Lilianne De La Caridad Beola Guibert

Hipertermia magnética basada en nanopartículas de óxido de hierro como terapia antitumoral: del cultivo celular tridimensional al modelo in vivo

Director/es
Gutiérrez Marruedo, Lucía
Grazú Bonavia, Valeria

http://zaguan.unizar.es/collection/Tesis

Universidad Zaragoza
1542

Tesis Doctoral

HIPERTERMIA MAGNÉTICA BASADA EN NANOPARTÍCULAS DE ÓXIDO DE HIERRO COMO TERAPIA ANTITUMORAL: DEL CULTIVO CELULAR TRIDIMENSIONAL AL MODELO IN VIVO

Autor

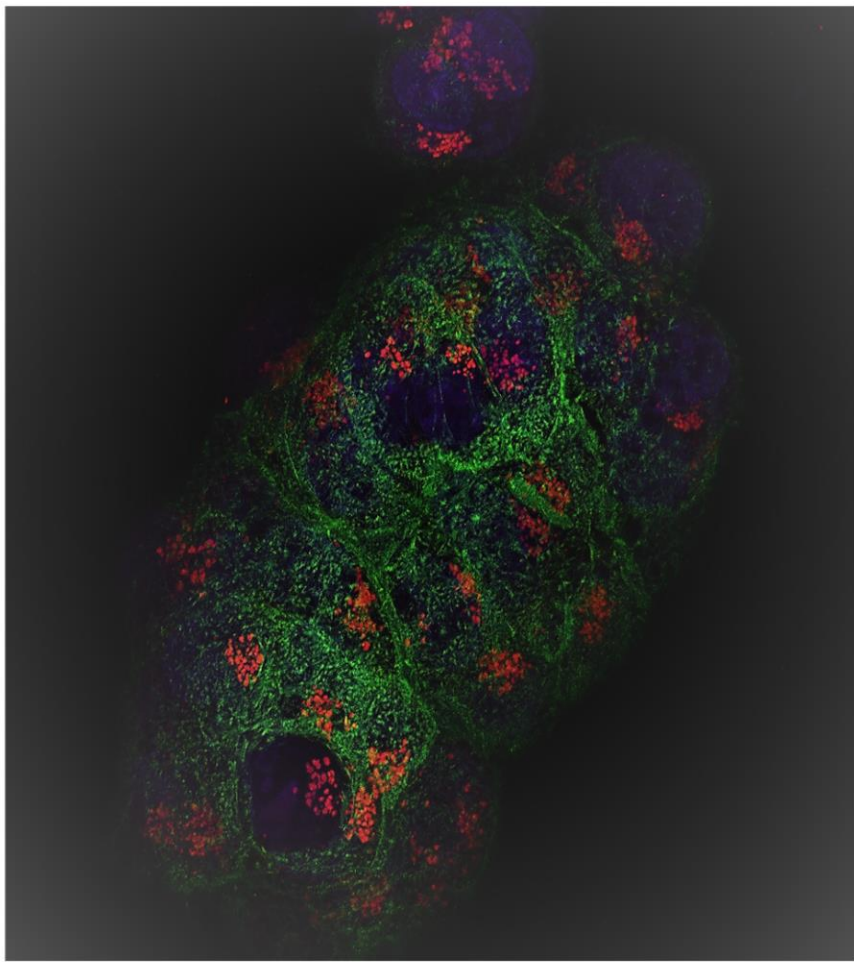## Lilianne De La Caridad Beola Guibert

Director/es

Gutiérrez Marruedo, Lucía
Grazú Bonavia, Valeria

UNIVERSIDAD DE ZARAGOZA
Escuela de Doctorado

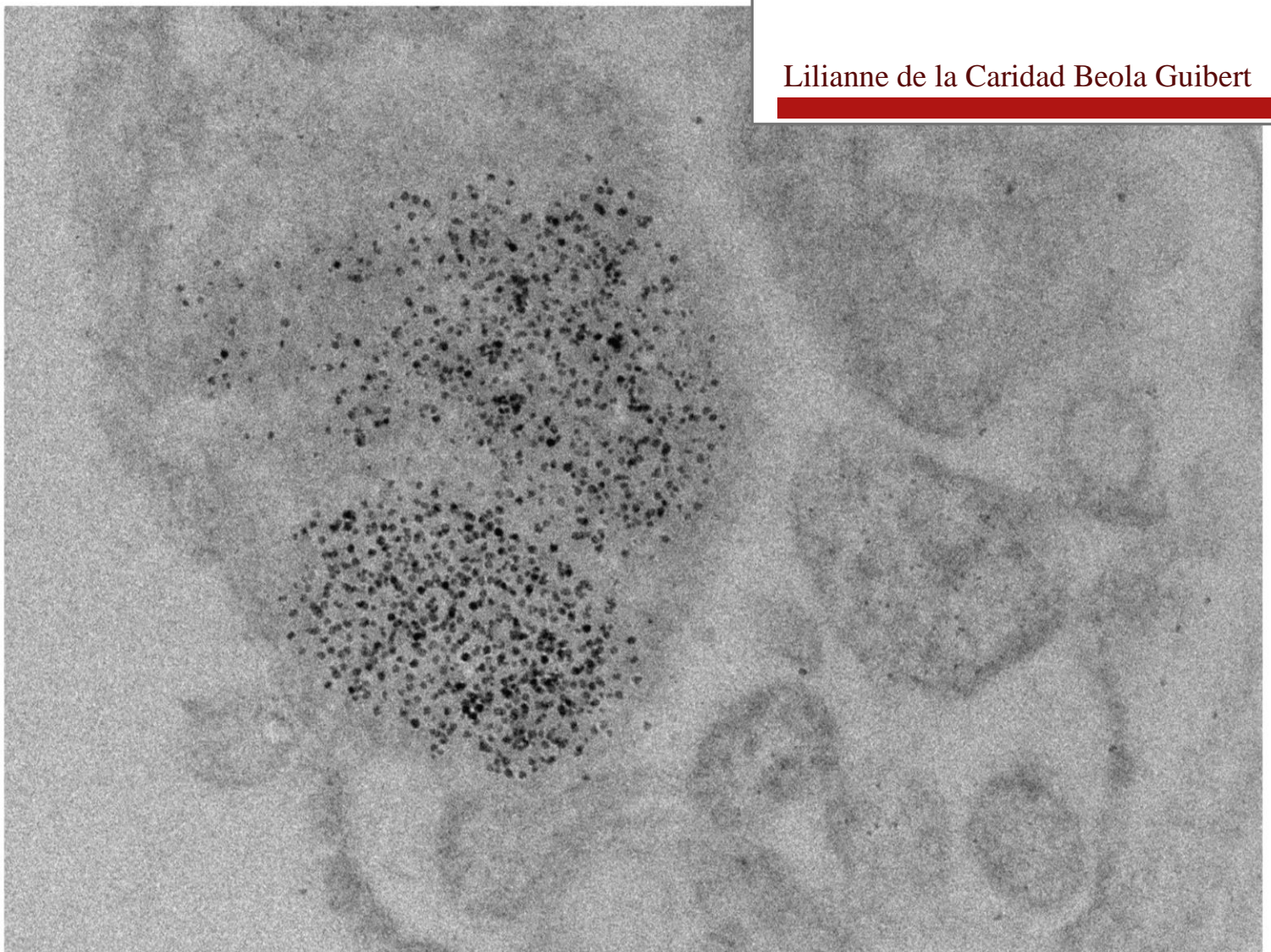Programa de Doctorado en Ciencia Analítica en Química

2020

Hipertermia magnética basada en nanopartículas de óxido de hierro como terapia antitumoral: del cultivo celular tridimensional al modelo in vivo

Universidad de Zaragoza
2020

Lilianne de la Caridad Beola Guibert

Hipertermia magnética basada en nanopartículas de óxido de hierro como terapia antitumoral: del cultivo celular tridimensional al modelo *in vivo*

Lilianne de la Caridad Beola Guibert

Memoria presentada para optar el grado de
Doctor por la Universidad de Zaragoza

Directores:
Lucía Gutiérrez Marruedo
Valeria Grazú Bonavia
Laura Asín Pardo

Departamento de Química Analítica
Zaragoza 2020

Dña. Lucía Gutiérrez Marruedo, Investigadora Ramón y Cajal, Dña. Valeria Grazú Bonavia, Investigadora Científica del CSIC y Dña. Laura Asín Pardo, Investigadora Contratada CIBER-BBN; pertenecientes al grupo Biofuncionalización de Nanopartículas y Superficies de la Universidad de Zaragoza

INFORMAN:

Que Lilianne de la Caridad Beola Guibert, licenciada y máster en Bioquímica y Biología Molecular, ha realizado bajo su dirección en el grupo de Biofuncionalización de Nanopartículas y Superficies de la Universidad de Zaragoza, el trabajo descrito en la presente memoria, que lleva por título "Hipertermia magnética basada en nanopartículas de óxido de hierro como terapia antitumoral: del cultivo celular tridimensional al modelo *in vivo*", y que presenta para optar al grado de Doctor.

Zaragoza, 2020

Dra. Lucía Gutiérrez
Marruedo

Dra. Valeria Grazú
Bonavia

Dra. Laura Asín
Pardo

"No temas a las dificultades. Lo mejor surge de ellas."

Rita Levi-Montalcini (1909-2012)

Aunque pueda parecer atípico comenzar unos agradecimientos con una cita, no puede ser de otra manera, porque si hay algo que he aprendido durante estos años es que hay decisiones que no solo te cambian la vida, sino que te transforman y te moldean el carácter, convirtiéndote en cada día en la mejor versión de ti mismo. Increíblemente han pasado 4 años desde que comencé el camino que hoy me ha traído hasta aquí, el cual hubiese sido imposible de recorrer sin la ayuda de tantas personas que han sido fuerza, apoyo, tesón, lágrimas y también risas en los momentos en los que más lo he necesitado. Así que primero que todo, agradezco a todos: a los que menciono aquí, a los que se me olvidarán por las prisas y emotividad del momento, y a todos aquellos que aún sin recordar sus nombres me tenderon una mano cuando más lo necesitaba.

Como no podría ser de otra manera, los primeros agradecimientos de esta tesis son para mis directoras (*Lu, Laurita* y *Vale*) por su formación durante estos años, por haberme dejado ser y experimentar, por escuchar, por corregir, por apoyar, por estar, y otros miles de por más…; porque son de esas cosas que ayudan a que sea fácil, incluso en los momentos más difíciles.

Amalia, gracias a ti comencé a experimentar en el mundillo de las nanos magnéticas, y fuiste mi guía y mi apoyo cuando en pleno Valle Grande (tú entenderás la referencia 😉) parecía que todo estaba perdido.

Infinitas gracias *Jesús (big boss :-p)* por aceptarme en tu grupo de investigación. El camino a recorrer hubiera sido más difícil de no haber contado con un grupo tan cohesionado y con tanto nivel científico y humano. Equipo "lo hacemos y ya vemos" (*Bea, Nessi, Soni, Albariño* y *Rafi*), sin nuestras escapadas de viajes, nuestros días eternos de labo y nuestras noches de risas y cenas, todo lo que conlleva mudarse de país y cambiar de vida hubiera sido mucho más difícil de sobrellevar, y eso os lo agradeceré siempre. Siempre compartiremos ese recuerdo del "huracán" en La Habana, y los mojitos en el malecón. *Bea* y *Nessi* mil gracias por ser tan especiales, por estar al tanto del mínimo detalle, por acompañarme en todo momento, y sobre todo por nuestras sesiones de terapia grupal hasta el cansancio. *Mari peque* gracias por tus ánimos y por esa dulzura tan natural y propia de ti que le impregnas a todo. *Alba (Tamara :-p)* y *Fra* gracias por vuestras sesiones de apoyo, por los dramas compartidos y por ese fabuloso

trabajadores de los *Servicios Científico Técnicos* del CIBA y a *todo el personal* de esa institución que un momento u otro me ha brindado su apoyo allí.

Mis más emotivos agradecimientos para los dueños del *Alfama Grill* en Lisboa y sus *trabajadores*, que estuvieron para mí y para mi familia casi sin conocerme, y que ocupan un lugar super especial en mi corazón. *Lore*, si hablamos de Lisboa estos agradecimientos no pueden terminar sin mencionarte, gracias por ser un gran amigo y compañero de trabajo.

Por último, quiero dar gracias infinitas a toda mi familia y amigos en Cuba, esa parte tan inmensa y tan importante de mi vida.

Rey, no hay palabras ni cariño suficiente por darte gracias por todos estos años de fuerza, apoyo y ánimos; sin ti claramente no hubiera sido lo mismo.

Abuelitos Tuta & Fermín y *Papá*, donde quiera que se encuentren, esta tesis está dedicada a ustedes, a su fuerza, a sus ánimos, a sus ganas de luchar y de vivir, y a su eterna sonrisa.

Mamá, no alcanzan las cuartillas, ni la vida para agradecerte tanto amor, tanta entrega, tanta incondicionalidad, tanta fuerza, tú eres y siempre serás mi ejemplo. A ti, madre querida, simplemente… GRACIAS POR TODO.

ABSTRACT

Magnetic hyperthermia is a promising therapy for the localized treatment of cancer. Under the exposure to an external alternating magnetic field, magnetic nanoparticles act as heating agents inducing cell death in the treated region. Understanding the molecular mechanisms involved in the cellular damage generated by this treatment is crucial for the successful application of this therapy.

In this thesis, 11 nm spherical magnetic nanoparticles were prepared by thermal decomposition, coated with PMAO (poly (maleic anhydride-alt-1-octadecene) and functionalized with glucose. In order to evaluate the influence of the nanoparticle location in the treatment efficacy, two different three-dimensional (3D) cell culture models, based on collagen gels, were prepared both in the murine macrophage cell line, RAW264.7, as in the human pancreatic tumor cell line, MIAPaca-2. One model kept all the particles inside the cells (*In Model*) while the other model had particles both inside and outside the cells (*In&Out Model*). In addition, the xenograft murine model of human pancreatic cancer based in the MIAPaca-2 cells was developed. The magnetic nanoparticle uptake and cell death mechanisms induced by different conditions of the hyperthermia treatment were evaluated by confocal microscopy, flow cytometry studies, molecular biology assays, histological analysis, magnetic measurements and other analytical characterization techniques. In addition, computational simulations to evaluate the intracellular heating effects were also performed.

In general, the *in vitro* and *in vivo* results obtained in this thesis, showed that magnetic hyperthermia had an important effect in the modulation of the extracellular matrix, as well as in the induction of immune-stimulation mechanisms. Phenomenon especially relevant in the search for new therapeutic strategies for pancreatic cancer. Moreover, the experimental results of this thesis showed that the type of cell death pathways triggered by the magnetic hyperthermia treatment depend on the number of intracellular nanoparticles. This is important in the understanding the molecular mechanisms that mediate the cellular response to this thermal therapy.

.

La hipertermia magnética es una terapia prometedora para el tratamiento localizado del cáncer. Bajo la exposición a un campo magnético alterno externo, las nanopartículas magnéticas actúan como agentes de calentamiento que inducen la muerte celular en la región tratada. La comprensión de los mecanismos moleculares implicados en el daño celular generado por este tratamiento es crucial para la aplicación exitosa de esta terapia.

Para esta tesis, se prepararon nanopartículas magnéticas esféricas de 11 nm por el método de descomposición térmica, que posteriormente se recubrieron con PMAO (poli (anhídrido maleico-alt-1-octadeceno) y finalmente se funcionalizaron con glucosa. Con el objetivo de evaluar la influencia de la localización de las nanopartículas en la eficacia del tratamiento térmico, se prepararon diferentes modelos de cultivo celular tridimensional (3D) basados en geles de colágeno, tanto en la línea celular de macrófagos murinos, RAW264.7, como en la línea de células tumorales pancreáticas humanas, MIAPaca-2. En un modelo, todas las partículas se encontraban localizadas dentro de las células (Modelo *In*), mientras que el otro modelo, contenía partículas tanto dentro como fuera de las células (Modelo *In&Out*). Además, se desarrolló un modelo murino de xenoinjerto de cáncer pancreático humano basado en las células MIAPaca-2. La internalización de las nanopartículas magnéticas, así como los mecanismos de muerte celular inducidos por diferentes condiciones de tratamiento de hipertermia se evaluaron por microscopía confocal, estudios de citometría de flujo, ensayos de biología molecular, análisis histológicos, medidas magnéticas y otras técnicas de caracterización analítica. Además, se evaluó el efecto del calentamiento intracelular inducido por las nanopartículas bajo acción del campo magnético mediante simulaciones computacionales.

En general, los resultados *in vitro* e *in vivo* obtenidos en esta tesis han demostrado que la terapia térmica con hipertermia magnética tiene un importante efecto en la modulación de la matriz extracelular, así como en la inducción de mecanismos de inmuno-estimulación. Fenómeno especialmente relevante en la búsqueda de nuevas estrategias terapéuticas para el tratamiento del cáncer de páncreas. Además, las evidencias experimentales de este trabajo demostraron que

las vías de muerte celular inducidas por el tratamiento con hipertermia magnética dependen del número de partículas localizadas en el interior de las células. Esto es importante para comprender los mecanismos moleculares que median la respuesta celular a esta terapia térmica.

ÍNDICE ·

1.1 Nanomateriales en biomedicina

El prefijo nano- es utilizado para referirse a objetos, sistemas o fenómenos con características derivadas de la escala nanométrica (nm=10^{-9} m). En el ámbito de los materiales según la recomendación (2011/696/EU) de la Comisión de la Unión Europea, puede definirse como nano: todo material "natural, incidental o manufacturado (…) donde una o más dimensiones externas están en el rango de tamaño de 1 a 100 nm".[1] El progreso alcanzado en el diseño y la síntesis de estos nanomateriales ha ido acompañado por su explotación paralela en varios campos de investigación, entre ellos la biología y la medicina, donde su impacto ha sido evidente por su relación directa con el cuidado de la salud y el desarrollo de la tecnología médica *(Figura 1.1)*.
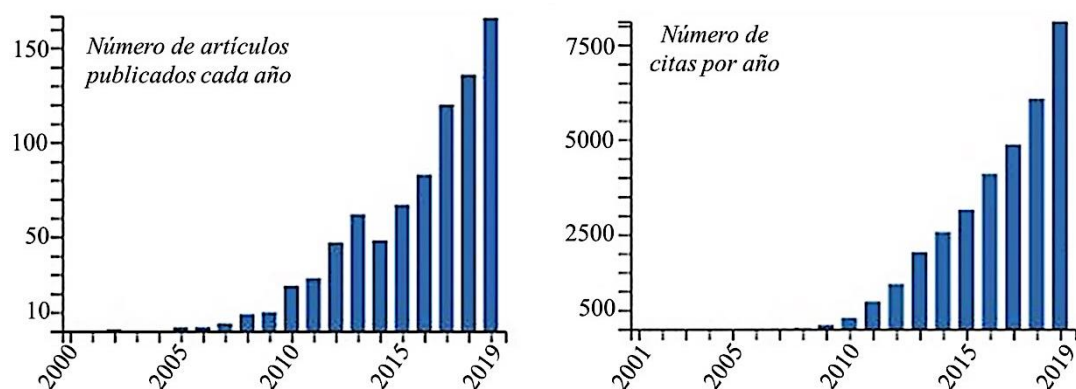
Figura 1.1 Estadísticas de artículos científicos publicados en el período 2000–2019 introduciendo los términos de búsqueda "nanomateriales" y "biomedicina". Fuente: Web of science.

La variedad de nanomateriales utilizados en biomedicina es extensa. Un listado breve, con menor o mayor impacto en el área, incluye puntos cuánticos, liposomas y una amplia variedad de nanopartículas metálicas y poliméricas *(Figura 1.2)*. Las excepcionales ventajas de su aplicación en el desarrollo de estrategias innovadoras de prevención, diagnóstico y tratamiento de enfermedades son múltiples: [2-4]

(i) Su tamaño nanométrico comparable a biomoléculas como proteínas y ácidos nucleicos les permite interactuar a niveles celulares, subcelulares e incluso moleculares; lo que contribuye a mejorar su interacción con las células diana, a la vez que minimiza el riesgo de efectos secundarios por acumulación en otros tejidos.

(ii) En dependencia de su tamaño, morfología o composición química, cada tipo de nanopartícula exhibe propiedades físico-químicas únicas (ópticas, magnéticas, catalíticas, mecánicas, etc.) que pueden ajustarse al tipo de aplicación médica o al fenómeno biológico que se desea estudiar.

(iii) El aumento de la relación área superficial /volumen les confiere una alta capacidad de carga de moléculas bioactivas u otras sustancias de interés biomédico, por lo que pueden ser diseñadas como nanoplataformas teragnósticas permitiendo simultáneamente la detección de la enfermedad y su tratamiento. A su vez, la conjugación o encapsulación de fármacos a las nanopartículas también permite superar problemas de solubilidad y estabilidad de formulaciones tradicionales basadas solo en biomoléculas, lo que contribuye a incrementar la disponibilidad sistémica del fármaco y con ello su acción terapéutica.

En la investigación biomédica, las nanopartículas se estudian y son ampliamente empleadas como transportadores para la liberación controlada de fármacos, producción de vacunas, así como en el desarrollo metodologías de regeneración tisular, modulación de la angiogénesis y formulaciones con actividad antimicrobiana.[5-7] En el ámbito del diagnóstico sus potencialidades son aprovechadas en el perfeccionamiento de biosensores y técnicas de imagen molecular para la detección temprana de múltiples patologías.[8-10] Mientras que en la terapia sus principales aplicaciones están dirigidas al desarrollo de tratamientos basados en mecanismos fotodinámicos, térmicos y magnetoterapia *(Figura 1.2).*
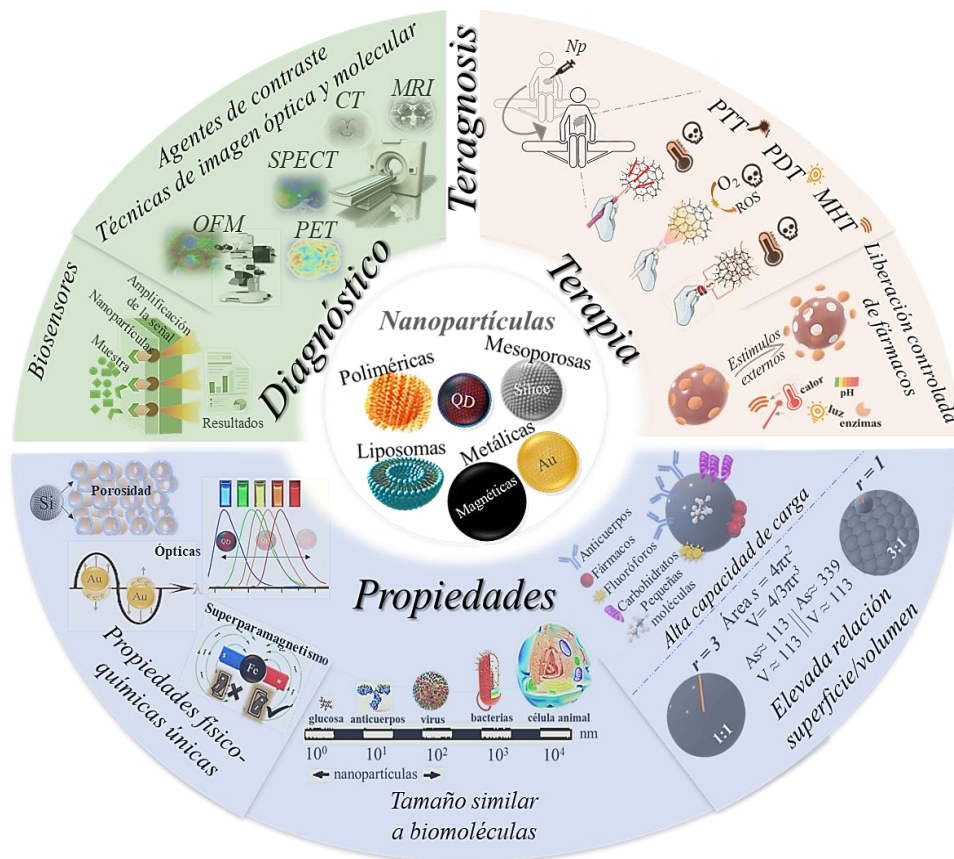
Figura 1.2 Propiedades y principales aplicaciones de las nanopartículas en biomedicina.
Abreviaturas: Oro (Au), Hierro (Fe); Puntos cuánticos (QD- del inglés"quantum dots"); Terapia fototérmica
(PTT- del inglés "photothermal therapy"); Dioxígeno (O₂); Especies reactivas del oxígeno (ROS- del inglés
"reactive oxygen species"); Terapia fotodinámica (PDT- del inglés "photodynamical therapy"); Terapia de
hipertermia magnética (MHT- del inglés "magnetic hyperthermia therapy"); Microscopía óptica de fluorescencia
(OFM -del inglés "optical fluorescence microscopy"); Tomografía computarizada (CT -del inglés "computed
tomography"); Resonancia magnética (MRI -del inglés "magnetic resonance imaging"), Tomografía
computarizada de emisión monofotónica (SPECT -del inglés "single-photon emission computed tomography");
Tomografía por emisión de positrones (PET -del inglés "positron emission tomography").

En la práctica clínica, la mayoría de las nanoformulaciones aprobadas para ensayos en pacientes están dirigidas al diagnóstico de diferentes tipos de cáncer mediante técnicas de imagen. Por otro lado, aunque en menor medida, también son empleadas en el tratamiento clínico de determinados tipos de tumores, principalmente en estadios de irrresecabilidad, ya sea de manera aislada o en combinación con procedimientos más convencionales como la radio- y quimioterapia.[11] Otras aplicaciones clínicas están relacionadas con el tratamiento de enfermedades como la anemia ferropénica, hepatitis y algunos tipos de neumonía. [12-14] Los nanomateriales más comunes empleados en este tipo de formulaciones se basan en liposomas y nanopartículas metálicas o derivadas de óxidos metálicos;[13-14] entre las que destacan las nanopartículas magnéticas de óxidos de hierro, cuyo uso es muy extendido y reconocido dentro de la biotecnología y la biomedicina por las excelentes potencialidades que ofrecen para disímiles aplicaciones diagnósticas y terapéuticas.

1.2 Nanopartículas magnéticas de óxido de hierro

El especial interés en la utilización de nanopartículas de óxido de hierro para biomedicina guarda estrecha relación con sus propiedades magnéticas únicas, su estabilidad coloidal y capacidad de ingeniería de superficie.[15-17] Aunque otros óxidos metálicos, como los derivados de níquel y cobalto también destacan por su comportamiento magnético,[18-19] el óxido de hierro constituye uno de los más investigados con estos fines debido a su elevada biocompatibilidad respecto a otros nanomateriales de este tipo.[20]

Numerosos tipos de óxidos de hierro pueden ser encontrados en la naturaleza y producidos en el laboratorio. Entre ellos, la hematita (α-Fe_2O_3), magnetita (Fe_3O_4) y maghemita (γ-Fe_2O_3), o una combinación no estequiométrica de estas dos últimas, son probablemente las composiciones químicas más comunes y tecnológicamente utilizadas. La magnetita, y la maghemita como producto de su oxidación, suelen ser las más empleadas para aplicaciones biomédicas debido a sus atractivas propiedades, que incluyen: alta magnetización (M, momento magnético por unidad de volumen), estabilidad química en condiciones fisiológicas y baja toxicidad.[15] Aunque sin lugar a dudas, el comportamiento superparamagnético que presentan en la nanoescala, es una de sus propiedades más interesantes para su aplicación en biomedicina.[21]

1.2.1 *Propiedades magnéticas*

Las propiedades magnéticas de las nanopartículas guardan estrecha relación con su tamaño. Los materiales masivos generalmente existen en un estado multidominio. Dentro de cada uno de estos dominios la magnetización (M) local se encuentra saturada, distribución que les permite disminuir la energía del sistema en ausencia de campo magnético. En consecuencia, estos materiales mantienen una respuesta magnética incluso cuando no se encuentra bajo la acción de un campo aplicado (H) *(Figura 1.3).*[22] A medida que se disminuye el tamaño de partícula, el mantenimiento de la pared del dominio requiere más energía. De manera tal, que por debajo un diámetro crítico, usualmente de unos pocos nanómetros (≈ 25 nm a temperatura ambiente),[23] mantener la estructura multidominio ya no es factible debido al costo energético que implica, lo que conduce a la formación de nanopartículas monodominio. En estos sistemas la energía térmica supera la energía de anisotropía, evitando la magnetización estable y dando como resultado un comportamiento superparamagnético *(Figura 1.3).*[24] La ausencia de coercitividad ($H_C=0$) que exhiben las nanopartículas superparamagnéticas cuando no hay campo aplicado, que se traduce en que solo se comporten magnéticamente en presencia del

estímulo magnético externo *(Figura 1.3)*, representa una ventaja excepcional al trabajar en sistemas biológicos ya que contribuye a evitar la agregación potencial de las nanopartículas una vez que son administradas, previniendo posibles efectos adversos *in vivo* como la obstrucción de los vasos sanguíneos.[25]
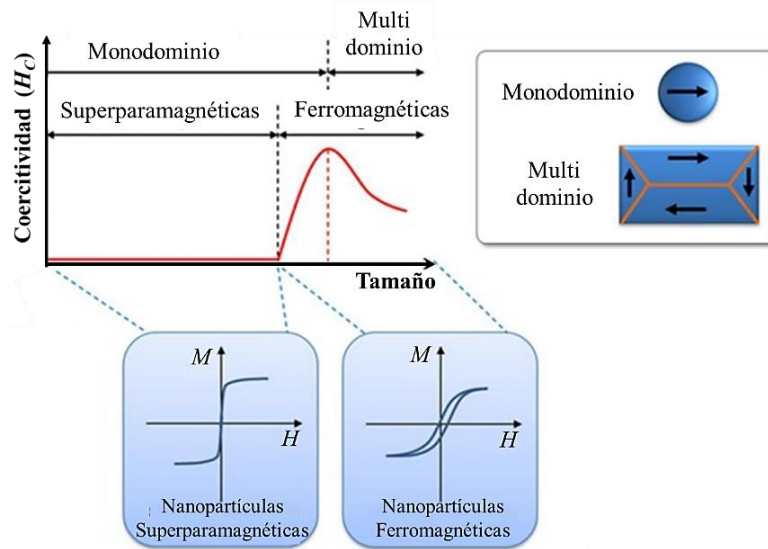
Figura 1.3 Comportamiento magnético de nanomateriales ferro- y superparamagnéticos. Adaptado: Theranostics. (2020); 10(8): 3793–3815. [26] Copyright (2020).

1.2.2 *Biocompatibilidad*

Otra propiedad que hace muy atractivo a estos sistemas para su aplicación en biomedicina es su baja toxicidad. El núcleo de óxido de hierro permite que las partículas sean degradadas y eliminadas de la circulación utilizando las rutas endógenas de metabolismo del hierro del organismo.[27-28]

Las nanopartículas después de su administración *in vivo* suelen ser capturadas por el sistema reticuloendotelial acumulándose principalmente en el hígado y el bazo, lo que conduce a su degradación por los macrófagos y las células de Kupffer hepáticas *(Figura 1.4)*.[29-30] El hierro metabolizado puede ser: (i) integrado a la síntesis de hemoproteínas, (ii) incorporarse a las reservas de hierro del organismo, o ser (iii) excretado a través de los riñones o las heces.[31] En tal sentido, se ha estudiado cómo la acumulación excesiva de nanopartículas en un área localizada puede tener implicaciones tóxicas.[32-33] Altos niveles de iones hierro libres, pueden conducir a un desequilibrio en la homeostasis y causar respuestas celulares aberrantes que incluyen citotoxicidad, estrés oxidativo, eventos epigenéticos y procesos inflamatorios. Al respecto, diversas investigaciones tanto *in vitro* como *in vivo* demuestran la seguridad y baja toxicidad de una amplia variedad de nanopartículas de óxidos de hierro a dosis de 100 µg Fe/ml

o superiores.[32, 34-40] Estudios en humanos, aunque más limitados en número, también evidencian efectos secundarios muy leves y de corta duración asociados a la administración de este tipo de partículas.[41-43]
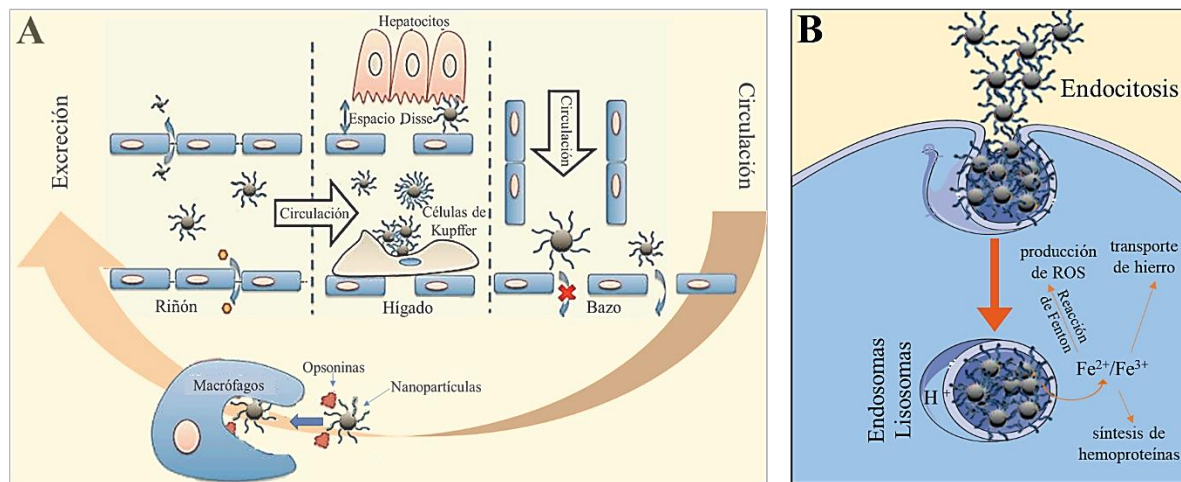
Figura 1.4 (A) Circulación de nanopartículas de óxido de hierro después de su administración in vivo. Adaptado: Chem. Soc. Rev. 2015; 44(23): 8576–8607.[27] Copyright (2020). (B) Internalización y metabolismo celular de las nanopartículas de óxido de hierro.

A nivel celular y molecular, la inducción de toxicidad por las nanopartículas de óxidos de hierro ha sido estrechamente relacionada con su capacidad de producir especies reactivas del oxígeno (ROS- del inglés "reactive oxygen species") mediante la reacción de Fenton,[44] efecto que guarda estrecha relación con el estado de oxidación de la partícula, ya que la magnetita puede oxidarse fácilmente para formar maghemita. En este sentido, dependiendo de las características fisicoquímicas de las nanopartículas, incluidos su tamaño, geometría o composición del núcleo metálico, estos procesos oxidativos pueden ser controlados mediante el uso de recubrimientos superficiales que disminuyan la reactividad de las partículas.[45]

1.2.3 *Síntesis y modificación superficial*

El tamaño y morfología de las nanopartículas, así como la química en superficie y su estado de agregación tienen una gran influencia en sus propiedades. Por lo cual, el desarrollo y perfeccionamiento de métodos de síntesis controlada constituye un requisito previo esencial para sus aplicaciones potenciales.

Los primeros estudios basados en la obtención de fluidos magnéticos estables fueron publicados por Rosensweig a inicios de la década de 1980.[46] Desde entonces, diferentes metodologías tanto físicas como químicas, se han descrito para sintetizar partículas estables,

con dimensiones controlables y propiedades magnéticas mejoradas.[47-48] Métodos físicos como la pirólisis láser [49-51] generan nanopartículas con un buen grado de cristalinidad, pero poseen como principal limitación, el requerimiento de instalaciones especializadas para desarrollar la síntesis. Por lo que suelen ser más costosos y complejos, además de presentar bajos rendimientos de producción. Otros, como la molienda mecánica [52-53] y condensación de gas inerte,[54-55] tienen la desventaja de ser poco efectivos para el control del tamaño, forma y composición de las nanopartículas, requiriendo adicionalmente su dispersión en medio líquido.[56] En este sentido, los métodos de síntesis química son los más utilizados cuando el objetivo es una aplicación biomédica.[15, 22, 57] La producción de nanopartículas de óxidos de hierro mediante técnicas químicas generalmente se basa en la reducción de iones metálicos a través de reductores químicos (citrato, alcohol, hidrazina, entre otros), o en la descomposición de precursores metálicos utilizando una fuente de energía. El proceso puede involucrar energía térmica (calor), sonoquímica, fotoenergía (luz ultravioleta y visible), electricidad u otras fuentes. Siendo de vital importancia la presencia de agentes estabilizantes (pequeñas moléculas y tensioactivos) en la dispersión coloidal para prevenir la agregación de las partículas y lograr una estrecha distribución de tamaños.[58] Numerosas metodologías químicas se han desarrollado para la producción de nanopartículas magnéticas de óxido de hierro basadas en sol-gel,[59] polioles,[60-61] microemulsión,[62] coprecipitación en medio acuoso,[63-64] síntesis hidrotermal,[65-67] descomposición térmica,[68-69] entre otros menos conocidos.[24] Dentro de este grupo, la descomposición térmica de precursores orgánicos del hierro es de lo métodos de síntesis más utilizados a escala de investigación por la elevada cristalinidad de las partículas obtenidas.[70-71]

La descomposición térmica de compuestos organometálicos en presencia de agentes tensoactivos tiene sus bases en el mecanismo de nucleación descrito por LaMer-Dinegar, [72] que comprende un corto período de nucleación de las partículas seguido por una etapa de crecimiento lento. En la literatura actual, la mayoría de las metodologías de obtención de nanopartículas de óxido de hierro por descomposición térmica se basan en el protocolo definido por Sun y colaboradores.[68-69] La síntesis mediante este método utiliza el acetilacetonato de hierro (III) como precursor orgánico, en presencia de ácido oleico, oleilamina y 1,2-hexadecanodiol como agentes estabilizantes. Las partículas derivadas de esta síntesis química se caracterizan por tener una elevada monodispersidad, aunque para su utilización sobre sistemas biológicos es requerido un paso adicional de transferencia a medio acuoso debido a la presencia de oleatos en su superficie.[73-74]

La manipulación de la química superficial de las nanopartículas es un aspecto clave para su transferencia del medio de producción al entorno biológico. Numerosos factores pueden comprometer la estabilidad de estos sistemas luego de su administración *in vitro* o *in vivo*:

(i)   Los medios de cultivo celular o los fisiológicos (tales como sangre, orina y linfa) pueden presentar una fuerza iónica muy diferente al medio de dispersión inicial en el que se encuentran las partículas tras la síntesis. Esto resulta en una supresión de la doble capa eléctrica que rodea las nanopartículas, generando una agregación parcial o total del sistema.[75]

(ii) La incorporación de las nanopartículas a compartimentos corporales específicos implica en muchos casos variaciones en el pH del medio, induciendo a su vez, la agregación de las mismas por efectos similares al descrito anteriormente.[76]

(iii) El contacto con la sangre, en casos de administraciones sistémicas, puede generar la adsorción superficial inespecífica de sales y proteínas plasmáticas, fenómeno que también facilita su aglomeración y además su eliminación por opsonización.[77-78]

Para prevenir tales efectos, se han desarrollado una amplia gama de recubrimientos superficiales que permiten diseñar la superficie de la nanopartícula para mejorar su estabilidad acuosa y su biocompatibilidad. Pequeñas moléculas tales como el ácido cítrico, ácido dimercaptosuccínico o dopamina,[79] así como una amplia diversidad de polímeros, entre los que puede citarse el polietilenglicol [80] o el ácido poli(anhídridomaleico-alt-1-octadeceno),[74, 81] son utilizados para intercambiar o intercalar con los oleatos de la superficie de las partículas. Estos procesos de recubrimiento superficial además de facilitar la estabilidad de las nanopartículas en soluciones fisiológicas, también proporcionan una plataforma sólida para su funcionalización con otros polímeros o biomoléculas que contribuyan al direccionamiento específico de las mismas hacia la célula o tejido diana . En relación a ello, varias estrategias de conjugación covalente que utilizan grupos amina, carboxilo, aldehídos o tioles expuestos en la superficie de las nanopartículas han permitido acoplar con éxito: anticuerpos o sus fragmentos, oligosacáridos, proteínas, péptidos miméticos o pequeños ligandos, contribuyendo a mejorar la internalización de las partículas, reducir su toxicidad y mantener su circulación por un tiempo suficiente para alcanzar su objetivo biológico.[21] Por otro lado, el recubrimiento superficial también permite la conjugación de las nanopartículas con otras moléculas funcionales, tales como agentes radioactivos o fluoróforos, que contribuye a ampliar su funcionalidad y mejorar su seguimiento sobre el sistema en el que se han administrado. [82-83] Lo que unido a la posibilidad de asociación o encapsulación de fármacos en superficie facilita la utilización de

las nanopartículas magnéticas de óxidos de hierro en una amplia diversidad de aplicaciones diagnósticas o terapéuticas.

1.2.4 *Aplicaciones biomédicas*

Numerosos enfoques prácticos han sido desarollados para la utilización de nanopartículas magnéticas en biomedicina. A escala diagnóstica, sus propiedades magnéticas intrínsecas permiten que sean utilizadas como *agentes de contraste* para la obtención de imágenes por resonancia magnética, por lo que presentan excelentes potencialidades en la detección de tumores y lesiones del sistema nerviso central.[84] El uso de nanopartículas magnéticas como agentes de imagen molecular en la investigación del cáncer permite el escaneo de alta resolución de la microvasculatura tumoral y la localización de áreas de inflamación, metástasis y proliferación vascular de tumores.[85] Incluso el uso clínico de determinadas formulaciones de este tipo se encuentra aprobado por las agencias regulatorias internacionales para la diferenciación de ganglios linfáticos cancerosos de los no malignos *(Tabla 1.1)*.[11] Por otro lado, la ingeniería superficial de las nanopartículas también ofrece ventajas excepcionales como matrices inmovilizadoras de una amplia variedad de marcadores de diagnóstico para el desarrollo de *biosensores*. Se ha demostrado que las nanopartículas pueden contribuir a mejorar la amplificación de la señal y las técnicas de lectura del analito respecto a las tecnologías más tradicionales.[8, 86] En este sentido, se investigan nuevas estrategias que aprovechan simúltaneamente la funcionalidad de las nanopartículas como agentes de contraste y su capacidad de ser utilizadas en la bio-detección, para desarrollar nanointerruptores detectables por resonancia magnética de imagen. Esta técnica se ha denominado resonancia magnética de diagnóstico, y es aplicable tanto en la detección de analitos muy pequeños, como en el desarrollo de herramientas de diagnóstico para detectar ácido nucleicos, proteínas o marcadores de cáncer en una muestra biológica.[87-88] Las propiedades magnéticas de las nanopartículas de óxido de hierro también ofrecen perspectivas interesantes para la separación selectiva de una amplia gama de entidades biológicas específicas bajo acción de un campo magnético externo. La *separación magnética* presenta características muy superiores a los métodos tradicionales de bioseparación, ya que al no requerir de pasos adicionales como la centrifugación o filtración previa, ni presentar limitaciones mínimas de difusión, asegura un proceso más simple y menos costoso.[89]

En la terapia, el uso de nanopartículas de hierro está aprobado para el tratamiento de anemias ferropénicas cuando la administración oral de otros medicamentos con base de hierro no es lo suficientemente eficiente *(Tabla 1.1)*.[14, 90] Otras aproximaciones terapéuticas se encaminan a

su utilización como portadores de agentes de interés clínico para la *liberación controlada de fármacos*, que maneja diferentes enfoques terapéuticos acorde al tipo de tratamiento considerado. En este sentido, la conjugación de ADN (ácido desoxirribonucleico) u oligonucleótidos a las nanopartículas es muy estudiado en el marco de la vectorización de genes o *terapia génica*. Las evidencias experimentales demuestran que la asociación de las partículas magnéticas con los ácidos nucleicos, además de protegerlos de la degradación por nucleasas, asegura una concentración altamente eficaz del vector genético en las células diana, lo que contribuye a promover la absorción celular, y con ello a la prolongación del efecto terapéutico.[91] Por otro lado, las nanopartículas también ha sido muy estudiadas para el suministro de fármacos dirigidos a reparar lesiones del sistema nervioso central debido a su capacidad potencial de superar diferentes barreras fisiológicas que limitan la accesibilidad al medicamento.[92] En la terapia oncológica las potencialidades de las nanopartículas magnéticas también han sido exploradas para la administración de agentes anticancerígenos al sitio del tumor.[93] Aunque en la mayoría de los casos, la *liberación controlada de fármacos* para el tratamiento del cáncer suele combinarse con una de las aplicaciones potenciales más estudiadas para el uso de las nanopartículas magnéticas en biomedicina, que se basa en su utilización como agentes de calentamiento local bajo acción de un campo magnético externo (AMF- del inglés "alternating magnetic field"), aproximación terapéutica conocida como *hipertermia magnética*.[94-96]

Nombre	Indicación clínica	Año de aprobación	Ensayos clínicos (ClinicalTrials.gov)
Venofer (American Regent)	Reemplazo de hierro para el tratamiento de la anemia en pacientes con enfermedad renal crónica	FDA (2000)	-2016: Venofer: 44 -2019: Venofer: 60
Feraheme (AMAG) Rienso (Takeda) Ferumoxytol	Deficiencia de hierro en pacientes con enfermedad renal crónica	FDA (2009)	-2016: Ferumoxitol: 57 (6 reclutamiento / activo para tratamiento de anemia; 22 reclutamiento / activo para aplicaciones de imagen) -2019: Ferumoxitol: 84 (6 reclutamiento / activo para tratamiento de anemia; 22 reclutamiento / activo para aplicaciones de imagen
Injectafer Ferinject (Vifor)	Anemia por deficiencia de hierro	FDA (2013)	-2016: Ferinject: 50 Injectafer: 8 -2019: Ferinject: 79 Injectafer: 24
Ferumoxtran-10 Combidex Sinerem (AMAG)	Imagen de metástasis de ganglios linfáticos	Disponible en Holanda	-2016: Ferumoxtrano-10: 11 (1 activo) -2019: Ferumoxtrano-10: 24 (1 activo; 6 reclutamiento)

Tabla 1.1 Listado de algunas formulaciones basadas en nanopartículas de hierro aprobadas para su uso en clínica a partir de los años 2000. Adaptado: Bioengineering & translational medicine (2019), 4 (3).[14] Copyright (2020). Abreviaturas: Agencia de Medicamentos y Alimentación (FDA- del inglés "Food and Drug Administration", Estados Unidos de América).

1.3 Hipertermia magnética

La hipertermia magnética es una terapia prometedora para el tratamiento de diversas enfermedades basada en la generación de calentamiento controlado sobre el tejido diana. En comparación con otras técnicas de hipertermia tradicionales (tales como: hipertermia capacitiva, por ultrasonido o microondas) tiene entre sus principales ventajas, la capacidad de focalización del calor a nivel celular y una mayor profundidad de penetración; lo que permite llegar a tejidos poco accesibles, haciendo posible su integración directa con otras terapias para mejorar su efectividad.[97-98]

El fundamento de la hipertermia magnética se basa en la exposición de las nanopartículas a un AMF, lo que genera una inversión continua en la dirección de su momento magnético. Esto se traduce en una conversión de la energía magnética a térmica a través de diferentes mecanismos físicos, permitiendo que la partícula se comporte como una fuente de calor. La eficiencia de esta transformación, y por ende el calentamiento generado, puede variar en órdenes de

magnitud dependiendo de las propiedades estructurales y magnéticas de las partículas, así como de su modificación superficial y la amplitud (H) y frecuencia (f) del AMF aplicado.[99]

El uso de nanopartículas superparamagnéticas para hipertermia muestra ventajas excepcionales respecto a otros agentes de calentamiento como las partículas ferromagnéticas; puesto que al no presentar magnetización residual una vez eliminado el estímulo magnético, contribuyen a minimizar los efectos de toxicidad asociados al tratamiento térmico.[100] En el caso de las nanopartículas superparamagnéticas, los mecanismos físicos responsables de convertir la energía magnética en calor bajo la acción del AMF se atribuye a las relajaciones de Néel-Brown *(Figura 1.5)*. El mecanismo de Néel tiene sus bases en los fenómenos de relajación del núcleo magnético interno y muestra una dependencia particular con el tamaño y la anisotropía intrínseca de la partícula (composición, superficie y forma).[101-102] Mientras que la relajación browniana se relaciona con la capacidad de las nanopartículas de reorientarse mediante rotación física en el medio donde se encuentran inmersas.[103] En nanopartículas superparamagnéticas ambos mecanismos pueden tener lugar simultáneamente y, en consecuencia, influir en su capacidad potencial de calentamiento. En aplicaciones *in vitro* e *in vivo*, se ha demostrado que la producción de calor ocurre esencialmente a través de la relajación de Néel,[104] debido a que la rotación libre de las partículas (mecanismo de Brown) se encuentra limitada por la alta viscosidad del medio biológico.
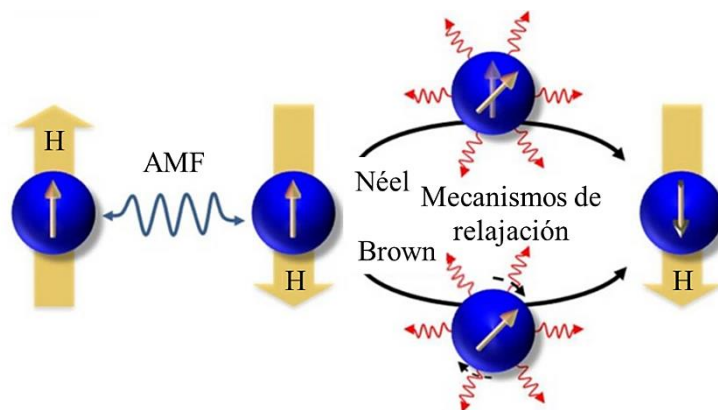
Figura 1.5 Mecanismos de relajación de nanopartículas superparamagnéticas de óxido de hierro. Adaptado: Theranostics. (2020); 10(8): 3793–3815.[26] Copyright (2020).

1.3.1 *Parámetros utilizados para reportar las propiedades de calentamiento de las nanopartículas magnéticas*

Un parámetro esencial a tener en cuenta en la utilización de nanopartículas para hipertermia magnética es su capacidad potencial de producir calor bajo la acción de un AMF. Esta eficiencia de calentamiento usualmente es reportada en términos de tasa de absorción específica (SAR- del inglés "specific absorption rate"), parámetro extrínseco que se basa en las características de la respuesta clínica a la potencia de calor entregada por unidad de masa; o como la pérdida específica de potencia (SLP- del inglés "specific loss power"), parámetro intrínseco basado en la capacidad de calentamiento del material.[105] En el contexto de la hipertermia magnética, el SAR (Ec.1) y el SLP (Ec.2) son considerados del mismo orden de magnitud. Sin embargo, aunque ambos términos utilizan las mismas unidades y se les ha atribuido el mismo significado, algunos autores consideran que el uso del SLP es más apropiado como terminología intrínseca para la hipertermia magnética.[106] Esto se debe al hecho de que las agencias reguladoras adoptaron la terminología "tasa de absorción específica" (SAR), en el contexto de la exposición a campos electromagnéticos de radiofrecuencia u otras formas de energía como el ultrasonido.[107] No obstante, ambos términos se continúan utilizando indistintamente para la hipertermia magnética y, su valor numérico es calculado mediante las ecuaciones: [26]

$$SAR = \frac{C}{m}\left(\frac{\Delta T}{\Delta t}\right) (Ec.1) \qquad SLP = \frac{C}{m/Vs}\left(\frac{\Delta T}{\Delta t}\right) (Ec.2) \;$$

donde C representa la capacidad calorífica específica de la muestra en su conjunto (considerando tanto el material como el medio de dispersión), m es la masa de material magnético utilizado en la medida, Vs es el volumen de la muestra y ($\Delta T/\Delta t$) es la pendiente inicial de la curva de calentamiento en función del tiempo (T/t: Temperatura / tiempo). En la mayoría de los casos el SAR es expresado en vatios por gramos de material magnético (W/g), aunque también puede ser enunciado en unidades volumétricas (W/m^3).[108] El uso de la pendiente inicial ($\Delta T/\Delta t$) en la curva T versus t (t → 0) es una de las metodologías más aceptadas para proporcionar una estimación del SAR, ya que las pérdidas térmicas iniciales durante el proceso de calentamiento siguen siendo insignificantes y la distribución de temperatura dentro de la muestra más homogénea.[105, 109]

En la literatura también se ha recomendado el uso de otro parámetro conocido como pérdida intrínseca de potencia (ILP- del inglés *"intrinsic loss power"*), para informar las medidas de generación de calor por hipertermia magnética; debido a que este valor normaliza el SAR

respecto a la frecuencia y la intensidad del AMF aplicado,[110-111] facilitando la comparación directa entre los valores reportados por los diferentes autores independientemente de las condiciones de campo aplicadas: $ILP = \frac{SAR}{H^2 f}$ $(Ec. 3)$. Sin embargo, el parámetro ILP no es completamente intrínseco y el sistema tiene que cumplir algunas consideraciones: las nanopartículas deben presentar tamaños cristalinos con un índice de polidispersidad mayor que 0,1 y los valores de intensidad de AMF aplicado deben estar por encima de la magnetización de saturación de las nanopartículas (*Ms*). A esto se suma que la frecuencia utilizada en el experimento debe ser del orden de los MHz, mientras que las pérdidas térmicas del sistema tienen que ser reproducibles.[112] Por estos motivos, la mayoría de los datos reportados en los estudios experimentales aún se continúan expresando en términos de valores de SAR.

1.3.2 *Principales ventajas del uso de hipertermia magnética en biomedicina*

La hipertermia magnética muestra grandes potencialidades terapéuticas dentro del campo de la biomedicina *(Figura 1.6)*.[113]
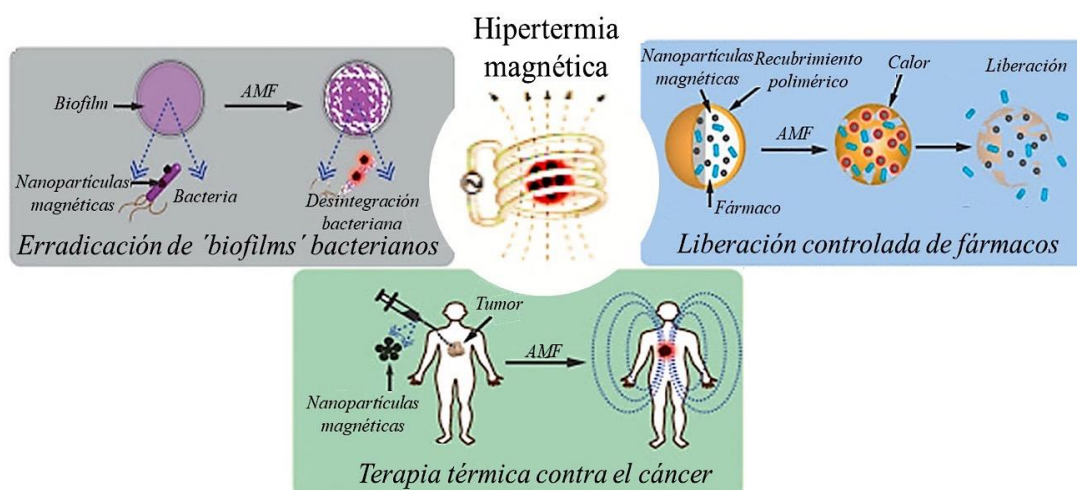
Figura 1.6 Diferentes tipos de aplicaciones biomédicas de la hipertermia magnética. Adaptado: Progress in Natural Science: Materials International Vol. 26, Issue 5, October (2016), Pag. 440-448.[101] Copyright (2020).

El incremento de temperatura inducido por las nanopartículas magnéticas bajo acción del AMF puede ser utilizado como un estímulo externo para la liberación de fármacos *(Figura 1.6)*.[7, 114] En comparación con otras metodologías de estimulación externa dedicadas a estos fines (tales como cambios de pH, condiciones enzimáticas, técnicas de calentamiento global, etc.), el efecto de calor localizado ofrece una alternativa prometedora para un control más específico del sitio de entrega, y una mayor precisión del tiempo activo de liberación de la carga

terapéutica. El suministro controlado de fármacos basado en hipertermia magnética puede ocurrir mediante diferentes mecanismos:[113-114]

(i) La ruptura o desestabilización de enlaces entre la molécula terapéutica y la matriz; de tal modo que el fármaco unido a las nanopartículas, a través de un enlace sensible al calor, sea liberado debido al aumento de la temperatura.

(ii) La degradación o transformación de la matriz de las nanopartículas, ya sea por el recubrimiento con polímeros termo-sensibles conjugados al fármaco, o mediante la encapsulación de la droga en estructuras conocidas como magneto-liposomas.

(iii) Mediante el desarrollo de las denominadas "compuertas conmutables". Este mecanismo se basa en el recubrimiento de las partículas magnéticas con materiales porosos sensibles al calor que contienen el fármaco retenido y, que en respuesta al tratamiento térmico hacen posible su liberación.

Otra aplicación de la hipertermia magnética en biomedicina está dirigida a reducir la viabilidad de patógenos bacterianos frente a una infección *(Figura 1.6)*. Numerosas evidencias científicas han demostrado la relación directa entre las infecciones bacterianas y la cronicidad de diversas enfermedades.[115] Un desafío crítico en el tratamiento de este tipo de infección es la capacidad de las bacterias de desarrollar ecosistemas microbianos organizados (biofilms) que les permiten generar resistencia a las terapias con antibióticos.[116] En este contexto, diversos estudios han evidenciado la eficacia de la hipertermia magnética para el tratamiento de biopelículas de diferentes tipos de bacterias.[117-118] Se ha observado que el aumento localizado de la temperatura mediante la activación dirigida de nanopartículas magnéticas por un AMF, puede inducir a la eliminación de las sustancias poliméricas extracelulares de estos sistemas bacterianos, incrementando así su sensibilidad de respuesta a los antibióticos convencionales. Otras evidencias experimentales también han demostrado que la aplicación de hipertermia magnética puede a la vez contribuir a potenciar la respuesta inmune innata del huésped para mejorar la eliminación de las bacterias intracelulares.[119]

La hipertermia magnética también ha sido ampliamente estudiada como aplicación terapéutica directa para la inducción selectiva de muerte celular por incremento de la temperatura *(Figura 1.6)*.[120] El nivel de daño generado por el tratamiento térmico varía por encima de cierto umbral de temperatura acorde a las condiciones del AMF aplicado,[99] y a las propiedades físico-químicas de las nanopartículas, que incluyen área y química de superficie, número de capas, dimensión lateral y grupos funcionales presentes en el recubrimiento.[101] Este concepto ha sido

particularmente aplicado al desarrollo de terapias antitumorales debido a la complejidad actual para el tratamiento de dicha patología.[121] El marcado interés clínico en el uso de hipertermia magnética para la terapia contra el cáncer tiene sus bases en la sensibilización de las células tumorales en respuesta a la elevación de la temperatura local. De manera tal que se induzca un efecto citotóxico específicamente localizado en el sitio del tumor, una de las principales limitaciones de las terapias tradicionales contra la enfermedad.[121]

1.3.2.1 Hipertermia magnética para el tratamiento del cáncer

El incremento de la temperatura corporal es un método de respuesta fisiológica a diversas lesiones, incluidas las infecciones virales y bacterianas, que produce los síntomas reconocidos como fiebre.[122] En este sentido, la influencia del aumento de la temperatura en la remisión del cáncer ha sido un fenómeno observado desde hace siglos. Las primeras evidencias de atenuación de la enfermedad a consecuencia de patologías febriles concomitantes fueron aportadas entre los siglos XVIII-XIX, e incluso, en la segunda mitad del siglo XIX, el uso de la terapia febril infecciosa, aparentemente era una práctica común para tratar diversas afecciones.[123] Sin embargo, no fue hasta la segunda mitad del siglo XX, con el auge de las actividades de investigación en términos de producción científica y tecnológica, que se proponen y especifican nuevas técnicas de generación controlada de calor para la terapia antitumoral.[112]

La característica común de las terapias de calentamiento se basa en el incremento de la temperatura de una parte del cuerpo (*hipertermia regional* e *hipertermia local*) o su totalidad (*hipertermia de cuerpo entero*), por encima de los límites fisiológicos durante un período de tiempo definido. La *hipertemia de cuerpo entero* es empleada a menudo en casos de cáncer metastásico,[124] mientras que la aplicación *local* es más utilizada en tumores localmente avanzados.[125] Las metodologías para generar calor en el organismo son numerosas y varían según la región objetivo. Estas incluyen desde calor administrado por contacto externo (mediante mantas o cámaras térmicas); hasta la radiación inducida por microondas; ultrasonidos; terapias de perfusión, acoplamiento capacitivo o inductivo de campos de radiofrecuencia y fotocoagulación intersticial con láser.[123] En general, pueden ser aplicadas de manera aislada o en combinación con otras técnicas, y aunque muchas representan enfoques de terapia más antiguos, aún son utilizadas en la práctica clínica. Sin embargo, a consecuencia de la severidad de los efectos adversos observados en la gran mayoría de tratamientos por *hipertermia de cuerpo entero*, las nuevas aproximaciones a la terapia antitumoral se han centrado en el desarrollo e implementación de metodologías de *hipertermia local*. Al limitarse

a áreas más pequeñas del organismo, el tratamiento antitumoral localizado suele inducir efectos secundarios más leves, por lo que ofrece una gama más amplia de posibilidades terapéuticas, especialmente si la temperatura del tumor puede mantenerse por encima de la del tejido normal circundante.

En la segunda mitad de la década de 1950, Gilchrist y colaboradores introducen como concepto, el uso de materiales magnéticos para el tratamiento localizado de tumores mediante hipertermia.[126] Esta metodología se ha ido perfeccionando con los años, como resultado de la obtención de nanomateriales con propiedades magnéticas y cristalinas mejoradas hasta llegar a convertirse en uno de los enfoques más prometedores para confinar el calor en áreas tumorales específicas, y evitar desajustes fisiológicos importantes a nivel de organismo.[127] El calentamiento magnético es atractivo como modalidad física para el tratamiento del cáncer debido a características específicas como la capacidad de control remoto, la resolución espacial a nanoescala y la especificidad a nivel molecular.[121, 128] A esto se suma el hecho de que las nanopartículas pueden ser diseñadas para su acumulación localizada en los tejidos cancerosos, lo que contribuye a mejorar la especificidad del tratamiento.[129] Respecto a otros nanomateriales con capacidad de inducir aumentos de temperatura localizada en una región objetivo, como el oro,[130] las nanopartículas magnéticas han atraído una atención considerable debido a su capacidad de generar calor de manera efectiva bajo un AMF sin limitaciones en la profundidad de penetración, lo que puede ser ventajoso para objetivos que residen incluso en el interior del sistema biológico. Por otro lado, el hecho de que el campo magnético causa efectos adversos mínimos sobre los tejidos, también constituye un beneficio distintivo para aplicaciones antitumorales no invasivas *in vivo*.[131]

El uso de hipertermia magnética ha sido planteado en oncología como terapia complementaria, adyuvante o concomitante, a los tratamientos tradicionales como la radio- o quimioterapia; aunque su aplicación pre- o postquirúrgica también ha sido valorada.[98, 132-134] La justificación del uso de hipertermia magnética en combinación con quimioterapia y radioterapia se basa en la heterogeneidad del tejido cancerígeno.[135-138] Los tumores pueden presentar extensas áreas de necrosis, hipoxia y acidificación del pH. Las células en estas zonas a menudo se encuentran en detención del ciclo celular (fase G_0), por lo cual son más resistentes a los fármacos que impiden el crecimiento (citostáticos) y al efecto de la radiación. Aunque en dependencia del tipo de tumor, aún no queda totalmente esclarecido si todos los tipos de células tumorales son más susceptibles al daño generado por calor, si se ha comprobado que un incremento relevante de la temperatura en el área patológica puede estimular la vascularización y aumentar la

oxigenación del tejido, contribuyendo a mejorar la concentración y eficacia de las drogas terapéuticas. Por otro lado, las células tumorales en proceso de replicación del ADN (fase S del ciclo celular) pueden mostrar una resistencia al tratamiento con radiaciones ionizantes. Al respecto, los estudios clínicos han demostrado que la elevación de la temperatura dentro del tumor tiene un efecto citotóxico importante en células radio-resistentes optimizando el efecto del tratamiento.[139] De manera análoga las ventajas de la termosensibilización en tratamientos clínicos adyuvantes o concomitantes con agentes quimioterapéuticos también han sido demostradas.[140-142]

Otra aproximación al uso de hipertermia magnética en la terapia contra el cáncer es su combinación con la inmunoterapia. Enfoque que ha comenzado a estudiarse en los últimos tiempos, basado en evidencias preclínicas que demuestran que el calentamiento del tumor puede iniciar una respuesta de inmunoactivación, que potencialmente sirve como complemento a los medicamentos inmunoterapéuticos en desarrollo o ya utilizados en la clínica.[143-145]

Aunque gran parte de la investigación actual se centra en el desarrollo de métodos de tratamiento dirigidos a disminuir la viabilidad celular en el tumor después de la hipertermia magnética; otros enfoques terapéuticos están más centrados hacia la respuestas de las células cancerosas a la terapia térmica. En este contexto, se han obtenido evidencias experimentales que señalan la maduración de células madres cancerosas (conjunto de células tumorales con propiedades de autorrenovación no regulada, que impulsan el crecimiento y la propagación del tumor [146]) hacia fenotipos más especializados, en respuesta a la generación de calor local tras el tratamiento con hipertermia magnética. Por lo cual, las potencialidades de una posible terapia de diferenciación por choque térmico también se estudia con perspectivas interesante para la oncoterapia.[147-149]

A escala *in vitro* y pre-clínica, las capacidades terapéuticas de la hipertermia magnética son exploradas en una amplia variedad de cánceres, que incluyen pulmón, mama, próstata, columna vertebral, cerebro, cabeza y cuello del útero, páncreas e hígado.[93-95, 98, 150-153] En la clínica, la aplicación de hipertermia magnética se plantea mayoritariamente en pacientes diagnosticados con tumores no resecables o complicados, o que buscan una alternativa a procedimientos quirúrgicos costosos y de alto riesgo. El uso de hipertermia magnética se encuentra aprobado en Europa como terapia adyuvante para tratar el glioblastoma multiforme (MagForce AG) en combinación con radioterapia. La terapia Nanotherm® también es clínicamente utilizada dentro de la Unión Europea para el tratamiento del cáncer de mama del sistema ganglionar, y

se prevé que su aprobación en Estados Unidos se encuentre en las etapas finales.[154] Otras formulaciones con uso clínico indicado para terapias de reemplazo de Fe o diagnóstico mediante imagen de resonancia magnética, como es el caso del Feraheme®, Ferumoxytol y Feridex®, también han sido aprobadas por la Agencia de Medicamentos y Alimentación de Estados Unidos para ensayos clínicos de hipertermia magnética.[155-156] Mientras que en Europa, la compañía MagForce, también ha llevado a cabo otros estudios clínicos basados en hipertermia magnética para el tratamiento del cáncer de próstata y cérvico-uterino.[157] Aunque estos ensayos representan un importante paso en el establecimiento de la hipertermia magnética como un procedimiento clínicamente estandarizado, aún persisten limitaciones para lograr el pleno potencial de esta prometedora terapia, que incluye en muchos casos la necesidad de altas dosis nanopartículas o la resistencia terapéutica derivada de los mecanismos de autoprotección de las células cancerosas contra el estrés térmico aplicado. Factores que a su vez guardan estrecha relación con la influencia que tiene el microambiente, la angiogénesis y muchos otros elementos de la biología del tumor en la modificación del resultado de la terapia térmica.[158] En este sentido, se hace imprescindible la búsqueda y desarrollo de modelos preclínicos que permitan estudiar desde una perspectiva mimética *in vivo* los efectos de la hipertermia magnética para lograr su translación efectiva a la clínica de pacientes.

1.4. Modelos biológicos para estudiar el cáncer

El cáncer engloba un conjunto genérico de enfermedades que pueden afectar diferentes partes del organismo.[159] En la sociedad actual, ha llegado a convertirse en uno de los trastornos de salud con mayor incidencia en las tasas de mortalidad y morbilidad debido a la complejidad de su diagnóstico y tratamiento *(Figura 1.7)*.[160]
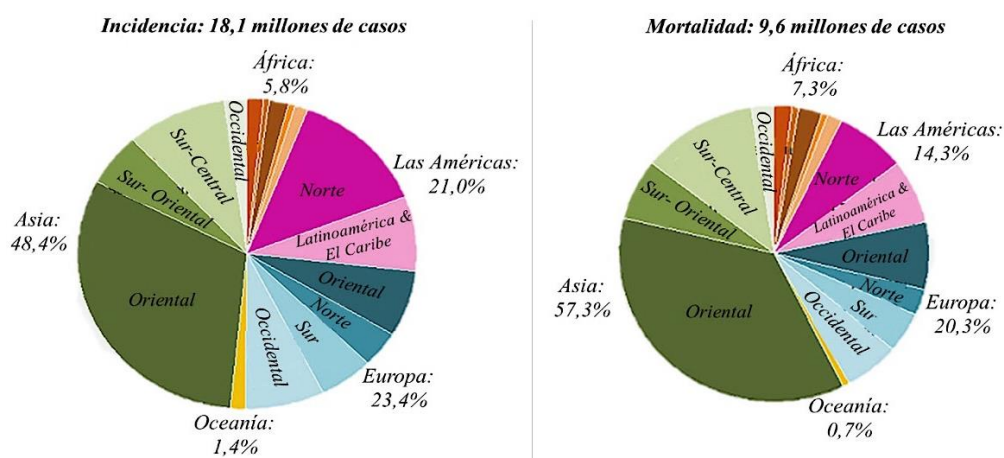
Figura 1.7 Estadísticas globales de incidencia y mortalidad del cáncer. Adaptado: Int. J. Cancer: 144, 1941–1953 (2019).[160] Copyright (2020).

El desarrollo del cáncer es un proceso complejo durante el cual las células acumulan anomalías genéticas, lo que conlleva a su proliferación incontrolada. Entre los años 2000 y 2001, Hanahan y Weinberg propusieron que la notable diversidad de enfermedades neoplásicas y sus mecanismos moleculares subyacentes, estaban íntimamente relacionados con un conjunto de procesos biológicos que determinaban la biología molecular y celular de la enfermedad, identificados como las "señales de identidad del cáncer" *(Figura 1.8)*.[161-162]
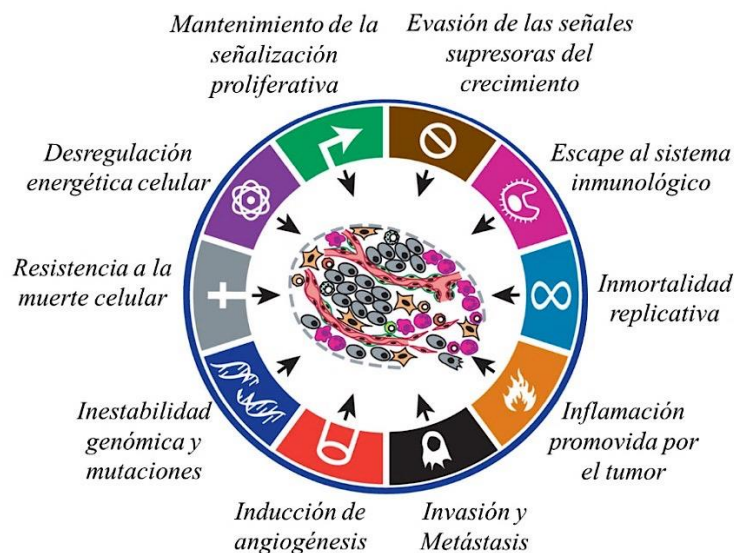
Figura 1.8 Señales de identidad del cáncer. Adaptado: Cell 144, March 4, (2011).[162] Copyright (2020).

El descubrimiento y conocimiento de los factores condicionantes de la biología tumoral maligna, aunque ha constituido una poderosa herramienta para el desarrollo y perfeccionamiento de metodologías de detección temprana y técnicas de tratamiento personalizado, también subraya la elevada complejidad molecular y celular de la enfermedad. La proliferación sistémica del cáncer requiere de la retroalimentación entre las células tumorales y su microambiente, en un contexto que involucra procesos inflamatorios, respuestas inmunológicas y cambios en el metabolismo celular.[162] Por otro lado, el microambiente tumoral también se caracteriza por la presencia de áreas de hipoxia, poblaciones heterogéneas de células (incluidas las células del estroma), zonas de proliferación celular variable, gradientes de señalización solubles y transporte diferencial de residuos metabólicos y nutrientes; que dificultan aún más el desarrollo de modelos biológicos que mimeticen el nivel de señalización celular que caracteriza el entorno real en el que residen las células tumorales humanas (*Figura 1.9)*.[163-164]

Región tumoral	Perfusión	Presión intersticial	pO₂	pH extracelular	Proliferación	Liberación de fármacos
Proliferativa	++	+	++	‹7,4	++	++
Quiescente	+	+++	+	≈ 6,5-7,00	+/-	+
Necrótica	+	+++	-	≈ 7,0-8,00	-	+/-
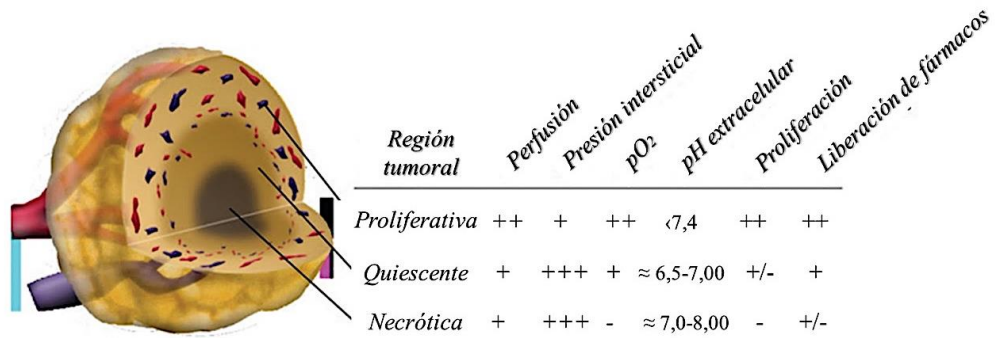
Figura 1.9 Representación esquemática de la heterogeneidad de las regiones tumorales en tumores espontáneos. La magnitud creciente de los parámetros fisiológicos se indica como: - ,+/-, +, ++, y +++. Adaptado: White paper (2015). BioTek Instruments, Inc.[165]

En este sentido, una amplia variedad de sistemas modelos tanto *in vitro* como *in vivo* han sido desarrollados para estudiar el cáncer humano *(Figura 1.10)*; y aunque cada uno presenta sus ventajas y limitaciones *(Tabla 1.2)*, constituyen pilares esenciales para la compresión de los mecanismos subyacentes en la efectividad de las nuevas aproximaciones al tratamiento antitumoral.[166]
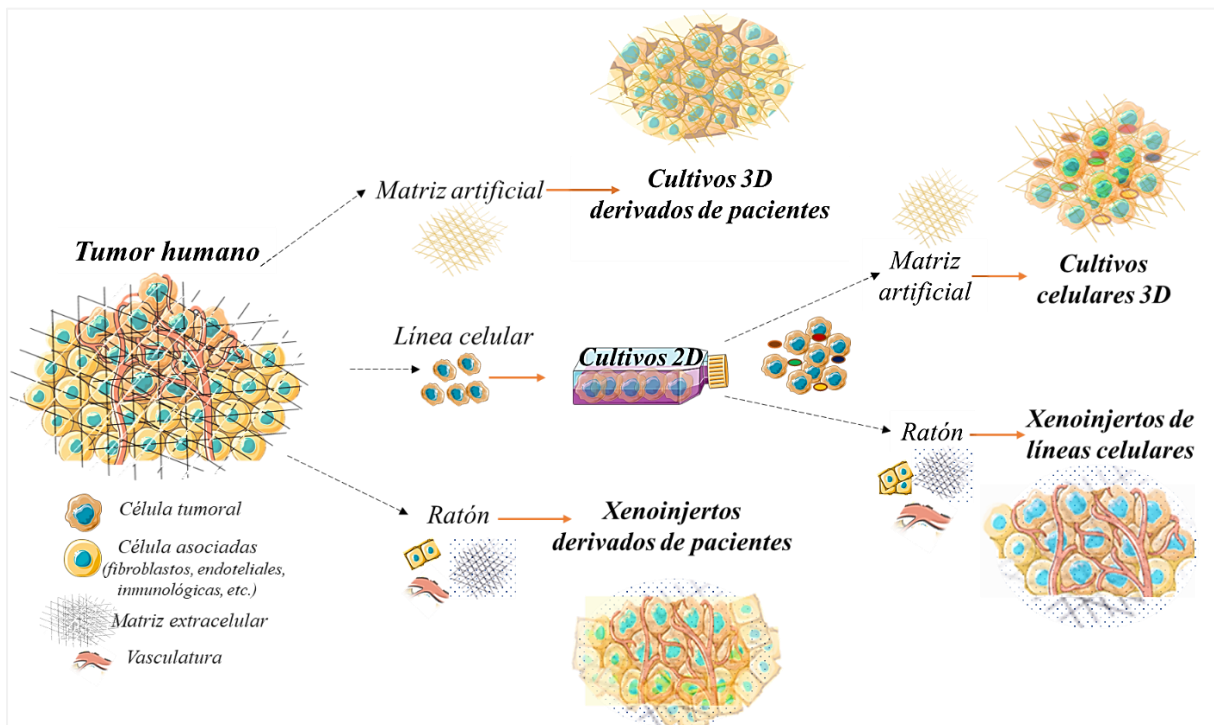
Figura 1.10 Generación de modelos biológicos para estudios de cánceres humanos. Nota: En modelos murinos de xenoinjerto de células tumorales humanas, los elementos de la matriz extracelular, vasculatura y células del estroma son aportadas por el ratón. En los cultivos tridimensionales (3D) la matriz es sintetizada artificialmente y los elementos celulares del estroma pueden añadirse en modalidades de co-cultivo (véase sección 1.4.1 y 1.4.2).

Características generales	Cultivo celular		Xenoinjertos tumorales
	2D	3D	
Requerimientos experimentales de establecimiento	+	++	+++
Requerimientos experimentales de mantenimiento	+	++	+++
Crecimiento 3D	-	++	+++
Interacción tumor-estroma	-	++	+++
Infiltración de células del Sistema Inmunológico	-	-/+ [1]	+ [2]

Tabla 1.2 Características generales de los modelos in vitro e in vivo de tumores humanos. Las características para cada modelo representado se indican como (-) nula, (+)bajo, (++) medio, y (+++) alto. Contenido adaptado: Current Opinion in Genetics & Development 2014, 24:68–73.[167] Copyright (2020). Nota: [1]posibilidad de co-cultivo; [2]células de sistema inmunológico del ratón (véase sección 1.4.1 y 1.4.2)

En esta tesis hemos trabajado en el cultivo bidimensional y tridimensional, así como en el desarrollo de modelos murinos de xenoinjertos de la línea celular de cáncer pancreático humano MIAPaca-2. También se ha trabajado el cultivo 2D y 3D de la línea inmortalizada de macrófagos murinos RAW 264.7 utilizada como modelos de internalización de las nanopartículas magnéticas. Por lo que profundizaremos en el establecimiento y desarrollo de estos modelos.

1.4.1. *Desarrollo in vitro de líneas celulares: cultivo bidimensional y tridimensional*

La investigación *in vitro* de la biología celular del cáncer, maneja dos tipos de células para el trabajo en el laboratorio: *primarias* e *inmortalizadas*.[168-169] Las *células primarias* son obtenidas de tumores sólidos (biopsias) o suspensiones celulares (perfusiones de órganos, derrames pleurales, sangre o ascitis), y posteriormente son transferidas a un medio de crecimiento artificial para su mantenimiento, denominado cultivo celular.[170] Las *células primarias* tienen la ventaja que mantienen la heterogeneidad del tumor clonal inicial. Sin embargo, la heterogeneidad en sí misma representa una desventaja para trabajar con ellas, ya que esta mezcla de fenotipos celulares puede dificultar el llegar a conclusiones irrefutables respecto a la respuesta celular ante un determinado estímulo.[171] Al respecto, aunque se han desarrollado diferentes metodologías para la obtención de poblaciones más homogéneas de *células*

primarias,[168, 172] una de las desventajas más importante para su desarrollo *in vitro* es la pérdida de su capacidad proliferativa (fenómeno conocido como senescencia), que limita en gran medida el tiempo que pueden ser mantenidas en cultivo.[173-174] En este sentido, el desarrollo de las técnicas de biología celular y molecular ha permitido solventar estas dificultades;[175-176] de modo tal que las células tumorales también pueden ser transformadas genotípicamente de manera espontánea (exposición a carcinógenos químicos o radiaciones ionizantes) o inducida (infección vírica o transfección de ADN) para evitar la senescencia y crecer indefinidamente, proceso conocido como inmortalización.[177-178] Estas células *inmortalizadas* se desarrollan en las denominadas *líneas celulares continuas* y se caracterizan por un crecimiento aberrante debido a que pierden la capacidad de inhibición de crecimiento por contacto. Por lo cual, la densidad celular, y en muchos casos el anclaje (adhesión celular a soportes), no representan una limitación para su proliferación.[179-180] Las *líneas celulares* tumorales son de los modelos más utilizados en la investigación biomédica del cáncer, ya que permiten el estudio de los mecanismos moleculares asociados a su desarrollo bajo condiciones altamente estables y controladas. A la vez que constituyen una plataforma básica para el control y seguimiento de nuevas formulaciones dirigidas al tratamiento de la enfermedad.[181-183]

El desarrollo de *líneas celulares* tumorales *in vitro* tiene múltiples ventajas:[184-185]

(i)   Las líneas celulares de cáncer retienen los perfiles genómicos de los tumores parentales, por la cual son consideradas representativas de tumores específicos y, por lo tanto, modelos válidos para la experimentación.

(ii) Las células tumorales en cultivo pueden ser modificadas genéticamente, utilizando diversos vectores de expresión u otras técnicas de modificación genética, para facilitar su mantenimiento y adaptarlas al proceso que desea estudiarse.

(iii) La presión selectiva de las condiciones de cultivo da lugar a una población celular altamente homogénea cuyas características se conservan durante varias generaciones; lo que proporciona una fuente renovable de células para la experimentación, a la vez que contribuye a garantizar la reproducibilidad de los experimentos y mejorar el tratamiento estadístico de los resultados.

Sin embargo, a pesar de sus múltiples ventajas, esta práctica experimental no se encuentra exenta de limitaciones:[186]

(i)   Los continuos procesos de congelación-descongelación, así como la dispersión enzimática o mecánica de las células adheridas, para su trasplante a un nuevo soporte de crecimiento

(subcultivo o pasajes celulares), puede conducir a inestabilidades genéticas que afectan tanto a la velocidad de crecimiento celular como a su capacidad para diferenciarse. Razón por la cual las condiciones de cultivo deben ser cuidadosamente controladas a largo plazo, ya sea limitando el número de pasajes celulares, o reponiendo las reservas congeladas después de un determinado número de generaciones, por células cultivadas en pases tempranos. En este sentido, la utilización de células que crezcan en suspensión también puede resultar ventajoso, ya que no requiere de disgregación celular previa para la generación de los subcultivos celulares. [174]

(ii) La administración de la mezcla de nutrientes y componentes habitualmente presentes en el plasma o fluido intersticial es otro parámetro esencial a controlar en el cultivo celular, ya que es la base bioquímica que permite a las células tumorales su desarrollo y diferenciación *in vitro*. Hecho que también condiciona en gran medida el instrumental requerido y el grado de preparación del personal encargado de los cultivos celulares.

(iii) El cultivo celular debe ser realizado en estrictas condiciones de asepsia debido a que la contaminación con otras fuentes de órganos u otros contaminantes habituales, tales como hongos, levaduras, bacterias, micoplasmas, también pueden afectar la fiabilidad y trazabilidad de los resultados obtenidos, así como el crecimiento y diferenciación de las células.

El cultivo celular en monocapas bidimensionales (2D) o en suspensión suele ser el escenario más sencillo para estudiar la biología de las células tumorales *in vitro*, manteniendo sus propiedades bioquímicas y genéticas.[187] La capacidad de controlar las condiciones físico-químicas (tales como el pH, temperatura, presión osmótica, presión parcial de O_2 y CO_2), y fisiológicas (ejemplos: hormonas, factores de crecimiento, densidad celular, etc.) del ambiente en que se desarrollan las células, permite evaluar con precisión la influencia de estos factores en la efectividad de las drogas terapéuticas antitumorales.[181] En el cultivo en *monocapa*, el anclaje al sustrato es un prerrequisito para la proliferación celular, ya que las células crecen adheridas a un soporte sólido de plástico o vidrio, por lo que no inician la proliferación hasta que se han adherido al sustrato. Por otro lado, el crecimiento en *suspensión*, es propio de células capaces de expandirse sin necesidad de adhesión porque son independientes del anclaje. Este tipo de cultivo es usualmente utilizado en células hematopoyéticas y algunas líneas celulares *inmortalizadas* o *células primarias* procedentes de tumores.[188] Sin embargo, entre las mayores limitaciones del cultivo en monocapa o en suspensión destaca la pérdida de la organización tridimensional (3D) que presentan los tejidos intactos, por lo que la modelación del

microambiente tumoral en estos casos es prácticamente nula *(Figura 1.10)*. A su vez, la carencia de arquitectura estructural 3D también conduce a una pérdida en la heterogeneidad de las regiones celulares que se observan dentro de los tumores humanos intactos *(Figura 1.9)*, debido a que las limitaciones de transporte de masa que se observan dentro de este tipo cultivo difieren en gran medida de las encontradas en un ambiente de desarrollo celular 3D.[189] Por lo cual, las células derivadas del cultivo bidimensional continuo suelen caracterizarse por una morfología y composición altamente uniforme, factor que también puede ser considerado una desventaja debido a que se pierde la heterogeneidad del tumor primario. En aras de solventar estas dificultades, actualmente se han desarrollado y se encuentran disponibles numerosos modelos de cultivo 3D, que incluyen matrices de hidrogeles, esferoides, organoides, así como variadas y novedosas metodologías de desarrollo e impresión de órganos *(Tabla 1.3)*.[190]

Técnica de cultivo 3D	Ventajas	Desventajas
Hidrogeles/ Soportes	-Aplicable a microplacas -Alta reproducibilidad -Capacidad de co-cultivo	-Arquitectura simplificada -Variabilidad entre los lotes de polímeros empleados
Esferoides	-Escalable a diferentes formatos de placas de cultivos -Capacidad de co-cultivos -Alta reproducibilidad	-Arquitectura simplificada
Organoides*/ Órganos en chips	-Arquitectura *in vivo* -Complejidad del microambiente *in vivo*	-Variabilidad -Falta de vasculatura -Dificultad para alcanzar la madurez celular observada *in vivo*
Bio-impresión 3D	-Arquitectura a medida -Gradientes químicos, físicos -Producción de alto rendimiento -Capacidad de co-cultivos	-Problemas con la maduración del tejido -Falta de vasculatura -Dificultad de adaptación a detección de alto rendimiento

Tabla 1.3 Principales ventajas y desventajas de las diferentes técnicas de cultivo celular tridimensional. Adaptado: Advancing the Science of Drug Discovery, (2015) 22(5), 456–472.[191] Copyright (2020). Nota: *de matriz blanda

El manejo adecuado del entorno celular tumoral es un componente clave en su capacidad de reprogramación, tanto para limitar como prevenir la carcinogénesis. Por lo cual el diseño y fabricación de estructuras 3D con características morfológicas y fisiológicas que permitan la mimetización *in vitro* del entorno en el que residen las células tumorales *in vivo*, se ha convertido en un requerimiento esencial para una modelación más realista de la arquitectura

estructural y funcional del cáncer humano.[192-193] En este sentido, los cultivos celulares tridimensionales de tumores permiten la modelación de un microambiente que garantiza las interacciones célula-célula, célula-matriz y, a su vez el contacto con el líquido intersticial; factores esenciales para mantener la función celular diferenciada que caracteriza el entorno 3D del tejido *in vivo*.[158, 194-195] Por otro lado, la heterogeneidad celular que puede alcanzarse dentro de estos modelos suele asemejarse más a los múltiples fenotipos encontrados en tumores sólidos, por lo que es mucho más realista que la homogeneidad encontrada en el cultivo en monocapa.[164-165] Esto es importante ya que se reconoce que la forma y el entorno de la célula pueden determinar su comportamiento y expresión génica. Por ejemplo, se ha observado que las mutaciones tipo *Kras*, que suelen relacionarse con la resistencia tumoral a fármacos anticancerígenos, pueden coincidir con el momento en que los tumores adquieren patrones de crecimiento 3D,[196-198] lo que reafirma la relevancia de estos modelos para evaluar fenómenos como la sensibilización de las células y la matriz extracelular en respuesta a la terapia térmica.

En el ámbito del cultivo 3D, los soportes extracelulares basados en hidrogeles son uno de los más utilizados para el crecimiento y diferenciación de líneas celulares tumorales *in vitro*.[194, 199] En este trabajo hemos desarrollado cultivos celulares tridimensionales basados en hidrogeles de colágeno, por lo cual profundizaremos en el diseño y fabricación de los mismos.

1.4.1.1 Hidrogeles para el cultivo celular tridimensional

Los hidrogeles son redes de polímeros altamente hidratados utilizados como materiales de soporte en el cultivo celular tridimensional y la impresión de órganos. Típicamente contienen del 1 al 20% de masa seca, y su integridad estructural depende de los enlaces cruzados entre las cadenas poliméricas que los componen, ya sea por unión covalente o mediante interacciones físicas. Las matrices de hidrogel pueden estar constituidas por polímeros naturales o sintéticos, pero en cualquier caso su función es proporcionar un entorno de apoyo para la supervivencia, proliferación y diferenciación de las células dentro de un entorno fisiológico *in vitro*.[200-201] La exitosa inclusión celular en este ambiente tridimensional requiere de hidrogeles que sean complementados con componentes biomiméticos (tales como proteínas del suero, medios de cultivo establecidos y/o factores de crecimiento, entre otras) y de matriz extracelular (tales como el colágeno y/o otras macromoléculas), para proporcionar señales biológicas que permitan la formación de un entorno de intercambio entre las células y su ambiente exterior, así como la generación de respuestas celulares específicas ante un estímulo aplicado, como puede ser la terapia térmica por hipertermia magnética.

La formación de los hidrogeles está mediada por la reticulación de los polímeros que lo conforman en respuesta a los cambios en su entorno. La reticulación, reacción química que media la formación de la red 3D por unión de las cadenas poliméricas, puede iniciarse utilizando estímulos físicos tales como cambios en la temperatura, el pH, fuerza iónica y fuerzas de cizalladura, o puede ser inducida químicamente a través de reacciones enzimáticas o por exposición a la luz (fotopolimerización).[202-203] La generación de hidrogeles a partir de estímulos externos es una metodología ampliamente utilizada para el desarrollo rápido y eficiente de prototipos celulares 3D, debido a que formación de la matriz del cultivo celular puede ser controlada tanto durante como después del proceso de formación del gel.[200, 204]

Numerosos tipos de matrices poliméricas son empleadas para el desarrollo de hidrogeles. Proteínas como el colágeno,[205] fibrina [206] o los soportes Matrigel [207] son los más comúnmente utilizados para el cultivo de células en 3D debido a sus propiedades biofísicas y adhesivas específicas. Entre ellos, los geles de colágeno son de los más ampliamente empleados para imitar las matrices extracelulares tumorales,[208] debido a que el colágeno (componente proteico fibroso más abundante de la matriz extracelular en mamíferos) desempeña un papel crucial en la progresión, invasión y metástasis del tumor, promoviendo tanto la adhesión como la migración celular.[209] Hidrogeles de colágeno tipo I han sido empleados como soportes de cultivos de numerosas *líneas celulares inmortalizadas* y *células primarias* de pacientes, tales como: esferoides multicelulares de osteosarcoma, células de cáncer de mama, de cáncer colorrectal humano, cáncer de próstata y páncreas, entre otros,[210-214] lo que ha demostrado la utilidad y aplicabilidad de este modelo tanto en la investigación fundamental del cáncer como en la detección de nuevas dianas terapéuticas.

1.4.2. *Modelos preclínicos de cáncer basados en ratones*

A pesar de los múltiples avances en el desarrollado de diversos sistemas *in vitro* para la experimentación del cáncer, el ensayo en modelos preclínicos continúa siendo un paso esencial en el proceso de traducción de opciones de tratamiento eficientes a la clínica.[215-216]

La medicina experimental del cáncer cuenta con una amplia variedad de modelos animales para la investigación de diversos procesos. Entre ellos, el ratón es el modelo utilizado por excelencia para ensayar nuevos enfoques terapéuticos a la enfermedad, aunque también han contribuido enormemente a la comprensión básica del cáncer. Las ventajas de los modelos murinos para la experimentación *in vivo* son múltiples: [217]

(i) Al tratarse de un mamífero, numerosos procesos bioquímicos son similares al de la especie humana; aunque no debe perderse de vista que también existen importantes diferencias en múltiples sentidos.

(ii) Los tiempos generacionales son muy cortos, por lo que son muy prolíficos y fácilmente adaptables a la vida en los animalarios o bioterios.

(iii) Existen una gran variedad de cepas experimentales genéticamente definidas debido a que es una de las especies de mamífero mejor estudiadas desde el punto de vista genético.

(iv) Poseen eficientes sistemas de desarrollo de células embrionarias pluripotenciales, lo que hace posible la introducción de mutaciones dirigidas y un gran número de arreglos cromosómicos, que permiten la evaluación de una elevada multiplicidad de escenarios terapéuticos .

(v) Existe un inmenso conocimiento acerca de los fenotipos mutantes, las características de las cepas, los mapas genéticos y la secuencia completa del genoma debido al trabajo acumulado durante años de investigación con este modelo. Hecho que también asegura un mejor control de las variables a evaluar en cada tipo de experimento.

Una amplia variedad de modelos murinos son utilizados para el estudio experimental del cáncer, que abarcan desde distintas líneas consanguíneas hasta cepas con mutaciones espontáneas y modificadas mediante ingeniería genética. Los modelos tumorales desarrollados en ratones, dependiendo del origen de la línea celular cancerosa, generalmente se dividen en tres categorías: *singénico*, *genéticamente modificado* y *xenoinjerto*. La selección del más adecuado dependerá del tipo de información que se desea obtener y las condiciones necesarias para su ensayo.[218-220] El estudio de las interacciones celulares en un contexto inmunológico funcional, requiere del uso de animales inmunocompetentes y sistemas *singénicos*. Los modelos *singénicos* son muy útiles como paradigmas al desarrollo tumoral en pacientes, ya que permiten monitorear la respuesta inmunológica antitumoral al tratamiento. Sin embargo, su principal desventaja es que se derivan completamente del sistema animal, y aunque los tumores humanos y de ratón comparten características similares, las interacciones tumor-huésped no siempre se conservan entre especies, lo que dificulta la traducción de los hallazgos encontrados en este tipo sistemas a la clínica de pacientes.[221-222] Por otro lado, los estudios traslacionales diseñados para descubrir y desarrollar terapias que aprovechan las anomalías oncogénicas, requieren del uso de animales con *modificaciones genéticas específicas*. La tecnología *transgénica* ha sido de particular importancia para el estudio de la expresión de oncogenes en animales, especialmente para evaluar aquellos procesos que no pueden ser abordados desde los

cultivos celulares. El principal desafío de este modelo, en muchos casos, es la escasez de promotores específicos del fenómeno a estudiar, y la dificultad para abarcar la complejidad genética de los canceres humanos, unido a los grandes volúmenes de trabajo, tiempo y recursos económicos necesarios para su establecimiento.[223-224] En este contexto, el uso de modelos de *xenoinjerto* se ha erigido dentro de la investigación preclínica del cáncer como el enfoque más directo para evaluar las respuestas terapéuticas en tumores malignos humanos.[222]

1.4.2.1 *Modelos murinos de xenoinjertos tumorales*

Los modelos tumorales de xenoinjerto son particularmente útiles para evaluar la tumorogénesis humana, tanto en los ensayos de respuesta *in vivo* al tratamiento como en el estudio de la histo-biología tumoral.[222] Los modelos murinos basados en xenoinjertos tumorales humanos tienen la ventaja principal de aportar un entorno fisiológico *in vivo*, que aunque en especies diferentes, contribuye a imitar las condiciones biológicas en la que se desarrolla el cáncer humano; por lo que ofrecen excelentes potencialidades para llevar a cabo estudios básicos y ensayos terapéuticos cuyas tasas de éxito pueden permitir una mejor predicción de la respuesta terapéutica en pacientes.[95, 225-228] Sin embargo, una desventaja importante es la limitación de la respuesta inmunológica, debido a que el establecimiento del modelo se encuentra estrechamente ligado al uso de animales inmunodeficientes para evitar el rechazo del tumor humano.[225] Razón por la cual no pueden representar con precisión la progresión de la enfermedad y la respuesta terapéutica observada en individuos inmunocompetentes.

Los modelos murinos de inmunodeficiencia disponibles para estudios de cáncer son variados.[229-230] Las cepas más utilizadas en la práctica experimental son: las de fenotipo desnudo (*nude*- del inglés) y las de inmunodeficiencia combinada severa (*SCID*- del inglés *"severe combined immunodeficient"*).[231-232] Los ratones *nude* se caracterizan por tener una limitación en la respuesta de células T, y presentan una mutación clásica (espontánea) tipo *(nu)*, que conlleva a la atimia y la alopecia total congénita.[233-234] Por otro lado, las cepas de *SCID* se originan por la mutación autosómica recesiva que le da su nombre y carecen de respuestas de células T y B, por lo que son incapaces de generar una respuesta inmune, tanto humoral como celular.[235] Debido a la ausencia de respuesta inmunológica a varios niveles que presentan los modelos murinos de inmunodeficiencia, los animales deben ser mantenidos en estrictas condiciones de asepsia, ya que presentan altas probabilidades de contraer infecciones graves recurrentes. La elección del modelo animal para el ensayo suele variar en dependencia del objetivo experimental, sobre todo si desea analizarse algún tipo de respuesta inmunológica a nivel innato como resultado de la terapia.[236]

Los modelos tumorales derivados de estos animales pueden establecerse a partir de (i) *líneas celulares tumorales* o (ii) *injertos derivados de pacientes (Tabla 1.4).* [225, 227, 237] En ambos casos, el trasplante de células o piezas de tumor al huésped inmunocomprometido puede manejar varios formatos: debajo de la piel (*subcutánea*), en la cavidad abdominal (*intraperitonea*l) o en el órgano de origen del tumor (*ortotópico*).[238] [226] El desarrollo de tumores fuera del órgano de generación primaria (ya sea de manera *subcutánea* o *intraperitoneal*) es conocido como implantación *heterotópica* o *alotrasplante*.[226] Aunque esta metodología puede ser considerada menos relevante en términos de evaluar la respuesta local en el tejido de origen, permite una elevada accesibilidad al tumor comparado con las implantaciones *ortotópicas* que generalmente maneja localizaciones más internas. Razón por la cual, la generación de tumores *heterotópicos* (fundamentalmente de manera *subcutánea*) puede ser considerado un método menos invasivo para el modelo animal,[226] debido a que la implantación del tumor no suele requerir de procedimientos quirúrgicos o estereotácticos de acceso a la cavidad o zona tisular interna que da origen al cáncer que se desea reproducir.

Modelos murinos	Ventajas	Desventajas
Xenoinjertos basados en líneas celulares	-Facilidad de establecimiento del modelo tumoral (especialmente en inoculaciones subcutáneas) -Mayor facilidad de translación de los resultados *in vitro* al modelo *in vivo*	-A menudo carecen de estroma -Dificultad para evaluar la respuesta inmunológica -Las líneas celulares pueden no ser representativas de la heterogeneidad celular de tumores primarios humanos
Xenoinjertos derivados de pacientes	-Recapitulación de la histopatología de los tumores humanos -Permite estudiar mecanismos específicos del paciente	-La eficacia del injerto no siempre es alta debido a la posibilidad de selección de tumores agresivos -Laborioso y costoso -Problemas de reproducibilidad (en muchos casos resultado de la especificidad de cada paciente)

Tabla 1.4 Principales ventajas y desventajas de los modelos murinos de xenoinjertos.

Los estudios realizados hasta el momento sugieren que la hipertemia magnética es una terapia prometedora para el tratamiento de tumores malignos. Sin embargo, existen muchos interrogantes acerca de los mecanismos moleculares involucrados en la muerte celular durante el tratamiento, así como de la influencia de la localización y distribución de las nanopartículas en la eficacia de la terapia térmica.

Teniendo en cuenta lo anteriormente mencionado el Objetivo General planteado para esta tesis doctoral fue: **Estudiar los mecanismos de respuesta a la terapia térmica antitumoral basada en nanopartículas magnéticas tanto *in vitro* como *in vivo***

Para ello identificamos los siguientes objetivos específicos:

1- Desarrollar modelos de cultivo celular tridimensional para el estudio de diferentes parámetros asociados al tratamiento con hipertermia magnética.

2- Estudiar el efecto del la hipertermia magnética en la matriz extracelular.

3- Estudiar los mecanismos de muerte celular activados por el tratamiento de hipertermia magnética.

4- Evaluar el efecto de la cantidad de nanopartículas internalizadas sobre los diferentes mecanismos de muerte celular inducidos por la hipertermia magnética.

5- Estudiar las condiciones óptimas de aplicación de la hipertermia magnética en modelos *in vivo* basados en líneas celulares tumorales humanas.

6- Estudiar la eficacia de la terapia antitumoral basada en hipertermia magnética.

7- Estudiar la respuesta inmunológica inducida por el tratamiento con hipertermia magnética.

CAPÍTULO 2 ·
RETOS A SUPERAR EN LA
ESTANDARIZACIÓN DE LA
HIPERTERMIA MAGNÉTICA

2.1 Introducción ampliada al tema

La hipertermia magnética ha sido particularmente estudiada en los últimos años para el tratamiento localizado del cáncer por su capacidad de dañar a las células tumorales causando lesiones mínimas a los tejidos normales, una de las principales metas de las terapias contra la enfermedad.[128] El incremento local de la temperatura, mediado por la exposición de las nanopartículas magnéticas a un AMF tras su administración al tumor, induce alteraciones en el crecimiento y diferenciación de las células cancerígenas promoviendo diferentes mecanismos de muerte celular.[121] En este sentido, los efectos biológicos de la hipertermia magnética son diferenciados en dos grandes categorías dependiendo del incremento de temperatura. La exposición de las células a temperaturas superiores a 45 ºC es denominado *termoablación* debido al potente efecto citotóxico que induce en el tejido tratado.[239-240] Mientras que el tratamiento hipertérmico a valores de temperatura entre 39-45 ºC es conocido como *hipertermia moderada*, y persigue una destrucción selectiva de las células tumorales a partir de la inducción de mecanismos de muerte celular programada.[241-242] El tipo de muerte celular promovido por la hipertermia magnética, su alcance citotóxico en el tejido, así como el impacto directo de estas rutas moleculares en la inhibición del crecimiento tumoral, dependen de múltiples factores intrínsecos de la terapia térmica que aún no han sido comprendidos ni dilucidados completamente. Parámetros tales como la influencia de la concentración, distribución y propiedades físico-químicas de las nanopartículas son determinantes en la respuesta biológica al tratamiento, y todavía se mantienen bajo investigación en aras de mejorar la comprensión actual que se tiene de la biología de la hipertermia magnética intracelular.

Un requisito esencial que persigue la aplicación de hipertermia magnética sobre sistemas biológicos es el aumento de la efectividad terapéutica con mínimos riesgos de toxicidad

asociados a la administración de las partículas. Experimentalmente, la cantidad de calor liberado por las nanopartículas en suspensión tras la exposición a un AMF puede ser cuantificado mediante la tasa de absorción específica (SAR) (véase sección 1.2.1).[243] Por lo cual, tanto para la experimentación *in vitro* como *in vivo*, se prefieren nanopartículas con altos valores del SAR ya que este parámetro es proporcional a la tasa de aumento de temperatura.[26] En general, un aumento en esta eficiencia de calentamiento para partículas basadas en un mismo material magnético (tales como el óxido de hierro) puede lograrse variando características morfológicas como el tamaño y la forma de las nanopartículas. Sin embargo, el valor del SAR también puede verse afectado por la agregación, la concentración y la viscosidad de las mismas, lo que evidencia la elevada complejidad del proceso de diseño, síntesis y caracterización de las nanopartículas para su uso en hipertermia magnética.[244-246] Al respecto, numerosas metodologías han sido descritas para obtener de manera eficiente nanopartículas de dimensiones y formas controlables, estrecha distribución de tamaños, propiedades magnéticas mejoradas y elevada estabilidad coloidal en medios biológicos complejos.[57] A pesar de ello, maximizar la eficacia del calentamiento producido por las nanopartículas durante la aplicación *in vivo* de la hipertermia magnética, aún constituye uno de los retos más desafiantes en la estandarización de esta prometedora terapia.

En este sentido, una alternativa para mejorar la eficacia en la producción de calor es el incremento de los valores de *f* y *H* del AMF aplicado.[247] Sin embargo, para la experimentación *in vivo* el aumento de estos parámetros se encuentra limitado por restricciones biológicas. Esto se debe a que la aplicación del AMF, además de inducir un efecto de calor terapéuticamente ventajoso por la presencia de las nanopartículas magnéticas, también puede originar corrientes parásitas (corrientes de Foucault o Eddy Current -del inglés) que resultan en un calentamiento inespecífico de los tejidos sanos.[248] En base a este criterio, experimentalmente se ha determinado la combinación óptima del producto de *H x f* para generar la dosis máxima de calor sin provocar molestias adicionales en el organismo. El valor máximo de $H \times f = 4.85 \times 10^8$ Am^{-1}s^{-1} para la aplicación de hipertermia magnética dentro del límite biológico fue determinado inicialmente a finales de la década de los 80.[249-250] Sin embargo, los estudios de Hergt & Dutz en 2007 demostraron que este producto crítico podía ser excedido hasta un valor de 5×10^9 Am^{-1} s^{-1} en dependencia de la extensión de la región expuesta al AMF y el estado de gravedad de la enfermedad.[251]

Los estudios realizados hasta la actualidad sugieren que la hipertermia magnética es una terapia prometedora para el tratamiento de tumores malignos.[26, 252-254] Sin embargo, aún persisten

discrepancias acerca de los mecanismos moleculares involucrados en la citotoxicidad inducida por el tratamiento, así como el rol específico de cada una de las propiedades físico-químicas de las nanopartículas en la respuesta observada. Por otro lado, la estandarización de estos procesos se ha visto dificultada con el paso de los años debido a la variedad de los resultados experimentales reportados en la literatura, que evidencian la necesidad urgente de desarrollar protocolos unificados y estandarizados tanto en el desarrollo del material magnético, como en las condiciones de aplicación del tratamiento térmico y los modelos *in vitro* e *in vivo* utilizados para evaluar la eficacia terapéutica. A continuación, se presentar un minucioso trabajo de revisión de literatura científica relativa al tratamiento de hipertermia magnética en modelos preclínicos.

2.2. A Roadmap to the Standardization of *In Vivo* Magnetic Hyperthermia

Lilianne Beola[1]; Lucía Gutiérrez , PhD[2]; Valeria Grazú, PhD[1] and Laura Asín, PhD[1]

[1]Instituto de Ciencia de Materiales de Aragón (ICMA), CSIC/Universidad de Zaragoza, C/ Pedro Cerbuna 12, 50009, Zaragoza, Spain. Centro de Investigación Biomédica en Red de Bioingeniería, Biomateriales y Nanomedicina (CIBER-BBN), Spain.

[2]Department of Analytical Chemistry, Universidad de Zaragoza and CIBER-BBN. Instituto Universitario de Nanociencia de Aragón (INA), Edificio I+D, C/ Mariano Esquillor Gómez, 50018, Zaragoza, Spain.

Authors contributions: Lilianne Beola is the principal author; Lucía Gutiérrez, PhD, Valeria Grazú, PhD and Laura Asín, PhD are the thesis supervisors. All the authors contributed to the discussion of the results.

Abstract: Despite the fact that magnetic hyperthermia seems to be a promising approach in cancer treatment, researchers working in this field have to face several drawbacks, as the lack of standardization in the treatment conditions and the difficulties measuring the biological effects. This chapter revises recent bibliography about *in vivo* pre-clinical studies and gives an overview of the current state of the art in this topic. Several aspects of the methodology are discussed, like the type of magnetic nanoparticles most commonly used, parameters of the application of the magnetic field, animal and tumor models, techniques used to follow the tumor growth and the evaluation of the treatment efficacy. The comparison and critical argumentation of all these points are expected to shed some light on the field of magnetic hyperthermia and to show the current tendencies in this kind of experiments.

Keywords: in vivo, magnetic nanoparticles, magnetic hyperthermia, animal models, tumor models.

1. Introduction

The heating of tumors by means of Magnetic Hyperthermia (MH) presents clear advantages over conventional hyperthermia techniques (e.g.: ultrasounds, microwaves and radiofrequency), as it is not limited by tissue depth, obstruction or reflection of the energy by bone structures and heat-sink effects near large blood vessels. In addition, other advantages include a more homogeneous temperature distribution in the tumor mass, a reduction of the treatment invasiveness while enhancing its specificity, and the fact that the treatment can be carried out at cellular level instead of at tissue or organ level.[128, 255]

The first phase I trial showing the feasibility of MH in human patients was carried out at Berlin Charité Hospital (2003-05). Since then, several clinical trials mostly on recurrent tumors (e.g. glioblastoma multiforme, prostate, esophagus, liver cancer) have shown promising results, not only in terms of systemic toxicity and morbidity but also in the improvement of the median overall survival of patients.[128] Specifically, in the case of glioblastoma, results obtained when MH was applied in combination with radiotherapy in 59 patients showed a median overall survival 10.6-16.2 months longer than the typical 6-month survival rate in these patients.[256] It is worth noting that these clinical studies started only 10 years after the group headed by Andreas Jordan initiated this field of MH [257] and not many pre-clinical studies were performed before that.

Despite these promising results, there are still several challenges to overcome for the establishment of MH in the clinical routine. In fact, many actual pre-clinical trials on MH are still trying to understand the importance of all the relevant parameters including physical, chemical, engineering, technological and biological aspects of this complex therapy strategy. Still, many knowledge gaps exist in the frame of in vivo MH applications. Of special relevance are the underlying physical mechanisms for heat generation, the cytotoxicity mechanisms that are triggered, the effect that the interaction of the magnetic nanoparticles (MNPs) with biological media/tissues and cells have on the MNPs heat efficiency, etc. In addition, there are several difficulties to reach the effective concentration in tumors when MNPs are administered through intravenous routes.[258] In this sense, it is important to highlight that in all the human clinical trials MNPs were injected intratumorally.

Another big obstacle that the research community involved in MH studies faces in the development of this technique is the general lack of standardization of the field, which makes very difficult to compare results among different laboratories. In this context, first of all,

standardization is required for the scaled-up production of MNPs with optimal magnetic characteristics for MH. This will imply to overcome the long scientific and technological challenge of developing synthetic methodologies with a good control of the particle size, size distribution, shape and crystal defects.[259] Another aspect that needs standardization is the fabrication and use of adequate alternating magnetic field (AMF) applicators. Hereof, there is still discussion about which is the best measurement methodology (calorimetric or magnetic measurements) and the best experimental conditions (adiabatic or non-adiabatic) to determine the heating efficiency in terms of the specific absorption rate (SAR) of the MNPs. This is also a crucial aspect as the higher the SAR, the lower the injected dose of MNPs needed for the patient treatment.[260] Besides, as SAR values strongly depend on the field amplitude generated by AMF generators, the calibration of MH setups in order to obtain results that could be compared among different models and different laboratories is fundamental.[261] Other aspects to be taken into account, besides the several well-known physical factors that influence the heating efficiency (e.g. amplitude (H) and frequency (f) of the AMF, magnetic anisotropy, magnetization, particle-particle interactions, size and size distribution of the MNPs, etc.), are biological issues. It has been reported that SAR values could shrink between 50% and 90% when either biomolecules are adsorbed onto the surface of MNPs or MNPs are located inside cells or tissues.[261] Therefore, it is recommended to check the actual magnetic response of MNPs in true biological environments and physiological conditions in order to understand the underlying reasons of the reduction of their magnetic heating (e.g. viscosity increase, aggregation) and thus engineer MNPs with robust heating efficiency regardless of the host medium. For this reasons, besides the need of more experimentation using in vitro models that mimic better the tumor and its microenvironment (3D cell cultures, tumor spheroids, etc.), the role of computational simulated models of *in vivo* heat dissipation will be also essential for the development of more reliable treatment planning.

Other important challenge of MH is to control heat generation in order to achieve a uniform thermal profile within the tumor. This strongly depends on the homogeneity of MNPs distribution inside the tumor and the route of administration. Thus, the development of efficient methods to selectively and uniformly deliver nanoparticles to the tumor is also an important area of research. So far, the administration mode selected in most *in vivo* studies is the intratumoral injection. However, this approach is not suitable for deep-seated and metastatic tumors. Moreover, intratumoral injection may cause tumor incongruence, invasiveness, and

recurrence, especially from under-treated tumor regions due to a non-homogeneous temperature distribution.

A number of review articles and book chapters have already dealt with the challenges mentioned above in order to transfer MH to the clinical practice. An analysis of MH literature illustrated in *Figure 1*, shows that more than 3000 articles were published from 1997 to date, dealing not only with the synthesis of adequate MNPs but also with the underlying physical factors that influence heating efficiency. Fewer articles (around 500) were published dealing with in vitro MH experimentation including the biological issues that affect SAR. Both aspects of MH have followed an exponential growth at the beginning of the 21st century.
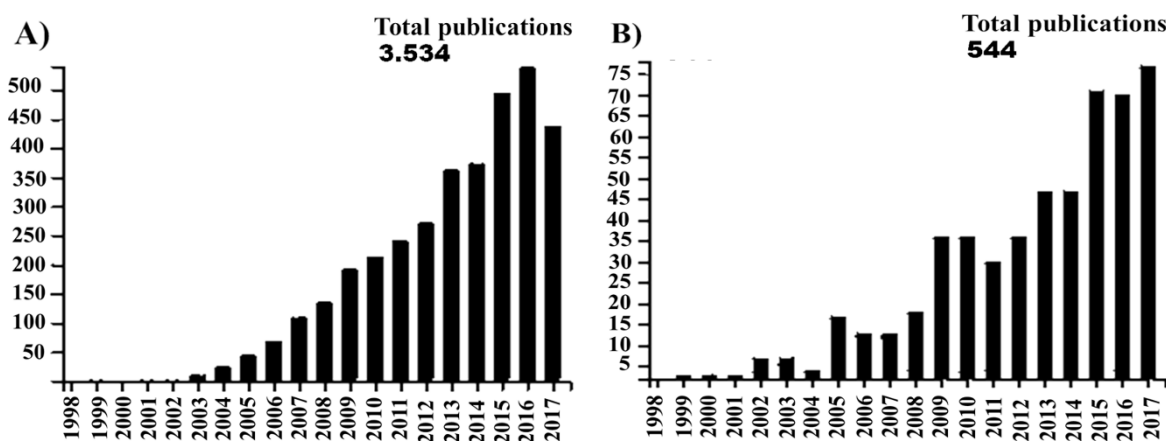
Figure 1. Number of published articles during the period 1997-2017 using the following search terms: A) "magnetic nanoparticles and magnetic hyperthermia", and B) "in vitro studies and magnetic hyperthermia".

The number of articles reporting *in vivo* MH experimentation is however low, and it is difficult to find an overview that includes a comparison in terms of type and quantity of MNPs, AMF applicator, AMF conditions, MNPs administration mode, tumor, animal model, and methodologies used to follow the biological effect of MH. This is the reason why this chapter focuses on the analysis of *in vivo* studies for preclinical applications of MH reported in the literature.

We have selected 33 studies published between 2001 and 2017, most of them are *in vivo* animal studies with only one research work on humans, and we compared the main relevant materials and methods used in all of them *(Table 1)*. In addition, we discussed the advantages and disadvantages of the different animal models and the methodologies used to measure the in vivo biological effects of MH. Lastly, as final remarks, we addressed key issues where

consensus must be reached by the MH community to make real progress toward clinical acceptance and implementation of MH in the clinical practice.

Ref.	MNPs				Animal model				
	Core	Size (nm)	SAR (W g^{-1})	H*f (A m^{-1} s^{-1})	Animal	Tumor	MNPs adm.	Technique used to follow tumor growth	Effect
[154]	IO	15	ND	1.8 x 10^9	HCT	A, O	IT	I (CT)	SR
[262]	IC	12	64	1.83 x 10^9	MIC	A, H	IT & IV	C	GI
[151]	IO	<20	ND	1.08 x 10^9	Rab IC	A, O	SM	Other	GI
[263]	IC	5–10x 1–4	620	1.83 x 10^9	M IC	A, H	IV	C	GI
[95]	IO	15, 12	658, 900	6.7 x 10^9	MID	X, H	IT	C	GI
[94]	IO	12	500	6.7 x 10^9	MID	X, H	IT	C	GI or CR
[264]	IO	20-50	ND	5.9 x 10^9	MID	X, H	IT	C	GI
[265]	IO	30	2614	6.6 x 10^9	MID	X, H	IT	C	GI
[150]	IO	19	500	8.x 84 10^9	Rat IC	A, O	IA	I (U)	GI
[266]	IC	15	ND	1.26 x 10^9	Rat IC	A, O	IT	I (U)	GI
[267]	IO	12	ND	9.84 x 10^9	MID	X, H	IT	C	GI
[268]	IO	19	137	2.64 x 10^9	MID	X, H	IT	C	GI
[132]	IC	NP	2,7	1.87 x 10^9	MID	X, O	IT	C, I	GI
[269]	IO	12	94	7.70 x 10^9	MIC	PT, H	IT	ND	HSP 70
[270]	IO	ND	29	4.23 x 10^9	MID	X, H	IV	C, I	GI
[271]	IO	ND	ND	ND	Rat IC	A, O	IT	I (MRI)	GI
[149]	Other	19	564	1.12 x 10^9	MID	X, O	IT	I (Fluo)	GI
[272]	Other	9	ND	7.58 x 10^9	MID	X, H	IT	C, I (MRI)	GI
[273]	Other	9	ND	4.87 x 10^9	MID	X, H	IT	C, I (MRI)	GI
[274]	IO	ND	210	8.18 x 10^9	M IC	A, H	IT	C	CR
[275]	IO	10 - 12	ND	ND	Rab IC	A, O	IT	C, I (U)	GI
[276]	IO	70-100	3050	1.2 x 10^9	MID	X, H	IT	C	GI
[277]	Other	60	ND	3 x 10^9	MID	X, O	IT	I (Fluo)	GI
[83]	IO	22	1497	4.3 x 10^9	MIC	A, O	IT & IV	C	GI
[278]	IO	16	360	1.8 x 10^9	MID	X, H	IT	C	GI
[279]	Other	30-50	ND	ND	MIC	A, H	IT	C	GI
[280]	IC	20	4850	1.05 x 10^9	MID	X, H	IT	ND	CR
[281]	IC	30	ND	ND	MID	X, H	IT	ND	CR
[282]	IO	22	264	4.3 x 10^9	MID	X, H	IT	C	GI
[283]	IO	10	76	ND	MID	X, H	IT	C	GI
[284]	IO	ND	ND	5.9 x 10^9	MID	X, H	IT	C	GI
[152]	IO	ND	ND	2.3 x 10^9	MID	X, O	INH	I (Fluo)	GI
[285]	IO	4	567	10 x 10^9	MID	X, H	IT	C, I (U)	GI
[286]	IC	30	76	5.9 x 10^9	MID	X, H	IT	I (CT)	CR

Table 1. Relevant Data From All the Papers Revised. A, allograft; C, caliper; CR, complete regression; CT, computed tomography; Fluo, fluorescence; GI, growth inhibition; H, heterotopic; HCT, human clinical trials; IT, intratumoral; IV, intravenous; IA, intraarterial; INH, inhalation; I, imaging; IO, iron oxides; IC, iron compounds; MIC, mice immunocompetent; MID, mice immunodeficient; MRI, magnetic resonance imaging; ND, not described; NP, not particles; O, orthotopic; Rab IC, rabbits immunocompetent; Rat IC, rat immunocompetent; SR, survival rate; U, ultrasounds; X, xenograft.

2. Nanoparticle design for MH *in vivo* application

One can theoretically design and synthetize nanoparticles with optimal heating properties when measured in the laboratory. However, some limitations to the optimum nanoparticle design regarding their composition, size, and agglomeration start to arise when we reach *in vivo* applications. Moreover, in order to go one step further and envisage reaching the clinical practice, other factors start gaining importance such as the possibility for large-scale production. In this section, all the implications on the nanoparticle design when focusing on MH are discussed in more detail.

3. Nanoparticle composition

MNPs with different chemical composition have been prepared during the past years to evaluate their heating efficiency for hyperthermia purposes in aqueous suspensions, including materials such as cobalt ferrites,[102] copper-nickel alloys [287] or copper-nickel [288] nanoparticles. However, when it comes to *in vivo* applications, toxicity issues arise and not all the chemical compositions are recommended given their potential toxicity. This is the main reason why the most commonly studied materials for *in vivo* magnetic hyperthermia treatments are iron oxides.[131] In fact, in our literature review of *in vivo* pre-clinical hyperthermia treatments described in *Table 1*, we have found that the core composition of ≈ 68 % of the materials tested was iron oxides (either magnetite (Fe_3O_4) or maghemite (γ-Fe_2O_3)); most of the remaining compounds contained iron in their composition (including metallic iron, molecular iron compounds, doped ferrites or alloys). Only one paper used a completely different material ($LaSrMnO_3$) *(Figure 2)*.[279]

MNP core composition

Other materials
3%

Iron containing
compounds
29%

68%

Iron oxides Fe_3O_4 or Fe_2O_3
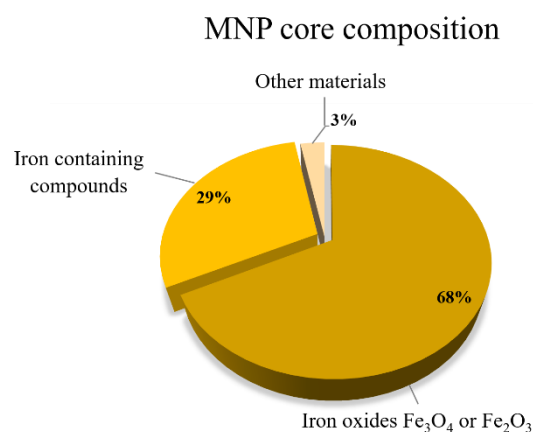
Figure 2. Analysis of the MNP core composition used in our review of in vivo hyperthermia studies (Table .1).

The main advantage of iron oxides is the existence in the body of metabolic mechanisms to manage iron atoms, being able to store and transfer iron released from the nanoparticles during their degradation process.[289] In fact, iron is such an important element in the treatment of widespread diseases (e.g. iron deficiency anemia among others) that several iron supplement formulations include iron oxyhydroxides (ferrihydrite or akaganeite) nanoparticles as part of their composition.[290] It is less frequent however, to use iron oxide (magnetite or maghemite) nanoparticles as iron supplements.[291] Iron oxides have also been approved by the Food and Drug Administration (FDA) of the USA as contrast agents for magnetic resonance imaging (MRI),[11] though most of the products have been discontinued since their approval.[292]

3.1. Nanoparticle size

It is known that, in case of intravenous administration, the size of nanoparticles has a strong impact on their biodistribution. Nanoparticles with sizes below 5 nm are easily eliminated through the kidneys and those with sizes above 100 nm are rapidly cleared by macrophages and transported to the liver.[293] These clearance routes limit the blood circulation time and, as a consequence, the possibility of reaching the targeting site in a concentration high enough for the clinical application. Therefore, for a better *in vivo* performance, nanoparticles should have sizes in the range between 5 and 100 nm. This is the case of all the materials that have been recently reported in the literature. When looking in more detail, the largest amount (47%) of nanoparticles used for the selected pre-clinical studies have sizes between 10 and 20 nm (*Figure 3)*. This data have to be taken cautiously, as around 15% of the works do not indicate particle core sizes. It has also to be mentioned that most of the reported materials have a spherical shape, with only two examples of significantly different shapes (rods [263] and rings [276]).

MNP size (nm)
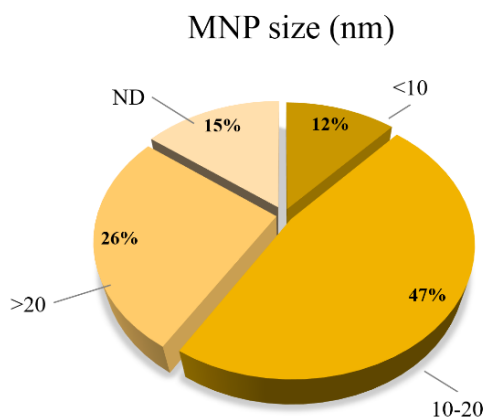
Figure 3. Analysis of the MNPs core size used in our review of in vivo hyperthermia studies (Table 12.1). (ND = Not described).

3.2. Nanoparticle agglomeration

Another limiting factor is nanoparticle agglomeration. The different colloidal properties that these materials present in aqueous suspension or in biological fluids may result in a strong agglomeration of nanoparticles *in vivo*. This has several consequences. On the one hand, it may generate adverse effects during intravenous administration, if agglomerates are big enough to obstruct blood vessels. On the other hand, agglomeration has a strong impact on the magnetic properties of the materials, subsequently altering their heating performance. Unfortunately, these factors are often not evaluated in research manuscripts dealing with *in vivo* experiments.

3.3. Nanoparticle synthesis route

All these limiting factors, required for *in vivo* applications and described above, may point to a specific nanoparticle design. However, achieving the desired MNPs through large-scale production is still a big challenge depending on the synthesis route.

Several synthesis routes are routinely followed to produce iron oxide MNPs. Each approach presents its corresponding advantages and drawbacks, resulting in a compendium of procedures that allow the preparation of a wide diversity of materials with varying size, shape, and aggregation degree. Briefly, organic decomposition synthesis routes provide highly monodisperse nanoparticles [294] and polyol mediated synthesis allows the production of multicore structures controlling the final morphology of the particles.[295] However, these two synthesis routes require high temperatures and the use of organic solvents. Aqueous protocols like the co-precipitation [296] and the hydrothermal aqueous routes [297] lead in general to aggregated nanoparticles with broader size distributions and not so well-defined morphology. However, these routes are low-cost, easy to scale-up and use non-toxic reagents.

From our literature review, regarding those studies using iron oxide nanoparticles, half of them provided a description of the preparation route of the nanoparticles *(Figure 4)*. The most common synthetic route for homemade particles was thermal decomposition (seven manuscripts), followed by co-precipitation (three manuscripts) and finally by polyol synthesis (one manuscript). Commercially available particles accounted for 18% of the studies analyzed (four manuscripts). Sadly, a significant percentage of the works (seven manuscripts, 32%) did not provide enough information of the synthetic route of the magnetic cores, even without giving references to previous works describing the material. This is a great inconvenience for the progress of knowledge, as the systematic lack of details prevents an easier comparison of the results.

MNP synthesis route
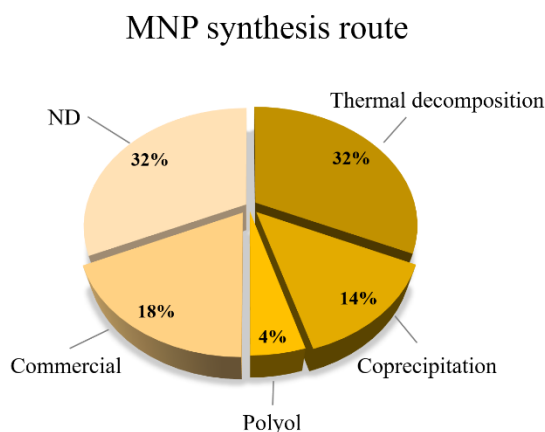
Figure 4. Analysis of the MNPs synthesis route used in our review of in vivo hyperthermia studies (Table 1). (ND = Not described).

The transference to the industry of all the knowledge acquired in the nanoparticle design is complex. The production of large amounts of some kind of materials is not straightforward due to scale-up difficulties resulting, in products not viable economically, and so it is with MNPs. Even though it may seem that thermal decomposition is the preferred synthetic route for the obtention of iron oxide MNPs for *in vivo* hyperthermia applications, it has to be pointed out that their production at large-scale (and under good manufacturing practices) is much more complex than that of the aqueous routes. When thinking on a clinical application, researchers should take into account the real possibilities of producing a given material at large-scale. In such case, aqueous routes should therefore be prioritized. Nevertheless, it should also be taken into account that scaling up processes are usually associated with a decrease in the homogeneity of the final product, and that it will be difficult to obtain exactly the same material for commercial purposes as the one obtained in smaller batches in research laboratories.

3.4. Nanoparticle sterility

Nanoparticles should be sterile for *in vivo* administration, to avoid the introduction of pathogens that may provoke undesirable biological effects in the animals and difficulties in achieving reproducible and consistent results.

In pre-clinical trials using MNPs for biomedical applications, before the in vivo administration, magnetic nanoparticles are generally sterilized by filtration through small pores (e.g. 0.2 μm) that allows the removal of bacteria that may be present in the suspension. This procedure is sometimes complicated in case of agglomerated nanoparticles with bigger hydrodynamic diameters. This procedure was reported in three of the papers analyzed in our literature review.

[94-95, 283] Some of the manuscripts describe the use of sterile MNPs although the sterilization process is not clearly detailed, [268] and some others precipitate the MNPs and just redisperse them in sterilized water.[269, 273] This last procedure is not the most appropriated one to achieve a complete sterilization of the material. Unfortunately, the vast majority of the manuscripts revised for this chapter do not provide specific information on the MNPs sterilization processes. If MNPs have not been sterilized, this may have consequences on the animal response to the treatment affecting the interpretation of the response to the therapy and making more difficult to get reproducible results.

It also has to be taken into account that filtration does not eliminate endotoxins, which are bacterially derived molecules that may be a source of variability for *in vivo* studies.[298-299] The analysis of the presence of endotoxins is generally neglected in the literature, and the use of synthetic protocols to avoid common endotoxin contamination should be implemented, such as using high purity water and depyrogenated labware, handling of containers with clean gloves and testing reagents for endotoxin presence before their use. Future standardization protocols for *in vivo* hyperthermia studies should include the evaluation of the presence of endotoxins as a routine technique to evaluate the sterility of the materials prepared before *in vivo* applications.

3.5. Nanoparticle heating properties

MNPs heating properties under an AMF are generally described by the specific absorption rate. SAR values are widely used to compare the heating capacity of different magnetic particles, although this extrinsic parameter depends on external factors such as the AMF amplitude and frequency, and the MNPs concentration. An alternative approach is the determination of the Intrinsic Loss Power (ILP).

In our literature review, SAR values were provided in ≈ 60% of the manuscripts, with values ranging from 3 to 4850 W g^{-1}. These values have limited interest, as the conditions in which they were measured are completely different from one work to another; in addition, the local concentration in the tissue samples is unknown. This is a consequence of the lack of real-time and accessible characterization techniques that provide a fast, cheap and reliable quantification of the MNPs in the tumor.

4. Magnetic hyperthermia conditions used *in vivo*

In this section, we are going to review and discuss some parameters of the MH application, such as the values of the magnetic field amplitude and the frequency used and the number of repetitions and duration of the AMF exposure from the studies detailed in *Table 1*.

4.1. Equipment

Here, our aim was to compare the equipment used in the literature manuscripts reported in *Table 1* to try to establish any trend on the instrumentation being used for in vivo applications. However, we have found that there is no clear trend on the equipment used, as the vast majority of the research papers reported homemade equipment.

The heterogeneity of instrumentation used for hyperthermia applications leads to a plethora of field amplitudes and frequencies resulting in a very broad range of conditions used for the in vivo experiments. Each of the described instruments produces an almost unique alternating current (AC) magnetic field, in terms of frequency and amplitude of the magnetic field. Therefore, it is almost impossible to compare the results among different studies. The frequency of the AC magnetic field ranged between 0.02 and 1300 kHz, being the most common ones ($\approx$ 62%) located in the range between 360 and 650 kHz *(Figure 5)*. In a similar way, field amplitudes used were in the range between 0.6 and 150 kA/m, being the most common ones ($\approx$ 47%) in the range between 9 and 20 kAm^{-1}.
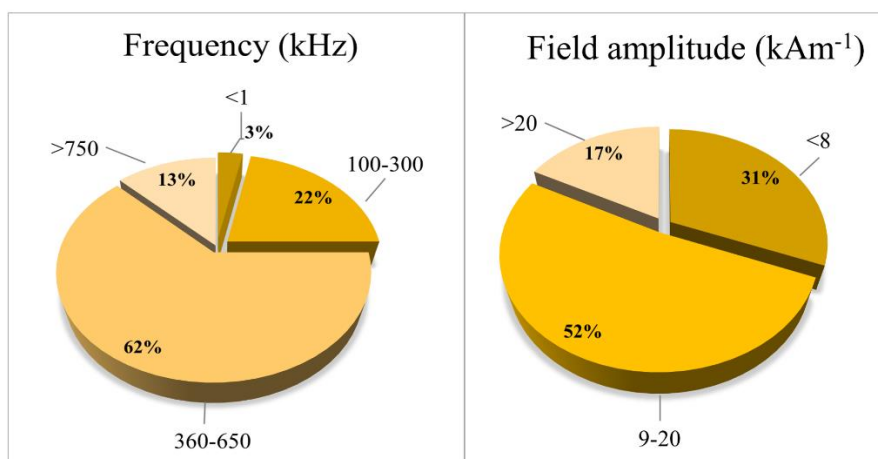
Figure 5. Analysis of the frequency and field amplitude used in our review of in vivo hyperthermia studies (Table 1).

Given the broad spectra of AMF conditions, the comparison of the results from the different studies is a complex task, especially taking into account that for a given frequency and amplitude of the applied magnetic field, the heating performance of magnetic particles depends on their size and composition.[300] In such scenario not all the nanoparticles may have the same behavior in every instrument.

Moreover, even if the particle size and composition were optimized for a given set of experimental frequency and amplitude of the AC magnetic field conditions, another factor, the nanoparticle concentration should be also taken into account, to achieve an optimal design.[104]

Given that so many different parameters have such a complex influence on the final clinical performance of MNPs during *in vivo* hyperthermia treatments, it is extremely difficult to design the optimum material for MH purposes. Therefore, even if MNPs and field conditions were designed together to achieve the most efficient combination for heat generation, this final combination should also take into account the sample dose needed for the clinical application to achieve the maximum efficacy.

4.2. *Biological safety of the AMF*

When an AMF is applied to tissues not only the therapeutically useful heating of MNPs takes place but also the tissue itself begins to non-selectively heat due to the generation of eddy currents. There exists an open deliberation about the most convenient values for amplitude and frequency parameters, concerning biological safety, since Atkinson et al. published in 1984 their very well-known paper where they established the range of usable frequencies in MH.[249] In that manuscript, the authors concluded that the value of the product $H \times f$ should not exceed 4.85×10^8 $Am^{-1}s^{-1}$. This was the highest well-tolerated condition that people receiving the treatment for more than one hour could withstand without major discomfort. They showed that the rate of heat produced per tissue is directly proportional to the square of $H \times f$ product and also to the square of the distance from the coil center. So, the smaller the radius of the region to be treated, the higher $H \times f$ values could be applied. As all the experiments were carried out with a coil designed to treat the thorax (about 30 cm), authors opened the possibility to use higher $H \times f$ limits for smaller applicators.

Hergt and Dutz established a new and weaker criterion for this limit for smaller coils and relating to the seriousness of the illness, dictating that the limit for the $H \times f$ product was 5×10^9 $Am^{-1}s^{-1}$. Thus, these authors made theorical calculations to maximize the SAR of MNPs when exposed to AMF respecting the biological safety parameters.[251]

If we analyze the AMF conditions used in the pre-clinical studies from *Table 1 (Figure 6)* we can see that none of the papers we have revised has used values of H and f that result in a $H \times f$ value below the limit proposed by Atkinson, 4.85×10^8 $Am^{-1}s^{-1}$. Half of the papers used AMF conditions between 4.85×10^8 $Am^{-1}s^{-1}$ and 5×10^9 $Am^{-1}s^{-1}$, so above the Atkinson limit but below the limit proposed by Hergt and Duzt. This range seems to be currently the most

convenient one, at least until new studies about the biological safety of the AMF are carried out. However, there are 35% of the studies that used H and f parameters resulting in $H \times f$ values above the biological safety limit.

The highest condition of the $H \times f$ product we have found is the article published by Guo et al. (10^{10} Am^{-1}s^{-1}), doubling the convenient limit. The application time used in this work was five minutes and the temperature of the surroundings was not measured. They combined MH with laser irradiation as some studies have demonstrated that Fe3O4 nanoparticles are able to exhibit strong photothermal effects when exposed to NIR laser irradiation.[301] So, after combining MH with laser irradiation and chemotherapy, the results obtained were good showing tumor growth inhibition after two weeks post-treatment.[285]

Not less important is to mention that some published studies (15%) do not describe the conditions of the AMF used, so it is quite difficult to correlate and position them within the research field of MH. Besides, with some papers, we have had difficulties to find the AMF conditions used, as it was necessary to track back a large number of previously published works. Our particular point of view in this respect is that when publishing a research work in this field some data need to be always mentioned, in particular, AMF conditions should always be provided.
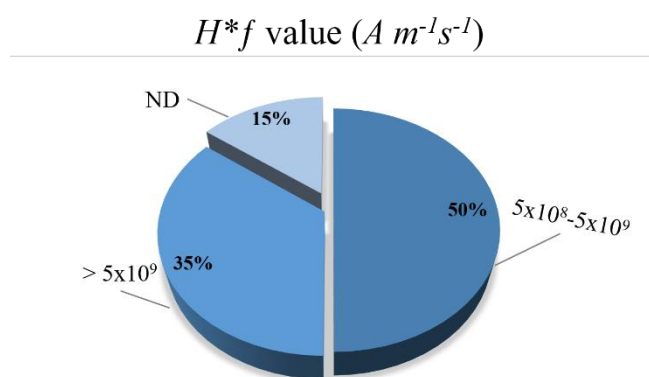
Figure 6. Representation of the H x f values used. Data taken from the papers detailed in Table 1.

4.3. Exposure to the AMF

The methodology followed for the application of the MH treatments varies between published works not only in the AMF conditions used but also in other aspects, such as the duration of the AMF exposure and the number of consecutive applications.

As shown in *Fig. 7* the duration of the AMF exposure in most of the reviewed studies (41%) is between 10 and 30 minutes. In 35% of the studies the exposure time is higher, between 30 and 60 minutes. Only 18% of the papers reveal exposure times below 10 minutes. Is it quite difficult to elucidate in advance which is the best exposure time to obtain the best antitumor effect. We tend to think that the longer exposure time, the stronger the effect because. But there exist some limitations that have to be considered in this aspect, for example, the technical limitations of the devices, as in some of them the AMF application cannot exceed certain duration. Also, the kind of dispositive used to maintain the temperature of the animals during the treatment is important. Some of the devices had a 3D temperature regulation system that prevented the animals from suffering hypothermia in a much better way than systems consisting of a hot surface where the animals are just laid down.

The number of repetitions of the AMF exposure and the intervals between them also differ between studies. As presented in *Figure 7*, 23% of the studies applied MH just once, 12% applied MH twice, 21% of the studies performed the MH three times, 9% of the papers performed four MH exposures and 6% of the studies reviewed applied the magnetic field five or more consecutive times. Again, it is hard to conclude which is the best treatment option, as the degradation of the MNPs in the tissues should be taken into account. In particular, MNPs degradation will strongly depend on their composition and coating.[289] It is now well known that the exposure of iron oxide MNPs to an acidic medium could dramatically affect their heating capability. As an example, experimental studies have shown how the heating capacity of iron oxide nanoflowers (with polyols as organic protecting shell) decreased 70% and 99% after 6 and 23 days respectively, under acidic media exposure.[302] It is quite obvious that the exposure of the animal to the AMF at certain time points after the MNPs injection if they have been degraded or removed from the target tissue will be ineffective.
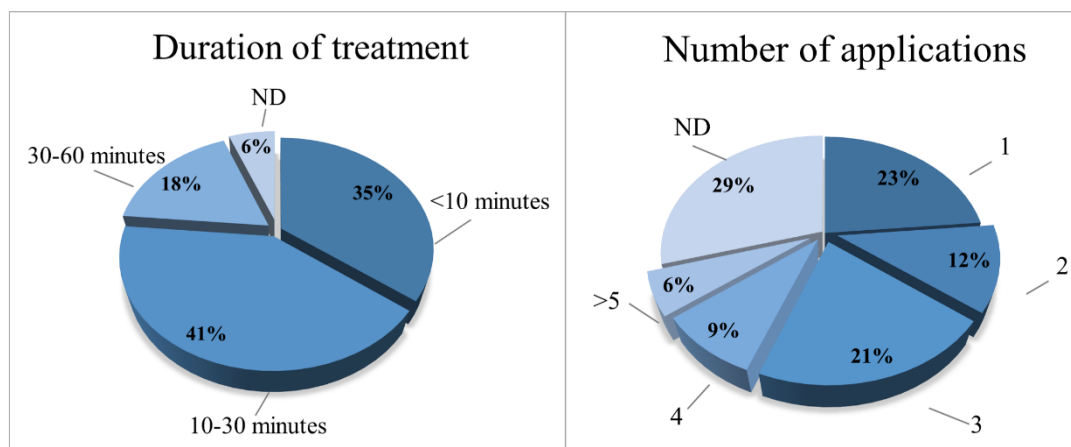
Figure 7. Representation of the duration of the AMF exposure and the number of consecutive repetitions of the treatment. Data taken from the papers detailed in Table 1.

From these results, it can be extracted that the most common protocol for this kind of experiments uses between one or three AMF applications (in alternating days) with a duration length between 10 and 30 minutes. It is noteworthy again the number of studies that do not provide enough details on the methodology used, thus hindering the standardization of *in vivo* MH experiments.

5. Animal models and biological effects

In this section, animal models, tumor models and MNPs administration routes are reviewed in the frame of the in vivo MH experiments selected and detailed in *Table 1*. Also, we discuss the biological effects that are analyzed after the MH treatment and the techniques currently used for their study.

5.1. Animal models

Evaluation of the MH treatment effectiveness in small animal models is a necessary pre-clinical step before reaching human studies. Although several animal models exist, murine models are by far the most extended ones for pre-clinical trials. This is also the case for MH studies. The majority of works published until now (85% of the reviewed papers) used mice as an animal model for in vivo hyperthermia studies *(Figure 8)*. Rats and rabbits have been used scarcely. The main advantages of mice relate to their small size, easy handling, fast reproductive cycles and their fully known genome.

Murine models can be further classified into two types, depending on the role of the immune system in the animals: immunocompetent and immunodeficient models. Immunocompetent

mice are the most commonly used model in oncoimmunology for the inoculation of histocompatible cancer cell lines.[230] However, in our literature review, they represent only a small proportion of the murine models used for *in vivo* hyperthermia studies (12%). In particular, the four studies that have used immunocompetent models have worked with C57Bl/6j mice, a commonly used strain for *in vivo* studies. Immunodeficient models are more frequently used (88% from the papers revised) *(Figure 8)* in our literature review. The main reason for this trend is that these mice can accept and develop normal and malignant grafts both from donors of the same species (allograft) as well as from different species (xenografts - usually from human origin). The main disadvantage of these animal models is the lack of a complete immunologic response. Although not deeply studied yet, there is some scientific evidence about the synergy between different thermal treatments (photothermal, MH, radiofrequency) and immunotherapy.[144] So, the lack of an immune system, which usually plays a key role to combat diseases, could negatively influence the treatments underestimating their real effect. There is also a study where the efficacy of the MH was enhanced due to the administration of immune-stimulators such as IL-2 (Interleukine-2) and GM-CSF (Granulocyte and Monocytes colony-stimulating factor), revealing the great importance of the immune response in the final efficacy of the treatment.[303]
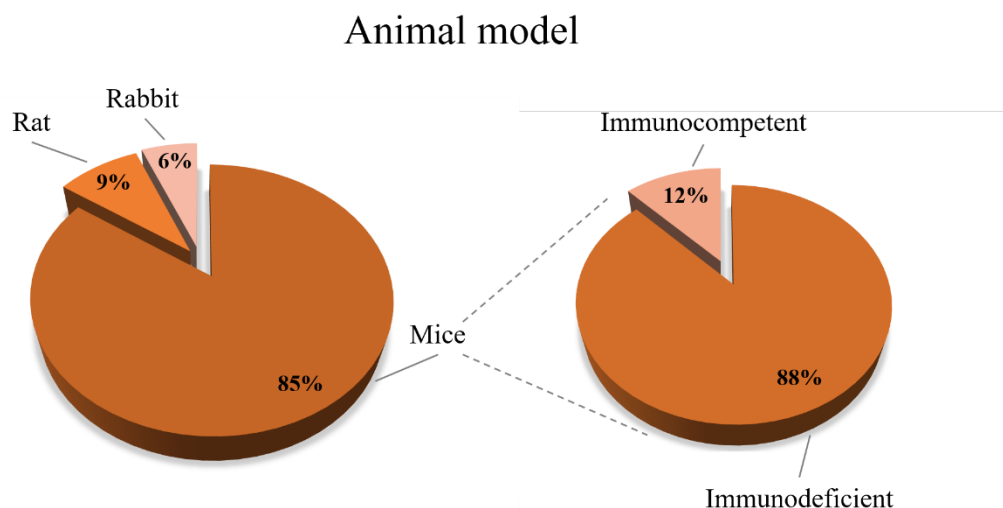
Figure 8. Schematic representation of the principal animal models used for in vivo hyperthermia studies. Data taken from the papers detailed in Table 1.

Several immunodeficient models, which are commercially available and that have been used in MH studies, are described next, detailing their specific advantages. One of the most commonly used immunodeficient models for hyperthermia studies are nude *(nu)* mice, named after their hairless phenotype. These mice are characterized by a severe reduction in the number of functional T cells as a result of having a dysfunctional and rudimentary thymus that remains small and cystic throughout the animals' life. As a consequence, failures in the maturation of their T cells occur. However, they present a response by the innate immune system and also humoral response. The homozygote model is the most widely distributed commercially and is available in various genetic backgrounds, consanguineous and non-consanguineous. The nude BALB/c type is the most reported in the literature, probably due to the fact that they are generally easy to breed and present minimal weight variations between females and males. Other models used to a lesser extent with nude mutation or $Foxn1^{nu}$ (forkhead box N1) are Athymic Nude-nu from Charles River (NCR-Foxn1nu) and Athymic nude from Naval Medical Research Institute (NMRI). The fact that nude mice have scarce normal hair follicles makes them an attractive model for evaluating the growth of subcutaneously established tumors since epilation is not necessary to follow-up tumor growth. Another advantage of this hairless model is that it allows following labeled tumor cells by fluorescence imaging or by bioluminescence acquiring whole body images of the animals.

In general, these kinds of nude mice are good models to establish rapidly growing tumor human cell lines. However, as they maintain a robust B and natural killer cell (NK) responses, nude mice are not adequate for blood-borne tumor lines such as leukemias or lymphomas. Moreover, they are also not adequate for human primary lines or heterogenetic tumor fragments. For this reason, another type of immunodeficient mice model used also *in vivo* MH experiments is the SCID (severe combined immunodeficiency) mouse model. The homozygous *scid/scid* (*Prkdc^{scid}*, catalytic subunit of DNA- dependent protein kinase) mice are phenotypically normal and have very low levels, or directly lack serum immunoglobulins. These animals have an inability to generate an immune response, both humoral and cellular (absence of mature T and B cells). This model presents superior success rate than the nude mice in human tumor transplants.[293] However, SCID mice mutations do not affect the myeloid and erythroid cell lines and therefore, these models exhibit normal levels of NK activity.

5.2. Tumor model and relationship with the administration routes

In general, one of the major problems observed when performing *in vivo* experiments using nanoparticles is the low amount of material that reaches the desired location after systemic administration. In fact, there is a recent study that, after revising more than one hundred papers, concluded that less than 1% of the intravenously administered dose arrives to the tumor.[304] This presents a real problem for biomedical applications that require a high amount of nanoparticles in the target tissue, as it is the case of MH. Because of this, the majority of the published studies (80%) use the direct injection of the magnetic material at the tumor site as main route, therefore ensuring that the highest possible MNPs content remains in this site *(Figure 9)*. However, this type of administration has the disadvantage that requires the establishment of subcutaneous tumors. Heterotopic tumors are the ones located outside the equivalent organ where the tumors should be grown, as the subcutaneous implants. The major drawback is that the tumor microenvironment in the subcutaneous model is very different from that of the primary cell or tissue type that generates the tumor. Precisely these interactions between the host envelope and tumor tissue strongly affect tumor cell proliferation, levels of growth factors and nutrients, both during tumor angiogenesis and in its metastatic behavior. All these reasons constitute the major limitations of subcutaneous tumor models. On the contrary, they are very easy to handle. The accessibility of subcutaneous tumors is a great advantage to monitor tumor growth progression and for the assessment of the direct effects of MH in its regression. For these reasons, this kind of tumor model is the most commonly used (74% reviewed papers) *(Figure 10)*.
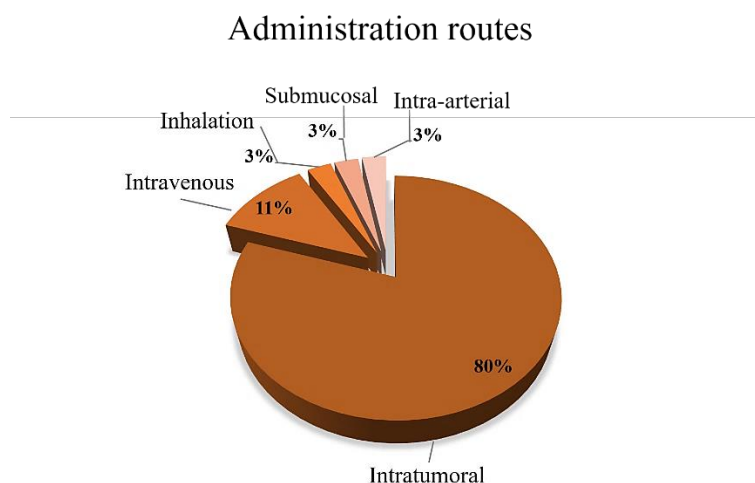
Figure 9. Schematic representation of the administration via of magnetic material for in vivo hyperthermia studies.

Orthotopic tumors are the ones implanted or generated into the equivalent organ from which the cancer originated. This type of implantation results in the correct microenvironment, which may more closely mimic the natural tumorigenesis in humans, as opposite to heterotopic models. These models are considered more clinically relevant and are better predictive models of drug effectiveness than standard subcutaneous models.
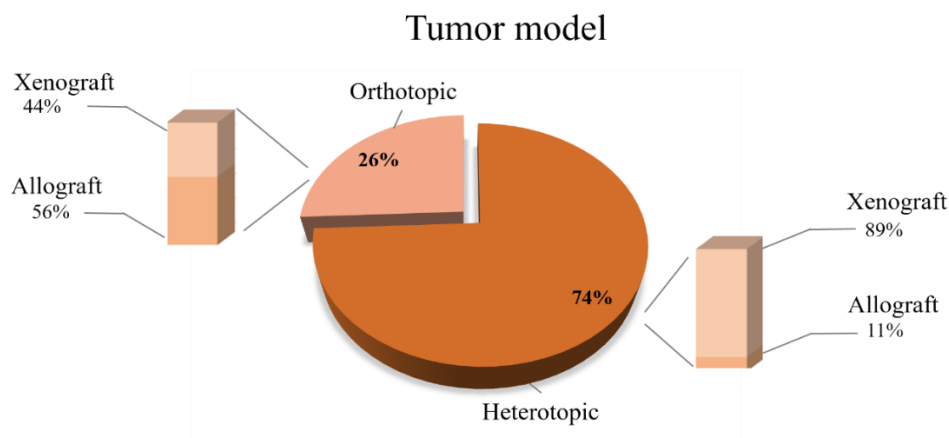
Figure 10. Schematic representation of the percentage of the different tumor models used for in vivo hyperthermia studies.

However, although orthotopic tumor models are considered ideal for evaluating the real impact of therapy, they have not been established yet as standard models. They require more complex imaging methods to follow their growth, and they also need more technical expertise and, in general, it can be said that it is a labor-intensive task. But one of the main reasons for the preference of the subcutaneous model over orthotopic tumors is the fact that currently this is the only way to ensure that most of the nanoparticles remain within the tumor for long periods of time. In the case of intratumoral injection of MNPs, it has been shown that around 89% of the injected MNPs get immobilized in the tumor tissue. MNPs are not only retained in the tumor interstitium, but they are also tightly packed inside endosomes of tumor cells and macrophages associated to the tumor. Besides, even after MH sessions using a combination of high field amplitude and frequency (25 kAm^{-1} and 400 kHz), they remained unaltered as homogeneous spots. However, it is noteworthy to highlight that not only their distribution within the tumor but also the time window where their heating capabilities are preserved before undergoing degradation must be determined for each type of MNPs.[261] Published studies of systemic administration require bigger doses to ensure that the necessary concentration of MNPs to produce a biological effect reaches the tumor site.[304] One alternative to solve this

problem is the intra-arterial administration of MNPs.[305] This administration route allows a more selective and at the same time more widely spread distribution of the hyperthermic agent. The main disadvantages are the technical difficulties and the possible escape of the therapeutic material to the general circulation, with its consequent toxic effects.

As can be seen in *Figure 10* when the tumor model is located subcutaneously (heterotopic) the majority of the studies, 89%, were carried out using immunodeficient mice where human tumors were implanted (xenograft tumor models). These models are a very easy and fast approach that renders an accessible tumor. However, at the same time, they do not provide the appropriate environment and lack the complete effect of the immune system. Thus, these are the easiest in vivo models for pre-clinical human tumors studies. Only the 11% of studies with heterotopic tumors of our selection were made with murine tumor cells in immunocompetent animals where the advantage is the contribution of the immune response. However, the scenario is different when analyzing the studies where an orthotopic tumor is used, where more than half of them consist of murine cells. As mentioned before, the technical experience needed for the development and follow up of these models is much higher, but in a more realistic tumor environment and is mimicked. However, a part of the reviewed orthotopic tumors (44%) were implanted in immunodeficient mice using human cells. It is true that in these cases the environment is much appropriate than in heterotopic tumors but there is a lack of immune system response.

Another aspect to take into account in the choice of the tumor model is the way the tumor is induced. Two main alternatives have been found in our literature research, either by injection of tumor cells or by surgical implantation of tumor fragments. Most of the studies reported used material from cell cultures for both heterotopic and orthotopic models. It should be noted that in the case of the latter some authors preferred to use fragments of tissue mainly in larger animal models such as rabbits and rats. These fragments (usually 1 mm^3) were usually obtained from previous tumor growth in the same animal model in which it will be subsequently grafted. However, a major disadvantage of models utilizing intact tumor tissue is the intrinsically heterogeneous nature of the different zones within the same tumor. This makes very difficult to standardize and compare results between tumors from different subjects. An alternative to avoid this heterogeneity is to resuspend in balanced saline pieces of the tumor tissue obtained from the different subjects (with a concentration of 100 pieces per milliliter), and then, inject this mixture to the experimentation subject.

5.3. *Biological effects observed and techniques used*

There are several techniques to study the antitumor effect of the MH treatment but there are two that stand out because they are the most commonly used. These two techniques are: physical measurement of the tumor dimension with a caliper and the use of imaging techniques to follow the tumor growth.

There are some advantages and drawbacks that have to be taken into account when one should decide which technique is going to be used to follow the tumor growth. The direct measurement of the tumor with a caliper is a very simple, fast and easy way to estimate the volume also allowing the possibility to daily follow their growth. But it is true that it is not the most accurate methodology because, for example, inflammatory tissue and necrosis zones may lead to an overestimation of the tumor volume. Besides, the operator in charge of such task should always be the same to minimize errors. The accuracy of the measurements will depend on the kind of tumor implanted and the animal model used. The tumor shape could be different and therefore, assumptions made to calculate the final volume may not be reliable. In this sense, the type of skin, color and presence of hair could facilitate or restrain the measurements. Furthermore, different equations to calculate final volume exist, the following two being the most used ones:

$$V = \frac{\pi}{6}\, a\, b\, c \ (Eq.\, 1) \qquad V = \frac{1}{2} a\, b^2 \ (Eq.\, 2)$$

Eq. 1 is the volume of an ellipsoid where a, b and c are the three tumor dimensions (length, width, and height). Eq. 2 corresponds to a modified ellipsoid equation where two dimensions, tumor height and width, are considered to be the same. The most accurate formula is the first one because it takes into account the three dimensions, although using a caliper to measure the height of the implanted tumors is not always an easy task. Thus, the modified ellipsoid volume formula is easier for the calculations as it makes the assumption that the height of the tumors is the same as the width. However, it should be taken into account that this assumption is not always correct. Nevertheless, using this approximation to compare tumor volumes from animals from the same experiment can be considered as relevant.

Other types of techniques used to follow the tumor growth are imaging techniques. They are more accurate than measurements made with a caliper but they are quite costly and have also their own technical limitations. There are several imaging techniques such as: i) MRI, which is based on the different relaxation times of the protons depending on their environment after being pulsed with a strong magnetic field in the range of radiofrequency, ii) computed tomography (CT), which detects different absorption of X-ray radiation between water, bone,

fat and air, iii) medical ultrasounds (diagnostic sonography), which is based on the differences in the time that takes for a pulse of sound to interact with a tissue and travel back to the probe depending on their different acoustic impedance and iv) bioluminescence and fluorescence imaging devices that detect the fluorescence or photons coming from the animal. This last technique requires having the tissue expressing a fluorophore protein or an enzyme that catalyzes bioluminescence reactions. The spatial resolution of all of these techniques is quite similar: MRI between 4-100 µm, CT 12-50 µm, ultrasound 50 µm and bioluminescence or fluorescence *in vivo* imaging also 50 µm.[306] However, MRI, CT and ultrasound are independent of the tumor depth, while bioluminescence and fluorescence imaging can only be used for real-time imaging when the tumor is subcutaneous. The most popular ones used in the revised bibliography were MRI and fluorescence imaging.

When we analyze the selected papers *(Figure 11)* we can see that more than half (57%) used only a caliper to calculate the volume of the tumors, while 23% of the studies followed tumor development with imaging techniques, whereas 17% of the studies combined both a caliper and imaging. This last combination allows correlating the signals obtained by the imaging techniques (e.g. photon flux in fluorescence) with tumor volume estimated with the caliper. This combination may not be necessary if the imaging approach is able to provide 3D reconstructions of the tumor volume.
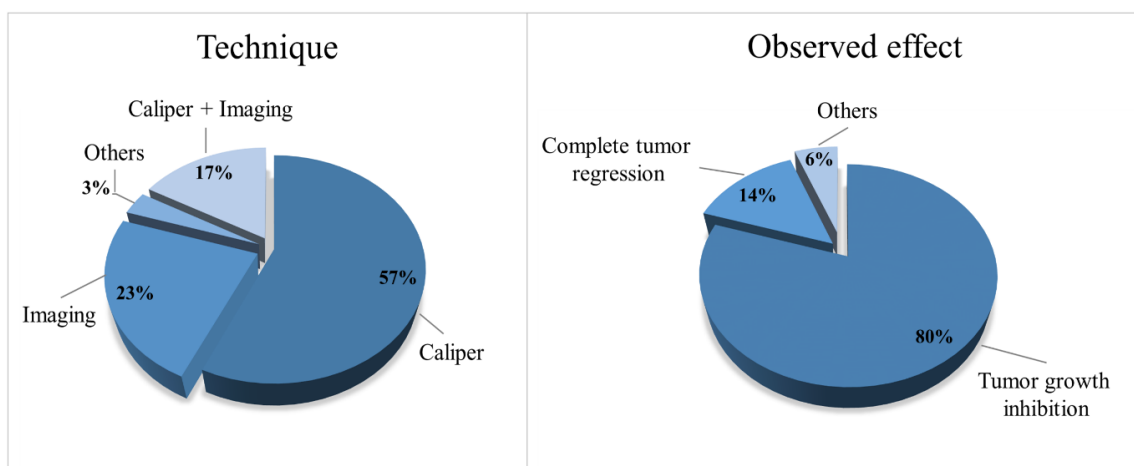
Figure 11. Representation of the techniques used to analyze the biological effect of the treatment. Data taken from the papers detailed in Table 1.

There is just one manuscript of the reviewed ones that used a different approach to determine tumor volume. It is the case of the study of the antitumor effect of the treatment described by Wang et al. that is based on the measurement of the achieved apoptosis rate by the analysis of the expression of Bax/Bcl-2 proteins, using terminal deoxynucleotidyl transferase dUTP nick end labeling (TUNEL) and Transmission Electron Microscopy (TEM) analysis.[151]

In spite of the diverse treatments conditions and methodologies used to check the MH efficacy, 80% of the revised works concluded that there is a tumor growth inhibition after the treatment. In addition, 14% of the cases reported a complete tumor regression, with no signs of tumor regrowth at least one month after ending the MH treatment.[281, 286] However, tumor volume regressions are sometimes difficult to compare among different studies as different time points are analyzed. It is truth that in some cases the antitumor effect produces a very slight inhibition of the growth. That is why many recent studies are now focusing on the synergistic effect of this treatment with other therapies such as chemotherapy or radiotherapy.

One conclusion that could be extracted from this comparison is that the MH studies that have been made are successful as tumor growth inhibition is observed in most cases. However, it is worth mentioning that negative results are often not published, which could lead to an overestimation of the efficiency of this treatment.

6. Limitations and future challenges

Right now, one of the major problems that the scientific community working on in vivo MH is facing is the difficulty to compare results from different laboratories, as little attention has been paid to the standardization of protocols. Also, in many cases, negative results are not being published.

Most of the manuscripts revised for this book chapter do not provide a complete description of the materials and methodology used. This is a consequence of the multitude of parameters that are involved in such complex animal experiments. However, the limited access to these details makes more complex the comparison between research works.

Part of these problems could be solved by a general use of commercial devices specifically designed for *in vivo* MH application, as this would imply a narrower range of AMF conditions. Moreover, it would also be ideal that each of the equipment was commercialized with a given type of MNPs, specifically optimized for the field conditions of the applicator. In this way, optimal heating properties would be achieved during the *in vivo* experiments.

The animal models used in the majority of the works revised consist of human cell lines subcutaneously implanted in immunodeficient mice. Although this kind of model is adequate as proof of concept of the treatment, more complex animal models involving the correct tumor environment and a complete immune response are needed for a better assessment of the treatment efficacy in real conditions. This implies the use of more complex imaging techniques to follow the progress of the tumor growth after the treatment. In addition, an effort should be made on evaluating the MH treatment efficacy in tumors with bad prognosis.

There are other two major issues that could also help to improve the MH treatments. Monitoring MNP localization using imaging techniques (e.g. MRI and CT imaging) [125, 307] before the treatment would allow the use of mathematical simulations to design personalized MH application conditions by calculating the heat generation depending on the nanoparticle location within the tumor. Being able to measure the in situ temperature in a non-invasive way during the MH application would also help to understand the efficacy of the treatment using different materials and conditions.

Despite the fact that this chapter has focused mainly on MH, the general trend is to use this treatment in combination with currently established ones such as chemotherapy, radiotherapy, surgery or immunotherapy. Synergies among these treatments may significantly improve the final antitumor efficacy.

Nevertheless, the main real future challenge would be to overcome the difficult gap between pre-clinical animal studies and the real clinical practice with humans.

2.3 Aportes al tema, visión crítica y perspectivas de futuro

La utilización de nanopartículas magnéticas para terapia térmica por hipertermia exige un diseño experimental que permita una mejora en los procesos físicos involucrados sin dejar de satisfacer los requerimientos biomédicos. Con este objetivo se han sintetizado nanopartículas de diversos tamaños y morfologías, que abarcan desde nanocubos, nanoesferas o estructuras "core-shell", en aras de mejorar la eficiencia de calentamiento de las mismas.[60-61, 64, 74, 81, 308-309] Sin embargo, la enorme variedad en los valores de SAR reportados, así como en las condiciones experimentales (tales como la amplitud y frecuencia del AMF) a partir de las cuales se realiza dicha determinación, dificulta la comparación directa entre ellos y, a la vez la elección de un tipo concreto de nanopartículas para su utilización en hipertermia magnética. Desafortunadamente, debido a que no hay estándares para la amplitud y frecuencia del AMF aplicado, cada grupo de investigación caracteriza sus partículas bajo diferentes condiciones y, en consecuencia, los valores de SAR obtenidos (incluso para la misma suspensión de nanopartículas) pueden ser diferentes debido a la heterogeneidad de los equipos utilizados para la realización de dichas medidas. Además, el valor del SAR informado en la gran mayoría de las investigaciones de hipertermia magnética se determina casi siempre suspendiendo las nanopartículas en agua. Por lo cual, no refleja la complejidad de los medios de dispersión fisiológicos en el que se encuentran las partículas después de su administración tanto *in vitro* o *in vivo*; donde se esperan fenómenos de disipación de calor a consecuencia del entorno biológico, e incluso cambios en el estado de oxidación, agregación o en las interacciones entre las nanopartículas, factores que también pueden afectar su capacidad potencial de generar un calentamiento terapéuticamente relevante.[310-313]

Por otro lado, el entorno biológico en el que son administradas las nanopartículas contribuye a la remodelación de sus propiedades químico-físicas, dotándolas de una identidad mucho más compleja de analizar en términos de predecir el posible nivel de daño inducido a la célula o tejido diana.[314-315] Aunque numerosos estudios *in vitro* evidencian que un aumento de la temperatura por encima de 43 ºC induce directamente a la muerte celular,[99, 120, 316-318] aún persiste una gran variabilidad entre los resultados publicados en la bibliografía, debido a que este umbral de temperatura puede variar dependiendo tanto de las condiciones del tratamiento como del tipo de célula tratada.[319] A su vez, los resultados *in vivo* suelen mostrar una heterogeneidad incluso mayor, y aunque en la mayoría de los casos se observa que la hipertermia magnética induce citotoxicidad local, y con ello una regresión del tamaño del tumor después de la terapia; los mecanismos fisiológicos implicados en estas respuestas no han

quedado totalmente esclarecidos.[316, 320-321] Entre otras razones, porque la diversidad en los esquemas de tratamiento aplicados es enorme, tanto en términos de dosis térmicas y tiempo de exposición a la terapia, como en la variedad del material magnético utilizado. En consecuencia, la comparación relativa entre estos estudios es compleja, ya que se dificulta el manejo de toda la información para llegar a conclusiones unificadas acerca de los factores que influyen en la efectividad del tratamiento térmico.

En el trabajo presentado en la sección anterior realizamos un estudio exhaustivo de los principales esquemas de tratamiento utilizados en la terapia *in vivo* antitumoral por hipertermia magnética, desde una perspectiva global que intenta abordar los parámetros esenciales a tener en cuenta para unificar los criterios de aplicación y análisis de resultados de esta aproximación terapéutica; paso previo esencial para su estandarización futura dentro de la práctica clínica. El análisis realizado abarca una multiplicidad de factores a tener en cuenta en la aplicación *in vivo* de la hipertermia magnética que incluyen, desde (i) la composición química de las partículas, (ii) sus principales rutas de síntesis y vías de administración, (iii) las condiciones de exposición a la terapia térmica (tipo de equipamiento, condiciones de H y f del AMF, etc.), (iv) los modelos animales de experimentación y la comparación entre ellos, hasta (v) la influencia de las técnicas de medición empleadas en la eficacia terapéutica observada. Nuestros resultados evidenciaron que a pesar de los continuos avances en el estudio de los mecanismos que median la hipertermia magnética tanto *in vitro* como *in vivo*, se hace necesaria una estandarización en el tipo de información reportada que permita la comparación de los resultados obtenidos entre los diferentes grupos de investigación, lo que continúa siendo uno de los grandes retos a los que se enfrenta este campo de investigación.

CAPÍTULO 3·
CULTIVO CELULAR 3D COMO MODELO PARA EL ESTUDIO DE LA EFECTIVIDAD DE LA HIPERTERMIA MAGNÉTICA

3.1 Introducción ampliada al tema

Numerosas investigaciones tanto *in vitro* como *in vivo* han demostrado la capacidad de las nanopartículas magnéticas de óxidos de hierro de inducir una hipertermia local bajo acción de un AMF externo, capaz de erradicar eficazmente las células dañadas en la zona tratada.[129] La temperatura a la que se alcanza la muerte celular varía dependiendo del tipo de línea celular, pero se conoce que está relacionada con la cantidad de calor necesaria para desnaturalizar las proteínas tanto citoplasmáticas como de la membrana celular.[319]

A nivel molecular, dosis térmicas por encima de 43 °C inducen daños irreversibles sobre las proteínas reguladoras encargadas de mantener la homeostasis celular, y en consecuencia las células mueren exponencialmente por apoptosis o necrosis *(Figura 3.1)*. En este sentido, la inducción de un mecanismo de muerte u otro dependerá de la temperatura alcanzada y de la duración del tratamiento térmico. Por otro lado, el calor generado a temperaturas inferiores a 43 °C generalmente no induce una citotoxicidad directa. Razón por la cual el efecto promovido por la hipertermia bajo estas condiciones es comúnmente denominado como sub-letal. Los mecanismos de termosensibilización celular inducidos a dosis térmicas sub-letales se basan en la desnaturalización y agregación de las proteínas; lo que conduce a la inhibición de la maquinaria de reparación del ADN y a la inactivación de las proteínas involucradas en la regulación del ciclo celular.[322-323] El calentamiento local inducido a estas temperaturas también puede alterar la viscosidad de la membrana plasmática, provocando alteraciones en sus funciones de transporte.[324] A su vez, la hipertermia sub-letal induce la sobreexpresión de las proteínas de choque térmico (HSP- del inglés "heat shock protein"); superfamilia proteica clasificada según su masa molecular, que tiene un papel esencial en la protección celular ante

diferentes tipos de estrés *(Figura 3.1)*.[325] Se ha descrito que la familia HSP tiene un efecto modulador sobre las cascadas inflamatorias que conducen a la generación endógena de ROS y mecanismos apoptóticos intrínsecos. Razón por la cual, pueden desempeñar un rol dual, tanto en la promoción de la muerte celular como en los mecanismos de supervivencia que contribuyen a su inhibición, dependiendo de su nivel de expresión.[326-328]

A nivel vascular, el tratamiento hipertérmico a temperaturas superiores a 43 °C suele provocar hemorragia y estasis (ausencia de flujo de sangre) de los vasos sanguíneos.[329] Mientras que la hipertermia sub-letal entre 40-42 °C se ha descrito que puede aumentar el flujo sanguíneo, la oxigenación del tejido[330] y el tamaño y permeabilidad de los poros microvasculares; lo que conduce a una mejora en la extravasación de las nanopartículas.[331] Estos cambios en la vasculatura tisular pueden contribuir además a la quimio- y radio-sensibilización observada en tumores después del tratamiento a estas dosis térmicas; y a la movilización de elementos de la respuesta inmunológica efectora, como los linfocitos T, hacia la región tumoral *(Figura 3.1)*.[135, 138, 329-330]
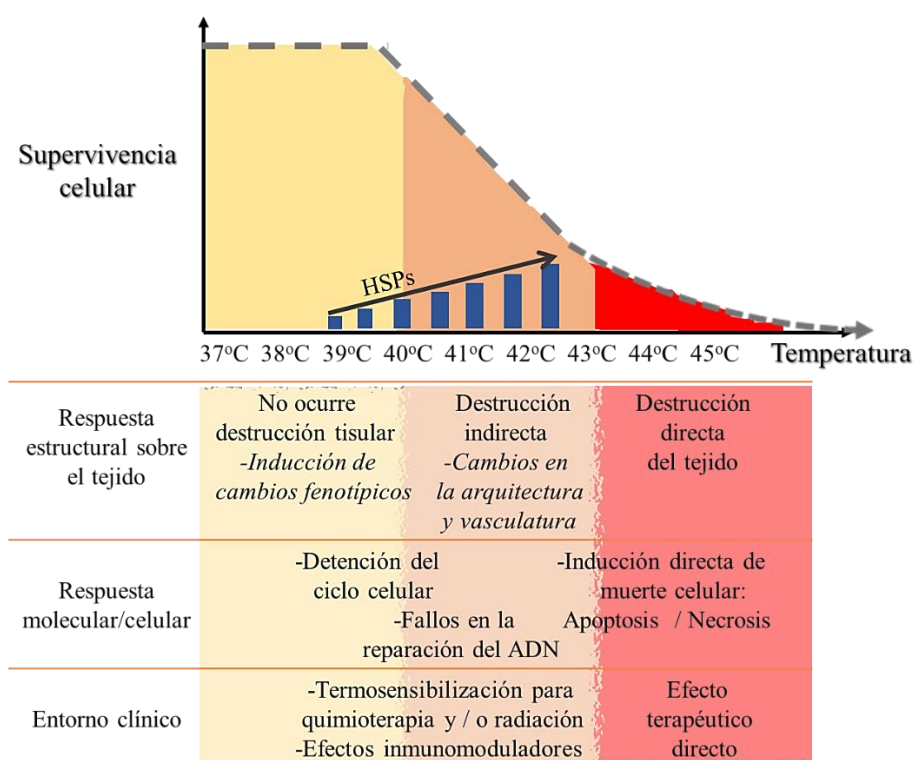
Figura 3.1 Diferentes niveles de respuesta al tratamiento térmico con hipertermia magnética. Contenido adaptado: European journal of cancer, 44(17), 2546-2554, (2008).[135] Copyright Elsevier (2020)". Abreviaturas: Proteínas de choque térmico (HSPs- del inglés "heat shock proteins"); Ácido desoxirribonucleico (ADN).

A nivel de tejido, el incremento de la temperatura también puede promover la permeabilización de la matriz extracelular; efecto relacionado con la inducción de cambios conformacionales sobre diferentes componentes del estroma tisular, como el colágeno.[332] En este contexto, se ha planteado el gran potencial que tienen las nanopartículas magnéticas como agentes térmicos, para degradar localmente la matriz extracelular y mejorar la efectividad del tratamiento antitumoral.[158] En comparación con los enfoques farmacológicos actuales dirigidos a alterar la matriz extracelular tumoral,[333-335] la hipertermia basada en nanopartículas podría exhibir ventajas únicas que incluyen alta especificidad, mínima invasividad y precisión selectiva espacio-temporal. Sin embargo, el papel de las nanopartículas en la modulación del microambiente tumoral, y especialmente su efecto sobre la matriz extracelular ha sido poco investigado hasta el momento.[211, 268, 317, 332, 336]

Los primeros acercamientos experimentales a los efectos multifacéticos de la hipertermia mediada por nanopartículas magnéticas, tanto en la inducción de un efecto citotóxico como en la modulación de la permeabilidad de la matriz extracelular, fueron realizados en modelos murinos de xenoinjertos tumorales.[268, 332] Sin embargo, debido a la multiplicidad de factores intrínsecos que median el tratamiento por hipertermia magnética (tales como, las condiciones de aplicación del AMF y características físico-químicas del material magnético), así como la complejidad y variabilidad existente en las respuestas de los diferentes tipos de tumores a la terapia térmica; se hace difícil encontrar en la práctica preclínica, un modelo único de predicción que mimetice todos los posibles escenarios de la respuesta terapéutica *in vivo*. En este contexto, contar con un sistema experimental *in vitro* que permita mimetizar las condiciones tridimensionales del ambiente celular tumoral *in vivo*, es un paso previo esencial para lograr un mayor acercamiento a las posibles respuestas preclínicas al tratamiento térmico. Al respecto, diversas estructuras 3D, diseñadas y desarrolladas como sistemas modelos de soporte celular, (véase sección 1.4.1) han permitido estudiar los efectos de la generación de calor sobre la matriz extracelular de una manera controlada tanto temporal como espacialmente.

En general, la matriz extracelular se comporta como un medio de integración fisiológica de naturaleza bioquímica compleja, que facilita la transmisión de las señales inter-celulares, y determina la estructura y función del tejido a través de los componentes secretados por las células hacia el medio extracelular.[337-338] Las matrices extracelulares están compuestas principalmente por tres tipos de macromoléculas: colágenos, proteoglicanos y glucoproteínas *(Figura 3.2)*. Los colágenos forman parte de un grupo de moléculas genéticamente distintas,

pero relacionadas a nivel estructural, que se encuentran representadas en la mayoría de las matrices extracelulares que rodean las células del cuerpo. El colágeno en la matriz extracelular suele estar modificado con carbohidratos y, una vez secretado fuera de la célula, forma largas fibras denominadas fibrillas de colágeno del organismo. Por otro lado, los proteoglicanos son un grupo de moléculas altamente polimórficas que también tienen distribuciones especializadas en los tejidos y en los diferentes tipos de matrices extracelulares. Mientras que la fibronectina se ha identificado como la principal glucoproteína del tejido conectivo, que junto con la laminina, está presente en las membranas basales.[337]
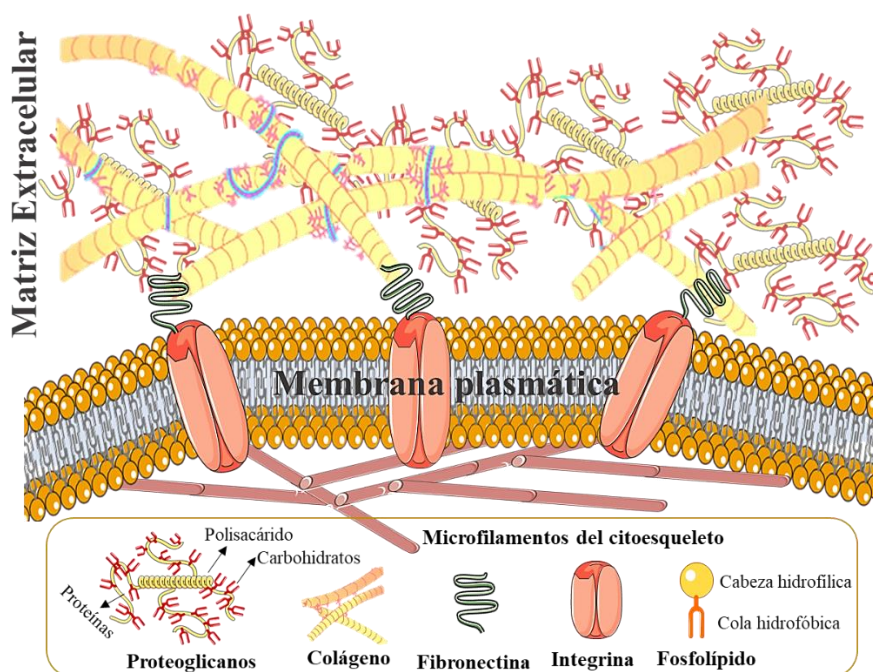
Figura 3.3 Esquema de los principales componentes bioquímicos de la matriz extracelular.

La composición molecular de la matriz extracelular varía en dependencia del tipo de tejido. En tumores, por ejemplo, el colágeno I es una de las moléculas más abundantes que proporciona integridad estructural y resistencia mecánica al tejido.[208] En este sentido, el hecho de que las fibras de colágeno puedan sufrir transiciones térmicas, constituye la base del uso de la hipertermia para alterar las propiedades mecánicas del tejido tumoral a nivel macroscópico. En particular, el colágeno tipo I exhibe una doble transición térmica en solución ácida.[339] A temperaturas en el rango entre 31- 37 °C suele producirse una transición reversible asociada a la despolimerización de las fibrillas más pequeñas.[340] Mientras que entre 37 °C y 55 °C dicha

transición se considera irreversible debido a la desfibrilación y completo desplegamiento de su estructura nativa de triple hélice.[341]

Los hidrogeles basados en colágeno son de los modelos más sencillos y de fácil establecimiento utilizados en el estudio de la respuesta mecánica de la matriz extracelular a estímulos externos como el calentamiento.[208, 342-343] Generalmente proporcionan una buena adhesión celular, y se caracterizan por ser mecánicamente débiles. Sus principales ventajas radican en que pueden ser procesados bajo condiciones suaves o incluso formarse *in situ,* lo que los convierte en modelos especialmente útiles para el posterior análisis de la respuesta biológica al tratamiento térmico. Por otro lado, al contener bajas cantidades de masa seca, los productos de su degradación son mínimos; por lo que el proceso de extracción de células mediante la digestión del gel con colagenasas, es tan eficiente como seguro, ya que los efectos citotóxicos asociados a la degradación polimérica del colágeno son mínimos.

3.2 Dual Role of Magnetic Nanoparticles as Intracellular Hotspots and Extracellular Matrix Disruptors Triggered by Magnetic Hyperthermia in 3D Cell Culture Models.

Lilianne Beola[1], Laura Asín, PhD[1], Raluca M. Fratila, PhD[1], Vanessa Herrero, PhD[1], Jesús M. de la Fuente, PhD[1], Valeria Grazú, PhD[1] and Lucía Gutiérrez, PhD[2]

[1]Instituto de Ciencia de Materiales de Aragón (ICMA), CSIC/Universidad de Zaragoza, C/ Pedro Cerbuna 12, 50009, Zaragoza, Spain. Centro de Investigación Biomédica en Red de Bioingeniería, Biomateriales y Nanomedicina (CIBER-BBN), Spain.

[2]Department of Analytical Chemistry, Universidad de Zaragoza and CIBER-BBN. Instituto Universitario de Nanociencia de Aragón (INA), Edificio I+D, C/ Mariano Esquillor Gómez, 50018, Zaragoza, Spain

Authors contributions: Lilianne Beola is the principal author; Raluca M. Fratila, PhD, and Vanessa Herrero, PhD synthetized the MNPs used in this work; Jesús M. de la Fuente PhD is the head of Bionanosurf group; Lucía Gutiérrez, PhD, Laura Asín, PhD and Valeria Grazú, PhD are the thesis supervisors. All the authors contributed to the discussion of the results.

Journal metrics: Impact factor 8.456 (2018) and Q1 ((Materials Science (miscellaneous); Medicine (miscellaneous); Nanoscience and Nanotechnology)

Abstract: Magnetic hyperthermia is a promising therapy for the localized treatment of cancer based on the exposure of magnetic nanoparticles to an external alternating magnetic field. In order to evaluate some of the mechanisms involved in the cellular damage caused by this treatment, two different 3D cell culture models were prepared using collagen, which is the most abundant protein of the extracellular matrix. The same amount of nanoparticles was added to cells either before or after their incorporation to the 3D structure. Therefore, in one model, particles were located only inside cells (*In model*), while the other one had particles both inside and outside cells (*In&Out model*). In the *In&Out model*, the hyperthermia treatment facilitated the migration of the particles from the outer areas of the 3D structure to the inner parts, achieving a faster homogeneous distribution throughout the whole structure and allowing the particles to gain access to the inner cells. The cell death mechanism activated by the magnetic hyperthermia treatment was different in both models. Necrosis was observed in the *In model* while apoptosis in the *In&Out model* 24 hours after the hyperthermia application. This was clearly correlated with the amount of nanoparticles located inside the cells. Thus, the combination of both 3D models allowed us to demonstrate two different roles of the magnetic particles during the hyperthermia treatment: i) the modulation of the cell death mechanism depending on the amount of intracellular particles, and ii) the disruption of the collagen matrix caused by the extracellular nanoparticles.
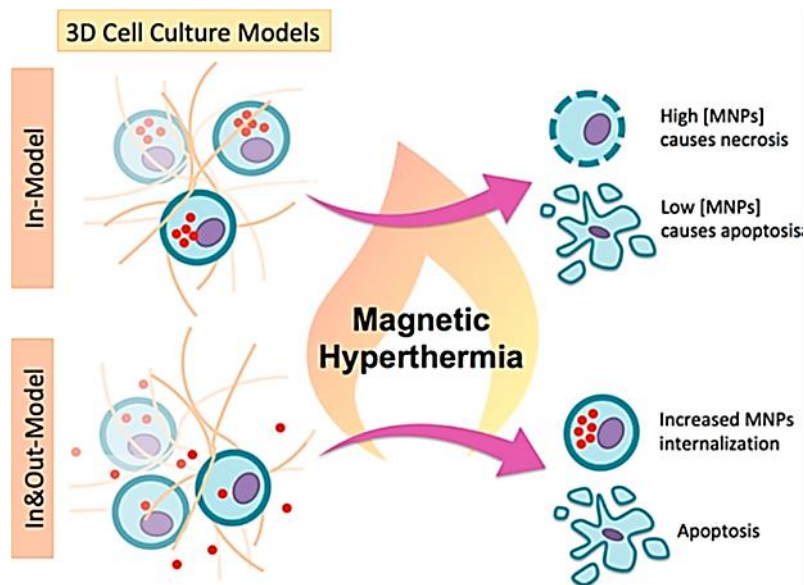
1. Introduction

Iron oxide magnetic nanoparticles (MNPs) are one of the most promising systems within the field of biomedicine and biotechnology.[74, 344-345] Their physico-chemical characteristics as well as their magnetic properties, provide unique opportunities for the development of a wide range of applications such as biosensors,[346-347] controlled drug delivery systems,[348-349] contrast agents for magnetic resonance imaging,[350-351] or cancer therapies such as magnetic hyperthermia.[352]

Magnetic hyperthermia (MH) has been particularly studied in recent years for the treatment of malignant tumours.[128-129, 353] It is widely known that cancer cells are more sensitive to heat than normal cells.[354] MNPs act as localized heating sources in the region where they are situated when submitted to an alternating magnetic field (AMF).[131] The local temperature increase in the tumour area induces cell death or alters the growth and differentiation of the cancer cells.[319] At the same time, MH has been used to promote synergistic effects when combined with other conventional treatments. In particular, it has been shown that MH treatment makes the cells more sensitive to radiation or to the action of certain chemotherapeutic drugs.[132, 355-356] A possible explanation of this synergistic effect between heat and chemotherapy was given by Krawczyk *et al.* who demonstrated that mild hyperthermia conditions provoked the degradation of BRCA2, a protein involved in the homologous recombination, which is a DNA repair mechanism by which the double strands breaks are repaired. If the cells are deficient in this DNA repair mechanism they become more sensitive to drugs that induce DNA damage.[241]

The cell death mechanisms activated by the MH treatment and the relevant parameters that control the triggering of each mechanism are not completely known yet. The classical conception of two cell death routes, apoptosis and necrosis, which take place independently, has been already refuted. Besides, some classical postulates about these two cell death mechanisms have been progressively abandoned and replaced for new ideas. It is known that necrosis can take place in a regulated way, like apoptosis, and that the apoptotic cells can sometimes be recognized by the immune system and trigger an adaptive immune response, like necrosis. Nevertheless, it is crucial to be able to control the activation of either necrosis or apoptosis mechanisms and to try to control the pro-inflammatory immune response that could be sometimes negative for tumour treatments, as it involves non-desirable processes such as the tumour invasion or metastasis. [357-359]

Currently, most of the *in vitro* studies that analyse the efficacy of the hyperthermia treatment are being performed in monolayer cell cultures.[244, 360-361] However, this traditional cell culture

method, in two dimensions (2D), has essential limitations in terms of inter-cellular communication, cell microenvironment and cell spatial behaviour.[192] Therefore, these 2D cell culture models cannot replicate the morphology and biochemical properties the cells have in the living organisms. They also lack the complex scenario that the MNPs face to reach the deeper areas of the tumours. One of the alternatives to solve these problems is the use of three dimensions (3D) cell culture models, such as spheroids, liquid spheres,[362-363] or 3D scaffolds.[364-365] 3D cell culture models are simple structures that mimic more accurately the tumour composition and structure [366] providing a more realistic environment to evaluate the cellular response to a treatment.[367] In addition, 3D cell culture models allow the production of a high number of identical replicas and provide a good alternative to perform preliminary tests before *in vivo* experimentation allowing the reduction of the number of animals needed. Until know, the number of studies using 3D cell culture models to evaluate the effect of magnetic hyperthermia is still scarce.[317] These previous studies have mainly used spheroids as 3D cell cultures, a model that lacks the presence of extracellular matrix.

In this work, we have developed two 3D cell culture models based on the use of a collagen matrix to evaluate the efficacy of magnetic hyperthermia treatment in a murine macrophage/monocyte cell line (RAW 264.7). Collagen was selected because besides being one of the major components of the extracellular matrix (ECM), it also plays a crucial role in the tumour ECM.[163] In particular, tumours with well-organized and highly interconnected collagen fibres display lower penetration of high-molecular-weight chemotherapeutic agents than those with disordered and loose collagen networks.[198, 368] Macrophages were chosen as model cells due to their known capacity of easily incorporating iron oxide nanoparticles.[30] This fact allowed working with a wide range of concentrations of nanoparticles inside the cells, which facilitated the study of the correlation between the amount of internalized particles and the cell death mechanism activated. The main difference between the two models is the moment in which MNPs are in contact with the cells along the 3D cell culture preparation protocol. In one model (*In Model*), cells in suspension are incubated with the particles and after washing away the MNPs that have not been internalized, the cells are transferred to form the 3D matrix, thus resulting in a homogeneous internalization of the MNPs amongst all the cells and also an exclusive intracellular location of the MNPs. The other model is based on the administration of the MNPs to the cells once they are already forming part of the 3D matrix resulting in a model where particles need time to penetrate and fill up the whole 3D matrix to gain access to inner cells. As a result, this model allows obtaining a different MNP distribution than the

former approach, having particles located both inside and outside the cells (*In&Out Model*) *(Figure 1)*. The combination of both models allows disentangling the effect that MNPs have on the extracellular matrix and the treatment efficiency.

In this work, we have used confocal microscopy and flow cytometry to study the MNP uptake, with and without exposure to an AMF. We have studied the evolution of the MNP location within the collagen matrix after the AMF exposure. We have also evaluated the cell death mechanisms triggered by the treatment at different times post-treatment (0, 24 and 48 h). Cell cycle and the cell viability studies allowed to discriminate the cell death mechanisms observed 24 h after MH treatment which was different on each 3D model: necrosis for the *In Mode* and apoptosis in the case of the *In&Out Model*. Besides, we have analysed the amount of MNPs internalized in each 3D model in order to establish a relationship between their concentration and the cell death mechanism observed after the treatment.
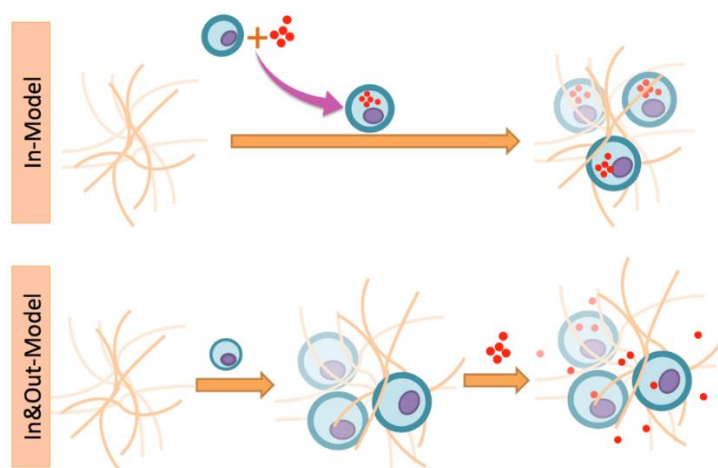
Figure 1. Representation of the formation of the two 3D models used in this work. In Model, where the MNPs are located just inside the cells. In&Out Model, where MNPs are located both inside and outside the cells.

2. Results and discussion

We have chosen spherical 11 nm iron oxide MNPs (11.2 ± 0.8 nm, *Figure 2*), as this diameter is within the most commonly studied range for *in vivo* magnetic hyperthermia experiments.[369] This diameter fulfils the requirements for *in vivo* experimentation, as it avoids fast renal clearance. This size is also considered to be in the range to achieve the better heating properties for magnetite/maghemite.[370]

MNPs have been prepared by thermal decomposition to have a careful control of the particle size and size distribution *(Fig. 2)*. The superparamagnetic behaviour at room temperature, desired in many biomedical applications to prevent the MNP aggregation associated to a permanent magnetic moment,[344] has been verified by magnetic measurements confirming the negligible coercivity and also indicating the good crystalline properties of the prepared material by a high saturation magnetization ($M_s = 81$ Am^2/kg Fe_3O_4) *(Figure 1)*.
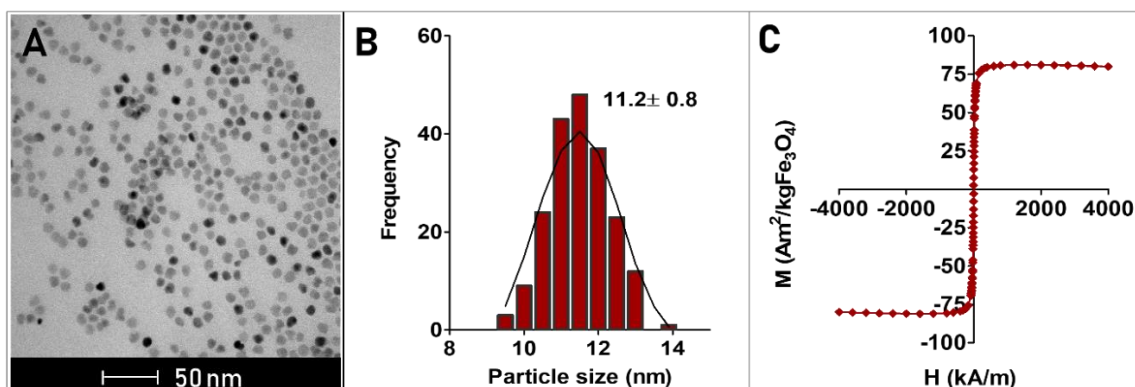
Figure 2. Magnetic nanoparticle characterization. (A) TEM micrograph, (B) Particle size distribution analysis and (C) Field dependent magnetization of the MNPs in water.

MNPs have been subsequently coated with a polymer (PMAO, poly (maleic anhydride-alt-1-octadecene) modified with a fluorophore (TAMRA, Carboxytetramethylrhodamine). The polymer coating allows the transference of the magnetic cores from the organic to the aqueous phase and provides carboxylic groups that allow both the incorporation of the fluorophore, to track the location of the MNPs in the *in vitro* experiments, and glucose, to prevent the aggregation in cell culture medium and provide an active targeting molecule for the particles uptake.[371] Glucose is especially interesting in our case as macrophages, as well as many tumour cells, due to their high energy requirements present upregulated glucose transporter proteins and subsequently the uptake of glucose-functionalized MNPs is enhanced.[372] The successful glucose functionalization, routinely used in our lab,[373] has been verified by ζ – potential measurements through a significant decrease of the MNP negative charge from -36 mV, before functionalization, to -13 mV after the glucose addition.

Several tests have been performed to assure that the material was suitable for *in vitro* experiments. Stability of functionalized MNPs has been assessed by dynamic light scattering (DLS) measurements, showing that the hydrodynamic size of the particles before and after the glucose functionalization remains below 70 nm for MNPs at pH = 7, suspended both in water

and complete culture medium (with 10% Foetal Bovine Serum) (*Table. S1*, Supporting Information). In addition, a sterility assay was performed and no evidence of the presence of microbial colonies has been observed after performing the test with the MNPs (*Figure S1*, Supporting Information). Finally, although the low toxicity of particles prepared following the same protocol has already been checked in the past,[242, 314] cell viability after the MNP administration was studied by flow cytometry in 2D cell culture models at different concentrations up to 100 µg of Fe per well (200 µg/ml), observing only a significant reduction of the cell viability at the highest concentration (*Figure S2*, Supporting Information). From these results, an iron amount of 100 µg of Fe per well has been chosen for the hyperthermia experiments, as it is the highest concentration tested in which the viability is not significantly different to the controls. The low toxicity of this amount of MNPs has also been confirmed by flow cytometry in the 3D cell cultures (*Figure S3*, Supporting Information).

The heating efficiency of the MNPs in water suspensions has been evaluated before the *in vitro* test. The Specific Absorption Rate (SAR) of the MNPs measured at an iron concentration of 1 mg/mL and using a field amplitude of H = 20 kA/m, and a frequency of 829 kHz is 253 W/g Fe. Establishing a correlation between the heating capacity of the MNPs in suspension and their ability to heat efficiently in *in vitro* experiments is not straightforward. First, it is difficult to determine and mimic the aggregation degree of the MNPs in the cellular environment. It is also a complex task to know the local concentration of the MNPs once they have been internalized by the cells. However, until all these problems are solved, the most common approach to validate that a specific material produces heat in the presence of an AMF is to measure the change of temperature over time in water at physiological pH, as at least it provides some information for comparison with other reported values.

2.1. Two different 3D cell culture models have been developed.

To achieve the generation of two 3D cell culture models we have followed two different strategies for the incubation of the cells with magnetic nanoparticles. As a proof of concept, macrophages have been selected as a model cell line, as they are known to easily uptake this kind of particles.[28, 30]

The first approach followed has been to incubate the detached macrophages with the MNPs and, after removal of the particles that were not internalized, to form the 3D cell culture with the cells containing the MNPs. This approach leads to a 3D cell culture in which the MNPs are homogeneously distributed amongst all the cells and only located inside them (*In Model*), as

observed by confocal microscopy and flow cytometry *(Figure 3)*, showing that almost all the cells (> 99%) contained MNPs after 1 h of incubation time.

The second approach has been to embed the macrophages within the 3D structure and then administer the MNPs. This way, particles need more time to penetrate the collagen structure to reach the inner cells. Although, after the incubation time, the supernatant is removed and the 3D structure is washed, some MNPs remain within the collagen matrix outside the cells. Because in this model particles could be found located both inside and outside the cells, we have named it "*In&Out Model*". The presence of particles both inside the cells and within the collagen matrix has been verified by confocal microscopy *(Figure 3)*. Interestingly, two different cell populations have been identified by flow cytometry: one population of cells with particles (58 ± 5%) and the other without particles (42 ± 8 %), indicating a slower rate of MNP uptake when compared to the *In Model* for the same incubation time of 1 h *(Figure 3)*, probably due to the time required for the movement of the MNPs towards the inner parts of the 3D structure. One of the advantages of using these two 3D cell culture models is that, although the same amount of particles has been administered to the cells, we have been able to achieve two different kinetic behaviours of MNP internalization.
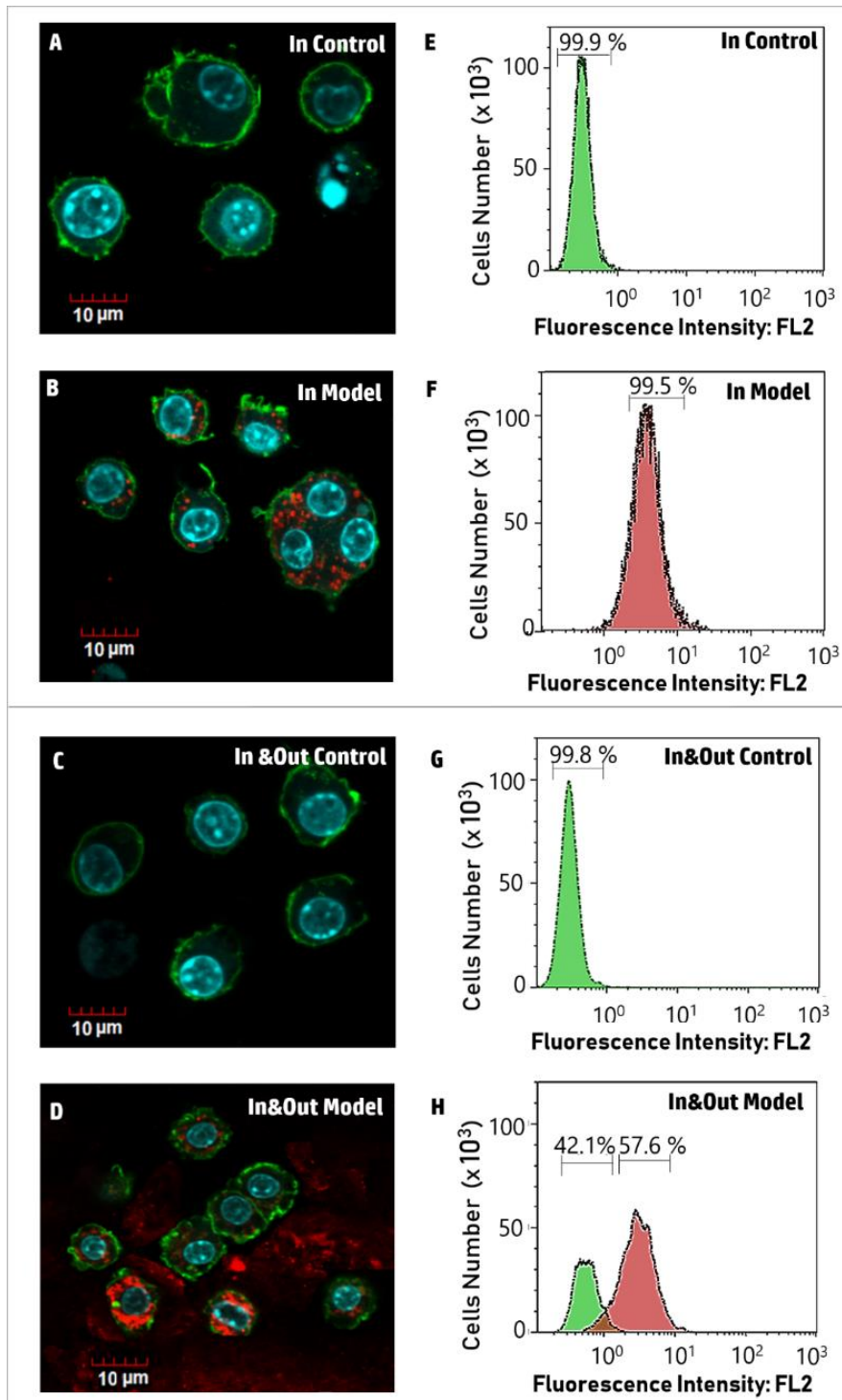
Figure 3. 3D cell culture characterization (A, B, C, D) Confocal images. The nucleus is shown in blue (DAPI), actin in green (Phalloidin_AlexaFluor488) and MNPs in red (TAMRA). Scale bar: 10 μm. (E, F, G, H) Flow cytometry analysis of nanoparticle uptake. Data have been selected as a representation of a series of five experiments.

2.2. AMF exposure enhances MNP uptake.

Once it has been verified that the two models were successfully generated, the transformations that may occur with time have been evaluated. In particular, the capacity of the cells to continue internalizing MNPs in the *In&Out Model* has been assessed. To evaluate the time frame of the MNP uptake in the *In&Out Model*, the evolution with time of the two different cell populations previously observed by flow cytometry (with and without MNPs) has been measured *(Table 1)*. Results have been compared also with 3D cell cultures of the *In&Out Model* after the AMF exposure to evaluate its impact on the MNP uptake.

The percentage of cells that contain MNPs in the *In&Out Model* increases with time, reaching a point at 24h after their addition where all cells contain MNPs *(Figure 4)*. This uptake, however, is significantly faster in the 3D cell cultures exposed to the AMF. It has been observed that immediately after the AMF exposure, a higher percentage of cells had uptaken MNPs (70 ± 3 %) in comparison with the control experiment with no AMF exposure in which only 58 ± 4 % of the cells showed MNP internalization. In addition, 3 h after the administration of the MNPs, the two populations of cells (with (69 ± 4 %) and without (31 ± 4 %) particles) were still observed in the 3D cell culture that had no exposure to the AMF while almost all the cells exposed to the AMF (99 ± 0.5 %) had uptaken MNPs. Nevertheless, although all the cells from the *In&Out Model* contain MNPs 24 h after the 3D cell culture generation, still many particles remain located outside the cells within the collagen fibres as observed by confocal microscopy *(Figure 5)*. As a conclusion of these results, flow cytometry studies in the *In&Out Model* demonstrate an enhancement in the rate of the MNP uptake by the cells triggered by AMF exposure *(Figure 4)*.

Experimental conditions	Time points		
	0 h	3 h	24 h
-AMF	58 ± 4 %	69 ± 4 %	99.5 ± 0.3 %
+AMF	70 ± 3 %	99 ± 0.5 %	99.2 ± 0.6 %

Table 1. Percentage of cells that contain MNPs in the In&Out Model at different time points, either in the control experiment with no AMF exposure (-AMF) or after the AMF exposure (+AMF). Data obtained by flow cytometry (n=5).
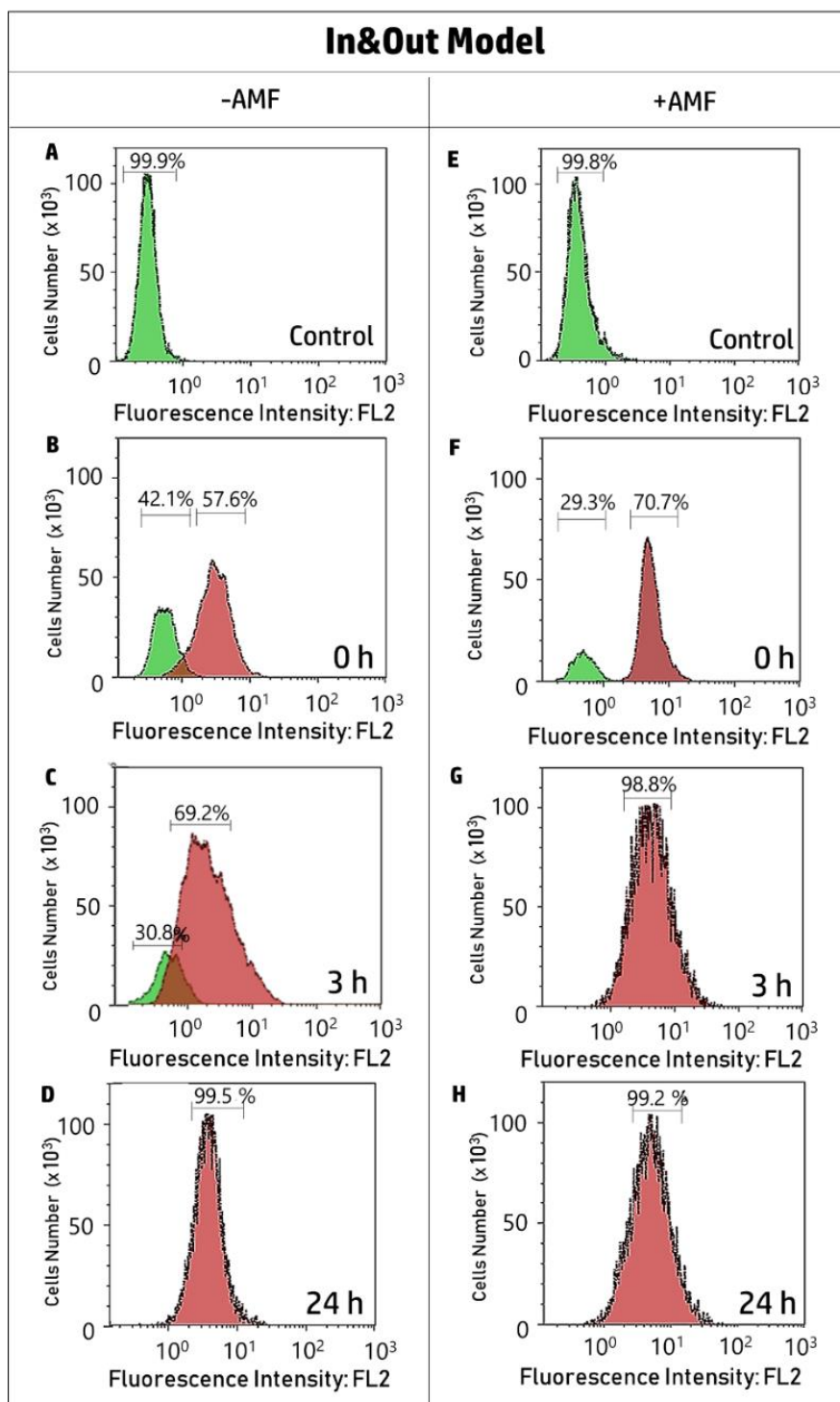
Figure 4. Flow cytometry analysis of the time dependent nanoparticles uptake in the In&Out Model. Left: Cells without exposure to the AMF (-AMF), Right: Cells after the AMF exposure(+AMF). (A, E) Control cells without MNP, (B, F) 0 hours, (C, G) 3 hours, (D, H) 24 hours. Data have been selected as a representation of a series of five experiments.
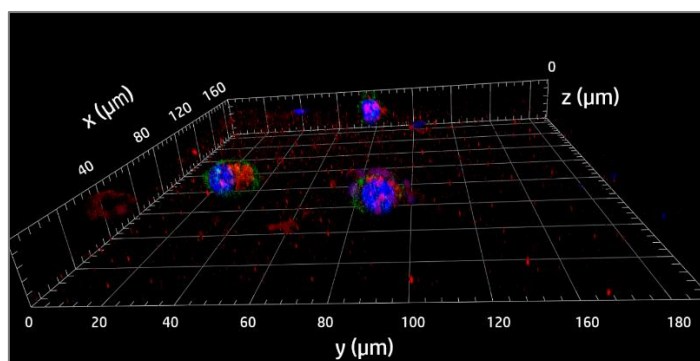
Figure 5. 3D reconstruction of confocal images acquired for the In&Out Model 24 h after AMF exposure. The nucleus is shown in blue (DAPI), actin in green (Phalloidin_AlexaFluor488) and MNPs in red (TAMRA). The presence of MNPs is still observed outside the cells 24 h after the AMF exposure.

To further investigate the mechanisms behind this MNP internalization enhancement mediated by AMF exposure, two 3D cell cultures of the *In&Out Model* have been prepared, and one of them has been exposed to the AMF. Images of the whole 3D structure have been acquired for the initial time point *(Figure 6)*. In the case of the cell culture not exposed to the AMF, most of the particles have not been able to diffuse towards the inner part of the collagen matrix, being mainly localized in the outer areas of the 3D structure. However, in the cell culture exposed to the AMF, particles have penetrated better and are more homogeneously distributed throughout the whole 3D structure. This phenomenon of a more uniform distribution of MNPs after the AMF exposure has also been previously observed in a spheroid model of triple negative breast cancer.[317] It has also been previously reported on a *in vivo* model where the nanoparticles where initially located in the collagen-rich outer areas of the tumour and penetrated more deeply into the core after the hyperthermia treatment.[268]

The enhancement of the MNP uptake may be associated with an increase in collagen permeability induced by the temperature rise during the MH treatment making the MNPs more "accessible" to the cells. It is known since a long time that the melting temperature of the triple helixes of the collagen type I, which is the most abundant in the nature, is few degrees above body temperature.[374] Most recent studies have shown that the denaturation of the collagen vitrified gels takes place in two steps: a reversible process that results in a meta-stable collagen matrix, and an irreversible process that takes place at 60 ºC, leading a random uncoiled collagen.[343] These results are relevant for the design of future preclinical treatments, as collagen is one of the major components of the tumour extracellular matrix present in breast,[197] prostate,[375] glioma,[376] or pancreatic [377] cancer. Therefore, the benefits of the application of

periodical cycles of AMF exposure would be to improve the permeability of the extracellular matrix and therefore the access of chemotherapeutic drugs or cells from the immune system to the inner areas of the tumour. In addition, the enhancement of the internalization of MNPs after each cycle could positively influence subsequent hyperthermia cycles and this amplification effect could have positive synergetic effects in the final effectiveness of the treatment.
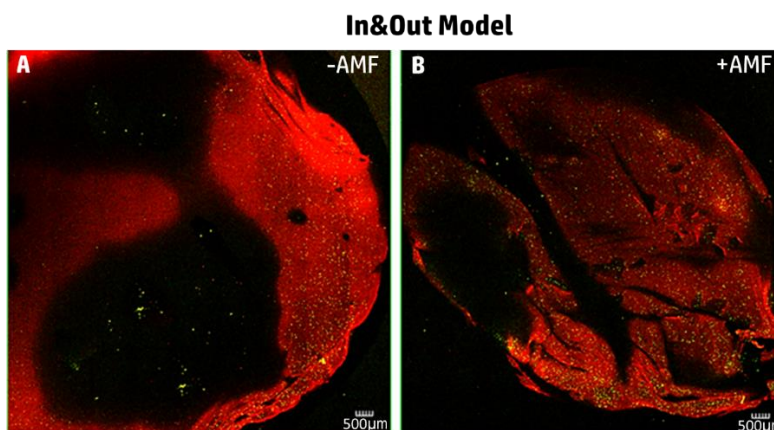
Figure 6. Map image of confocal microscopy of 3D cell culture without (A) and with (B) the AMF exposure for the In & Out Model (0 hours). The image shows the overlay of two channels: green fluorescence of the labeled cells and red fluorescence of the MNPs. Scale bar is 500 µm.

2.3. Magnetic Hyperthermia treatment induces different cell death mechanisms in the two 3D cell culture models.

To evaluate the effect of the differences between the two models on the cell death mechanisms we have evaluated the activation of the cell death routes at three different time points (0, 24 and 48 h) after the hyperthermia treatment. Interestingly, the results have shown differences in the cell death mechanism between the two models. Just after the hyperthermia treatment (0 h) most of the cells remain alive in both models, being negative for Propidium Iodide (PI) and Annexin V staining. PI is a small molecule that enters in the cells and binds DNA only when the lipid bilayer membrane is disrupted, which happens in the late stages of the apoptosis and in the necrosis mechanism. Annexin-V binds phosphatidylserine (PS), a phospholipid that is normally located on the inner side of the cell membrane but translocates to the extracellular side in the first stage of the apoptosis. Therefore, cells that are positive for PI and negative for Annexin V have their cell membrane integrity altered without exposing the phosphatidylserine, a process typical from the beginning of necrosis, while cells that are positive for both markers indicate a late necrosis or late apoptosis stage.[378]

One day after the treatment, the *In Model* shows a significant population of necrotic cells (39.02 ± 4%) (positive for PI and negative for Annexin V), 60.09 ± 4.5% of cells that are still alive (negative for both markers) and a small percentage of cells (0.89 ± 0.1%) that are probably in a late necrosis stage (positive for both markers). On the contrary, at 24 h, the *In&Out Model* presents a very different situation where 38 ± 5.6% of the cells are undergoing apoptosis (positive for Annexin V and negative for PI) and the rest of the cells (61 ± 5.8%) are alive *(Figure 7)*. As a conclusion we can say that the *In&Out Model* results in a more controlled cell death pathway while the response to the MH treatment in the *In Model* is more aggressive.
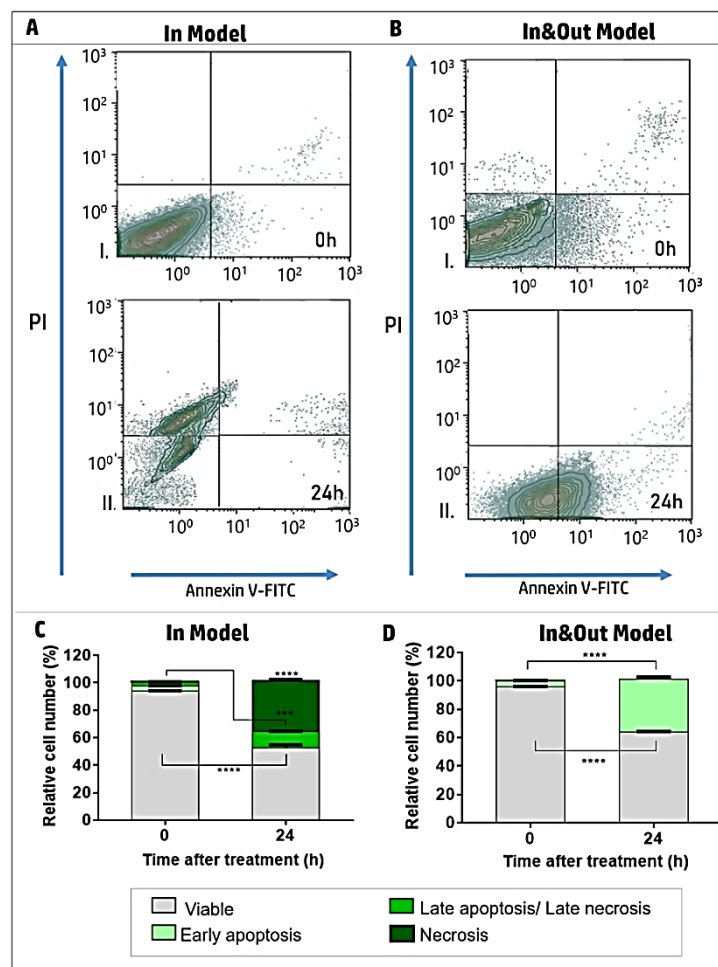
Figure 7. Analysis of magnetic hyperthermia-induced cell death (Annexin V and PI staining). Selected density plot (representative of 5 experiments) obtained at 0h and 24h after MH treatment for the In Model (A) and In&Out Model (B). (C and D) Summarized flow cytometry data resulting from five independent experiments shown as mean ± SD. Statistical significance between the means at the different times was determined using a two-way ANOVA with Sidak's multiple comparisons test (**** p < 0.0001; *** p < 0.001; p > 0.05 no significance).

To evaluate the status of the cells that remain alive 24 h after the treatment, the cell cycle has been analysed by flow cytometry *(Figure 8)*. It has been previously shown that among the crucial events triggered by a heat shock stress are the changes in the cell cycle progression. Depending on the duration and the intensity of the heat shock, cells can enter into a transient or permanent cycle arrest that can take place either in the G1 or G2/M transition. Cells accumulate at these so-called checkpoints because the activity of the proteins that regulate these transitions (cyclin-dependent kinases) decreases.[379] G1 checkpoint checks several aspects of the cells such as the size, nutrients and DNA damage before entering in the replication phase, and G2 checkpoint is focused on analysing DNA damage after the replication and replication completeness. So, depending when the DNA damage occurs the cells will be arrested in different phases. Previous results have shown that mild heat shock provokes a cell-cycle arrest in the G2/M phase.[147]

Cell cycle analysis of the control 3D cell culture has revealed that around 40% of cells are in the G2M phase in both models. This phase includes both cells undergoing the G2 phase, where cells prepare themself for mitosis, and also those cells that are dividing (M phase).[380] The observation of an important percentage of cells in this sub-phase suggests a normal replication of the cells after the 3D model construction. In contrast, the analysis of the cell cycle from the cells that remained alive 24 h after the MH treatment for both models has revealed a significant decrease on the percentage of cells in the G2M and S phases, accompanied by an increase on the percentage of cells in the G0/G1 phase. These results indicate an arrest of the cells in the G0/G1 phase that does not allow the cells to duplicate its DNA and undergo the mitosis process. Therefore, it can be concluded that cells are suffering damages that are being detected by the key proteins preventing the cell replication process. The arrest is however more pronounced for the *In Model*. This result is probably a consequence of the heterogeneous distribution of MNPs along the 3D structure of the *In&Out Model* when the AMF is applied, as the core of the 3D cell culture would probably contain cells that have not incorporated MNPs or that are far away from other extracellular MNPs that act as heating agents. However, in order to have a more detailed explanation of the mechanisms involved, further experiments on the expression and activity of some proteins such as p-53 and some cyclin-dependent kinases should be performed in future studies.

It should also be briefly discussed that a small decrease in the percentage of cells in mitosis phase is observed in the In Model in comparison with the *In&Out Model*. This effect has been observed both in the model with cells incubated with MNPs and the control incubated without

MNPs and is probably due to the protocol of the 3D model preparation. In the *In Model*, the cells have been maintained in suspension during 1 hour for the incubation period. As RAW–264.7 are adherent cells, the suspension step is less favourable for the normal cell development in comparison with the *In&Out Model*, where the cells are directly located into the collagen matrix.
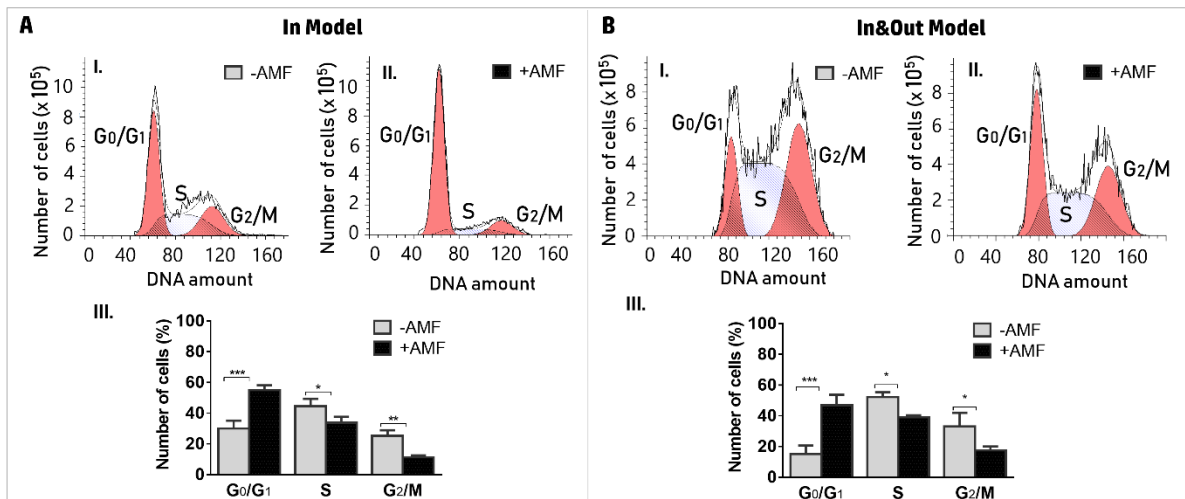
Figure. 8. Effect on cell cycle distribution 24 h after magnetic hyperthermia treatment. (A) In Model (B) In&Out Model. The distribution of cells in each phase is given in the case of no MH treatment (I); after MH treatment (II) and the comparison of both experiments (III). Results are represented as average ± S.D. and are based on three independent experiments. Statistical significance was determined using a one-way ANOVA with Bonferroni post-test (***p<0.001; **p<0.01; *p<0.05).

To further evaluate the effects of the cell cycle arrest observed 24 h, the experiment was extended and the number of dead cells was determined by flow cytometry up to 48 h after the MH treatment for both models. A significant decrease on the number of cells alive is observed in both models at 48 h, presenting only ≈ 4% viability *(Fig. 9)*. Despite the fact that different cell death routes are followed, these results indicate that the hyperthermia treatment is able to kill most of the cells just 48 h after the treatment.
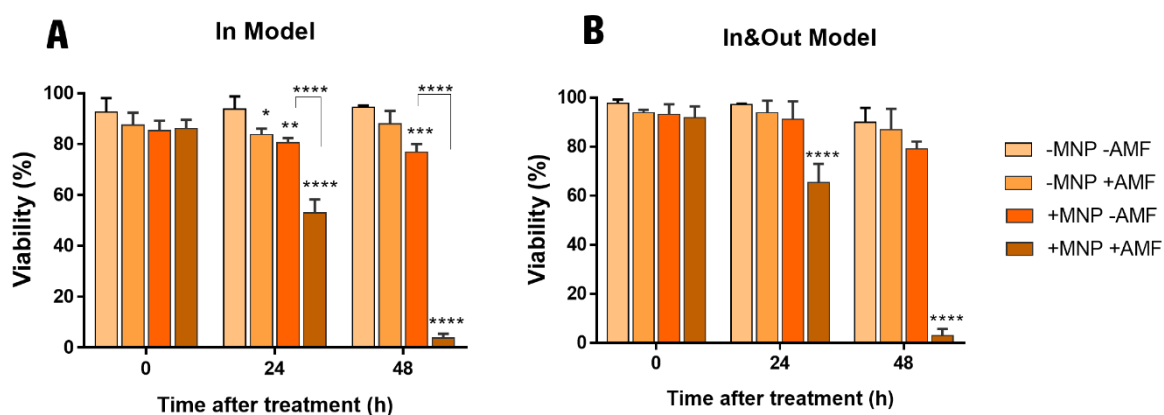
Figure 9. MNPs cell viability evaluated in 3D models at different times after the Magnetic Hyperthermia treatment. (A) In Model and (B) In&Out Model. Cell viability has been evaluated by Flow Cytometry for the two models and compared different controls: with (+MNPs) or without (-MNPs) magnetic nanoparticles, and with (+AMF) or without (-AMF) exposure to the magnetic field. Results from five independent experiments are shown as mean ± SD. Statistical significance between the means respect to the control (-MNP -AMF) was determined using a two-way ANOVA with Dunnett's multiple comparisons test (****p<0.0001; ***p<0.001; **p<0.01; *p≤0.05; p>0.05 no significance). In cases where more than one group generated significant differences with respect to control, the means between those groups were also compared.

2.4. Magnetic Hyperthermia treatment induces different cell death mechanisms depending on the intracellular amount of MNPs.

An important factor to take into account in the discussion of the previously shown results is that although the cells from both models have been incubated with the same amount of MNPs, due to the way the 3D models are prepared, cells from the *In Model* end up incorporating a higher amount of MNPs. To evaluate the amount of MNPs uptaken by the cells in both models, cells have been removed from the collagen structure and their iron content has been quantified (*Table. S2*, Supporting Information). When administering 100 µg of iron to both models, the intracellular iron content has been determined to be 10-fold higher for the *In Model* (8.7×10^{-8} mg Fe/cell) in comparison with the *In&Out Model* (8.1×10^{-9} mg Fe/cell) *(Figure 10)*. This difference has been also verified after performing a magnetic characterization of the 3D cell cultures (*Figure S4*, Supporting Information).

It is important to highlight that these values of iron uptake confirm the high amount of MNPs that macrophages are able to internalize (depending on the incubation conditions). It is also worth mentioning that the amount of internalized MNPs in the *In&Out Model* is of the same

order as the observed in other cell lines [99, 381] validating the interest of our model as a tool to better understand the cellular mechanisms triggered after the AMF exposure.

Several 3D cell cultures of the *In Model* have been prepared using decreasing amounts of MNPs to assess the iron amount internalized by the cells *(Figure 10)*. Our findings show that it is necessary to decrease 10 times the amount of iron added to the cells in the In Model in order to achieve an intracellular amount of MNPs of the same order of magnitude (1.8×10^{-8} mg Fe/cell) as for the *In&Out Model (Figure 10)* prepared with the highest MNPs concentration.

In order to evaluate the effect of the iron content on the cell death mechanism in the *In Model*, macrophages incubated with 10 times less MNPs than in the previous experiments have been placed in a 3D matrix (*In Model-lowFe*) and exposed to the AMF. In such scenario, 24 hours after the treatment, 50% of the cells are undergoing an early apoptotic death, 35% of cells are in a late apoptosis/necrosis stage and 15% of cells remain alive *(Figure 10)*. These results indicate a strong influence of the MNP concentration inside the cells on the cell death mechanism triggered by the MH treatment, as a higher MNP concentration triggers a necrotic pathway *(Figure 7)* while the lower MNP concentration triggers an apoptotic pathway.
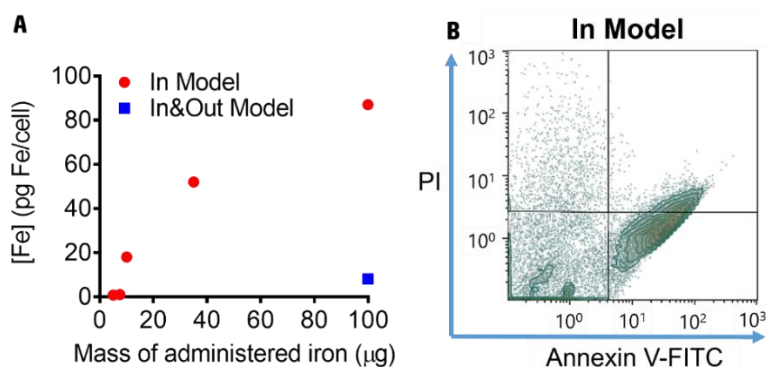
Figure 10. Effect of the iron concentration inside the cells. (A) Intracellular iron content for both 3D models as a function of the administered iron amount. (B) Flow cytometry analysis of the cells in the In Model-lowFe (incubated with 10 times less MNPs) 24 h after MH treatment.

It is important to highlight that the amount of MNPs internalized by the cells is able to modulate the cell death mechanism after the exposure to an AMF. However, we are still far from the complete control of the treatment. Some studies that compare the heating capacity of different MNPs when they are either in suspension or inside the cells, have shown a clear reduction of the SAR values when the MNPs are located in cellular vesicles.[130] However, a non-monotonic

relationship between MNP concentration and their heating capacity has been recently described.[104] The MNPs heating performance as a function of their packing density is a complex scenario where several factors (interactions,[104] viscosity of the medium,[382] collective behaviour, etc.) are responsible of causing either an increase or a decrease of the MNP heating capacity when decreasing the MNP concentration. Given that determining the local concentration produced as a result of the strong agglomeration of the MNPs within the cell is a complicated task, it is difficult to make predictions about the impact of the different doses on the resulting heating effects for an specific kind of material.

To evaluate the effect of such possible differences of the MNPs aggregation could have on their heating capacities, and therefore on the cell death mechanism triggered, the magnetic properties of both 3D models prepared with the higher concentration of MNPs have been measured, prior to any AMF exposure. The AC magnetic susceptibility in the 10–200 K temperature range has been measured for both models as this kind of measurements is able to detect the effect of dipolar interactions caused by local aggregation (when particles are closely packed, interparticle distances decrease and the dipolar interactions among particles increase).[383] Both samples display the characteristic features of the presence of superparamagnetic particles with a maximum in the in-phase susceptibility maxima accompanied by an out-of-phase susceptibility maximum at slightly lower temperatures.[384] The temperature dependence of the out-of-phase susceptibility, χ'' (T), shows a maximum located at slightly different temperatures for both models *(Fig. 11)*. Still, the differences observed in these two models do not justify a significant different MNP aggregation degree that could lead to different heating properties.[104] These results are in agreement with previous studies evaluating the aggregation of MNPs in macrophage models that had shown negligible dipolar interactions among particles even during intracellular MNP aggregation.[28]
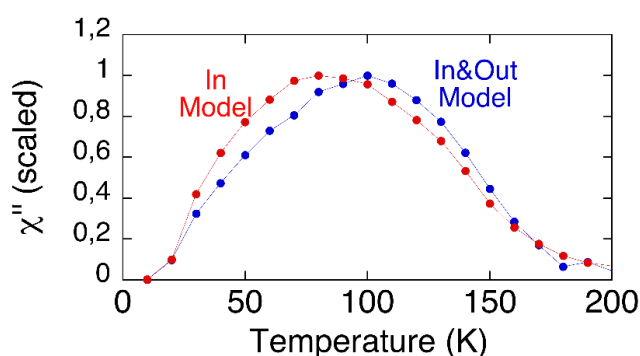
Figure 11. Magnetic characterization of the 3D cell cultures. Temperature dependence of the out-of-phase susceptibility scaled to their maximum of the two different models.

2.5. *The heterogeneous distribution of the magnetic nanoparticles within the 3D structure affects the rate of cell death.*

To evaluate the importance of the model on the MH treatment effect, the cell death rate observed for the *In Model-lowFe* has been compared with the *In&Out Model* (having a similar amount of internalized MNPs). In such scenario, although in both cases an apoptotic cell death mechanism is triggered, the rate of cell death is higher for the *In Model-lowFe* than for the *In&Out Model*. This is probably a consequence of the heterogeneous distribution of the MNPs amongst all the cells. It has been previously shown that, in the *In&Out Model* before the AMF exposure most of the MNPs are located at the outer areas of the 3D collagen structure *(Figure 6)* and a significant number of cells do not contain any MNPs *(Figure. 4)*. Therefore, only those cells containing MNPs and/or located in the outer areas of the 3D structure would feel the effect of the temperature increase, leading to a slower death rate. From all these results we can conclude that, even with a similar average amount of iron per cell, both models respond differently to the AMF exposure because of the initial location of the MNPs within the 3D structure.

These results highlight the importance of the development of 3D cell culture models that mimic the complex scenario of a tissue with inhomogeneous MNPs distributions. It can be foreseen that the results from studies in 2D cell cultures are probably providing misleading results that do not relate to the effect of the hyperthermia treatment as a consequence of the different incorporation of the MNPs by the cells. Furthermore, our results indicate that repetitions of the AMF exposure, once the MNPs are more homogeneously distributed throughout the 3D structure, or a delay between the MNPs administration and the AMF application to achieve a better distribution of the particles may result in a more effective treatment *in vivo*.

3. Conclusions

We have prepared two different 3D cell models using a collagen matrix to mimic different possible tumour scenarios. In both models, cells have been exposed to the same amount of nanoparticles, however, while in the *In Model*, the MNPs are only located inside the cells and homogeneously distributed amongst all of them, in the *In&Out Model* a heterogeneous distribution is achieved with particles heterogeneously distributed outside the cells and also cells with and without MNPs.

The time dependence of the MNP uptake on the *In&Out Model* has been evaluated. At the initial time point, most of the MNPs are located in the outer areas of the 3D structure and

therefore not all the cells have incorporated MNPs. Then, after 24h, all the cells from the 3D cell culture show the presence of MNPs inside their cytoplasm. In addition, it has been observed that this process of MNP uptake with time is faster after the exposure to the alternating magnetic field. These results are crucial for the design of *in vivo* hyperthermia treatments, as a delay between the MNP administration and the AMF exposure, or repeated cycles of AMF exposure, may improve the treatment effectiveness.

Our results demonstrate that MH induces the change in the collagen matrix that results in a more homogeneous distribution of the particles within the 3D cell culture. This observation may be of great relevance to use magnetic hyperthermia as a tool to disrupt the tumours extracellular matrix and improve the effect of other cancer treatments that have limitations to cross this barrier.

The development of these two different 3D models has allowed us to evaluate the effect of the nanoparticles concentration on the cell death mechanisms after the AMF exposure. In the *In Model*, that contains a higher amount of internalized MNPs, the main cell death mechanism observed 24 h after the MH treatment is necrosis, while in the *In&Out Model* and the *In Model-Low Fe* (containing a similar amount of MNPs as the *In&Out Model*) only apoptosis is observed at the same time point.

We have proved that the way MNPs are administered to the tumour area has a strong impact on the cell death mechanisms activated after the application of an AMF. MNPs administration route affects both the nanoparticle location within the 3D structure and concentration inside the cells and the accurate control of these two parameters is fundamental to develop an efficient and safe hyperthermia cancer treatment.

We believe that the development of these two 3D models, will have a strong impact in the study of other therapies based on magnetic nanoparticles, such as their use in photothermal therapies using laser sources.[130] However, several aspects such as the depth of the light penetration need to be optimized before.

4. Materials and Methods

4.1. *Magnetic nanoparticle synthesis, functionalization and characterization*

Iron oxide MNPs were synthesized by thermal decomposition in organic media based on a previously reported seed-mediated growth method [69] using iron (III) acetylacetonate (Fe(acac)$_3$) as a precursor.[314] This procedure rendered oleic-acid coated hydrophobic MNPs

that were then transferred to water using a protocol based on the conjugation of the oleic acid with a hydrophilic polymer (poly(maleic anhydride-alt-1-octadecene, PMAO, MW 30000–50000 Da) modified with TAMRA (tetramethylrhodamine 5(6)-carboxamide cadaverine (Anaspec, Seraing, Belgium), a fluorophore that allows the *in vitro* tracking of the MNPs.[314]

Then, the coated MNPs were functionalized with glucose to provide further stability in biological media. The coated nanoparticles (1 mg of iron) were incubated with 42 μmol of N-(3-dimethylaminopropyl)-N'-ethylcarbodiimide hydrochloride (EDC) and 30 μmol of 4-aminophenyl β-D-glucopyranoside in 250 μL of SSB buffer (50 mM of boric acid and 50 mM of sodium borate) at pH 9. After 3 h at room temperature, the excess of reagents was removed by washing the sample with phosphate-buffered saline buffer (PBS) at pH 7.4 in a centrifugal filter.[74] Finally, nanoparticles were passed through syringe filters with a pore size of 0.22 μm (Merck Millipore, Darmstadt, Germany).

Dynamic light scattering and ζ-potential measurements were performed in water and in complete Dulbecco's Modified Eagle's Medium GlutaMAX™ Supplement (cDMEM; Gibco®, Thermo Fisher Scientific) on a Malvern Zetasizer Nano-ZS, using ten runs per measurement and five replicates at 25 °C and pH 7.

Particle size and morphology were studied by Transmission Electron Microscopy (TEM) using a Tecnai T20 (FEI company, OR, USA) microscope operating at 200 kV. The sample was prepared by placing a drop of a diluted suspension of the MNPs in water onto a carbon-coated grid and allowing it to dry. Particle size was determined by manual measurement of 200 particles using the Digital Micrograph software.

The heating capacity of the MNPs was determined using a commercial Alternating Magnetic Field generator (DM100; Nanoscale Biomagnetics, Spain). A 1 mg Fe/mL MNP sample was placed in a closed container centred in the inductive coil. The AMF was applied for 5 min using a field amplitude of H = 20 kA/m, and a frequency of 829 kHz while the temperature was recorded using an optic fiber sensor incorporated in the equipment.

For the magnetic characterization, the MNPs liquid sample was allowed to dry at room temperature deposited into a piece of cotton wool that was subsequently placed into a gelatine capsule. Field dependent magnetization measurements were performed in a Quantum Design (USA) MPMS-XL SQUID magnetometer at 300 K with a maximum field of 5 T.

4.2. Sterility assay

Swab and Samplers Test Kits (Merck Millipore) were used for the quality control of the MNPs sterility. The microbiological analysis aimed at detecting bioburden levels of bacteria, yeast or mold (Coli-Count™, Heterotrophic Plate Count and Yeast and Mold Samplers). The MNPs were tested in the sampler membrane, covered with growth medium for specific microorganism, at the common dilution used for the *in vitro* studies following the incubation conditions specified by the manufacturer (Coli-Count 35 °C, 22-24 h; Yeast and Mold 28-32 °C, 48-72 h; Heterotrophic Plate Count (HPC) Sampler 25-35 °C, 48-72h). After the incubation, the filter surface was examined with an illuminator to identify the presence of microbial colonies.

4.3. Cell line

The murine macrophage RAW–264.7 cell line (ATCC® TIB71™) was cultured and maintained in cDMEM supplemented with 10 % fetal bovine serum (FBS, Invitrogen), 100 U/mL penicillin G (sodium salt) and 100 µg/mL streptomycin sulfate (Invitrogen) at 37 °C in a humidified atmosphere at 5 % CO_2. To detach the cells, a two-step protocol was followed trying to enhance the cells viability. First, cells were incubated with Trypsin EDTA solution (Sigma Aldrich) for 5 minutes at 37 ºC and then, the cells were scrapped from the flask. Finally cells were collected in fresh cDMEM.

4.4. Formation of 3D cell culture models

3D cell culture gels were prepared as follows. First, 250 µL of a $4x10^6$ cells/mL suspension in complete culture medium were mixed with fetal bovine serum (Invitrogen) and Modified Eagle's Medium 10x (MEM w/Earle´s salts, w/o Glutamine, w/o Sodium Bicarbonate, First Link UK Ltd) in a 1:1:1 volumetric ratio. The resulting cell suspension was added to an ice-cold mixture of 1.25 mL rat tail Collagen type I (Protein concentration 2.05 mg/mL in 0.6 % acetic acid, First Link UK Ltd) solution and 0.5 mL 0,1 % sodium hydroxide (NaOH) solution. Then, some drops of NaOH were added while gently shaking until the medium turned pink. After that, the final mixture was added quickly to a 24 well plate (600 µL / well, $\approx 10^6$ cells / well, Thermo Scientific Nunc Cell-Culture) and incubated at 37 °C for 30 min. After collagen gellification, 0.5 mL of complete culture medium was added per gel.

Two different strategies for the incubation with magnetic nanoparticles were followed. The first model where nanoparticles are located only inside the cells - In Model- was prepared by incubating detached cells ($4x10^6$ cells/mL in complete medium) with the MNPs (0.2 mgFe/mL)

during 1 h at 37 ºC and then washing the particles that had not been uptaken by centrifugation (161 rcf, 6 min) twice. After that, the cells were used to form the collagen gel.

The second strategy produced the 3D cell culture where the particles are located both inside and outside the cells - In&Out Model, and also have a heterogeneous localization within the 3D structure. To achieve this, the 3D model containing the cells was formed as described before. Just after collagen solidification, 500 μL of a MNP solution of 0.2 mg Fe/mL in complete medium were added and incubated at 37 °C for 1 h. After that, the supernatant was removed, the 3D cell culture was washed twice, and 500 μL of complete culture medium were added to the 3D model.

4.5. MNPs toxicity.

2D cell cultures were incubated during 1 h with increasing amounts of iron (10, 20 50, 100 and 200 μg) prepared in a final volume of 500 μL. 3D cell cultures were incubated with 100 μg of iron during 1 h. Cell viability was assessed by flow cytometry.

4.6. Magnetic Hyperthermia treatment

Before starting the AMF exposure and during the treatment, 3D cell cultures were thermalized at 37 °C using a water bath pump (Stryker - Medical Devices & Equipment Manufacturing Company) connected to a water tubing jacket. Then, the 3D cell cultures were exposed to an AMF during 30 min at a frequency of 377.5 kHz and field amplitude of 13 kAm^{-1} using a commercial AMF generator (DM3, nB nanoscale Biomagnetics, Zaragoza, Spain).

4.7. Flow cytometry studies

Cells were released from the 3D cell cultures using a treatment with collagenase type I (isolated from *Cl. histolyticum* lyophilized, non-sterile, Gibco™ Thermo Fisher Scientific) at 2 mg/mL in HBSS (Hank's Balanced Salt Solution) during 30 min at 37 ºC. Then, cells were washed by centrifugation (161 rcf, 6 min) and re-suspended in PBS (Phosphate Buffer Saline pH=7.4). All samples were analysed in a Gallios™ Flow Cytometer (Beckman Coulter) and the data interpreted with Kaluza 1.5a Software (Beckman Coulter).

To determine the MNPs uptake, cells re-suspended in PBS at a concentration of 2.5×10^4 cells/mL were analysed by flow cytometry.

To study the cell viability, cells were re-suspended in 1X Annexin V Binding Buffer (10 mM Hepes/NaOH (pH=7.4) 140 mM NaCl, 2,5 mM CaCl$_2$) at a concentration of 10^6 cells/mL. Then, 5 μl of the Annexin V-FITC (Fluorescein Isothiocyanate) and 5 μL of Propidium Iodide

(PI) were added to 100 µL of cell suspension and incubated at room temperature for 15 minutes in the dark (FITC-Annexin V Apoptosis Detection Kit). After the incubation period, 400 µL of 1X Annexin binding buffer was added and the sample was analysed by flow cytometry.

To evaluate the cell cycle, cells were fixed with cold ethanol (70%) during 24 h and, after that, incubated with propidium iodide during 30 min in dark for analysis by flow cytometry. The data obtained was treated with the MODFIT LT 3.0 Verity Software (G0/G1, G2/M and S indicate the cell cycle phase while sub-G0/G1 refers to the proportion of apoptotic cells.)

4.8. Confocal microscopy

To study the MNP internalization, the 3D cell cultures were fixed during 20 min with 500 µL of paraformaldehyde (4%). Then, the nuclei were stained with DAPI (4′,6-diamidino-2-phenylindole) and the cytoskeleton with Phalloidin488. An Olympus FV10i Confocal Laser Scanning Microscope equipped with 405 nm (18 mW), 473 nm (12.5 mW) and 635 nm (10 mW) lasers was used to acquire images of the cells. The images were then processed using Olympus Fluoview FV10-ASW 3.1 Viewer software (Olympus Canada, Markham, ON, Canada). The three dimensional projection images of the 3D cell cultures were obtained with a Zeiss LSM 880 Confocal Microscope with a 63x/1.40 Plan Apochromat objective. The laser sources used were 458 nm, 488 nm (Argon Ion), 561 nm (DPSS- Diode-pumped solid state). ZEN Microscope and Imaging Software were used for the image analysis.

4.9. Magnetic characterization

3D cell cultures were freeze-dried and placed into gelatine capsules for their magnetic characterization. AC (alternating current) magnetic susceptibility measurements were performed in a Quantum Design (USA) MPMS-XL SQUID magnetometer with an AC amplitude of 0.41 Oe, in the temperature range between 10 and 200 K and at a frequency of 11 Hz.

4.10. Iron quantification

Iron concentration was determined using a standard colorimetric procedure.[82] For the MNPs, an aliquot was digested with aqua regia for 15 min at 60 °C and diluted with Milli-Q water.

For the cells, 3D cell cultures were treated with collagenase (2 mg/mL) 30 min at 37 °C and after that the cells were spun down in a mini spin centrifuge. The digestion of the cells was performed heating with HNO_3 (Panreac) and then with H_2O_2 (Panreac) (both steps at 90ºC and during 1 h each). A calibration curve was prepared by dilution of an Iron standard solution 1

mg/mL Fe in 2% HNO_3 (Acros Organics, USA). The digested samples were incubated at room temperature for 15 min after the addition of KOH (4 N), 4,5-dihydroxy-1,3-benzenedisulfonic acid disodium salt monohydrate (Tiron) and sodium phosphate buffer (0.2 M pH=9.7). Finally, sample absorbance (480 nm) was measured on an UV/Vis spectrophotometer (Thermo Scientific Multiskan™ GO MA, USA) and compared to a calibration curve.

4.11. Statistical analysis

Data are expressed as mean ± SD of a minimum three biological replicas. Statistical significance of difference in means was performed using GraphPad Prism v7.00 Student´s test and one-way ANOVA test were used for the analysis of the data. The confidence interval was 95%. Bonferroni post-test was used to determine which means differed.

5. Associated content

Complementary results are supplied as Supporting Information:

Sample	Suspension media	Hydrodynamic size (nm)	PDI	ζ – potential (mV)
MNP@PMAO-TAMRA	Water	48	0.4	-36
MNP@PMAO-TAMRA@Glucose	Water	67	0.4	-13
MNP@PMAO-TAMRA@Glucose 1h After cDMEM incubation	Cell culture media	55	0.5	-7.81

Table S1. Hydrodynamic size (Intensity) and ζ – potential of magnetic nanoparticles coated with PMAO and TAMRA (MNPs@PMAO-TAMRA) measured in water and the same particles after the functionalization with Glucose (MNPs@PMAO-TAMRA@Glucose) measured in water and in cell culture media (cDMEM).

	[Fe]$_{located\ inside\ the\ cells}$ (mg Fe/cell)	
Iron administered	**In-model**	**In&Out Model**
100 µL	8.7×10^{-8}	8.1×10^{-9}
35 µL	5.2×10^{-8}	Below DL
10 µL	1.8×10^{-8}	Below DL
7.5 µL	1.0×10^{-9}	-
5 µL	8.1×10^{-10}	-
2.5 µL	Below DL	-
1 µL	Below DL	-

Table. S2. Iron concentration located inside the cells in both models after the incubations with different amounts of magnetic nanoparticles.
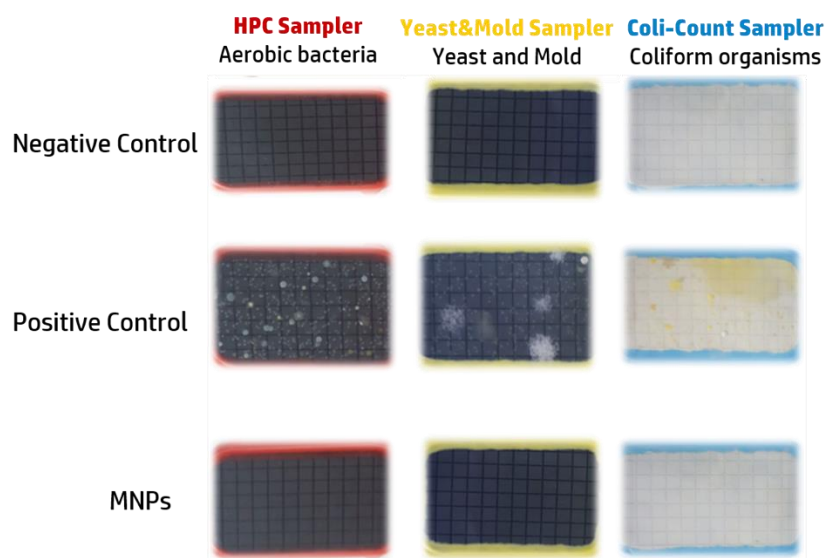
Figure S1. Sterility assay. (Red) Heterotrophic Plate, (Yellow) Yeast and Mold and (Blue) Count Coli-Count™ Samplers. A sample of garden soil has been used as the positive control and sterile water (W4502 Sigma) has been used as negative control. Particles coated with PMAO and TAMRA and further functionalized with glucose (MNPs@PMAO-TAMRA@Glucose) had not shown evidence of microbial colony.
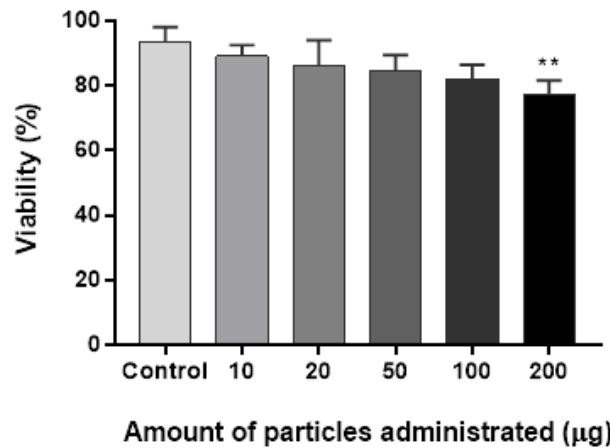
Figure S2. MNPs toxicity assay. 2D cell cultures of macrophages have been incubated during 1 h with different amounts of MNPs corresponding to 10, 20 50, 100 and 200 µg of iron. Cell viability has been evaluated by Flow Cytometry using an Apoptosis Detection Kit (Annexin V-FICT/PI) . Only a significant reduction on the cell viability respect to control (cells without MNP)has been observed at the highest concentration (** p < 0.01) One way ANOVA Analysis followed Dunnett's multiple comparisons test . GraphPad Prism 7.00.
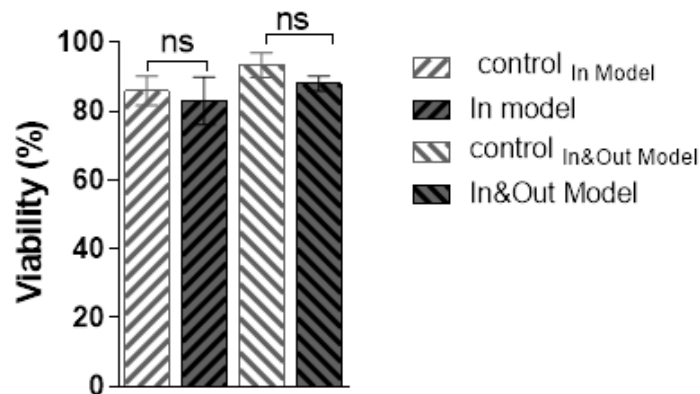
Figure S3. MNPs toxicity assay evaluated in 3D models. Cell viability has been evaluated by Flow Cytometry (Apoptosis Detection Kit Annexin V-FICT/PI) in the two different 3D models studied after the incubation during 1 h of MNPs corresponding to 100 µg of iron. No significant reduction on the cell viability has been observed in these conditions ([ns] p > 0.05) One way ANOVA Analysis followed Dunnett's multiple comparisons test. GraphPad Prism 7.00.
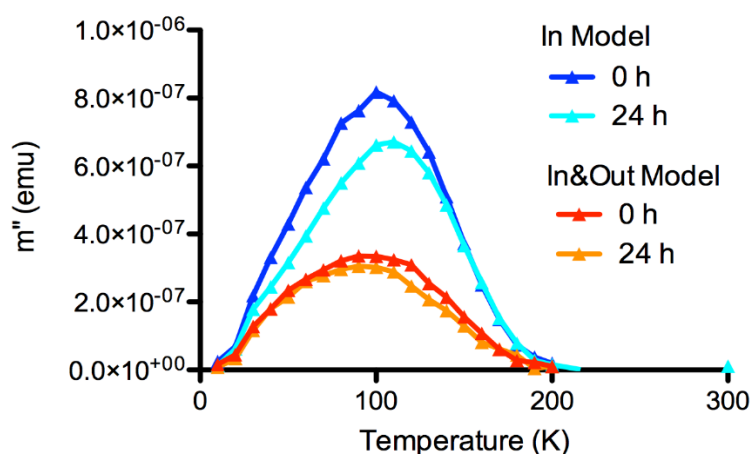
Figure S4. Magnetic characterization of the 3D models. Temperature dependence of the out-of-phase susceptibility for both models at two different times after the AMF application. The height of the susceptibility maximum acts as a surrogate measurement of the MNPs concentration, indicating the higher amount of particles in the In-model. Magnetic measurements of the 3D cell cultures indicate that the MNPs concentration in the In-Model is three times higher. It should also be noted that in the In&Out Model, both the MNPs inside and outside the cells are detected, so the differences in the amount of internalized MNPs are, therefore, higher.

6. Acknowledgment

3.3 Aportes al tema, visión crítica y perspectivas de futuro

La sensibilización de la matriz extracelular mediante la aplicación de hipertermia local ha sido estudiada desde hace décadas para mejorar la eficacia terapéutica de los fármacos anticancerígenos convencionales.[385-388] En este sentido, uno de los enfoques más novedosos que ofrece la hipertermia magnética para mejorar las terapias actuales contra el cáncer, es la posibilidad de generar un efecto terapéutico dual.[336] De manera tal, que a la vez que se induzca citotoxicidad sobre las células tratadas, sea posible afectar la integridad de la matriz extracelular.[158, 332] El especial interés en la modulación de la matriz extracelular para la terapia antitumoral, [377] tiene sus bases en el papel dominante que desempeña esta estructura en los diferentes procesos que determinan la carcinogénesis (*Figura 1.8*; sección 1.4), tales como la conexión y migración celular, la regulación y estimulación de la diferenciación tumoral, así como la expresión de proteínas específicas implicadas en la inhibición farmacológica e inmunosupresión observada en tumores.[198, 389-391] A diferencia de las estrategias farmacológicas basadas en la administración sistémica de enzimas modificadoras de la matriz extracelular y agentes antifibróticos;[195] la actuación controlada de nanopartículas bajo estímulos externos ajustables como el AMF, tiene grandes potencialidades para la generación de daños altamente localizados sobre componentes específicos de la matriz extracelular (ej. colágeno),[332] que a su vez pueden ser adaptables al contexto clínico del paciente y a la combinación con otras modalidades terapéuticas. Sin embargo, a pesar de sus prometedoras y múltiples ventajas, se ha estudiado muy poco acerca de cómo esta modulación matricial, inducida por la estimulación de las nanopartículas en presencia de un campo magnético, influye en la respuesta del sistema biológico ante el estímulo hipertérmico.

Trabajos publicados por Kolosnjaj-Tabi y colaboradores entre 2014 y 2017,[309, 332] demostraron, en un modelo murino de xenoinjerto de carcinoma epidermoide, que el calor generado por las nanopartículas magnéticas tiene un impacto directo sobre la reorganización de las fibras de colágeno de la matriz tumoral; lo que mejora notablemente la distribución intratumoral de las partículas incluso después de una única dosis de hipertermia. Sin embargo, aunque valiosos, los xenoinjertos presentan limitaciones importantes. En primer lugar, en modelos de xenoinjerto, son las células del huésped las que producen la matriz extracelular, y esto es un factor significativo a tener en cuenta, ya que la matriz en estos casos se conforma principalmente por células del tejido tumoral humano y células epiteliales provenientes del ratón (*Figura 1.10*; sección 1.4); lo que pueda plantear serias implicaciones con respecto a las interacciones entre el tumor y las células del estroma, así como en la señalización celular,

dependiendo del modelo tumoral analizado.[197, 377] Por otro lado, el ensayo con animales requiere de instalaciones especializadas y, en su mayoría costosas (véase sección 1.4.2), que en muchos casos no se encuentran accesibles para todos los grupos de investigación. Además de plantear importantes desafíos científicos y éticos, por lo que debe ser completamente justificada la consistencia y utilidad del estudio para la realización de la investigación.[217, 392-393] Por estas razones, un objetivo primordial para alcanzar el máximo potencial de la hipertermia magnética *in vivo*, es el desarrollo y optimización de modelos predictivos *in vitro*, que permitan estudiar los diversos cambios mecánicos y celulares inducidos por el calor, desde las diferentes perspectivas fisiológicas que pueden encontrarse en los ensayos clínicos y preclínicos.

En este contexto, la novedad y la importancia de nuestro estudio radica en el desarrollo de una metodología de cultivo 3D, sencilla pero fisiológicamente relevante, que sirve de base para la evaluación y comprensión de la naturaleza de la interacciones célula-matriz extracelular, desde dos perspectivas de reconocida relevancia para la clínica: (i) una localización de nanopartículas totalmente intracelular; objetivo anhelado durante muchos años tanto en la práctica preclínica como clínica para lograr un concentración más específica del calor dentro de las células y (ii) una localización más heterogénea, que no se restringe solo a las células, sino también a la matriz extracelular que las rodea; efecto más cercano a lo observado *in vitro* e *in vivo* después de la administración del nanomaterial magnético. En este trabajo, demostramos la capacidad de las nanopartículas magnéticas de inducir una hipertermia subletal terapéuticamente relevante, con potencialidades para afectar: (i) tanto la estructura de la matriz extracelular, hecho que resultó en una evidente redistribución de las nanopartículas en el gel, y en consecuencia en una mejora de su internalización celular; (ii) como la viabilidad celular, a través de la inducción de mecanismos de muerte tanto apoptóticos como necróticos. En resumen, los resultados de este estudio evidenciaron que los hidrogeles basados en colágeno I son modelos adecuados para generar un entorno *in vitro* de matriz extracelular, que permita estudiar el efecto de la hipertermia en un ambiente biomimético y fisiológicamente relevante. Hallazgos que sentaron las bases y promovieron los posteriores estudios *in vitro* sobre matrices tridimensionales realizados en esta tesis.

Hasta el momento de la publicación de nuestro trabajo, solo encontramos un estudio *in vitro* que abordaba este efecto dual de la hipertermia magnética desde el cultivo 3D, y se encontraba específicamente dirigido a estudiar los efectos de la terapia térmica sobre las metástasis pulmonares del cáncer de mama triple negativo.[317] Un estudio posterior al nuestro también

abordó la remodelación de la arquitectura del colágeno en modelos de esferoides basados en cáncer pancreático.[211] Sin embargo, en el caso particular de administrar nanopartículas para producir calor, una desventaja importante del estudio de la respuesta mecánica y biológica al tratamiento hipertérmico desde la generación de modelos tumorales específicos, radica en que los resultados observados para un tipo de tumor, no suelen ser fácilmente extrapolables a tumores de otros tipos, debido a las notables diferencias en la capacidad de endocitar nanopartículas que presentan las diferentes líneas celulares tumorales. Por esta razón, en nuestro trabajo, para abordar el efecto de la distribución y concentración de las nanopartículas, en la modulación de las respuestas de las células y su entorno a la hipertermia magnética, seleccionamos como sistema modelo de internalización células RAW264.7, procedentes de una línea celular de macrófagos peritoneales murinos. La elección de trabajar con una línea modelo de captación celular, como base para la comprensión de los mecanismos que median estos efectos, nos permitió modular de manera estandarizada diferentes rangos de concentración intracelular de nanopartículas, para evaluar y comprender su impacto en los efectos observados en respuesta al tratamiento térmico. La línea celular RAW264.7 ha sido previamente utilizada en la literatura como modelo de internalización de nanopartículas magnéticas de óxido de hierro; por lo que las múltiples vías endocíticas involucradas en la internalización y degradación de las partículas en los compartimentos intracelulares, sus posibles mecanismos de excreción, así como la toxicidad dependiente de la dosis, han sido ampliamente descritos para estas células.[315, 394-397]

Interesantemente, nuestros resultados demostraron que el mecanismo de muerte celular en respuesta a la terapia térmica cambiaba de apoptosis a necrosis dependiendo de la concentración intracelular de nanopartículas. En células con altas concentraciones de partículas, el tratamiento térmico indujo una rápida necrosis; mientras que cuando la concentración intracelular de nanopartículas era 10 veces menor, las células morían por apoptosis. Sin embargo, aunque pueda parecer evidente que un incremento en la internalización de nanopartículas promueva dosis térmicas más elevadas, y con ello diferentes vías de muerte celular; algunos autores han demostrado que la viabilidad celular puede disminuir significativamente después de la terapia térmica, sin que se observen cambios perceptibles en la temperatura global del área objetivo.[398-400] Este efecto denominado "hot spot",[401] enfatiza una visión donde la inducción de la muerte celular puede ser menos dependiente de la cantidad de material magnético usualmente requerido para aumentar considerablemente la temperatura macroscópica de las células, y estar más relacionado con un perfil de temperatura local

generado en las proximidades de las nanopartículas. Sin embargo, los mecanismos subyacentes en las múltiples respuestas de las células al efecto térmico intracelularmente localizado, no han sido ni comprendidos, ni dilucidados totalmente. Razón por la cual, en esta tesis decidimos evaluar la influencia de la concentración y distribución intracelular de las nanopartículas sobre las diferentes vías de señalización de muerte celular regulada inducida por la hipertermia magnética; tema que se desarrolla en detalle en el próximo capítulo.

CAPÍTULO 4 ·
HIPERTERMIA MAGNÉTICA
Y MUERTE CELULAR

4.1 Introducción ampliada al tema

La respuesta molecular y celular al calentamiento local inducido por la hipertermia magnética es diversa (véase sección 3.1); y el alcance de la misma depende de numerosos factores que van desde el tiempo de exposición y la temperatura alcanzada durante la terapia térmica, hasta las características físico-químicas del material magnético utilizado como agente de calentamiento.[99] En este contexto, los mecanismos de muerte celular pueden cambiar de "programado" (ej. apoptosis) a "accidental" (ej. necrosis) por encima de cierto umbral de temperatura. [321, 336, 402] Sin embargo, se ha planteado que la distinción semántica entre la muerte celular "programada" (implícitamente fisiológica) y "accidental" (implícitamente patológica) no es totalmente realista, debido a que en muchos casos es simplemente la intensidad de la señal o el nivel de estrés generado, lo que determina si la muerte celular ocurre a través de una ruta más apoptótica o más necrótica.[403] Por otro lado, aunque el término "muerte celular programada" se ha utilizado de manera generalizada durante años como un sinónimo de apoptosis, en contraste con la necrosis considerada como una consecuencia "accidental" del estrés no fisiológico; se ha demostrado que la necrosis también puede ser un evento programado tanto en su curso como en su aparición.[403-405]

En la literatura, la muerte celular ha sido clasificada acorde a múltiples criterios: según sus características morfológicas (apoptótica, necrótica o autofágica), aspectos funcionales (programada o accidental), criterios enzimológicos (con y sin la participación de distintos tipos de proteasas), o características inmunológicas (inmunogénica o no inmunogénica).[403-407] Debido a la gran diversidad de denominaciones utilizadas para describir las distintas modalidades de muerte celular, el Comité de Nomenclatura sobre Muerte Celular comenzó a realizar recomendaciones periódicas a partir del año 2005,[403-405, 408-410] que abogaban por el empleo de criterios más unificados sobre la definición y formulación de los distintos tipos de

muerte celular, en aras de facilitar la comunicación y comparación de los resultados obtenidos dentro de la comunidad científica. En este sentido, las alteraciones morfológicas macroscópicas que identifican a la muerte celular, han sido utilizadas históricamente para su agrupación en tres modalidades diferentes:[404]

(i) *Apoptosis* o muerte celular de tipo I. Las células en apoptosis se caracterizan por un rápido estrechamiento del citoplasma y la pérdida de contacto con sus células vecinas debido alteraciones en las moléculas de adhesión de la membrana plasmática. En el núcleo, el material genético se compacta (condensación de la cromatina/ picnosis) y es segregado hacia la membrana nuclear para su fragmentación (cariorrexis). La condensación del citoplasma induce ampollas en la membrana plasmática, que culminan con la formación de pequeñas vesículas aparentemente intactas, comúnmente conocidas como cuerpos apoptóticos. Los cuerpos apoptóticos son captados de manera eficiente por las células vecinas con actividad fagocítica, y finalmente son degradados dentro de los lisosomas. Señales bioquímicas como la exposición de fosfatidilserina, fosfolípido que usualmente se mantiene en la cara interna de la membrana plasmática, hacen posible el reconocimiento molecular de las células apoptóticas para garantizar la fagocitosis.

(ii) *Autofagia* o muerte celular de tipo II. La característica principal de la muerte celular autofágica es la vacuolización masiva del citoplasma de las células, que también culmina con la captación fagocítica y la consiguiente degradación lisosomal.

(iii) *Necrosis* o muerte celular tipo III. Las células necróticas suelen mostrar una marcada inflamación citoplasmática (oncosis), con el consiguiente abultamiento de los orgánulos que lo constituyen; acompañada de la ruptura de la membrana plasmática y una condensación moderada de la cromatina. Su característica distintiva es la liberación del contenido celular al microambiente circundante, en ausencia de compromiso fagocítico y lisosomal evidente.

Sin embargo, a pesar de que la comunidad científica aún mantiene una clasificación general de las modalidades de muerte celular, conservadora y morfológica; detrás de cada uno de estos mecanismos subyacen complejas vías de señalización que deben ser evaluadas cuidadosamente.[405, 409-411] Por lo cual, incluso morfologías de muerte celular aparentemente similares, a menudo ocultan un elevado grado de heterogeneidad funcional, bioquímica e inmunológica, dependiendo del estímulo que desencadena la muerte de las células. En este sentido, se ha propuesto una clasificación actualizada de las modalidades de muerte celular, que engloba un conjunto de mecanismos "regulados", agrupados acorde al estímulo molecular

que induce a las células a la muerte. Estos mecanismos incluyen rutas de apoptosis intrínseca e extrínseca, necroptosis, ferroptosis, muerte celular dependiente autofagia, muerte celular dependiente de lisosomas, entre otras *(Figura 4.1)*.[410] Cada una de estas modalidades de "muerte celular regulada" se desencadena y amplifica mediante cascadas de señalización molecular, que presentan un elevado grado de interconectividad entre ellas, por lo aún se mantienen bajo estudio para lograr su completo esclarecimiento. En marcado contraste con la "muerte celular accidental", mediada por la erradicación instantánea y catastrófica de las células expuestas a graves daños de naturaleza química, mecánica o física (ej. dosis térmicas elevadas); la "muerte celular regulada" tiene sus bases en una maquinaria molecular controlada, lo que implica que puede ser modulada (es decir, retrasada o acelerada) mediante intervenciones terapéuticas como el tratamiento térmico a dosis subletales o moderadas con hipertermia magnética.
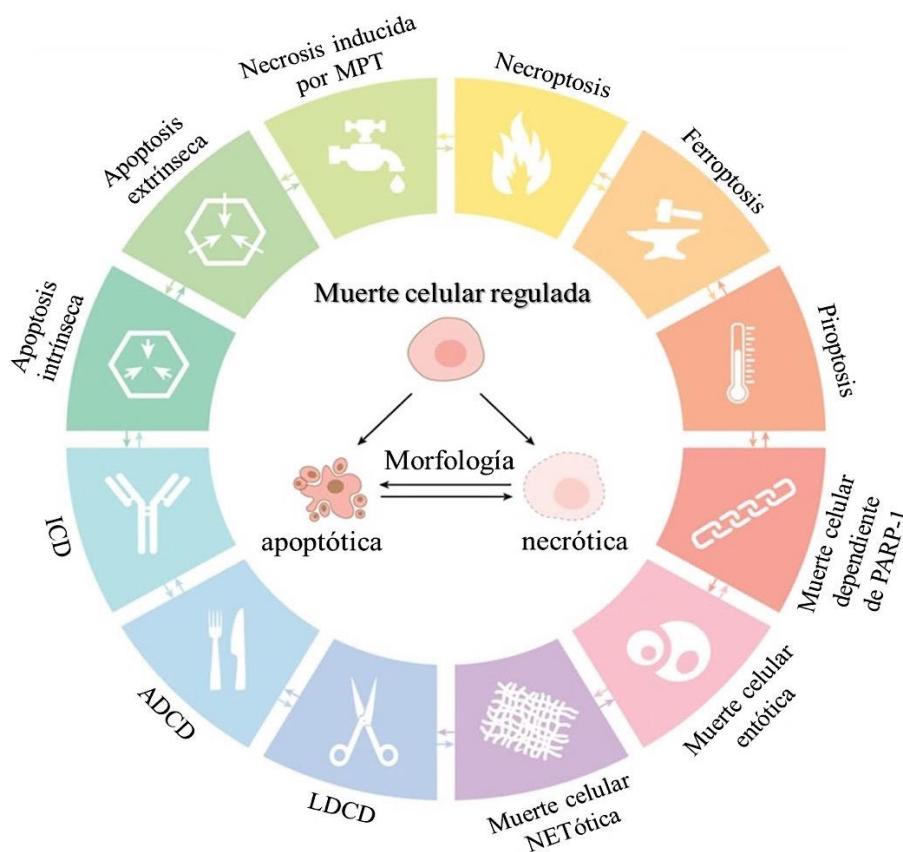
Figura 4.1 Principales modalidades de muerte celular regulada. Adaptado: Cell Death & Differentiation 2018, 25 (3), 486-541.[410] Copyright (2020). Abreviaturas: Muerte celular dependiente de autofagia (ADCD- del inglés "autophagy-dependent cell death"); Muerte celular inmunogénica (ICD- del inglés immunogenic cell death); Muerte celular dependiente de lisosomas (LDCD- del inglés "lysosome--dependent cell death"); Transición de permeabilidad mitocondrial (MPT- del inglés "mitochondrial permeability transition"); Trampas extracelulares de neutrófilos (NET- del inglés "neutrophil extracellular traps") ; Poli [Adenosín Difosfato-ribosa] polimerasa-1 (PARP-1- del inglés "Poly [Adenosine DiPhosphate-ribose] polymerase 1")

De manera general, los estudios tanto *in vitro* e *in vitro* demuestran que las principales rutas que median la muerte celular después del tratamiento con hipertermia magnética son la apoptosis y la necrosis. Usualmente, dosis térmicas inferiores a 45 °C inducen la activación de rutas de muerte apoptóticas, mientras que la necrosis suele ser desencadenada en condiciones de hipertermia más severas.[99, 120, 242, 244, 317-318, 321, 412] A diferencia de los mecanismos anteriores, el papel de la autofagia en la muerte celular mediada por hipertermia es cuidadosamente considerado. Al respecto, aunque algunos estudios sugieren que la autofagia inducida en respuesta al calentamiento celular puede regular favorablemente vías de señalización relacionadas con la apoptosis o determinados componentes de la ruta de necrosis; también se conoce que participa activamente en la protección de las células al estrés por calor, contribuyendo a inhibir el efecto letal del tratamiento hipertérmico para garantizar la supervivencia celular. [397, 413-416]

En el contexto de la aplicación terapéutica de la hipertemia magnética, particularmente en enfermedades como el cáncer, la apoptosis es uno de los mecanismos citotóxicos más estudiados. Esto se debe a que la inducción de necrosis se asocia a menudo con daños patológicos irreversibles, así como a una potente actividad pro-inflamatoria local; que puede no ser deseada dependiendo del tipo de tratamiento, o contribuir a apoyar el crecimiento tumoral si no es promovida de manera controlada.[415, 417-418] Mientras que la autofagia, además de ser un proceso lento y espacialmente restringido a las zonas del citoplasma donde ocurre la vacuolización, también puede constituir una defensa celular contra el estrés agudo.[403, 414] La apoptosis, en cambio, representa un programa de muerte celular activamente controlado, que garantiza una rápida y efectiva eliminación de las células dañadas, bajo condiciones fisiológicas estrictamente reguladas.[403, 405, 410]

En su representación más clásica, la apoptosis se desencadena casi exclusivamente cuando se activan las caspasas, una familia de enzimas de tipo proteasas, caracterizadas por la presencia de residuos de cisteína (Cys) en su sitio activo.[419] Las caspasas normalmente se encuentran presentes en todas las células animales como enzimas precursoras inactivas (pro-caspasas), que se activan durante la apoptosis por escisión proteolítica en un residuo conservado de ácido aspártico (Asp). Una vez activadas, proceden a la destrucción de las células apoptóticas desde el interior celular, a través de la proteólisis de las proteínas diana, siempre después de un residuo de Asp; hecho que les confiere su pseudónimo de "*caspasas*" (*c*isteinil-*a*spartato protea*sas*).[420] En función de su posición en la cascada de señalización apoptótica, las caspasas son clasificadas como: *iniciadoras (-2, -8, -9, -10)* o *efectoras (-3, -6 ,-7)*.[421-423] Las *caspasas*

iniciadoras se activan por auto-proteólisis (dimerización), ya sea a través de adaptadores (ej. Caspasa -8) o por la translocación a compartimentos específicos en el citosol (ej. Caspasa -9), en respuesta a diversos daños celulares *(Figura 4.2)*.[424-426] Por otro lado, las *caspasas efectoras* son las principales responsables de los cambios morfológicos y bioquímicos que ocurren en las células apoptóticas; y son activadas por las caspasas iniciadoras, ya que no presentan capacidad de auto-proteolizarse.[423, 427] Este proceso donde la activación inicial de una caspasa provoca una reacción en cadena que conduce a la activación de las otras, se le conoce como cascada de activación de las caspasas, y tiene un rol fundamental en la amplificación de las señales pro-apoptóticas.[421] En este sentido, existen dos cascadas principales para la activación de las caspasas, que a su vez determinan dos vías diferentes de inicio de la apoptosis: *intrínseca* o *extrínseca (Figura 4.2)*.[428] La activación de una vía u otra depende de diversos factores, entre los que destaca el tipo de célula, y la naturaleza e intensidad del estímulo lesivo aplicado.

Figura 4.2 Cascada de señalización de la apoptosis dependiente de caspasas. Abreviaturas: Factor-1 activador de las proteasas apoptogénicas (Apaf-1- del inglés "apoptosis protease-activating factor-1"); Ligando de muerte (DL- del inglés "death ligand"); Receptor de muerte (DR- del inglés "death receptor"); Dominio de muerte (DD- del inglés "death domain") de las proteínas adaptadoras; Dominio efector de la muerte (DED- del inglés "death effector domain"); Complejo de señalización inductor de muerte (DISC- del inglés "death-inducing signaling complex").

La vía *intrínseca* involucra a la mitocondria, y puede ser iniciada por una amplia variedad de perturbaciones intracelulares *(Figura 4.2)*. Su paso crítico desencadenante es la permeabilización de la membrana externa mitocondrial, que es controlada por los miembros de la familia de proteínas BCL-2, cuya principal función es el control de la estabilidad mitocondrial, permitiendo o inhibiendo el flujo de proteínas apoptogénicas desde la mitocondria.[429] La familia BCL-2 se encuentra constituida por proteínas homólogas, algunas de las cuales evitan la apoptosis (anti-apoptóticas), mientras que otras la promueven (pro-apoptóticas).[429-430] Miembros anti-apoptóticos como el propio BCL-2, localizados en la membrana externa de la mitocondria, actúan bloqueando la oligomerización de proteínas pro-apoptóticas como BAX y BAK para preservar la viabilidad celular ante factores de estrés.[430] La regulación positiva de BAX y BAK es asociada con la permeabilización de la membrana mitocondrial y la liberación de proteínas apoptogénicas desde el espacio intermembrana al citosol.[431] Alternativamente, ciertos miembros pro-apoptóticos como BID pueden actuar promoviendo la oligomerización e inserción en la membrana de BAX,[432] y con ello, contribuir con la salida desde la mitocondria de proteínas como el Citocromo c y Apaf-1, que una vez en el citosol, se unen en presencia de trifosfato de desoxiadenosina (dATP -del inglés "deoxyadenosine triphosphate"), atrayendo a la pro-Caspasa iniciadora -9 para su activación en el complejo supramolecular denominado apoptosoma, lo que inicia la cascada de activación *intrínseca* de las caspasas *(Figura 4.2)*.[433] Se ha demostrado que durante la aplicación de dosis térmicas subletales de hipertermia magnética, la inducción de altos niveles de ROS,[434] puede sensibilizar eficazmente a las células a la *muerte apoptótica intrínseca* como resultado de los daños en el ADN, oxidación de proteínas, privación de factores de crecimiento y el consecuente daño mitocondrial.[323, 435] La evidencia experimental también demuestra que el tratamiento con hipertermia magnética a temperaturas entre 41-45 °C puede incrementar la permeabilización mitocondrial, y con ello la liberación de factores pro-apoptóticos intrínsecos como el Citocromo c, seguido de la consiguiente activación de las Caspasas iniciadoras y efectoras -9, -7, -6 y -3.[436-439]

La *vía extrínseca*, por otro lado, es controlada por los "receptores de muerte"; una familia de citoquinas que se caracteriza por la presencia de dominios transmembrana en su estructura, lo que les permite establecer conexiones con el espacio extracelular (recibiendo señales pro-apoptóticas desde el exterior y de las células vecinas), a la vez que hace posible la transducción de la señal apoptótica al interior celular *(Figura 4.2)*. [440-441] Dos familias de receptores se han identificado en el contexto de la muerte celular: la proteína FAS y el factor de necrosis tumoral

(TNF- del inglés "tumor necrosis factor").[442-444] Ante perturbaciones micro-ambientales extracelulares, tales como la pérdida de la matriz extracelular o liberación de citoquinas ("ligandos de muerte"), desencadenadas en respuesta a lesiones celulares agudas como el elevado estrés térmico; dichos receptores son activados por la unión con su ligando correspondiente. La activación del receptor induce su trimerización, y con ello el reclutamiento de proteínas adaptadoras intracelulares y caspasas, desencadenando la formación de un complejo de señalización inductor de muerte (DISC- del inglés "death-inducing signaling complex").[426] En este complejo supramolecular, las pro-caspasas iniciadoras (-8 y/o -10) son convertidas a su forma activa a través de la auto-proteólisis de su denominado "dominio efector de la muerte", para activar subsecuentemente a las pro-caspasas efectoras de la muerte celular (ej. Caspasa -3) *(Figura 4.2)*.[445-447] La vía de señalización *extrínseca* también puede generar señales hacia la mitocondria. La Caspasa iniciadora -8, una vez activa, puede fragmentar a BID, miembro pro-apoptótico de la familia BCL-2, generando un fragmento proteico (tBID) que se transloca a la membrana mitocondrial, y en consecuencia también puede activar la vía *intrínseca*.[448-449] Evidencias experimentales tanto *in vitro* como *in vivo* han demostrado que la exposición de las células a condiciones de hipertermia moderada (43-45 °C) puede inducir cambios significativos en la expresión de genes apoptóticos implicados en la señalización de la *vía extrínseca*, tales como *FAS y TNF-a*.[437, 439, 450] También se han observado niveles significativamente elevados de las Caspasas -8, -7, -6 y -3, específicamente después del tratamiento con hipertermia magnética a dosis térmicas superiores a 43 °C.[437, 439] Otros resultados también indican la activación de las Caspasas -8, -9, el receptor TNFR1 (- del inglés "TNF receptor type 1") y proteínas adaptadoras como TRADD (- del inglés "TNFR1-associated death domain") y FADD (- del inglés "FAS-associated death domain"), tanto a 43 °C como a 45 °C, lo que sugiere la activación de las *vías apoptóticas* tanto *extrínsecas* como *intrínsecas* en respuesta a la hipertermia magnética.[439]

Por otro lado, recientemente se ha planteado el papel de la permeabilización de la membrana lisosomal en las vías de señalización apoptóticas inducidas por la hipertermia magnética.[451-453] De manera general, la implicación de los lisosomas en la muerte celular comenzó a ser considerada hace solo un par de décadas; a partir de observaciones experimentales que desafiaban el papel exclusivo de las caspasas en los diferentes mecanismos de muerte celular regulada.[414] Durante muchos años, la ruptura del lisosoma fue considerada un cambio celular que ocurría solamente en las últimas etapas de la muerte, debido a que la ultraestructura lisosomal suele observarse intacta en las células apoptóticas analizadas bajo microscopía

electrónica.[414] Sin embargo, a principios de los años 2000, otros estudios revelaron que en lisosomas con una aparente ultraestructura normal, parte de las enzimas lisosomales eran filtradas al citosol, lo que sugería que la permeabilización lisosomal no solo podía ocurrir de manera temprana en diversos mecanismos de muerte celular, sino que también podía ser la causa desencadenante de la misma.[414, 454] A nivel bioquímico, la permeabilización de la membrana lisosomal, resulta en la liberación de su contenido al citoplasma, incluidas las enzimas proteolíticas de la familia de las catepsinas, cuyo papel en la muerte celular ha sido más que demostrado.[455-458] Al respecto, ha sido propuesto que niveles de estrés moderados pueden desencadenar una liberación limitada del contenido lisosomal al citoplasma, seguido de apoptosis u otro mecanismo de muerte celular regulada.[410] Mientras que un estrés de alta intensidad puede conducir a una ruptura lisosomal generalizada y a una rápida muerte celular accidental *(Figura 4.3)*. [454, 459]
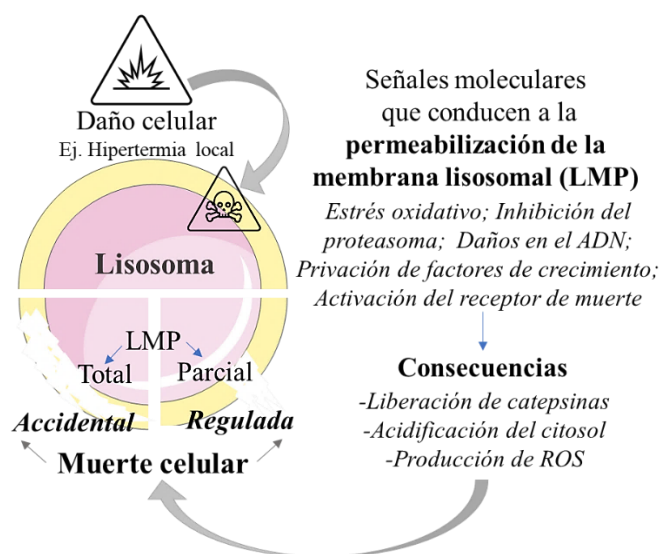
Figura 4.3 Causas y consecuencias de la permeabilización de la membrana lisosomal que pueden desencadenar la muerte celular. Abreviaturas: Permeabilización de la membrana mitocondrial (LMP- del inglés "lysosome membrane permeabilization")

Los mecanismos moleculares implicados en la regulación de la muerte celular por permeabilización lisosomal aún no han sido completamente esclarecidos, pero sí existen evidencias experimentales que demuestran la participación del lisosoma en las diferentes rutas de señalización de la apoptosis. En general, el mecanismo propuesto por el cual las proteasas lisosomales promueven la vía *intrínseca* de la apoptosis, se asocia a su actuación directa sobre las mitocondrias para inducir y/o potenciar la disfunción mitocondrial, y con ello, con la

liberación de factores apoptogénicos como el Citocromo c.[458] Se ha demostrado además que las proteasas lisosomales pueden promover o potenciar la ruta mitocondrial, ya sea escindiendo, activando, así como facilitando la translocación o liberación de diferentes mediadores de la apoptosis, como caspasas y proteínas de la familia BCL-2.[457] Por otro lado, la generación de ROS en la mitocondria debido a la permeabilización de la membrana mitocondrial- dependiente de catepsina y del ROS lisosomal, puede a su vez retroalimentar al lisosoma para maximizar la permeabilización lisosomal y, al mismo tiempo, el daño mitocondrial*(Figura 4.4)*.[460] Los efectos letales de la permeabilización lisosomal y las catepsinas no están limitados a la activación de la vía de apoptosis *intrínseca*. Alternativamente, la permeabilización lisosomal también puede participar en la ejecución de la muerte celular en respuesta a estímulos apoptóticos de la vía *extrínseca*. Se ha planteado que la catepsina D podría escindir y activar BID en el ambiente ácido del compartimento endo-lisosomal después de la internalización del receptor TNFR1,[461] lo que sugiere que la expresión de BID también podría servir como un conector entre las señales de muerte celular de los lisosomas y las mitocondrias.[455] Otros autores han demostrado que la unión de ligandos de muerte, como el TNF-α , con su receptor, paso que media la activación de la Caspasa-8 (principal responsable de escindir Bid) también puede favorecer la permeabilización de la membrana lisosomal y la liberación de la catepsina B *(Figura 4.4)*. [462] En este contexto, numerosos estudios han planteado que en función del tipo de células y la intensidad del estímulo lesivo, la participación lisosomal en la apoptosis puede ser distinta.[463] En el caso particular de la hipertermia magnética, se ha observado que bajo acción de un AMF, las nanopartículas acumuladas en los lisosomas actúan como "hot spot" aumentando la temperatura muy localmente, lo que mejora la producción de ROS lisosomal a través de la reacción de Fenton.[453] Esta sobreproducción de ROS promovida por el tratamiento térmico, induce peroxidación lipídica de la membrana del lisosoma promoviendo su permeabilización, y la consecuente liberación de su contenido proteolítico *(Figura 4.4)*.[451-453] El mecanismo de activación de la muerte celular apoptótica dependiente de lisosoma es complejo, y aún se continúa estudiando para esclarecer el papel de los componentes del contenido lisosomal en la activación de las diferentes rutas de señalización.[463] En este sentido, los estudios de hipertermia magnética intra-lisosomal, aunque pocos,[451-453, 464] han planteado que la inducción de apoptosis puede depender de una liberación temprana de las proteasas lisosomales, especialmente las de tipo catepsinas, debido a un elevado incremento de la temperatura local alrededor de los lisosomas.[453, 464] Por otro lado, los efectos citotóxicos de la permeabilización lisosomal, al parecer, también podrían depender de la activación de las diferentes rutas de señalización

apoptótica, u otras vías de muerte celular regulada, y contribuir a la amplificación de la señal de muerte.[452] Los resultados experimentales obtenidos hasta el momento sugieren que cada uno de estos dos mecanismos pueden estar implicados en la muerte celular regulada inducida por la hipertermia magnética, pero esto aún no se ha determinado con mayor precisión.
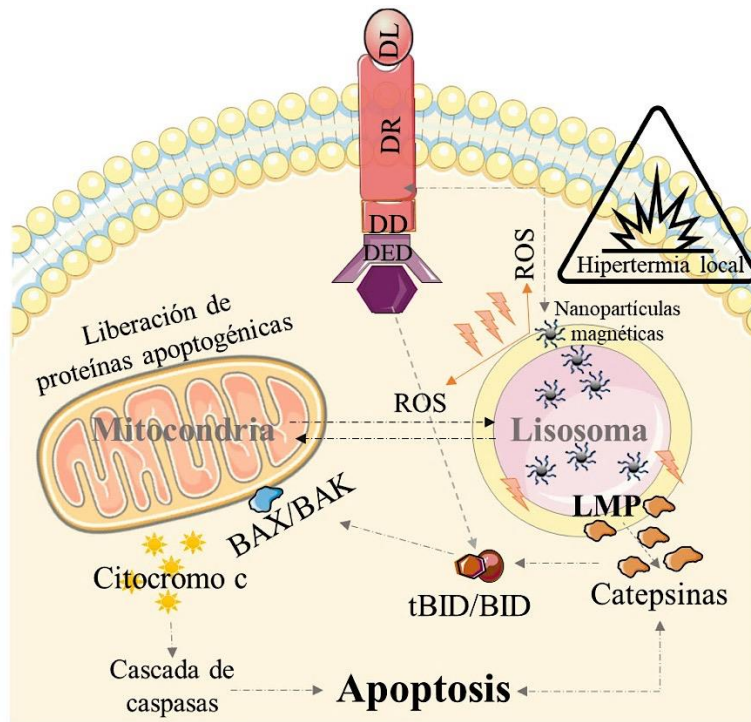
Figura 4.4 Representación esquemática de la posible implicación de la permeabilización de la membrana lisosomal en la señalización de la muerte celular apoptótica mediada por hipertermia magnética.

4.2. Intracellular number of magnetic nanoparticles modulates the apoptotic death pathway after magnetic hyperthermia treatment.

State of the article: Under revision

Lilianne Beola[1], Laura Asín, PhD[1], Catarina Roma-Rodrigues, PhD[2]; Yilian Fernández-Afonso[1], Raluca M. Fratila, PhD[1]; David Serantes, PhD[3]; Sergiu Ruta, PhD[4]; Roy W. Chantrell, PhD[4]; Alexandra R. Fernandes, PhD[2]; Pedro V. Baptista, PhD[2]; Jesús M. de la Fuente, PhD[1];Valeria Grazú, PhD[1] and Lucía Gutiérrez, PhD[5]

[1]Instituto de Ciencia de Materiales de Aragón (ICMA), CSIC/Universidad de Zaragoza, C/ Pedro Cerbuna 12, 50009, Zaragoza, Spain. Centro de Investigación Biomédica en Red de Bioingeniería, Biomateriales y Nanomedicina (CIBER-BBN), Spain.

[2]UCIBIO, Departamento de Ciências da Vida, Faculdade de Ciências e Tecnologia, Universidade Nova de Lisboa, Campus da Caparica, 2829-516 Caparica, Portugal

[3]Applied Physics Department and Instituto de Investigacións Tecnolóxicas, Universidade de Santiago de Compostela, 15782 Santiago de Compostela, Spain

[4]Department of Physics, University of York, Heslington, York YO10 5DD, United Kingdom

[5]Department of Analytical Chemistry, Universidad de Zaragoza and CIBER-BBN. Instituto Universitario de Nanociencia de Aragón (INA), Edificio I+D, C/ Mariano Esquillor Gómez, 50018, Zaragoza, Spain

Authors contributions: Lilianne Beola is the principal author; Yilian Fernández-Afonso made the magnetic measurements of this work; Catarina Roma-Rodrigues, PhD, Alexandra R. Fernandes, PhD and Pedro V. Baptista, PhD supervised the molecular biology experiments of this work during the research fellowship in Lisbon of Lilianne Beola; David Serantes, PhD, Sergiu Ruta, PhD and Roy W. Chantrell PhD made the theorical calculations of this work; Raluca M. Fratila, PhD synthetized the MNPs used in this work; Jesús M. de la Fuente PhD is the head of Bionanosurf group; Lucía Gutiérrez, PhD, Laura Asín, PhD and Valeria Grazú, PhD are the thesis supervisors. All the authors contributed to the discussion of the results.

Abstract: Magnetic hyperthermia is a cancer treatment based on the exposure of magnetic nanoparticles to an alternating magnetic field in order to generate local heat. In this work, 3D cell culture models were prepared to observe the effect that a different number of internalized particles had on the mechanisms of cell death triggered upon the magnetic hyperthermia treatment. Macrophages were selected by their high capacity to uptake nanoparticles. Intracellular nanoparticle concentrations up to 7.5 pg of Fe per cell were measured both by elemental analysis and magnetic characterization techniques. Cell viability after the magnetic hyperthermia treatment was decreased to < 25% for intracellular iron contents above 1 pg per cell. The theoretical calculations of the intracellular thermal effects that occurred during the alternating magnetic field application suggested a localized temperature increase in smaller vesicles. In contrast, the predicted effect on the global cell temperature was much lower. Different apoptotic routes were triggered depending on the number of internalized particles. At the low magnetic nanoparticle concentrations tested (below 1 pg of Fe per cell), the intrinsic route was the main mechanism to produce apoptosis, as observed by the high *Bax/Bcl-2* mRNA ratio and low caspase-8 activity. In contrast, at higher concentrations of internalized magnetic nanoparticles (1 – 7.5 pg of Fe per cell), the extrinsic route was favored to trigger apoptotic events, observed through the increased activity of caspase-8. Nevertheless, both mechanisms may coexist at intermediate iron concentrations. Knowledge on the different mechanisms of cell death triggered after the magnetic hyperthermia treatment is fundamental to understand the biological events activated by this procedure and their role in its effectiveness.
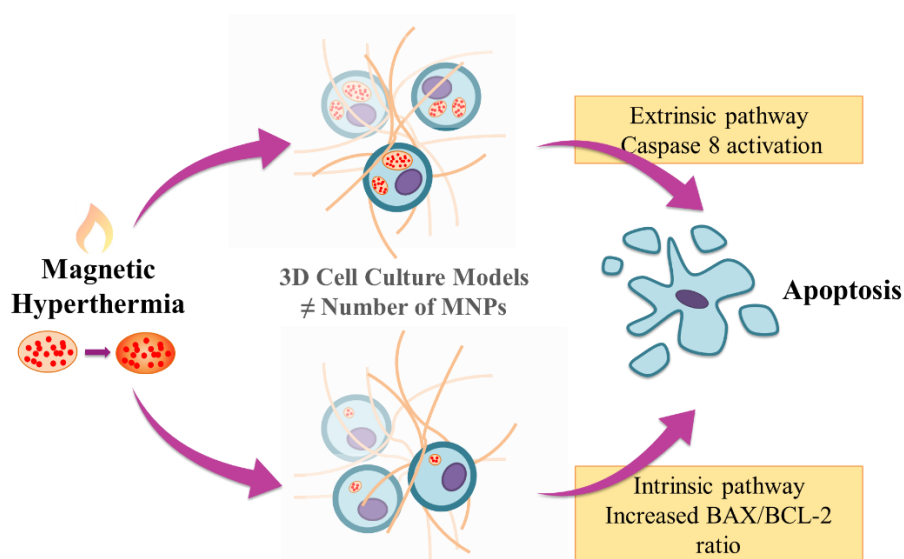
Keywords: iron oxides, nanoparticles uptake, magnetic hyperthermia, apoptosis, cell death pathways, 3D cell culture, macrophages

1. Introduction

Magnetic hyperthermia (MH) has been proposed as a promising strategy for cancer treatment.[128] Iron oxide nanoparticles are the most commonly used material for this purpose, given their biocompatibility associated to their physical and chemical properties.[254] Upon exposure to an external alternating magnetic field (AMF), the local temperature near the magnetic nanoparticles (MNPs) increases, which in turn may trigger cancer cell death. Nevertheless, there is still a lack of control on the cell death mechanisms that are induced depending on the heat released during the treatment.[129]

It is fundamental to understand the type of cell death mechanism triggered by the MH treatment, as they might induce distinct cancer cell responses. When analyzing the effect of the global temperature increase in the mechanisms of cell death, it has been previously described that at high temperatures (above 55 ºC) necrosis - an accidental cell death (ACD) - is the main cell death pathway, causing a structural dismantling of the cells and releasing their intracellular content in an uncontrolled manner. In such case, the lack of molecular activation of specific molecular pathways could result in undesired inflammatory and cytotoxic responses. In contrast, at lower temperatures (42-47 ºC) regulated cell death (RCD) mechanisms are the main mechanisms that are triggered by a molecular machinery leading to a preservation of the plasma membrane integrity and, therefore, not inducing inflammatory response.[99, 120, 242, 321, 336, 465] Mixed events - RCD and ACD - could also be occurring in cell populations depending on the temperature stimuli. Therefore, a careful control of the temperature should be achieved during hyperthermia treatments in order to prevent ACD and promote RCD.

In the particular case of using nanomaterials to produce heat, as in the case of MH, the mechanisms involved in the cell death signaling have not completely been described yet. In general, it is accepted that many iron oxide nanoparticles are often internalized by the cells remaining in intracellular vesicles, such as endosomes or lysosomes, depending on the time since the internalization.[228, 466-468] Then, upon exposure to the AMF, hot spots can be produced inside the cell, leading to non-homogeneous temperature profiles. In fact, it has been previously described that during the magnetic hyperthermia treatment a local temperature increase is observed near the particles, while no global temperature increase occurs.[398-400] The energy released from the particles may cause lysosomal membrane permeabilization (LMP).[452-453] As a consequence, the release of the lysosome proteolytic content to the cytosol occurs, inducing cell death that could even cause a bystander effect impacting surrounding cells. [454, 456, 459, 469]

Such cell death may occur by different routes (included in both RCD and ACD categories) depending, for example, on the magnitude of the membrane permeabilization.

The possibility of modulating the different cell death pathways would allow to control their associated biological consequences. For instance, the immune system activation might be different. Immunogenic cell death (ICD), described initially as an exclusive cell death mechanism to protect the body against pathogens, is nowadays known as a cell defense mechanism in the absence of pathogens. In fact, apart from necrosis that has been classically considered as immunogenic, other types of cell death such as regulated necrosis [470] and apoptosis [366, 407, 471] trigger also immune response because of the generation of danger-associated molecular patterns (DAMPs). It has also been demonstrated that caspases involved in the intrinsic apoptosis pathway offer an immunosuppressing effect, silencing the immune response of this pathway.[371-372] Cell death mechanisms are not exclusive, and it seems reasonable to consider that a specific stimulus could trigger a mixture of unpredictable events. All this new knowledge makes it very interesting to try to elucidate the death routes triggered under different conditions of MH treatment, because of the biological implications, like the immunogenicity and the final effectiveness of the treatment.

In a previous work we observed the effect of the MNP concentration on the cell death mechanisms after the MH treatment.[336] In cells with a higher amount of MNPs, necrosis was observed 24h after exposure to the AMF. In contrast, when a lower amount of MNPs were localized inside the cells, cell death was mainly induced by the apoptosis pathway. Other studies also described the cell death mechanisms associated with heat production during the magnetic hyperthermia treatment.[99, 412, 472] However, little has been evaluated about the influence of MNP concentration on the molecular mechanisms that determine the different apoptotic pathways triggered during the treatment.

In the present work, we used a 3D cell culture model previously reported,[336] as this kind of model mimics in a more realistic way the cellular environment than 2D cell cultures.[317, 473] A highly phagocytic macrophages cell line (RAW264.7) [315] was used and cells challenged with different amounts of MNPs. MNP uptake was evaluated by flow cytometry (FC), confocal microscopy, Inductively Coupled Plasma Optical Emission Spectrometry (ICP-OES) and magnetometry. Apoptosis induction 24h after the exposure to AMF was also evaluated by flow cytometry. Computational analysis was performed to evaluate the different heating performance between in-water experimental SAR characterization and the heating performance

after cell internalization. In addition, after the MH treatment, *Bcl-2* and *Bax* gene expression as well as caspase-8 activity were determined through Reverse Transcriptase quantitative polymerase-chain-reaction (RT-qPCR) and a protein colorimetric assay, respectively. This approach was designed to elucidate the molecular mechanisms of apoptosis induced by the MH treatment as a function of the number of internalized particles. The possibility of controlling the activation of such mechanisms could be the basis to establish the optimal conditions of the MH treatment and to predict the future efficacy of the therapy.

2. Results & Discussion

2.1 Preparation and characterization of MNPs

The synthesis and functionalization of 11 nm superparamagnetic iron oxide MNPs coated with PMAO (poly(maleic anhydride-alt-1-octadecene) and functionalized with glucose (Glc) was discussed in a previous published work.[336] Their core size *(Figure 1)*, low polydispersity, magnetic properties and low cytotoxicity,[336] previously demonstrated their suitability for *in vitro* MH studies and, therefore, we chose the same material for the present work. The polymeric coating with PMAO allowed the transference of the MNPs from organic solvents used during the synthesis to aqueous medium. In this study, PMAO was modified with the fluorophore, TAMRA (carboxytetramethylrhodamine), to be used for FC and confocal microscopy studies.[82, 314] The glucose functionalization prevented nanoparticle aggregation in cell culture medium supplemented with Fetal Bovine Serum (FBS) allowing good cell nanoparticle internalization (Supporting Information, *Figure S1*).
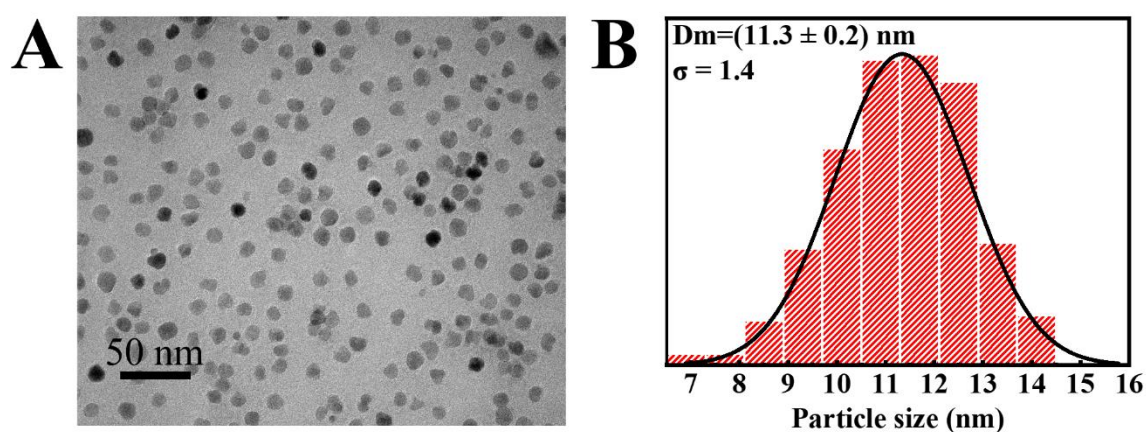
Figure 1. (A) TEM image of the MNPs. (B) Particle size distribution analysis.

The efficacy of the polymer coating (PMAO modified with TAMRA), as well as the glucose functionalization was verified by analysis of electrophoretic mobility (Rf) and ζ potential. The MNP characterization evidenced a decrease on the MNP negative charge from -22.0 ± 0.1 mV, before functionalization, to -9.0 ± 0.6 mV after glucose addition. In agreement with these changes, a decrease in MNP mobility during electrophoresis was observed after the glucose functionalization, in agreement with previously reported functionalization (Supporting Information, *Figure S1*). The hydrodynamic size of the Glc-functionalized particles suspended in PBS at pH = 7 was 85 ± 7 nm.

The specific absorption rate (SAR) was also evaluated before the *in vitro* MNP studies to determine the heating efficiency in suspension. The SAR value was 104 W/g Fe ([Fe] = 1 mg/mL, H= 20 kA/m, f= 829 kHz). Although the SAR measurement in suspension may not be representative of the physical behavior of the MNPs once internalized in the cells, when combined with theoretical analysis it allows estimation of the MNPs heating capacity in the conditions used for the *in vitro* experiments, as will be described below.

2.2 Validation of the cell culture models with different amounts of MNPs per cell

As mentioned earlier, one of our main objectives was to evaluate the effect of different amounts of MNPs internalized by the cells on the efficacy of MH treatment and the pathway triggered towards cell death. For that purpose, the generation of a reproducible 3D cell culture model was a better option to mimic the *in vivo* environment compared to the classical 2D cell culture models.[197-198, 375, 473] Our 3D model was based on a highly phagocytic cell type, such as the macrophages cells (RAW264.7) that present a high capacity to phagocyte the MNPs due to their biological functions,[30, 474] and a collagen matrix, which is a major component of the extracellular matrix in the tumor tissue. In addition, the use of collagen provided a very easy system to release the cells from the 3D culture for a-posteriori analysis, through a fast, simple and low cytotoxic enzymatic procedure.[336]

Our approach was based on the preparation of 3D cell culture models containing different amounts of particles per cell, named M1, M10, M25, M50, M75 and M100 depending on the iron amount used to treat the cells. To achieve this, cells in suspension (0.5 mL) were incubated with different MNP amounts for 1 h (Total amount of iron = 1, 10, 25, 50, 75 and 100 µg). Then, cells were washed to remove all the extracellular MNPs. After that, cells were transferred to the 3D cell culture. The nanoparticles uptake by the cells was evaluated and quantified through ICP-OES, magnetic measurements and FC.

Intracellular iron quantification was performed by ICP-OES. As expected, increasing amounts of total intracellular iron were obtained when increasing the concentration of MNPs during the incubation step *(Figure 2A, Table 1)*. The highest intracellular iron amount per cell was 7.5 pgFe/cell, which is in good agreement with data published about MNPs internalized in similar phagocytic cell lines.[465] In addition, the intracellular iron content was also determined through AC magnetic susceptibility measurements and subsequent data analysis *(Figure 2B, S2)*. This technique, contrary to ICP-OES measurements, allowed quantifying the iron forming part of the MNPs, as it can be distinguished from other iron-containing species.[475] In order to do that, the height of the signal of the out-of-phase susceptibility corresponding to the relaxation phenomenon of the particles was compared to that of the original particles. The iron amount per cell calculated by both methods (ICP-OES and AC magnetic susceptibility analysis) was very similar *(Figure 2A)*, indicating that most of the intracellular iron was in the form of MNPs. These results allowed calculating the internalized number of particles, N, for each model *(Table 1)*. Interestingly, the detection limit of the magnetic quantification was lower, allowing to determine ≈ 0.1 pg of iron (in the form of MNPs) per cell for the M1 model *(Figure 2A)*.
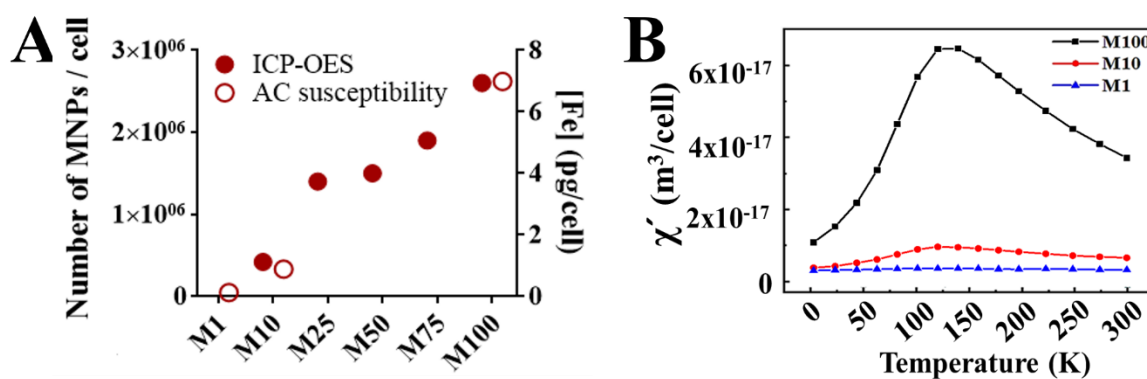
Figure 2. (A) Iron amount from MNPs per cells determined by ICP-OES and magnetic measurements. (B) Temperature dependence of the in-phase component of the AC magnetic susceptibility in three selected models.

These two techniques (ICP-OES and magnetometry) provided average data for the cell fraction. Nevertheless, it could not be assumed that the distribution of MNPs was homogeneous among all cells. As such, we further evaluated the particle distribution by confocal microscopy and flow cytometry.

Flow cytometry showed that almost all the cells incubated with the highest amounts of MNPs had internalized MNPs (about 94 % of the total number of cells for models M50, M75 and M100) *(Figure 3, Table 1)*. When decreasing the amount of MNPs during incubation, a lower percentage of cells contained MNPs. In particular, in M25 and M10 models the percentage of cells containing MNPs decreased to 86 % and 57 %, respectively. Furthermore, in M1 only 6% of the cells had incorporated MNPs *(Figure 3A)*.
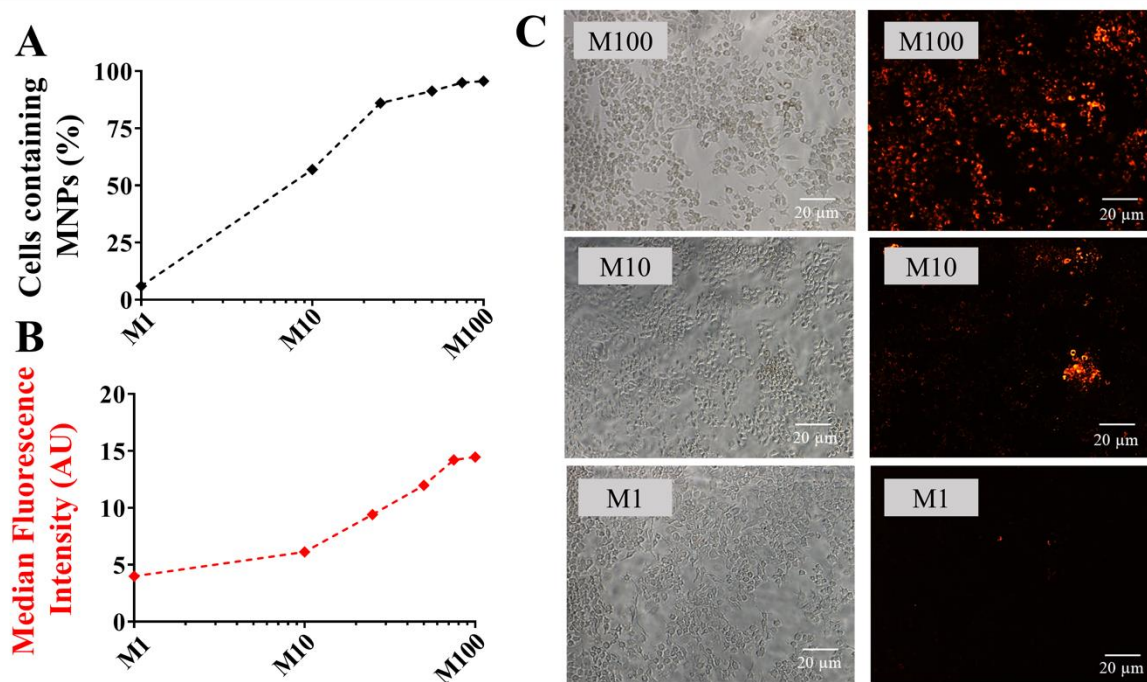
Figure 3. (A) Percentage of MNPs-loaded cells and (B) Median Fluorescence Intensity values of the different models studied. Data obtained from flow cytometry analysis. (C) Bright field (left) and fluorescent red channel (right) images of cells culture from four of the models studied. Scale bar: 20 µm.

The median fluorescence intensity (MFI) data showed that, although the percentage of cells containing MNPs was similar at the highest concentrations, their corresponding MFI kept increasing as a function of the amount of MNPs during incubation (MFI $_{M50}$=11.9; MFI $_{M75}$=14.2; MFI $_{M100}$=14.5) *(Figure 3B)*. These data indicated that a higher amount of MNPs were internalized per cell for increasing iron concentrations, in agreement with the quantification assays performed.

These results further agreed with the fluorescence and optical microscopy images *(Figure 3C)*. Images showed that for the system with the highest number of internalized particles (M100), all cells contained large aggregates of particles, associated to the entrapment of the MNPs inside

intracellular vesicles, probably lysosomes, as previously demonstrated by our group using similar particles with the same coating and functionalization.[371] The images from the model M10 showed that, in general, a lower fluorescence signal coming from the MNPs per cell was detected. In addition, cells with no apparent signal from the particles (or at least under the detection limits of the technique) were also observed. With this technique, it was also possible to determine that the intracellular distribution of the MNPs was not homogeneous as some cells contained large aggregates of particles.

Taken together, the ICP-OES, the magnetic characterization, the FC and the microscopy supported the achievement of 3D cell culture models with different internalized number of particles. Nevertheless, it should be considered that for the system with the lowest number of internalized particles, a significant number of cells did not contain any particles.

Model	Fe amount administered (µg)	MNP-loaded cells (%)	[Fe] internalized (pg/cell)	Number of particles/cell
M100	100	95.6	7.5	2.6×10^6
M75	75	94.9	5.4	1.9×10^6
M50	50	91.3	4.4	1.5×10^6
M25	25	86.1	3.9	1.4×10^6
M10	10	57.0	1.2	4.2×10^5
M1	1	6.0	<MCD	<MCD

Table 1. Summarized values related to the magnetic nanoparticles uptake in the different models analyzed. The percentage of MNP-loaded cells has been calculated from flow cytometry data. The amount of internalized iron and the corresponding number of particles per cell has been calculated from the ICP-OES measurements.

In summary, these results confirmed a correlation between the MNP amount administered during the incubation time and the number of MNPs taken up by cells, although intracellular distribution was not homogeneous. Despite some limitations of this model, we had the capability to control the number of particles inside the cells, a key development to study the effect of the magnetic hyperthermia treatment on cell death as a function of the intracellular heat production.

2.3 Effect of the magnetic hyperthermia treatment on the cell death

Cell viability was evaluated 24h after the exposure of the 3D cell cultures, previously incubated with the different amounts of MNPs (M1 to M100), to mild hyperthermia conditions (H= 13 kA/m; ƒ= 377 kHz; t= 30 min) *(Figure 4A)*. As control, cell viability was also assessed in cells

not exposed to MNPs or AMF, in cells only exposed to AMF and in M100 cells without AMF *(Figure S3)*. Cell viability after AMF treatment decreased drastically with increasing amounts of internalized MNPs *(Figure 4A)*. The combination of AMF treatment with the highest amounts of MNPs (M75 and M100) led to a high reduction of cell viability (down to 9 ± 4 % of viable cells for both models). It should be noted that for both controls (M100 cells not exposed to AMF or cells only exposed to AMF) a small reduction of cell viability was observed (≈ 80 % viable cells, *Figure S3*), indicating that the high reduction observed for M100 is due to the combination of both treatments, MNPs and AMF. Exposure of M10, M25 and M50 models to AMF induced also a significant loss of cell viability (23 ± 5, 20 ± 2 and 16 ± 2 % of viable cells respectively, *Figure 4A*). Finally, in model M1, a less severe effect was observed (65 ± 7 % of viable cells, *Figure 4A*). In order to further understand the mechanism underlying the loss of cell viability induced by the combination of AMF and MNPs, we evaluated apoptotic markers.

The number of viable cells, apoptotic (early and late) cells and necrotic cells was monitored by FC using two fluorescent markers: Annexin V (a cellular protein that binds to phosphatidylserine (PS)) modified with FITC (Fluorescein isothiocyanate) and propidium iodide (PI).[378] The loss of cellular membrane asymmetry is an early event in the apoptotic process and can be measured through the detection of PS residues in the outer side of the membrane, marked with Annexin V. The paired labelling with PI, a DNA intercalator agent which is not able to penetrate intact membranes, was used to detect the plasma membrane disruption typical of late apoptotic / necrotic events.

The FC analysis demonstrated a strong correlation between the amount of intracellular MNPs and the response to AMF (Figs. 4 and S3). A general trend was observed when analyzing the percentages of both early apoptotic (AnnV+PI-) and late apoptotic (AnnV+PI+) cells after AMF *(Figure 4B)*. An increase in the percentage of AnnV+ cells was observed with the increase of internalized MNPs *(Figure 4B)*. The increase of AnnV+PI+ cells was particularly high for the M50, M75 and M100 models, with 7, 9 and 15% of cells in the late apoptotic state respectively (Fig. 4B). Interestingly, almost no viable cells were observed when cells were incubated with the highest amount of MNPs (M100) and exposed to AMF *(Figure 4B)*. Once again in M100 cells in the absence of AMF we observed a high percentage of viable cells *(Figures 4C and S3)* indicating that the loss of viability and apoptosis induction was due to the treatment combination. Additionally, for all the tested conditions almost no cells in necrosis were observed *(Figures 4 and S3)*.
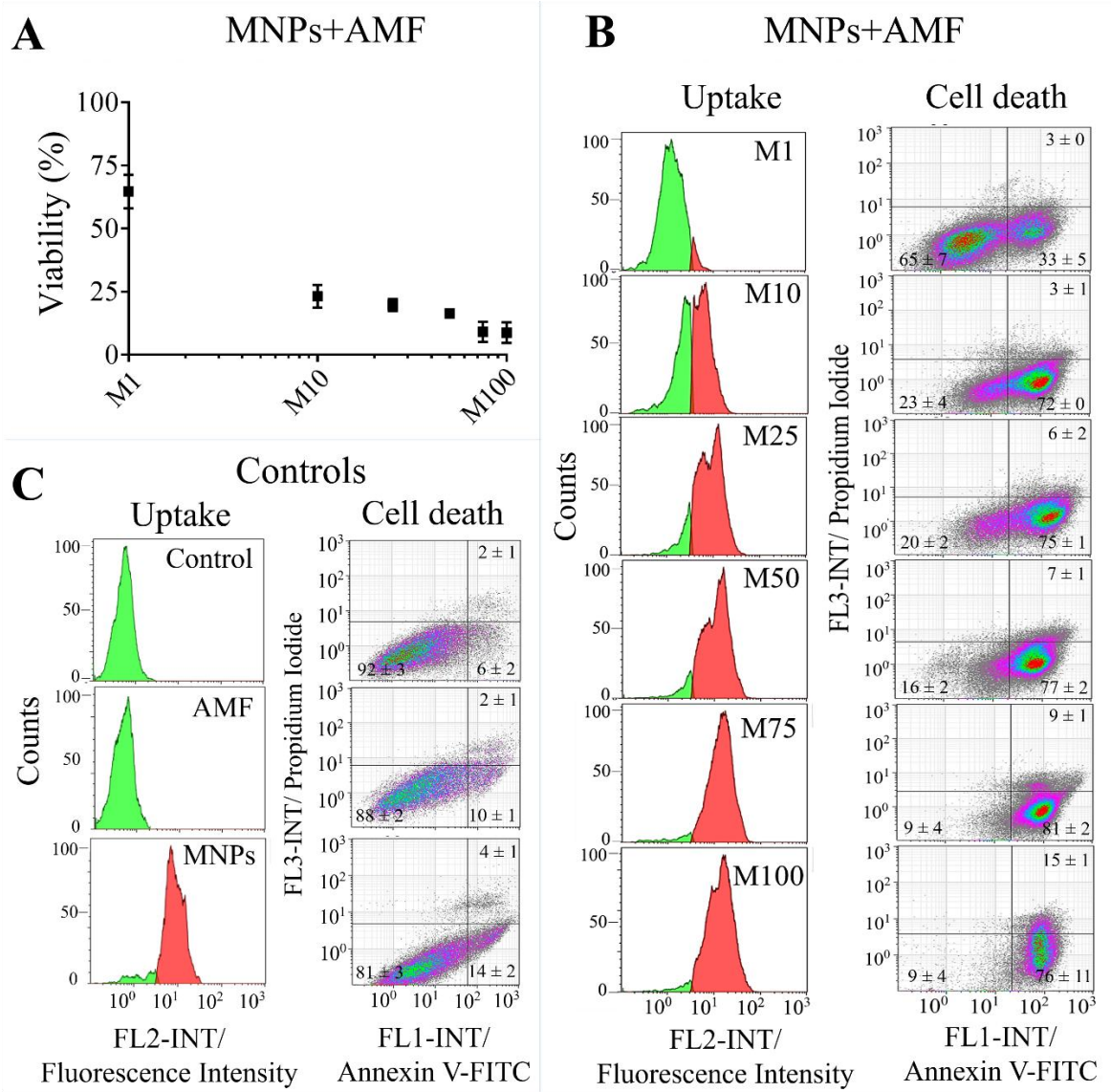
Figure 4. Flow cytometry analysis of nanoparticles uptake and cell death. (A) Viability analysis for all the samples containing MNPs and exposed to the AMF (See supporting information for the analysis of the control samples, Fig. S3), (B) Cells from different models containing MNPs treated with MH (M1 to M100), (C) Control samples, including untreated cells, cells exposed to the AMF and cells incubated with MNPs (same amount as M100) but not exposed to the AMF.

Taken together, these results indicated a correlation between the number of internalized particles and the corresponding cell response, triggering apoptosis, as a consequence of the alternating magnetic field exposure. As no overall temperature increment (ΔT) of the cells was observed during the MH experiment, localized thermal effects had to be evaluated.

2.4 Local thermal effects occur during the AMF exposure

As mentioned before, different global temperatures have been associated with different cell death mechanisms.[321, 360] However, it has been previously observed that, counterintuitively, MH experiments leading to cellular death do not necessarily lead to a global temperature increase.[398, 400, 452] Little is known about the effect of increased temperature locally inside the cells. It has been shown that nanoparticles could produce a significant temperature increase near their surface,[242] but little has been evaluated about the impact on the heat produced in such hot spots on the whole cell temperature.[398, 452-453] Measuring temperature with the required resolution to evaluate these processes remains a very complicated task.

In order to provide an understanding of the thermal effects occurring within the cells during the AMF exposure a theoretical simulation was performed *(Figure 5)*, particularly focusing on elucidating the feasible heating performance when the particles are internalized by the cells, under different interparticle interactions and field conditions. In addition, a simple estimate of the temperature increase within the lysosome and the entire cell was made as a function of the internalized number of particles obtained from the ICP-OES and magnetic susceptibility measurements.
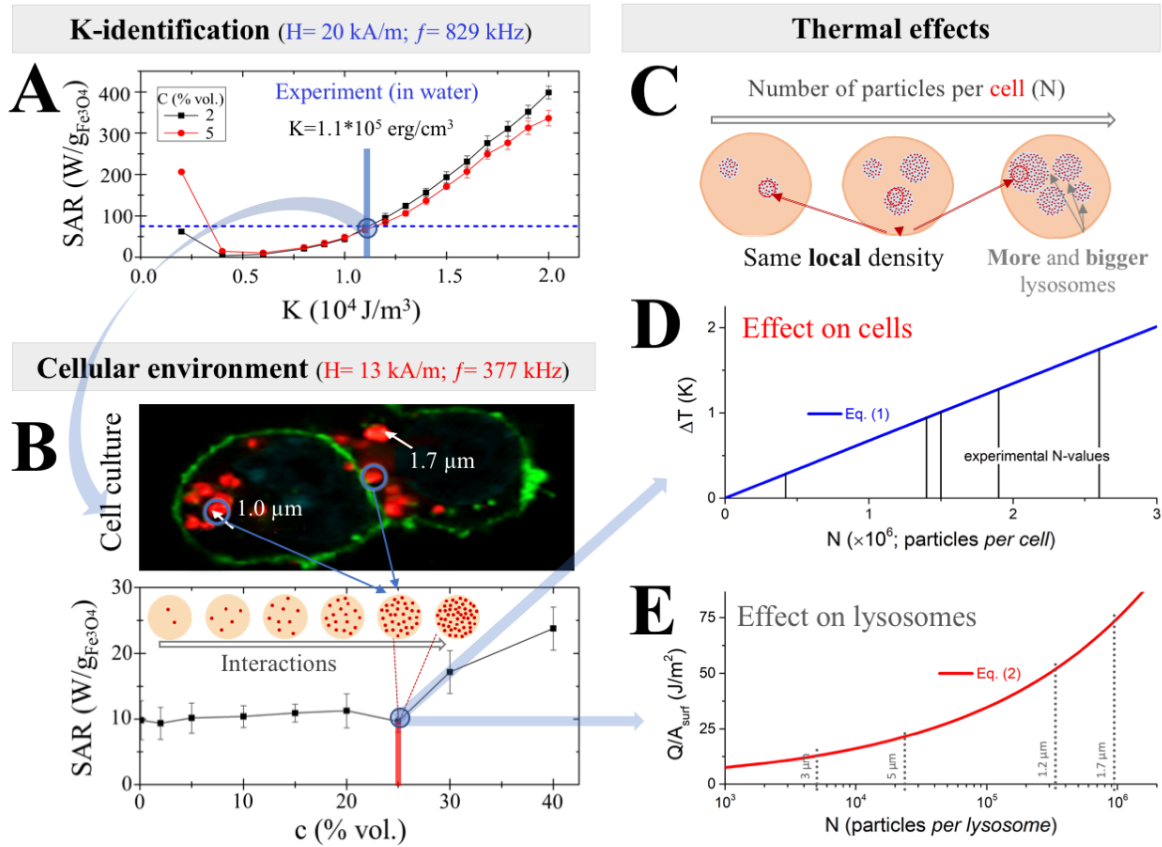
Figure 5. Computational Analysis of the thermal effects. (A) Identification of the anisotropy constant of the particles, K, through the comparison of computationally predicted SAR and the experimental value measured in water (K-identification). (B) estimation of the SAR performance of the particles occurring during the in vitro conditions, using the previously identified K value (Cellular environment). (C)Schematic representation of the number and size of lysosomes in the different models depending on the number of particles per cell. (D) estimation of the dependence on number of particles (N) of ΔT of the whole cell with the obtained SAR for the cellular environment. (E) estimation of the dependence on number of particles (N) of flow of energy density through the lysosome wall with the obtained SAR for the cellular environment.

Given that the field conditions and the interparticle interactions during the *in vitro* experiments were different than those used for SAR characterization, a previous step was necessary to estimate the heating power of the particles within the conditions of the *in vitro* experiments, especially, given the strong effect that interparticle interactions may have on the SAR values.[476-477] Firstly, the anisotropy constant of the particles (K), key parameter for heat generation, was identified (Figure 5A). [104, 478-479] To do so, the SAR measured for the particle suspension (MNPs occupying about 2% of the volume, H= 20 kA/m, *f*= 829 kHz) was simulated using a computational kinetic Monte Carlo technique and considering K as a free parameter (see supporting information - section computational details - for more information).[480] The K value

was identified as the one at which experimental and simulated SAR values matched, resulting in K=1.1*10^5 erg/cm^3, in reasonable agreement with related studies. Results illustrated the complex role of interactions, which can either decrease or increase the SAR depending on K (*Figure 5A* for 2% and 5% of occupied volume fraction).[104]

Secondly, this K was used to simulate the SAR of the particles when internalized by the cells, where the particles were closely packed within the lysosomes. The SAR corresponding to the *in vitro* conditions (H= 13 kA/m, f= 377 kHz) was calculated assuming a packing fraction of magnetic material of about 25%, that was obtained considering the particle iron core size and a 2 nm coating associated to the PMAO linked to the iron oxide surface *(Figure 5B)*.[82] Note that the large number of particles per lysosome (thousands) allowed discarding finite-size clustering effects. The SAR value obtained in such conditions was ≈ 14 W/g Fe, significantly lower than the one measured experimentally for the water suspension. This reduction in the SAR values would be a consequence of the different AC field measuring conditions and the different local particle concentration. In fact other studies had previously indicated the large reduction of the SAR values once the particles were internalized by the cells.[311, 468, 481-483] Nevertheless, as observed in the previous section *(Figure 4)*, this heating capacity was still able to induce cell death.

The SAR value obtained for the *in vitro* conditions was then used to estimate the increase in temperature both in the lysosomes and in the whole cell. For the analysis of ΔT inside the lysosomes, first, it was considered that the heat did not flow rapidly out of the lysosome. This unrealistic adiabatic approximation suggested a quick temperature rise of ΔT ≈ 63 K in about 20 seconds (see S.I. for details of the numerical estimate). An important aspect of these calculations was that, since local packing fraction was assumed to be the same *(Figure 5C)*, the achieved ΔT was independent on the number of particles within the lysosome (i.e. there was no dependence on lysosome size).

The analysis of ΔT within the whole cell was performed considering that the heat was released from the lysosomes to the entire cell. Assuming that the heat flowed from within the lysosomes to the surrounding cell but that flow outside the cell was negligible (based on the observed global ΔT ≈ 0 K), ΔT as a function of N was naïvely estimated as (see S.I. for details)

$$\Delta T_{cell} = \frac{SAR \cdot \Delta t \cdot N \cdot \rho_{MNP} \cdot d^3}{c_{H_2O} \cdot \rho_{H_2O} \cdot d_{cell}^3} \ (1),$$

where SAR was the value obtained from Figure 5B; Δt is the time variation during the assumed adiabatic behavior; ρ_{MNP} (c_{MNP}) and ρ_{H2O} (ρ_{H2O}) is the density (specific heat capacity) of the magnetic nanoparticles and water, respectively (note that the heat capacity of the cell is assumed to be the same as that of water); d is the particle diameter and d_{cell} stands for the average cell size. Using Eq. (1) with $\Delta t = 20$ s (based on our own experimental observations of ΔT $vs.$ Δt linearity), for the experimental conditions it was obtained an essentially linear behavior (Figure 5D). The relatively small absolute values predicted were concordant with the observed global $\Delta T \approx 0$ K and the intuitive idea of higher heating with larger number of internalized MNPs.

Assumptions made for Eq. (1) made it only valid for a small initial time interval. Alternatively, a more sophisticated model was developed considering the rate of heat flow (ΔQ) through the lysosome wall. The areal density of heat flow through the lysosome membrane, which depends on the lysosome size was estimated as (see S.I. for details)

$$\frac{\Delta Q}{S_{ly}} = \frac{1}{6} SAR \cdot \Delta t \cdot N^{\frac{1}{3}} \cdot \rho_{MNP} \cdot d \cdot c^{\frac{2}{3}}, \quad (2)$$

where c is the volume fraction (0.25) and S_{ly} is the surface area of the lysosomes. The results as a function of N (Figure 5E), indicated a non-linear growth of ΔQ with particle number. For bigger lysosomes a much larger heat flux per surface area was predicted in comparison with the values obtained for smaller lysosomes. In our models, we observed that both the number and the size of the lysosomes was increased significantly with the number of internalized particles, reaching diameters up to 1.7 µm for model M100 while for model M10 lysosome diameters only reached 1 µm. These differences may play a very important role in the way the heat is transmitted to the rest of the cell and further investigations should be performed to elucidate the real influence that the lysosome size has in the thermal effects occurring during the AMF exposure

Taken together, all these results indicated that in our cell models a significant increase in temperature within the lysosomes may have occurred at very short times during the MH experiment. When the heat produced was transferred to the whole cell, the average cell temperature did not change significantly. However, the lysosome size was identified as a fundamental parameter in the heat flux between these organelles and the cells. It can be envisaged that lysosomes are a key organelle to evaluate in order to control the biological response to the heat produced during the MH treatment.

2.5 The number of intracellular MNPs affects the activation of different cell death pathways

So far, our results suggested that the MH treatment induced a clear apoptotic response with different intensities depending on the amount of internalized MNPs (Fig. 4) and that according to the model calculations different thermal effects could be occurring with higher and lower number of internalized particles *(Figure 5)*. The analysis of the ratio of cells in early and late apoptotic stages indicated, as expected, that higher intracellular amount of MNPs produced a more intense and faster apoptotic cell death *(Figure 4)*. However, Annexin V-FITC/PI FC assay by itself did not provide any additional information concerning the type of apoptotic pathway triggered in the presence of the different amounts of MNPs and hyperthermia.

At the molecular level, apoptosis is characterized by the activation of caspases (cysteinyl, aspartate specific proteases) *(Scheme 1)*. There are two main pathways for activation of apoptosis depending on the stimuli: through external death receptors (an extrinsic pathway) or through internal signals linked to the mitochondria (intrinsic pathway).[363] Activation of the extrinsic cell death pathway occurs by the binding on the cell surface of specific ligands (e.g. TNF-related apoptosis-inducing ligand, TRAIL), coming from the environment or neighboring cells,[366] to death receptors. This binding induces activation of pro-caspases (8 and / or 10) that are the initiators of apoptosis through the extrinsic pathway.[484-485] The intrinsic route is activated by intracellular danger signals and controlled by the BCL2 protein family through mitochondrial permeabilization. This route can be activated by numerous intracellular death signals, such as DNA damage, oncogene activation, growth factor deprivation or microtubule disruption.[472, 485] Both pathways are also connected. In some types of cells, the extrinsic pathway is often not enough to produce cell death and requires an amplification via the intrinsic pathway.[363] In such cases, signaling starting through the death receptors (extrinsic pathway) may also lead to apoptosis *via* the intrinsic pathway through the activation of the BID/tBID proteins (also part of the BCL2 family).

It has been previously described that in Magnetic Intra-Lysosomal Hyperthermia (MILH) the heat produced by the particles located inside the lysosomes causes lysosomal membrane permeabilization [44, 48, 50] resulting in the leakage of lysosomal enzymes into the cytosol.[463]. The molecular mechanisms of cell death induced upon lysosomal membrane disruption are extensive and have not yet been completely understood. The different lysosomal cathepsins that

release into the cytosol following of LMP can trigger different signaling pathways to promote both the intrinsic and extrinsic apoptosis pathways.[463] However, their mutual importance varies depending on the stimulus that triggers the total or partial permeabilization of the lysosomal membrane.[457]
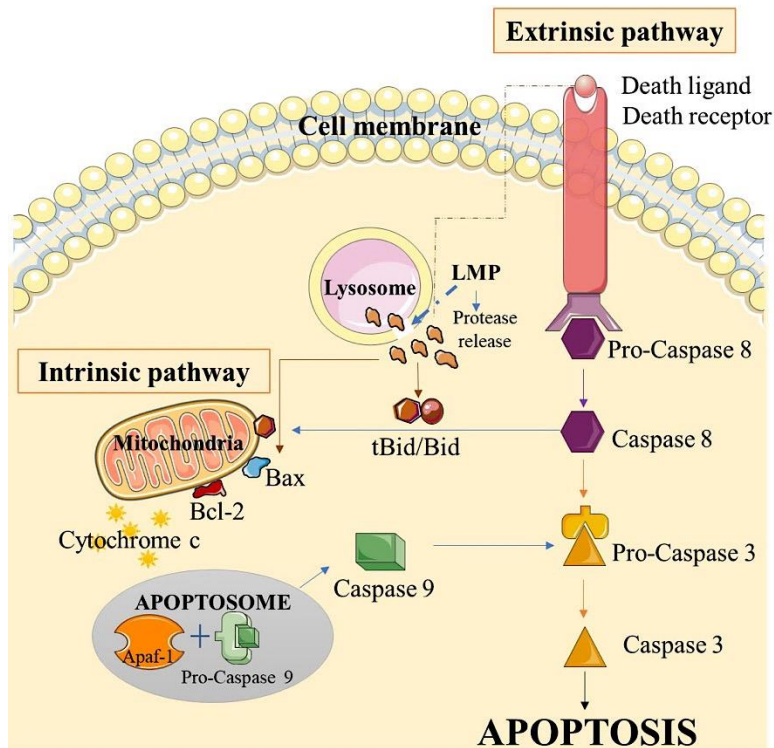
Scheme 1: Schematic representation of the molecular events triggered by both extrinsic and intrinsic apoptotic pathways.

To further clarify the apoptotic route triggered during the MH treatment, *Bax* and *Bcl-2* expression levels, associated with the intrinsic pathway and caspase-8 activity, associated with the extrinsic pathway were assessed in 3D cell culture models exposed to the AMF and the different amounts of MNPs. In addition, *Bid* expression was also monitored to evaluate the crosstalk between the extrinsic and the intrinsic pathways that would allow the initiation through the extrinsic pathway and finalization through the intrinsic pathway.

First, we studied the impact of the internalization of MNPs on the *Bax* and *Bcl-2 mRNA* levels in cells not exposed to the AMF *(Figure 6A)*. Our results showed that there were no significant differences in the expression levels of *Bax* (pro-apoptotic) in the samples incubated with different amounts of MNPs. In contrast, an important overexpression was observed in the *Bcl-2* (anti-apoptotic) levels, that increased with increasing amounts of internalized MNPs until

model M50, meaning that cells could counteract the presence of MNPs and did not need to trigger intrinsic apoptosis *(Figure 6A)*. Interestingly, at the two highest amounts of internalized MNPs (M75 and M100), there was a down-regulation of *Bcl-2* expression and a trigger of intrinsic apoptosis (increase of *Bax/Bcl-2* ratio up to values ≈ 2, between 10 and 100 times higher than for the rest of the models) *(Figure 6A)* This result was in line with the previous data indicating that, for the M100 cells, a more intense stress is observed triggering an apoptotic response *(Figure 4A)*with concomitant loss of cell viability (20%; *Figure 4A*).
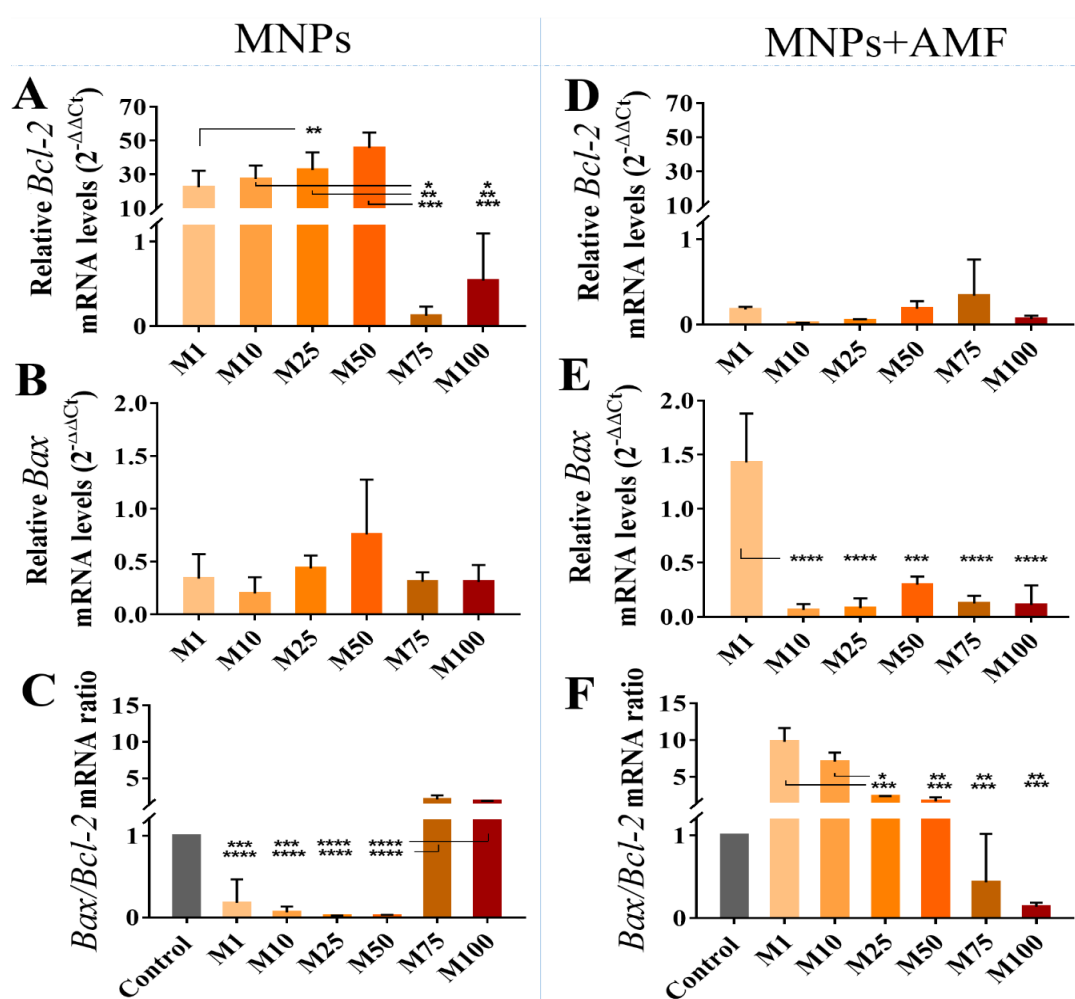
*Figure 6. Analysis of the mRNA expression involved in the mitochondrial cell death apoptotic pathways of the different models studied before (A, B, C) and 24h after (D, E, F) exposure to an AMF. Relative Bcl-2 (A and D) and Bax (B and E) mRNA levels were calculated normalizing each sample by the control cells´ value. In panels A, B and C, the control consisted of just cells, and in panels D, E and F the control consisted of cells without MNPs but exposed to AMF. Besides, Bax/Bcl-2 ratio (C and F) was calculated in order to compare the level of the intrinsic apoptotic pathway with respect to the controls. Results show a clear upregulation of that pathway in the cells incubated with lower amounts of MNPs and exposed to the AMF. Statistical significance between the means was determined using a one-way ANOVA followed by Tukey's multiple comparisons test (****p < 0.0001; ***p < 0.001; **p < 0.01; *p ≤ 0.05; p > 0.05 no significance).*

We then analyzed the mRNA expression of these two genes in cells incubated with the MNPs and exposed to the AMF *(Figure 6B)*. For the model with the lowest MNP concentration, M1, a clear overexpression of the *Bax* mRNA levels was observed that, together with a decrease of the *Bcl-2* mRNA levels, resulted in a notable increase of the ratio *Bax*/*Bcl-2*, indicating that, under these conditions, the apoptosis was likely to take place through the intrinsic pathway. For the remaining MNP concentrations (M10 to M100), the mRNA levels of the anti-apoptotic gene *Bcl-2* remained stable and low and the mRNA levels of the pro-apoptotic gene *Bax* decrease compared to the level attained for M1, giving rise to a dose-dependent decrease of the *Bax*/*Bcl-2* ratio compared to the M1 sample. Values of *Bax*/*Bcl-2* ratio increased 7 and 10-fold for the M1 and M10, respectively and decreased down to 0.1 in the sample incubated with the maximum dose of MNPs, M100 *(Figure 6)*.

It is worth mentioning that the apoptotic population after MH treatment increased with the increase of MNP amounts. However, the implication of the intrinsic pathway seemed to decrease with increasing MNP amount. These results clearly indicated that the increase in the apoptotic cell death, up to certain concentration (M10), could be attributed mainly to the intrinsic pathway and justified by the increase of the observed *Bax*/*Bcl-2* ratio. However, for higher MNPs concentrations the increase in the apoptotic response did not fit with the levels of *Bax*/*Bcl-2* detected for these samples, indicating that other apoptotic routes might be playing a role. To evaluate this hypothesis, the activation of the extrinsic pathway by MH treatment was assessed *via* caspase-8 activity, since caspase-8 is a key player in the activation of apoptosis through the extrinsic pathway. Four different samples were selected for this assay: a control without MNPs (AMF) and samples incubated with high (M100), intermediate (M10) and low (M1) amounts of MNPs and exposed to the AMF (MNP+AMF). The caspase activity was evaluated 24 h after the MH treatment. The analysis revealed that caspase-8 activity increased as expected M1 < M10 < M100 *(Figure 7)*.
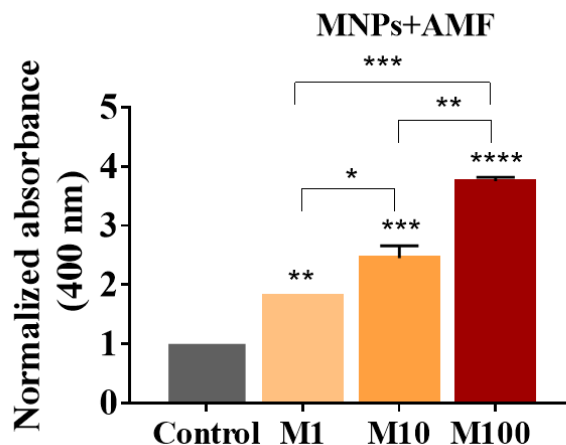
Figure 7. Analysis of the caspase-8 activity involved in the extrinsic cell death apoptotic pathways in three of the different models studied that evidence differences in the BAX/BCL-2 expression. Statistical significance between the means was determined using a one-way ANOVA followed of Tukey's multiple comparisons test (****p < 0.0001; ***p < 0.001; **p < 0.01; *p ≤ 0.05; p > 0.05 no significance) comparing with the control group (0.0 µFe). In cases where more than one group generated significant differences with respect to control, the means between those groups were also compared.

As described before, following the activation of caspase-8, two possible routes could be followed: the continuation of the extrinsic pathway, or the initiation of the intrinsic pathway through BID, but in this case the BCL-2 family proteins would also be implicated resulting in an increase in the ratio *Bax*/*Bcl-2*. To further verify that the intrinsic pathway was not triggered through BID for the models containing the highest amount of intracellular MNPs, *Bid* expression was analyzed for M1, M10 and M100 samples. Following the same trend as *Bax*/*Bcl2* ratio, a reduction of the *Bid* expression was observed for increasing concentrations of MNPs (+AMF), suggesting that the extrinsic pathway was favored in the case of the highest intracellular MNP concentrations (Supporting information, *Figure S4*).

Cell death mechanisms cannot be treated as exclusive, and it seems reasonable to consider that a specific stimulus could trigger a mixture of events. However, comparing all these results we observed a detectable tendency in triggering mainly an intrinsic or extrinsic mechanism depending on the MNP amount. As mentioned before, for the model with the lowest MNP content (M1) the increase in the apoptosis was in total agreement with the increase of the ratio *Bax*/*Bcl-2*, indicating that, at these MNP levels, after the MH treatment the mechanism triggered was mainly intrinsic apoptosis. However, in cell models from M10 to M100, where a significant number of cells containing MNPs was achieved and where a significant decrease on the cell viability was observed, very low levels of *Bax* and *Bcl-2* mRNA expression were observed. The

increase of the activity of the caspase-8 indicated that for these higher MNP amounts a trigger of the extrinsic mechanism occurs. These results indicated that depending of the amount of MNPs internalized, different apoptotic pathways were triggered in response to the MH treatment. The different apoptotic pathways may be related to the total or partial permeabilization of the lysosomal membrane. Further experiments are needed to continue elucidating other mechanisms involved in the cell response to the MH treatment.

3. Conclusions

We established a series of 3D cell culture models containing different amounts of internalized MNPs. These models were of extreme use for the evaluation of the impact of the amount of intracellular MNPs on the death mechanisms triggered after a MH treatment.

Theoretical calculations indicated a large SAR drop after cell internalization, primarily due to the different field conditions. Additionally, a simple estimate suggested that a correlation between the number of particles and size of the vesicles where the particles are trapped after their internalization might result in different localized effects, particularly due to the different energy density per surface area through the lysosomes' membrane. In contrast, the global cell temperature may not increase significantly.

Flow cytometry and *Bax* and *Bcl-2* mRNA levels showed that, although internalization of the MNPs did not lead to observable toxicity, there was an overexpression of the anti-apoptotic gene *Bcl-2*, which might be related to a protection mechanism. At the highest concentrations of MNPs (M75 and M100), a slight cytotoxic effect could be observed. However, when exposing cells to the AMF, the amount of internalized MNPs was the key factor triggering different apoptotic routes.

Results indicated that, at the lowest concentrations, the apoptotic mechanism was mainly intrinsic. However, when increasing the amount of MNPs the intrinsic pathway became less important and the extrinsic pathway played a fundamental role on the cell death.

Together, these results are of great importance in the field of magnetic hyperthermia and for the support of MH as antitumoral treatment. In fact, our data clearly show that depending on the amount of intracellular MNPs, the cell death mechanism is different as well as the subsequent biological events triggered. Modulating the amount of MNPs and, therefore, the death pathway would be a key tool when facing preclinical experiments to evaluate the real effectiveness of this approach before effective translation to the clinic.

4. Materials & Methods

4.1 Magnetic Nanoparticles: synthesis, functionalization and characterization

Superparamagnetic iron oxide nanoparticles with an average size of around 11 nm were synthesized by thermal decomposition in organic medium. Then, the magnetic cores were transferred to aqueous medium (PMAO-TAMRA (carboxytetramethylrhodamine)) and functionalized with glucose based on a previously reported method.[336] Finally, MNPs were resuspended in phosphate-buffered saline buffer (PBS) and filtered with a syringe filter with a pore size of 0.22 μm (Merck Millipore, Darmstadt, Germany) to guarantee their sterility. Iron concentration was determined using a standard colorimetric procedure based on the use of 4,5-dihydroxy-1,3-benzenedisulfonic acid disodium salt monohydrate (Tiron). [82] Sample absorbance (480 nm) was measured on an UV/vis spectrophotometer (Thermo Scientific Multiskan GO MA, USA) and compared to a calibration curve. An electrophoresis agarose gel 1% 0.5 Tris-borate-EDTA (TBE) was performed in order to corroborate the efficacy of the functionalization. The electrophoresis was performed at 90 V during 30 min. After this time, the gel was scanned with a Bio-Rad Gel Doc EZ equipment and the quotient of the migration distances of the MNPs samples before and after of the glucose functionalization was determined as quality control of the procedure. The image analysis of the agarose gel was performed with Gel Analyzer 2010 Program. Particle size and morphology were studied by transmission electron microscopy (TEM) using a Tecnai T20 (FEI company, OR, USA) microscope operating at 200 kV. The sample was prepared by placing a drop of a diluted suspension of the MNPs in water onto a carbon coated grid and allowing it to dry. Particle size was determined by manual measurement of around 200 particles per sample using the Digital Micrograph software. The magnetic heating capacity of the MNPs was determined using a commercial alternating magnetic field generator (DM100; Nanoscale Biomagnetics, Spain). A 1 mg Fe/mL MNPs sample was placed in a closed container centered in the inductive coil. The AMF was applied for 5 min using a field amplitude of $H = 20.10$ kA/m and a frequency of 829 kHz, while the temperature was recorded using an optic fiber sensor incorporated in the equipment. For the magnetic characterization, the MNPs liquid sample was allowed to dry at room temperature deposited into a piece of cotton wool that was subsequently placed into a gelatin capsule. Field dependent magnetization measurements were performed in a Quantum Design (USA) MPMS-XL SQUID magnetometer at 300 K with a maximum field of 5 T. Dynamic light scattering (DLS) was measured in Milli-Q water on a Malvern Zetasizer Nano-ZS, using ten runs per measurement and five replicates at 25 °C and pH 7. MNPs prepared to a final concentration of

0.1 mg/mL were incubated at room temperature with different biological media (cell culture medium with serum, cell culture medium without serum and PBS 1x) using 96-well plates. After 24 h, the samples were observed under optical microscope (Nikon Eclipse, TE2000-S) to observe the aggregation effects.

4.2 Cell culture

The murine macrophage RAW−264.7 cell line (ATCC® TIB71) was cultured and maintained in complete Dulbecco's Modified Eagle's Medium GlutaMAX™ Supplement (cDMEM; Gibco®, Thermo Fisher Scientific) supplemented with 10 % fetal bovine serum (FBS, Invitrogen), 100 U/mL penicillin G (sodium salt) and 100 µg/mL streptomycin sulfate (Invitrogen) at 37 °C in a humidified atmosphere at 5 % CO_2. Every four or five days in dependence of the confluency, the cell culture was diluted to 1:10. To detach the cells, these were incubated with Trypsin EDTA solution (Sigma Aldrich) for 4 minutes at 37ºC, in order to increase the viability. Then, the cells were scraped from the flask. Finally, cells were collected in fresh cDMEM.

To prepare the 3D cell culture models, the cells in suspension were incubated with different amounts of MNPs (1 µg; 10 µg; 25 µg; 50 µg; 75 µg and 100 µg) during 1h at 37 ºC in 0.5 mL of cDMEM. After the incubation time, the medium with MNPs was discarded and the cells washed by centrifugation (300 xg, 5 min) twice and then, were mixed with the collagen gel. Just after of the collagen gelling, 0.5 mL of cDMEM was added to the gel [336].

4.3 Cellular localization and uptake quantification of MNPs

A Zeiss LSM 880 confocal microscope with a 63x/1.40 PlanApochromat objective was used to visualize MNPs localization in the 3D cell culture. The gels were fixed during 20 min with 0.5 mL of paraformaldehyde (4%). Then, the nuclei were stained with DAPI (4′,6-diamidino-2-phenylindole) and the cytoskeleton with Phalloidin488. The laser sources used were 458 nm, 488 nm (Argon Ion), and 561 nm (DPSS; Diode-pumped solid state). ZEN Microscope and Imaging Software was used for the image analysis.

Flow cytometry and Inductively Coupled Plasma Optical Emission Spectrometry (ICP-OES) were used to determine the MNPs uptake and intracellular concentration, respectively. For the sample preparation, the same incubation protocols as described above were followed. In the flow cytometry studies, a concentration of $2.5x10^4$ cells/mL resuspended in PBS were analyzed using the FL2 channel at 575 nm (Gallios™ Flow Cytometer, Beckman Coulter). For the ICP-OES studies, cell pellets from the different incubations were digested by heating with HNO_3

(Panreac) and then with H_2O_2 (Panreac) (both steps at 90 °C and during 1 h each). Finally, the samples were diluted until a final volume of 10 mL with MiliQ water and the concentration was determined using the Thermo Elemental IRIS Intrepid ICP-OES.

AC magnetic susceptibility measurements were performed in a Quantum Design (USA) MPMS-XL SQUID magnetometer using an AC amplitude of 0.41 Oe and a frequency of 11 Hz in the temperature range between 10 and 300 K. Freeze-dried cell pellets of around 350.000 cells were placed into gelatin capsules for the measurements. The MNPs used for the quantification protocol were prepared in two different ways. One sample was prepared by placing a known volume of the original MNPs suspension into a cotton wool piece and another sample was diluted in a hot agar solution and maintained immersed in an ultrasound bath during the cooling down process to achieve a homogeneous dispersion of the particles within the sample and therefore reduce the interparticle dipolar interactions.

4.4 Magnetic hyperthermia treatment

3D cell cultures were thermalized at 37 °C using a water bath pump (Stryker - Medical Devices & Equipment Manufacturing Company) connected to a water tubing jacket. Then, the cell cultures were exposed to an AMF (DM3, nB nanoscale Biomagnetics, Zaragoza, Spain) during 30 min. The frequency used was 337 kHz and the field amplitude of 13 kA/m.

4.5 Cell death studies

Cells were released from the 3D cell cultures [336] and re-suspended in 1X Annexin V Binding Buffer (10 mM Hepes/NaOH (pH=7.4) 140 mM NaCl, 2,5 mM $CaCl_2$) at a concentration of $1x10^6$ cells/mL. Then, 5 µl of Annexin V-FITC (Fluorescein Isothiocyanate) and 5 µL of Propidium Iodide (PI) were added to 100 µL of cell suspension and incubated at room temperature for 15 minutes in the dark (FITC-Annexin V Apoptosis Detection Kit). After the incubation period, 400 µL of 1X Annexin binding buffer was added and the sample was analyzed by flow cytometry. All samples were analyzed in a Gallios™ Flow Cytometer (Beckman Coulter) and the data interpreted with Kaluza 2.1 Software (Beckman Coulter).

4.6 Computational details

The thermal fluctuation and external field driven magnetisation behaviour of interacting magnetic particles was modelled by using kinetic Monte-Carlo approach [1,2]. The model described in ref. 2 is based on the following system energy:

$$E = \Sigma \left(-K_i V_i \left(\hat{k}_i \cdot \hat{m}_i \right)^2 - M_s V \hat{m}_i \cdot \left(\vec{H}_{app} + \vec{H}_i^{mag} \right) \right) \quad (1)$$

with V_i being the volume of a particle i; M_s the saturation magnetisation; and $\hat{k}_i$ and $\hat{m}_i$ the anisotropy vector and magnetisation moment, respectively, both normalized to unity. The effective local field acting on particle i is given by the sum of the external applied field ($\vec{H}_{app}$) and the magnetostatic interaction field ($\vec{H}_i^{mag}$). The time dependent transition for a particle moment $\hat{m}_i$ to switch between the up ("1") and down ("2") states is:

$$P_i = 1 - exp(-t/\tau_i) \quad i = 1,2 \quad (2)$$

where the relaxation time constant τ_i is a reciprocal sum of the transition rates τ_i^+ and τ_i^- dependent on the energy barriers $\Delta E_i^{1,2}$ seen from the "1" and "2" states via the standard Neel-Arrhenius law [3]:

$$\tau_i^{1,2} = \tau_0 exp\left(\Delta E_i^{1,2}/k_B T\right) \quad (3)$$

The k_B is the Boltzmann constant and T the temperature. The energy barrier, $\Delta E_i^{1,2}$, depends on the intrinsic particle properties, such as V_i and K_i.

The calculations were done considering log-normal distributions of anisotropy value of 10% and a 15% distribution in particle size. Example of the hysteresis loops for the in-water and in vitro conditions are shown in *Figures S5* and *S6* respectively. For the second case, the role of packing density was illustrated by considering packing densities between 2% and 40%.

4.7 RNA extraction and RT-PCR analysis

RNA was extracted from the same samples as described in the previous section. For this procedure, 2.5×10^5 cells were centrifuged at 500 rcf during 5 min at 4ºC and the supernatant was discarded. The pellet was gently resuspended in 0.5mL of Trisure (Bioline) and incubated 5 min to room temperature. After this time, 0.2 mL of chloroform was added and mixed vigorously during 15 min, then the solution was centrifuged to 12000 rcf during 5 min and the upper phase (aqueous phase) was transferred to a new tube. Ice cold isopropanol was added in a ratio of 1: 2.5 with respect to the volume recovered and incubated during 10 min to 4 ºC. The solution was centrifuged to 12000 rcf, during 5min at 4ºC, and the supernatant was discarded. The pellet was washed with 0.5 mL of ethanol 75 % (v/v), mixed using a vortex and then centrifuged at 7500 rcf during 5 min. Finally, the supernatant was discarded and the pellet dried. For the quantification, the samples were resuspended in 0.05 mL of ultrapure water using a tip with filter.

For the RT-PCR studies, 350 ng of total RNA in each sample was reverse-transcribed into first-strand cDNA using NZY M-MuLV First-Strand cDNA Synthesis Kit. Five reactions were prepared (using flame) in dependence of the mRNA volume needed. The final volume was 10 μL. RNA samples were added and gently mixed with the reaction components (out of the flame area) and incubated in the thermocycler with the following program [486]: 1) 25 °C for 10 min; 2) 37 °C for 50 min; 3) 85 °C for 5 min. Then,1 μL of NZY RNase H (*E. coli*) was added to the reaction mix, that was incubated in the thermocycler to 37 °C during 20 min. cDNA obtained was used as template for the qPCR amplification. The qPCR was performed on a Corbett Rotor-Gene 6000 thermal cycler (QIAGEN) using the NZY qPCR Green Master Mix (2x) with the following primers, at a concentration of 0.1 μM each: *Bax* forward (5´-TGGCAGTGACATGTTTTCTGAC-3′) and *Bax* reverse (5′-TCACCCAACCACCCTGGTCTT-3′); *Bcl-2* forward (5´-CTTCGCCGAGATGTCCAGCCA-3´) and *Bcl-2* reverse (5´-GCTCTCCACACACATGACCC-3´); *18S* forward (5´-GTAACCCGTTGAACCCCATT-3´) and *18S* reverse (5´-CCATCCAATCGGTAGTAGCG-3´); *Bid* forward (5'-CTTGCTCCGTGATGTCTTTC-3') and *Bid* reverse (5'-TCCGTTCAGTCCATCCCATTT-3').[486-487] qPCR conditions included an initial denaturation at 95 ^{0}C for 10 min and 40 cycles of 95 ^{0}C for 20 s, 55 ^{0}C (*18S* and *Bid*) or 65 ^{0}C (*Bcl-2* and *Bax*) for 20 s, and 72 ^{0}C for 30 s (18S) or 20 s (*Bcl-2* and *Bax*). qPCR data were analyzed by the Ct method ($2^{-\Delta\Delta Ct}$),[488] where relative gene expression is given by quantification of the gene of interest (*Bid*, *Bax* or *Bcl-2*) relative to internal control gene (RNA*18S*), normalized to the control condition (non-treated cells).

4.8 caspase-8 Assay

For protein extraction, 4×10^6 cells were centrifuged to 500 rcf during 5 min at 4ºC and all the supernatant was removed. Then 0.1 mL of fresh cold lysis buffer (4 ºC) was added to each sample to solubilize the pellet. The mix was incubated at -80 ºC overnight. After this time, samples were thaw gently on ice. To disrupt the cell membranes, cycles of ultrasound bath in ice cold water were made (6 cycles, 2 min 30 s, the samples were setting on ice during 30 s between each cycle). Finally, the samples were centrifuged to 5000 rcf during 5 min at 4 ºC and the supernatant transferred to a clean tube for protein quantification using a colorimetric Bradford test. The levels of caspase-8 were further determined using a colorimetric test – caspase-8 Assay Kit (ab39700). For that 10 μL of 1M DTT stock solution was added to 1 mL of 2X Reaction Buffer (100 mM DTT final concentration) and 50 μL of 2X Reaction Buffer/DTT mixture was added into each reaction well containing 50 μg of protein (sample and background control wells). The solution was mixed well by pipetting up and down. Finally, 5

µL of IETD-pNA substrate (4M stock) was added into each well (200 mM final substrate concentration) and mix well by pipetting up and down. The plate was covered and incubated at 37°C for 2 hours. After this time the absorbance was measured on a microplate reader at OD 400 nm.

4.9. Statistical Analysis

Data are expressed as mean ± SD of a minimum three biological replicas. Statistical significance of difference in means was performed using GraphPad Prism v7.00. One-way ANOVA tests were used for the analysis of the data. The confidence interval was 95%.

5. Associated content
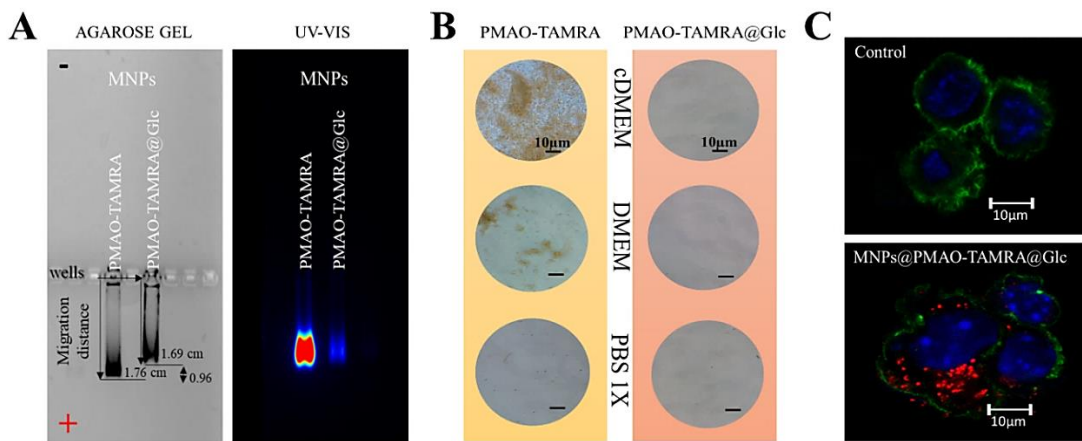
Figure S1. Characterization of the MNPs glucose functionalization efficacy (A) Agarose 1% gel image analysis and (B) stability study in different biological media - before (PMAO-TAMRA) and after (PMAO-TAMRA@Glc) after of the glucose addition (C) Confocal images of the MNP uptake after Glc functionalization. The nucleus is shown in cyan (DAPI), actin in green (PhalloidinAlexaFluor488), and MNPs in red (TAMRA). Scale bar:10 µm.
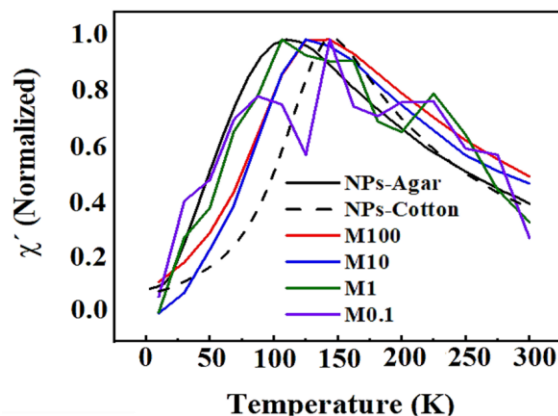
Figure S2 Temperature dependence of the out-of-phase susceptibility data scaled to the maximum to observed the differences on the location in temperature of the maxima for the different samples.
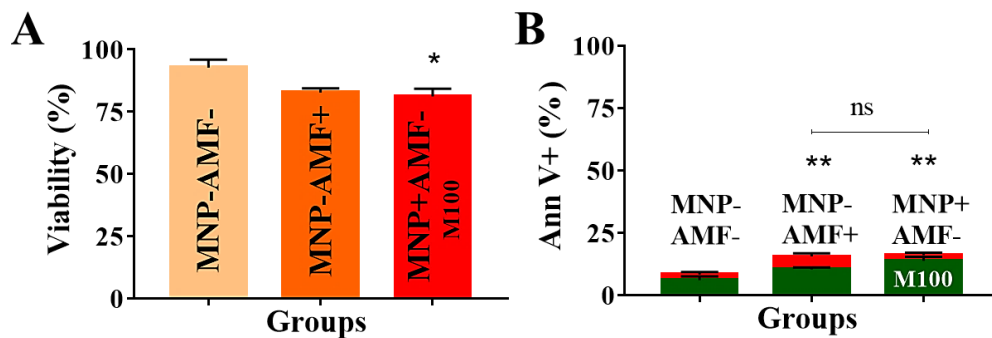
Figure S3. (A) Viability analysis and (B) Percentage of cells positive for Annexin V (+) that are either positive or negative for propidium iodide of the control samples from Figure 4C, D. Statistical significance between the means was determined using a one-way ANOVA followed of Dunnett's multiple comparisons test (A) and two-way ANOVA followed of Sidak's multiple comparisons test (B) (**p < 0.01; *p ≤ 0.05; p > 0.05 no significance).
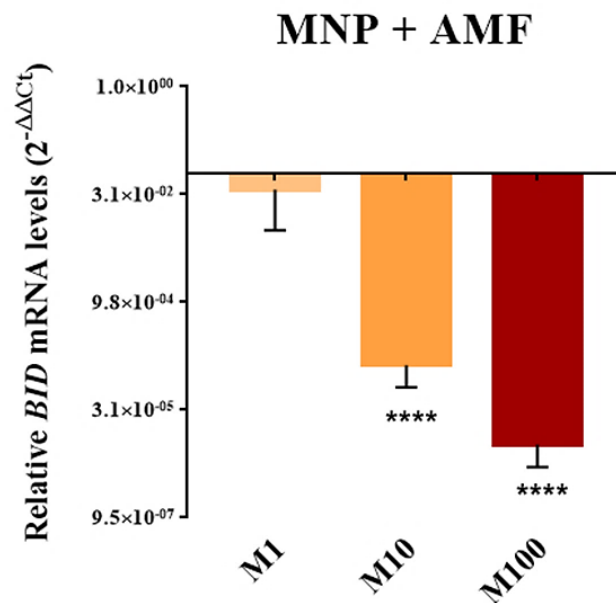
Figure S4. Expression of BID mRNA after 24h after the exposure to AMF in the presence of different concentrations of MNPs (M10 to M100). Values were normalized to a control sample without MNPs (AMF). Statistical significance between the means was determined using a one-way ANOVA followed of Tukey's multiple comparisons test (****p < 0.0001).

Computational details
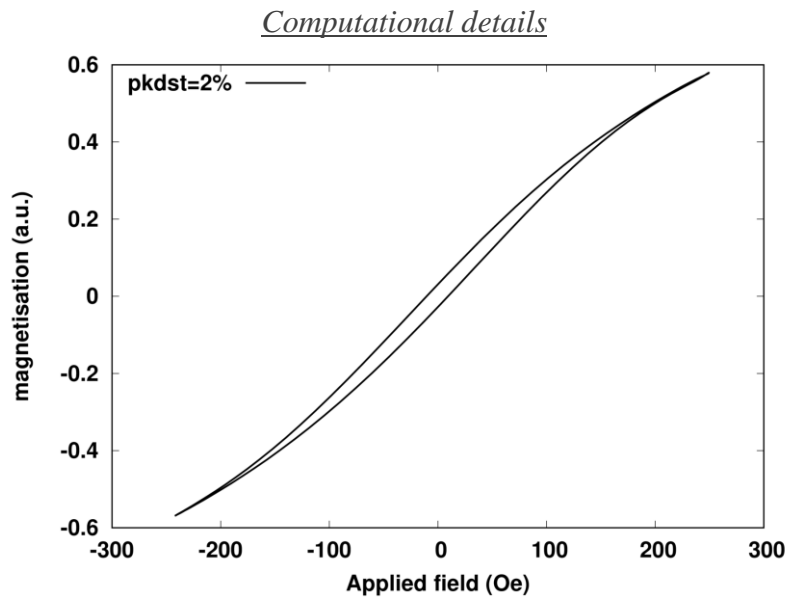
Figure S5. Hysteresis loop for anisotropy of 1.1*105 erg/cm3, applied field of 20 kA/m and frequency of 829kHz at a low packing density of 2%.
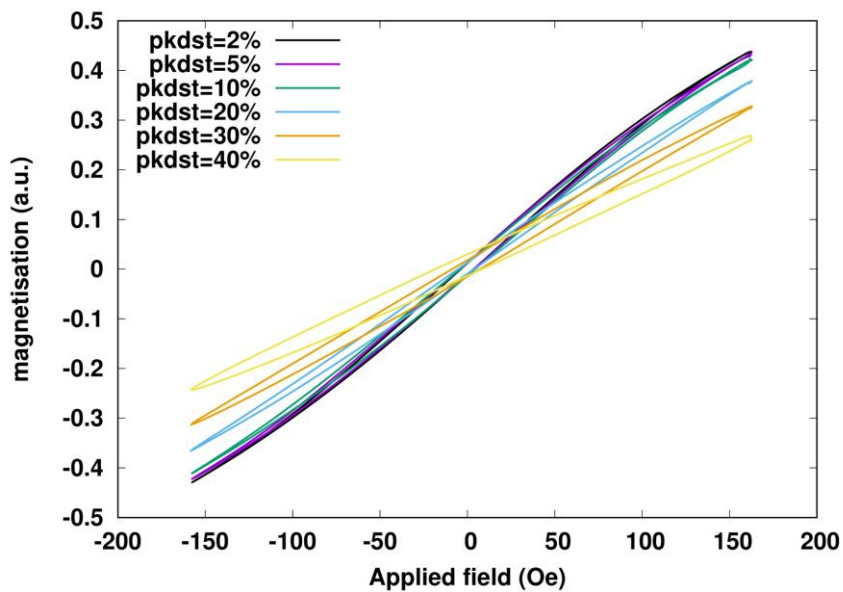
Figure S6. Hysteresis loops at 379 kHz and applied field of 13 kA/m for different packing densities between 2% and 40%.

To do the estimates of ΔT and $\Delta Q/Sly$, we considered that the heat released by the particles during a certain time interval Δt, given by

$$\Delta Q_{MNPs} = SAR \cdot \Delta t \cdot m_{MNPs}, \qquad (4)$$

with mMNPs the mass of the nanoparticles, results in an adiabatic temperature change of the entire system:

$$\Delta Q_{MNPs} = c \cdot m_{TOT} \cdot \Delta T , \qquad (5)$$

with c the specific heat capacity and mTOT the total mass being heated. Depending on whether we consider each lysosome or the entire cell the containing system, different expressions for ΔT shall be obtained. Thus, if to begin with we consider that the system containing the particles during the adiabatic heating process is an isolated lysosome, then its temperature variation is given by

$$\Delta T_{lys} = \frac{SAR \cdot \Delta t \cdot m_{MNPs}}{(c_{H_2O} \cdot m_{H_2O} + c_{MNP} \cdot m_{MNPs})}, \qquad (6)$$

using that c*mTOT=cH$_2$O*mH$_2$0+cMNP*mMNPs, i.e. the total mass is that of the lysosome (associated with water parameters), plus that of the contained particles. Since we assume that the volume density of particles within the lysosomes is very similar for all lysosome sizes,

$$c = \frac{V_{MNPs}}{V_{lys}} = 0.25 . \qquad (7)$$

It is convenient to rewrite Eq. (6) in terms of lysosome (water) and particles volume, using that mMNPs=N*ρMNPs*V1MNP and mH2O= ρH$_2$O*VH$_2$O (being N the number of particles within the lysosome, ρMNPs (ρH$_2$O) the density of the particles (water), and V1MNP and VH$_2$O the volume of one particle and that of water within the lysosome, respectively). Using that Vlys=VH$_2$O+VMNPs=VH$_2$O+N*V1MNP, it is obtained that

$$m_{H_2O} = \rho_{H_2O} \cdot \left(\frac{1}{c} - 1\right) \cdot NV_{1MNP} \qquad (8)$$

This is to say, the fact that the volume concentration is always constant implies that both the mass of particles and that of the surrounding water within the lysosome are directly proportional to the number of particles N, so that Eq. (6) results in a size-independent ΔT:

$$\Delta T_{lys} = \frac{SAR \cdot \Delta t \cdot \rho_{MNPs}}{\left(\frac{1}{c}-1\right) \cdot c_{H_2O} \cdot \rho_{H_2O} + c_{MNPs} \cdot \rho_{MNPs}} \qquad (9)$$

for the particular conditions of the present experiments, which results in close packing of the particles within the cells, the 2-nm thickness coating results in an effective volume fraction (of magnetic material) of about 25%, so that $(1/c-1)=3$, and $\Delta Tlys \approx 63$ K.

To estimate ΔT of the cell, $\Delta Tcell$, we performed analogous reasoning but, in this case, taking in addition the total size of the cell (its average diameter, dcell) as a key parameter. Thus,

$$\Delta T_{cell} = \frac{SAR \cdot \Delta t \cdot m_{MNPs}}{c_{cell} \cdot m_{cell}} . \qquad (10)$$

In this case ccell*mcell=cH$_2$O*mH$_2$0+cMNP*mMNPs, but since mMNPs << mH$_2$0, we can safely approximate ccell*mcell $\approx$ cH$_2$O*mH$_2$0 = cH$_2$O*ρH$_2$O*Vcell, resulting in

$$\Delta T_{cell} = \frac{SAR \cdot \Delta t \cdot N \cdot \rho_{MNP} \cdot d^3}{c_{H_2O} \cdot \rho_{H_2O} \cdot d_{cell}^3} , \qquad (11)$$

with d and dcell the average particle and cell diameters, respectively. In this case there is a clear dependence on the number of particles, as expected since the particle concentration per cell is different.

To estimate the heat flow per surface area of the lysosomes we followed similar reasoning. Firstly, using that c=NV1MNP/Vcell, we write the average lysosome diameter in terms of the volume concentration,

$$d_{cell} = \left(\frac{6NV_{1MNP}}{\pi c} \right)^{\frac{1}{3}} = d \left(\frac{N}{c} \right)^{\frac{1}{3}} . \qquad (12)$$

The surface area of the lysosomes, Sly=4π(dlys/2)2 can hence be written in general as

$$S_{ly} = \pi d^2 \left(\frac{N}{c} \right)^{\frac{2}{3}} \qquad (13)$$

Now, using Eqs. (4) and (13), we directly obtain the energy flow per surface area of the lysosomes, $\Delta Q/Sly$, as shown by Eq. (2) in the main text.

6. Acknowledgments

4.3 Aportes al tema, visión crítica y perspectivas de futuro

Durante muchos años las investigaciones de hipertermia magnética se han centrado en alcanzar una distribución más homogénea de nanopartículas para obtener dosis térmicas terapéuticamente relevantes.[103, 127, 133, 247, 254, 310, 478, 489-494] En este sentido, numerosos estudios han descrito que el calentamiento global de las células a una temperatura inferior a 45 °C conduce a la muerte celular preferentemente por vía apoptótica.[99, 316, 320-321, 412, 492] Sin embargo, la inducción de apoptosis bajo estas condiciones a menudo es ineficaz, ya que las células pueden adquirir tolerancia al estrés hipertérmico, y por consiguiente volverse más resistentes a los daños letales posteriores inducidos por el choque térmico.[493, 495-496] En este contexto, se ha sugerido que el calor generado por las nanopartículas bajo acción de un AMF, podría estar altamente localizado dentro del entorno circundante de las partículas, con un efecto menor o nulo sobre el calentamiento macroscópico.[398, 496] Por lo cual, la capacidad de dirigir nanopartículas a estructuras subcelulares específicas, se ha estudiado como un enfoque atractivo para estimular diversos mecanismos de muerte celular regulada.[398, 451-453, 497]

Evidencias experimentales de varios grupos de investigación han demostrado que un aumento de las temperaturas subcelulares, debido a la acumulación de nanopartículas en estructuras como los lisosomas, puede conducir a una reducción significativa de la viabilidad celular, incluso sin observar cambios perceptibles en la temperatura global de la célula.[398, 452-453, 464] En dichos trabajos, la muerte celular se atribuyó a la permeabilización de la membrana lisosomal acompañado de la consiguiente liberación de sus enzimas proteolíticas al citosol, que se conoce que pueden activar y/o participar en diversos mecanismos de muerte celular regulada.[414, 454] Por otro lado, estudios en diversas líneas celulares tumorales y no malignas, también han reportado la activación de las vías apoptóticas extrínsecas e intrínsecas en respuesta a la hipertermia magnética.[436-437, 439] Sin embargo, hasta donde sabemos, no hay estudios previos donde se haya correlacionado el efecto de la cantidad intracelular de nanopartículas y la producción de un calentamiento sub-celularmente localizado, con la inducción específica de una vía de muerte apoptótica u otra. En este contexto, el cambio global en la expresión de genes pro-apoptóticos y anti-apoptóticos que observamos en nuestro trabajo (véase sección 4.2), sugieren que la vía de señalización de la apoptosis inducida por el tratamiento de hipertermia magnética puede cambiar de intrínseca a extrínseca dependiendo de la concentración intracelular de las nanopartículas. En condiciones *in vitro*, las nanopartículas se acumulan preferencialmente en los lisosomas, donde se encuentran altamente concentradas.[228, 371, 396, 467-468] Teniendo en cuenta lo anterior, los análisis computacionales del efecto térmico realizados

en este trabajo, sugieren que la muerte celular parece estar mediada por una liberación de calor muy local dentro de los lisosomas, en lugar de por un calentamiento global de las células. Los resultados de nuestro estudio revelaron que a bajas cantidades intracelulares de nanopartículas, el tratamiento de hipertermia magnética conduce a la muerte celular apoptótica por vía intrínseca o mitocondrial. Mientras que a elevadas cantidades intracelulares de nanopartículas, la apoptosis ocurre a través de la vía de señalización extrínseca.

En este sentido, aunque los mecanismos moleculares subyacentes en la muerte celular apoptótica pueden exhibir una superposición considerable, cada uno de ellos está involucrado en diferentes escenarios celulares. En general, la muerte celular apoptótica puede ocurrir, por un lado, en ausencia de perturbaciones ambientales exógenas, y por lo tanto, funcionar como un programa fisiológico completamente programado. Mientras que por otro lado, la apoptosis puede originarse en respuesta a perturbaciones del microambiente intracelular o extracelular, debido a estímulos lesivos como la hipertermia. Cuando el daño inducido por el estrés térmico, es demasiado intenso o prolongado para generar una respuesta adaptativa que restaure la homeostasis celular (termotolerancia), diferentes vías de señalización moleculares son activadas para inducir a la apoptosis y garantizar la eliminación las células dañadas, evitando así su multiplicación. [412, 498] Por lo cual, la promoción de apoptosis intrínseca o extrínseca en respuesta al estrés térmico, también constituye una estrategia para la preservación del equilibrio biológico. Sin embargo, a diferencia de las respuestas adaptativas como la termotolerancia, que operan a nivel celular, los mecanismos muerte regulada operan directamente a nivel del organismo.[499] De manera tal, que su función homeostática no solo se refleja en la auto-eliminación de las células dañadas a partir de las señales de perjuicio provenientes de su interior (tales como daños en el ADN o disfunción proteica) que pueden desencadenar la vía apoptótica intrínseca; sino también en la capacidad de estas células moribundas para exponer o liberar moléculas que alertan al resto sobre una amenaza potencial (ej. restos de membrana plasmática, sobreexpresión de citoquinas como TNF y FAS, etc.), conduciendo a las células vecinas a su eliminación para evitar disfunciones en el tejido (vía apoptótica extrínseca). Razón por la cual, se podría sugerir acorde con nuestros resultados teóricos y experimentales, que bajas intensidades de estrés térmico intra-lisosomal (orgánulo por excelencia donde se acumulan las nanopartículas después de su internalización) podrían desencadenar una permeabilización parcial del lisosoma, seguido de una liberación limitada de su contenido proteolítico al citoplasma, que puede favorecer la disfunción mitocondrial y, por ende la apoptosis intrínseca. Mientras que un estrés térmico de alta intensidad, asociado con una mayor transferencia

térmica a la membrana lisosomal (debido al aumento del número de nanopartículas en el lisosoma), podría conducir a una ruptura lisosómica generalizada; lo que unido a un efecto térmico más global, relacionado con el aumento del tamaño y número de lisosomas con nanopartículas ocupando el espacio citosólico celular, podrían desencadenar el reclutamiento y la activación de receptores de muerte para favorecer la vía apoptótica extrínseca.

Aunque nuestros resultados son consistentes con informes anteriores que demuestran la regulación positiva del gen *Bax* (vía apoptótica intrínseca) exclusivamente a dosis bajas de estrés térmico; no encontramos estudios previos donde se reportara un incremento de la respuesta de la caspasa iniciadora -8 ante el aumento del estrés térmico. Al respecto, los datos experimentales encontradas en la literatura, o bien muestran patrones idénticos de actividad Caspasa-8 tanto a bajas como a altas dosis térmicas,[439] o no proporcionan evidencia de su activación bajo estrés por calor.[437, 500] Estas diferencias pueden ser atribuidas a la utilización de diferentes condiciones experimentales (tales como, variaciones en las condiciones de aplicación de la terapia térmica, cinética de exposición y utilización de diferentes tipos de células, etc.), lo que indica la importancia de utilizar una plataforma experimental optimizada para evaluar el efecto de las exposiciones hipertérmicas *in vitro*. En este sentido, a diferencia de los informes previamente mencionados, nuestro estudio fue realizado utilizando un modelo de cultivo 3D basado en hidrogeles de colágeno I (véase sección 3.2),[336] que nos permitió evaluar del efecto del calentamiento magnético en un entorno tanto bio-mimético como fisiológicamente relevante. Por otro lado, el uso de un modelo celular de internalización de nanopartículas basados en la línea de macrófagos murinos RAW264.7 facilitó el análisis, compresión y profundización del impacto biológico de las diferentes concentraciones intracelulares en la respuesta celular al estrés térmico inducido por la hipertermia magnética; ya que debe tenerse en cuenta que las grandes diferencias que muestran las líneas celulares tumorales en la endocitosis de las nanopartículas, dificulta en muchos casos la extrapolación de los resultados experimentales entre una línea tumoral y otra. A pesar de estas ventajas, una limitación del modelo fue la dificultad de obtener imágenes de co-localización lisosomal de las nanopartículas mediante el uso de sondas fluorescentes. Una explicación plausible de nuestras observaciones, es que debido a la alta actividad fagocítica de esta línea celular, la sonda fuera eliminada rápidamente por las sustancias reductoras dentro del citoplasma antes de que llegara a los lisosomas, o que el límite de detección de la sonda utilizada fuera demasiado alto para discriminar los compartimientos ácidos de estas células. Por lo cual, este protocolo necesita de más estudio para su estandarización. No obstante, la localización lisosomal de nanopartículas

de hierro después de su internalización en macrófagos ha sido ampliamente demostrada en la literatura mediante diversas técnicas experimentales;[228, 395-397] y además la co-localización específica en lisosomas de nanopartículas de óxido de hierro de similar tamaño de núcleo, recubrimiento y funcionalización a las utilizadas en este trabajo, también ha sido demostrada en trabajos previos con otras líneas celulares.[371]

Los mecanismos moleculares que median la muerte celular regulada son complejos e interconectados, y presentan variaciones dependiendo del tipo de célula y la intensidad y naturaleza del estímulo aplicado. Por lo cual, aunque este trabajo aporta evidencias teóricas y experimentales que contribuyen a la elucidación de los efectos del calor intracelularmente localizado en la inducción de varias rutas de muerte celular apoptóticas, también reafirma la necesidad de una mayor profundización en estos fenómenos para lograr su total esclarecimiento. Al respecto, estudios futuros podrían estar dirigidos a evaluar la cinética de internalización de las nanopartículas en los lisosomas utilizando diversas líneas celulares tumorales, y con ello, la influencia del calentamiento local que inducen bajo acción de un AMF, en aspectos tales como: la producción de ROS, el daño mitocondrial y lisosomal, así como la expresión de diversos receptores y ligandos de muerte celular. Por otro lado, la optimización de las nanopartículas para maximizar la muerte celular requiere una comprensión de la distribución espacial de sus propiedades de calentamiento dentro de los lisosomas; por lo que la combinación de estudios de co-localización lisosomal de partículas (dependiendo de la concentración y la cinética de acumulación de las mismas) con análisis computacionales del efecto térmico, también sería muy interesante para optimizar el efecto terapéutico de la hipertermia magnética.

Finalmente, somos conscientes de que aunque valioso, el modelo celular ensayado no representa la elevada complejidad de las líneas celulares tumorales utilizadas en la práctica *in vitro* e *in vivo*, por lo que se requiere de la contextualización y claramente la adaptación de los resultados obtenidos al modelo tumoral que se desee estudiar. Razón por la cual, después de optimizar e identificar algunos de los principales factores (tales como concentración y distribución intracelular de las nanopartículas) que modulan las vías de señalización de la muerte celular en diferentes modelo de cultivo celular 3D de células RAW264.7, decidimos evaluar el efecto de la dosis térmica, tiempo de exposición, y diferentes localizaciones de nanopartículas de óxido de hierro en una línea celular de cáncer pancreático humano; tema que se aborda en detalle en el siguiente capítulo.

CAPÍTULO 5 ·
HIPERTERMIA MAGNÉTICA COMO ENFOQUE PARA EL TRATAMIENTO DEL CÁNCER DE PÁNCREAS

5.1 Introducción ampliada al tema

El cáncer de páncreas es una de las neoplasias malignas con mayores índices de letalidad a nivel mundial.[501] A principios del siglo XXI, el número estimado de cánceres pancreáticos en todo el mundo era de 110,000 con una tasa de mortalidad global estimada del 98%,[502] y pocos años después, en 2018, ya era clasificado como el 11° cáncer mundial más común, contando con 458,918 casos nuevos y causando 432,242 muertes (4,5% de todas las muertes causadas por cáncer) en ese año.[160] Las razones de estas altas tasas de mortalidad suelen asociarse al diagnóstico tardío de la enfermedad, ya que los pacientes que la desarrollan no suelen manifestar síntomas claros hasta una etapa avanzada; a lo que se une, que en muchos casos, los esquemas de tratamientos aplicados en la clínica no logran remitir la enfermedad.[503] Por un lado, si bien la cirugía de resección tumoral puede aumentar los índices de supervivencia en un 5% durante un período de cinco años, más del 80% de los pacientes con cáncer de páncreas no son candidatos elegibles a estos procedimientos, debido a que a menudo presentan metástasis regionales y distantes a consecuencia del diagnóstico de la enfermedad en un estadio avanzado.[504] Por otro lado, los tumores pancreáticos se caracterizan por tener un estroma denso y un microambiente tumoral altamente inmunosupresor, lo que hace que las terapias convencionales como la radiación y quimioterapia, u otros esquemas de tratamiento más emergentes como la inmunoterapia, sean menos efectivas.[237, 505-507]

En este contexto, el uso de hipertermia magnética basada en nanopartículas entregadas específicamente al sitio del tumor, proporciona una metodología terapéuticamente prometedora para el tratamiento del cáncer pancreático debido a que el impacto del calentamiento local resultante se puede observar tanto a nivel ultraestructural, para facilitar la disrupción de la

gruesa matriz extracelular que los caracteriza;[211] como a nivel macroscópico, ya que los daños localmente inducidos por la terapia térmica alteran la homeostasis promoviendo diversos mecanismos de muerte celular; tal y como se ha demostrado en los anteriores capítulos de esta tesis.[336] A diferencia de los agentes farmacológicos convencionales utilizados para el tratamiento del cáncer, o de otras metodologías de hipertermia de cuerpo entero o regional (tales como mantas térmicas, ultrasonidos, etc.), en la hipertermia magnética el calentamiento de las nanopartículas permanece local y depende de la presencia simultánea de las partículas y su excitación con un campo magnético alterno. Hecho que contribuye a minimizar los efectos secundarios sistémicos, y permite una mejor recuperación de las células u órganos sanos vecinos debido a que no se aplican elevados niveles de estrés al entorno biológico circundante del tejido tratado.[26, 121, 129, 260, 508] Por otro lado, es conocido que el tratamiento a dosis térmicas moderadas también permite estimular diversos elementos de la respuesta inmunológica tanto innata como adaptativa contra la propagación del tumor.[144, 509] Fenómeno especialmente prometedor en el tratamiento de tumores con marcadas características inmunosupresoras y de difícil acceso a la terapia como es el caso de los derivados del cáncer de páncreas, lo que convierte a la hipertermia magnética en una alternativa muy atractiva tanto para su aplicación como esquema de tratamiento individual, como en concomitancia con quimio-, radio- e inmunoterapia para mejorar y/o potenciar su efectividad terapéutica. [510-512]

La investigación de nuevas alternativas de tratamiento para el cáncer de páncreas hacen urgente la búsqueda de modelos que permitan predecir los resultados clínicos de estos enfoques terapéuticos, en términos de imitar las interacciones micro-ambientales heterotípicas que parecen ser la clave en la patogénesis de la enfermedad. Para estudios *in vitro* del cáncer pancreático humano, donde la matriz estromal puede llegar a representar casi el 90% del volumen tumoral en reposo,[513] el desarrollo de modelos tridimensionales de cultivo ofrece excepcionales ventajas respecto a los convencionales modelos de cultivo en monocapas bidimensionales, ya que imita el microambiente tumoral 3D y proporciona un nivel intermedio de complejidad tumoral para ensayar diversos enfoques terapéuticos previos al ensayo *in vivo*.[514] En este sentido, una amplia variedad de modelos 3D de cáncer pancreático humano se han desarrollado para estudios básicos y traslacionales de la biología de las células tumorales pancreáticas, y como plataforma en la identificación y validación de nuevos biomarcadores específicos para el tratamiento de la enfermedad.[514-515] Por ejemplo, el modelo esferoidal desarrollado por Gutiérrez-Barrera y colaboradores utilizaba células tumorales pancreáticas del epitelio ductal humano para imitar características morfológicas y de señalización (tales como,

regiones del lumen, apicales y basales) de los cánceres pancreáticos en la clínica.[516] Mientras que otro modelos 3D basados en matrices de Matrigel, metilcelulosa y alginato también se han elegido para imitar componentes de la matriz extracelular, y proporcionar señales intrínsecas que permiten estudiar el desarrollo tumoral y su respuesta a la terapia.[517-518] Sin embargo, el establecimiento de modelos individualizados de cáncer de páncreas que permitan mimetizar la mayoría de los escenarios encontrados en la práctica clínica, se ha visto dificultado debido a la elevada complejidad estromal y ubicación interna de este tipo de tumor. En este sentido, uno de los modelos matriciales de mayor relevancia en el estudio de la modulación del microambiente tumoral pancreático, y específicamente de la matriz extracelular, son los basados en colágeno.[390, 519] Precisamente, porque la desmoplasia, una producción aberrante de matriz extracelular que resulta en la formación de una densa red fibrosa enriquecida en colágeno fibrilar y altamente infiltrada con los denominados fibroblastos asociados a cáncer, se considera como un marcador predictivo de malignidad del cáncer pancreático. [515] La respuesta desmoplástica aberrante del tejido tumoral pancreático no se limita solo una restricción física pasiva, sino también que activa directamente diversas vías de señalización inmunosupresoras, a la vez que promueve la agresión tumoral.[390, 519] Por lo cual, evaluar el impacto de la hipertermia basada en el uso de nano-calentadores inducibles como las nanopartículas magnéticas utilizando modelos tridimensionales basados en colágeno, es un paso esencial para comprender el impacto de la hipertermia magnética en la normalización de la rigidez tumoral, y por ende, la respuesta de sensibilización del tumor a diferentes esquemas de tratamiento. En lo que concierne a los estudios *in vivo*, los modelos tradicionales de cáncer pancreático humano se basan en la implantación y desarrollo de células tumorales humanas o fragmentos de tumor derivados de pacientes en ratones inmunodeficientes.[514, 520-521] Aunque la traducción de estos conocimientos para el beneficio de los pacientes ha sido lenta debido a las complicaciones asociadas al desarrollo de modelos preclínicos óptimos que permitan imitar el desarrollo del cáncer pancreático humano, los avances alcanzados en estos años parecen ser prometedores en la translación de las observaciones, tanto *in vitro* como *in vivo,* al tratamiento clínico de la enfermedad.

Al respecto, uno de los mayores desafíos de la hipertermia magnética *in vivo* es lograr una concentración de material magnético en el tumor que permita alcanzar dosis terapéuticamente relevantes. Para la experimentación *in vivo*, las nanopartículas magnéticas pueden ser inyectadas directamente en la región tumoral o por vía sistémica (ej. intravenosa, intraperitoneal, etc.). En este último caso, suelen preferirse nanopartículas con altos valores de

SAR para maximizar el efecto de calentamiento local,[254] debido que una vez que las nanopartículas entran en contacto con los fluidos biológicos pueden ser capturadas por los monocitos y macrófagos de tejidos residenciales resultando en su inespecífica acumulación en órganos como el hígado y el bazo *(Figura 1.4)*,[12, 522] lo que va en detrimento de las cantidades efectivas acumuladas en el tumor. Sin embargo, también debe tenerse que el valor de SAR, además de depender de los parámetros intrínsecos de la partícula (tales como, la geometría, tamaño, etc.), también depende de los parámetros de AMF utilizados para realizar las mediciones, por lo cual su magnitud puede variar dependiendo del equipo empleado para realizar el tratamiento térmico.[101, 105, 246] Por otro lado, la agregación de nanopartículas, que a menudo ocurre en el entorno celular, también limita la eficiencia de calentamiento macroscópico de las partículas magnéticas.[310, 312-313] Razón por la cual, a pesar de los avances en la síntesis y desarrollo de nanopartículas con capacidades magnéticas óptimas, la administración sistémica sigue estando limitada por la necesidad de lograr una alta concentración local del material magnético en el tumor; ya sea aprovechando las características propias de las vasculatura tumoral,[523] o mediante la funcionalización de las nanopartículas con anticuerpos o ligandos específicos al tumor. [524] Esto unido a los posibles efectos tóxicos asociados a la liberación de las partículas a la circulación, [40, 525-527] han derivado en el hecho de que en la mayoría de las investigaciones pre-clínicas, e incluso las aplicaciones clínicas actuales para terapia del cáncer por hipertermia magnética, se favorezca la administración intratumoral sobre la inyección sistémica.[369]

Tanto a nivel pre-clínico como clínico, la administración intratumoral de nanopartículas ha demostrado ser una herramienta eficiente para la generación de dosis térmicas que favorecen la remisión parcial o total del tumor.[154, 321, 369, 511, 528] Al respecto, la mayoría de modelos preclínicos en los cuales se utiliza esta metodología, se basan en el tratamiento de tumores implantados subcutáneamente debido a que las nanopartículas son inyectadas directamente en el tumor (véase sección 2.2).[369] A pesar de esto, en la práctica clínica también se ha demostrado la factibilidad de la administración intratumoral mediante el uso de métodos estereotácticos de aplicación del material magnético.[154, 490] De hecho, probablemente el desafío más importante para esta metodología sea la obtención de una acumulación homogénea de nanopartículas después de la inyección. Entre otras razones, porque las altas presiones intersticiales en el área del tumor pueden conducir a patrones de distribución irregulares, e incluso ralentizar la tasa de infiltración de las partículas.[529] A lo que se une, que la naturaleza heterogénea de las regiones tumorales *(Figura 1.9)* también dificulta un suministro uniforme, ya que algunas áreas del

tumor (ej. zonas en proliferación) pueden metabolizar las partículas más rápido en comparación con otras (ej. zonas necróticas o quiescentes). En consecuencia, la eficacia terapéutica puede verse disminuida debido a la heterogeneidad de las dosis térmicas que se alcanzan dentro del tumor una vez que las partículas se exponen al AMF, o por la existencia de zonas que al no contener nanopartículas escapan de la exposición a la temperatura.[402, 490, 530] Por este motivo, la biodistribución del nanomaterial magnético después de la inyección intratumoral, aunque poco estudiado hasta el momento,[154, 490, 529, 531] debe ser cuidadosamente analizado para garantizar la efectividad de la terapia térmica, y con ello un mejor control de las respuestas biológicas inducidas por el tratamiento.

5.2 Effect of the field conditions, MNP biodistribution and immune response in the treatment of a xenograft pancreatic cancer model with magnetic hyperthermia.

Lilianne Beola[1]; Valeria Grazú, PhD[1]; Yilian Fernández-Afonso[1]; Raluca M. Fratila, PhD[1]; Marcelo de las Heras, PhD[2]; Jesús M. de la Fuente, PhD[1]; Lucía Gutiérrez, PhD[3] and Laura Asín, PhD[1]

[1]Institute of Materials Science of Aragón, Universidad de Zaragoza, CSIC, Campus Río Ebro, Edificio I+D, Mariano Esquillor Gómez, 50018 Zaragoza, Spain. Centro de Investigación Biomédica en Red de Bioingeniería, Biomateriales y Nanomedicina (CIBER-BBN), Spain.

[2]Department of Animal Pathology, Veterinary Faculty, University of Zaragoza, C/ de Miguel Servet, 177, 50013, Zaragoza, Spain.

[3]Department of Analytical Chemistry, Universidad de Zaragoza and CIBER-BBN. Instituto Universitario de Nanociencia de Aragón (INA), Edificio I+D, C/ Mariano Esquillor Gómez, 50018, Zaragoza, Spain.

Abstract: Magnetic hyperthermia (MH) has been used to treat a tumor model of pancreatic cancer. This type of tumor is characterized by the presence of dense stroma that acts as a barrier for chemotherapeutic treatments. Therefore, the use of 2D in vitro models imitates even worse *in vivo* conditions. This is why several parameters that have an important effect on MH treatment effectiveness have been tested using 3D cell culture models before going to *in vivo* experiments. Indeed, several alternating magnetic field (AMF) conditions have been tested first using 3D culture to determine which one was producing the stronger effect on the cell viability. Once this optimal AMF condition was applied *in vivo*, the activation of the immune response after the MH treatment has been evaluated indirectly, observing an increased expression of Chaperone calreticulin (CALR) molecules in those cells containing magnetic nanoparticles. Moreover, the distribution of the nanoparticles within the tumor tissue has been assessed in histological analysis of tumor sections, observing that the exposure to the alternating magnetic field results in the migration of the particles towards the inner parts of the tumor. The results obtained therefore showed that MH could trigger tumor cell death either directly and/or indirectly through biological effects due to induction of local heat or the activation of an immune response, respectively. In the case of this last anti-tumoral mechanism, the observed disruption of the tumor stroma by the MH treatment results in a key-enabling factor. Finally, a relationship between an inadequate biodistribution of the particles after their intra-tumoral injection and a significant decrease in the effectiveness of the MH treatment has been found. Animals in which most of the particles remained in the tumor area after injection have shown higher reductions in the tumor volume growth in comparison with those animals in which part of the particles had been transported to the liver and spleen. Therefore, our results point out several factors that should be considered in order to achieve successful results on the use of magnetic hyperthermia for the treatment of pancreatic cancer.

Keywords: iron oxide magnetic nanoparticles, magnetic hyperthermia, intratumor administration, biodistribution, immunological effect, pancreatic cancer

1. Introduction

Pancreatic ductal adenocarcinoma (PDAC), the most frequent type of pancreatic cancer, is characterized by the generalized presence of extremely dense stroma. This stroma is responsible for the increased rigidity of these tumors[532] and acts as a barrier not only against chemotherapeutic drugs, decreasing their effectiveness, but also impairing infiltration of antitumor immune cells.[533-534] This, amongst other factors, is one of the reasons of the bad prognosis of this type of cancer, with average five-year-survival rates of 10 %. Therefore, new therapeutic strategies for the treatment of this disease are urgently needed that not only addresses triggering the selective death of tumor cells, but at the same time tackles the disruption of stromal molecular and cellular components.

Over the past decades, nanotechnology has been extensively exploited in the quest for new and advanced tools for diagnosis and therapy of diseases. Different types of nanomaterials have been proposed as biosensors, as contrast agents for different imaging techniques, or as nanocarriers able to improve the efficacy, long-term stability and biodistribution of drugs.[535-536] In the frame of pancreatic cancer, several nanoparticle-based strategies have been investigated for the development of new diagnostic and therapeutic platforms, some of them showing potential for the modulation of the PDAC microenvironment. Most of the proposed strategies are focus on drug delivery combining in the same nanoplatform the release of different therapeutic agents for both modulating the stroma and triggering tumor cell death. However, the diversity of animal models, tumor location, selected drugs and nanomaterials makes difficult to extract solid conclusions when comparing all the results.[515] Our strategy is also centered on both achieving a change in the stroma permeabilization and provoking tumor cell death. However, in our case, we propose to do it without combining different drugs but with a single kind of treatment that have showed a dual role;[336] an indirect antitumor effect due the physical stroma disruption and a direct antitumor effect due to the heat produced in the tumor cells that could trigger the immune system response and the cell death.

The proposed therapeutic approach for achieving the above-mentioned effects in PDAC is nanoparticle-based magnetic hyperthermia (MH). In this kind of therapeutic treatment, magnetic nanoparticles (MNPs) are able to convert energy absorbed from an external alternating magnetic field (AMF) into local heat. This treatment has been proposed as both as a stand-alone method or in combination with other treatments.[93, 121, 537] In the clinical practice, the European Medical Agency (EMA) has approved MH treatment after the success of clinical

trials for glioblastoma (Berlin, Charité Hospital, 2003 to 2005). It has also been approved as an adjuvant therapy for recurrent glioblastoma in combination with radiotherapy in 2012.[154] Currently, the company Magforce is undergoing clinical trials in USA to validate its use also for prostate cancer.[239]

Despite these advances, researchers working in the field of magnetic hyperthermia for cancer treatment still face several challenges and practical problems such as the difficulty to achieve enough magnetic material in the tumors after intravenous administration, or the heterogeneous distribution of the particles in the whole tumor volume even after intra-tumoral injection.[402] This limitation becomes even more important when using the MH to treat PDAC because of its unique tumor environment. However, we consider that the enhancement of MNPs penetration in 3D cell models observed in our group after the MH treatment will help to overcome this restriction.[336] In addition, there are still many knowledge gaps in the frame of *in vivo* MH applications, like the cytotoxicity mechanisms triggered directly by the treatment and/or since to an activation of an immune response to tumor antigens stimulated by the treatment. Antitumor immune response is a key player, and often quite forgotten, that contributes in the effectiveness of all the possible antitumor treatment combinations. Gaining knowledge on how the MH treatment could affect the immune system function would allow taking advantage of natural defense mechanisms against tumors. One of events that can be evaluated to assess the response of the immune system to a treatment is the presence of Damage-associated molecular patterns (DAMPs) in the treated cells. One of the several DAMPs that could be analyzed is the expression in the cell surface of the chaperone calreticulin (CALR), which takes place early in the course of the immunogenic cell death (ICD). In general, DAMPs bind to pattern recognition receptors (PRRs) in the immune cells, leading the activation of both innate and adaptive immune responses. Stimulating the immune system with the MH treatment would lead to very important advantages, such as generating a systemic antitumor reaction that could act in metastatic tumors and triggering an immune memory effect that could prevent the patients from relapses.[145, 510]

Very recently, our work using 3D cell culture models composed of collagen, which is the main component of the extracellular matrix, has shown that the heat produced by magnetic nanoparticles has a dual role as it was able to produce cell death triggered by intracellular hotspots and also to improve the permeability of the collagen acting as extracellular (ECM) matrix disruptor allowing the penetration of the nanoparticles towards the inner part of the 3D structure.[336] These results are especially relevant in the frame of PDAC, in which the stroma

can account for up to 80% of the tumor volume, acting as a biological barrier against anti-PADC treatments and therefore reducing their effectiveness. Nevertheless, our previous studies were performed using a macrophage cell line, known by its high MNP internalization capability. Therefore, to evaluate the feasibility of using MH for treating PDAC, further studies were required to analyze the feasibility to achieve the same observed effects *in vitro*, but using a pancreatic tumor cell line, which typically has less internalization capability than macrophages. As this was the case, we went a step further by also evaluating the effect of MH *in vivo*.

In summary, the general objective of this study was to evaluate the antitumor effectiveness of MH for pancreatic cancer treatment both *in vitro* and *in vivo*. A 3D cell culture model using a pancreatic tumor cell line (MIA PaCa-2) was selected for the *in vitro* optimization of the AMF conditions. Then, using the optimal AMF conditions, the MH treatment was tested in a heterotopic xenograft mouse model. The expression of calreticulin in tumor cells after *in vivo* application of MH treatment was measured in order to assess the effect of the treatment on the potential activation of immune response. Finally, the impact of MNP biodistribution after their intra-tumoral injection on the effectiveness of the MH treatment was also evaluated.

2. Results and Discussion

2.1 *In vitro* experiments

2.1.1 *MNP internalization and distribution after MH treatment*

Magnetic nanoparticles from the same synthetic batch as in our previous work were used in this study.[336] Briefly, oleic acid-coated 11.3 ± 0.2 nm spherical iron oxide nanoparticles (Fig. S1) obtained by thermal decomposition were stored in hexane. The magnetic cores were then submitted to a water-transference step by performing new coating with PMAO (poly(maleic anhydride-alt-1-octadecene) modified with a fluorophore (TAMRA, carboxytetramethylrhodamine). Finally, their functionalization with glucose was performed to produce the final material used in this work. This functionalization step is carried out in order to prevent aggregation in complex biological media and improve the particle uptake by the cells. The Specific Absorption Rate (SAR) value for these particles was 104 W/g Fe, (measured at H= 20 kA/m and f= 829 kHz, using [Fe] = 1 mg/mL). Stability was verified by Dynamic Light Scattering measurements yielding a hydrodynamic size of 85 ± 7 nm *(Figure S1)*.

As in our previous work[336], we prepared two different 3D cell culture models mimicking different *in vivo* scenarios of MNP internalization. We called the first model "*In Model*". In this model, cells were incubated with the MNPs during 1 h, washed to remove the unbound MNPs, and then used to form the 3D collagen gel. This procedure resulted in a high percentage of MNP-loaded-cells, as shown by flow cytometry (FC) (68.5 ± 2.6 %, *(Figure 1B)*). In this model, as expected no extracellular MNPs were found in the collagen matrix, as it was verified with fluorescence microscopy *(Figure 1A)*. The second model, named "*In&Out Model*", consisted of a collagen gel where the cells have been previously embedded and that were subsequently incubated with MNPs during 1 h and washed afterwards to remove unbound particles. In this model a lower number of MNP-loaded-cells was found (28.5 ± 4.5%, *(Figure 1E)*) in comparison with the other model. In addition, MNPs were still found in the collagen matrix outside the cells *(Figure 1D)*. It is noteworthy that, although the percentage of cells that internalized MNPs in both cases was very different (being much higher the number of cells with internalized MNPs in the *In Model* than in the *In&Out* one), the average amount of MNPs internalized per cell is very similar. This could be inferred by the values of median fluorescence intensity (MFI) of both positive populations (10.2 ± 0.8 and 10.4 ± 1.2 for *In Model* and *In&Out Model*, respectively) pointing out to a similar internalization capability of the cells in both models. We have previously shown that the procedure used to incubate the 3D gel with the MNPs in the *In&Out Model* yields a heterogeneous distribution of the particles within its structure, where most of the particles are located in the outer areas of the 3D structure.[336] The difficulty of the MNPs to reach the inner parts of the 3D structure in this model is the reason for the lower number of cells that are able to internalize MNPs, when compared to the *In Model*.

In previous experiments made with macrophages, we observed that extracellular MNPs in the *In&Out Model* diffuse with time to the inner part of the structure.[336] This migration is faster if the 3D cell culture is exposed to an AMF, probably because the heat generated by the particles disrupt collagen fibers increasing the permeability of the 3D collagen structure.

In this work we studied the influence that the exposure to an AMF had in the MNP internalization in tumor cells. Three different combinations of magnetic field amplitude (H) and frequency (*f*) were used (AMF 1: 110 kHz and 31.9 kA/m, AMF 2: 377 kHz and 13 kA/m and AMF 3: 228 kHz and 23.9 kA/m). In all cases the AMF exposure was 30 minutes. AMF2 were the conditions used in our previous work[336] and the other two AC field conditions (AMF 1 and AMF 3) were selected in order to test other field amplitude and frequency conditions,

but always maintaining their product around the biological limit of 5 x 10^9 A/ms[251, 254] (AMF1: 3.5 x 10^9, AMF2: 4.9 x 10^9 and AMF3: 5.4 x10^9 A/ms).

As expected, in the In Model both the percentage of MNP-loaded cells and the MFI remained the same before and after the AMF application due to the absence of extracellular MNPs (Fig. 1C). In contrast, in the *In&Out Model*, while the percentage of MNP-loaded cells did not change significantly before and after the AMF application, the average amount of MNPs internalized per cell increased after the MH treatment *(Figure 1F)*. These results indicated that probably longer times are needed to achieve a complete internalization of the particles by the cells that are located in the inner part of the 3D structure.

Interestingly, the increase of the number of MNPs internalized per cell in the *In&Out Model* after the AMF treatment was significantly different depending on the AMF conditions. In particular, the highest increase of the MNP internalization was observed for the AMF3 conditions (MFI = 15.0 ± 0.9 a.u.). This value was the highest from all the conditions tested both for the *In* and *In&Out Models* at the different AMF conditions *(Figures 1C, F)*.

Probably, the variations in the AMF conditions produced a different heating profile on the collagen matrix that had an effect on the diffusion of the MNPs within the 3D structure. Unfortunately, several technical and experimental limitations prevented us from knowing the exact local temperature reached near the particles. First, technical limitations prevented us from measuring the SAR values at these field amplitude and frequency conditions. Nevertheless, even if we could have been able to measure the SAR values in these conditions, it would have been difficult to decide at which MNP concentration the experiments should have been performed, as it is very difficult to know the local MNP concentration in the 3D cell culture, a key parameter affecting the interparticle dipolar interactions and thus their heating efficiency.[477] Several approaches have been described to measure temperatures locally, although all of them needed a significant alteration of the MNPs,[82, 538] and therefore, the results may not be a precise reflection of the real heating conditions. Further studies using theoretical simulations[104] would be required to completely understand the heat being released by the particles in our conditions and optimize the treatment.
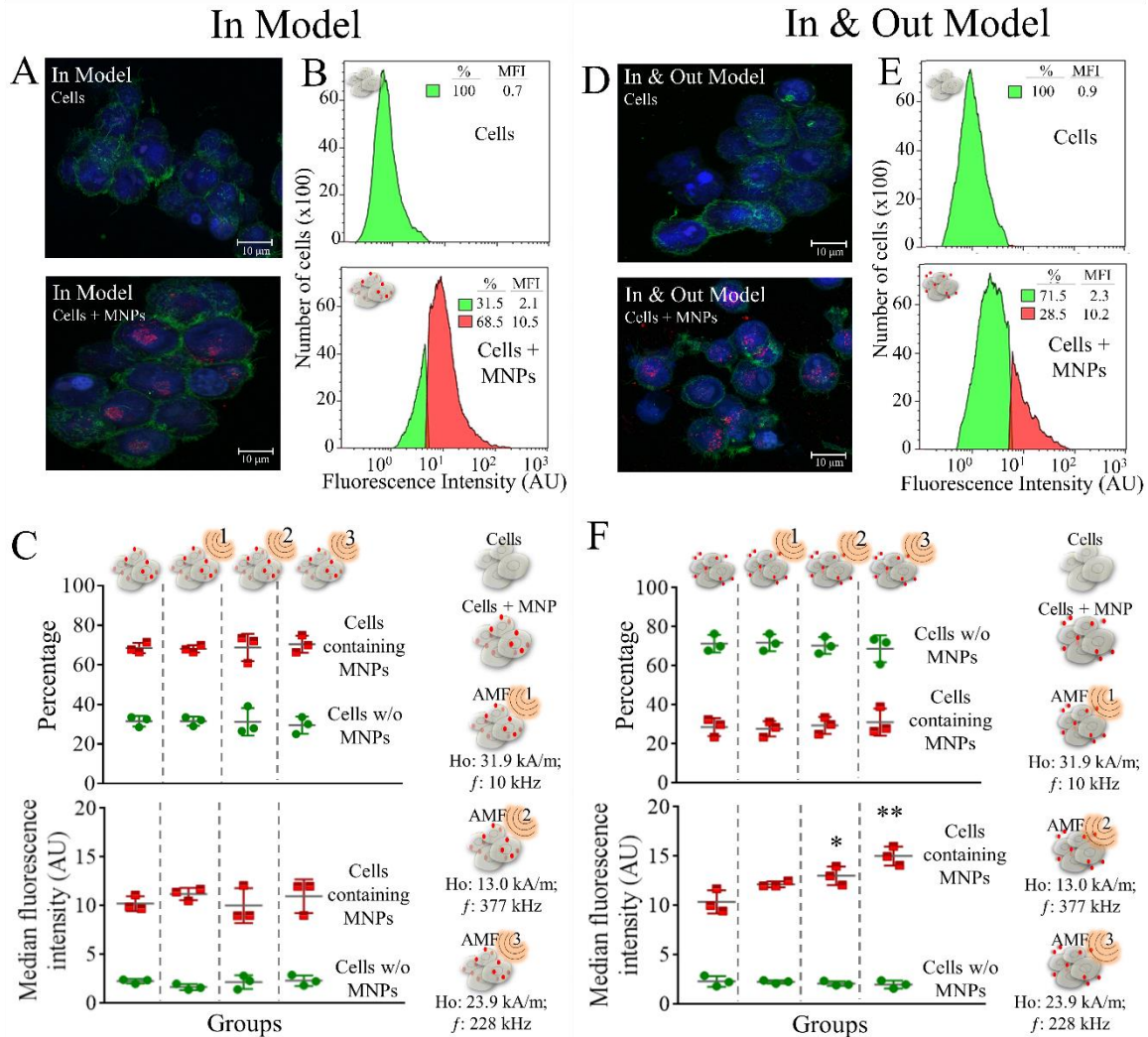
Figure 1. 3D cell culture models characterization: In Model (left), In &Out Model (right). (A, D) Confocal images. Red: MNPs (TAMRA). Blue: DAPI (nucleus). Green: Alexa Fluor® 488 Phalloidin. Scale bar: 10 μm. (B, E) Selected nanoparticle uptake histogram representative of three independent experiments. (C, F) MNP uptake before and after exposure to different AMF conditions (AMF 1: 110 kHz; 31.9 kA/m. AMF 2: 377 kHz; 13 kA/m. AMF 3: 228 kHz; 23.9 kA/m) measured as percentage of cells with MNPs and the changes in the MFI. Statistical differences were determined using a two-way ANOVA followed by a Sidak's multiple comparisons test (**p < 0.01; *p < 0.05; p > 0.05 no significance).

These results confirmed that the internalization of MNPs present in the extracellular environment continues after the MH treatment. This observation could have an important effect in clinical settings, as in most *in vivo* studies the MNPs are being injected intratumorally[265, 278, 320, 369], where a remarkable percentage of MNPs remains in the extracellular matrix (ECM). In such case, a positive effect of the repetition of the AMF exposure on consecutive days to enhance the effect of the MH treatment may occur. Additionally, an increase of the ECM

permeability after the AMF exposure could be of great help not only because of the MNP internalization enhancement but also because it could be used to allow the infiltration of antitumor drugs or immune system cells towards inner parts of the tumor that would contribute to improve the final antitumor effectiveness.[332, 539-540]

2.1.2 In vitro antitumor efficiency of the MH treatment

After studying the MNP internalization and the effect the AMF exposure has on it, we examined the cell viability after the MH treatment at the three conditions of magnetic field above detailed. For that purpose, the cell viability of the different treatments was tested by flow cytometry. We used Propidium Iodide (PI), which enters into the cell as result of the plasmatic membrane disruption, and Annexin V, which binds Phosphatidyl Serine, a phospholipid that translocates to the outer leaflet of the plasmatic membrane at the beginning of the apoptosis process.

Figure 2 shows the results of the cell viability studies 24 hours after the MH treatment for both 3D models, *In Model* and *In&Out Model*. It can be seen that, for both models, all the controls presented a viability above 80% confirming that the AMF and the MNPs *per se* do not produce any cytotoxic effect. When analyzing the results of cell viability after the complete treatment using three different AMF conditions it was observed that, in both models, when using AMF 1 and AMF 2 conditions the cell viability was similar to the control groups. These results indicated that the heat released by the MNPs in these conditions was not enough to produce detectable cellular damage in MIA PaCa-2 cells at least 24 hours after the treatment. However, results were different for the AMF 3 condition where the cell viability decreased in both models (52.9 ± 2.8% for the *In Model* and 72.0 ± 2.6% for the *In&Out Model*). In these conditions, cells positive for Annexin V (undergoing early apoptosis) and cells positive for both PI and Annexin V (undergoing apoptosis or necrosis) were detected. The differences of dead cells percentages observed for the two models under the exposure to AMF 3 were probably due to the different percentage of MNP-loaded cells. In the case of the *In Model* the percentage of cells that internalized MNPs was much higher than for the *In&Out Model*, as previously shown in *Figure 1*. These results agreed with the results observed for the internalization of the MNPs in the previous section, pointing to the fact that these field amplitude and frequency conditions were the ones in which our system released more heat.

The cell death pathway was likely to be the same in both models, observing some cells in an early apoptosis stage and other population in a late necrosis/apoptosis stage. Having the same

death route in both 3D models agreed with the fact that the average amount of MNPs per cell was the same in both of them.
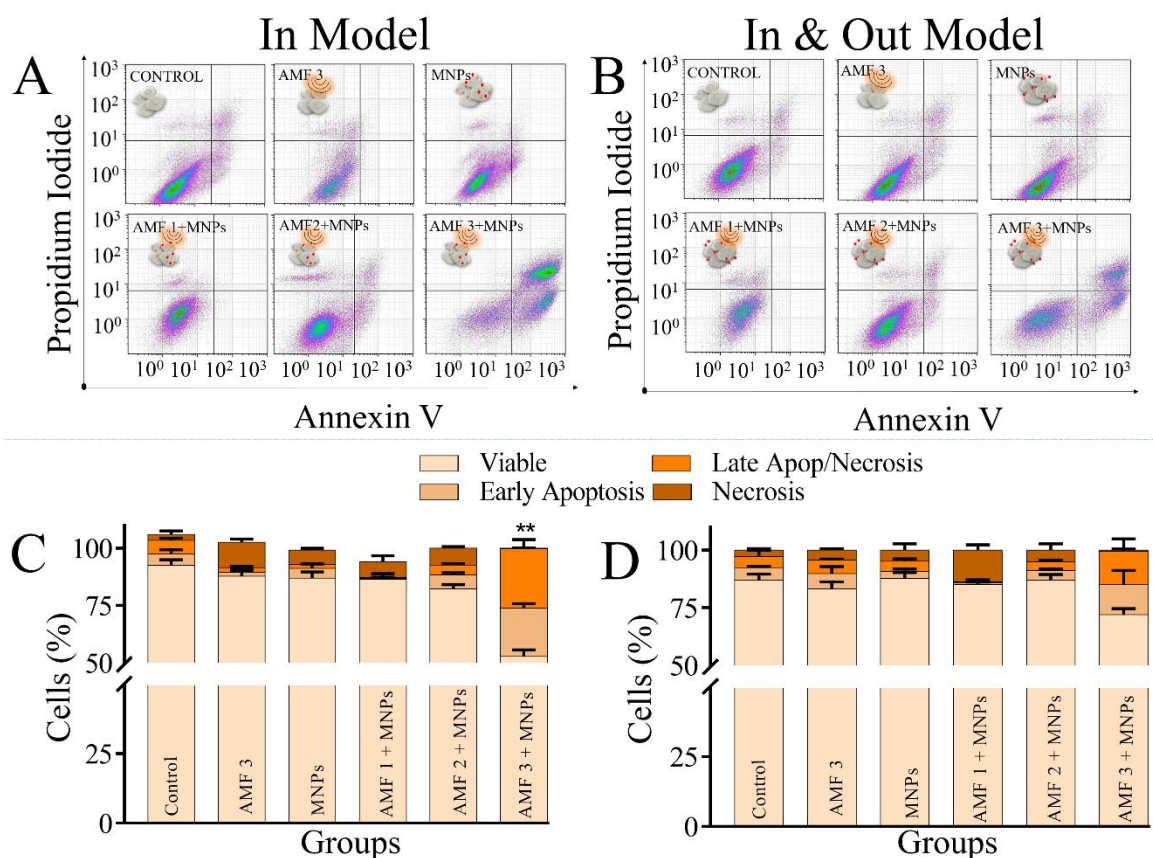
Figure 2. Cell death induction (Annexin V/PI staining) 24 h after a single administration of a magnetic hyperthermia treatment using different AMF conditions (AMF 1: 110 kHz; 31.9 kA/m. AMF 2: 377 kHz; 13 kA/m. AMF 3: 228 kHz; 23.9 kA/m) for In Model (left) and In & Out Model (right). (A, B) Selected density plots representative of three independent experiments. (C, D) Summarized results data resulting from three independent experiments shown as mean ± SD. Significant differences respect to the control group were analyzed using a two-way ANOVA followed by a Bonferroni's multiple comparisons test (** p < 0.01; p > 0.05 no significance).

2.2 In vivo experiments

2.2.1 In vivo assessment of the immune response activation

The effect of the MH treatment in an animal model was then studied. A nude mice strain was selected for the subcutaneous implantation of MIA PaCa-2 cells that led to the development of a pancreatic tumor in the right flank of the animals. It is important to bear in mind that these animals lack part of the immune system, which may lead to an underestimation of the real effectiveness of the treatment.

Approximately 14 days after the MIA PaCa-2 cells injection, the tumors were small but detectable, with an appropriate size (around 100-200 mm^3) for MNP injection (0.15 mg Fe/tumor). Animals were randomly distributed in four groups, four mice in each control group and 8 in the one receiving the complete treatment. The different experimental groups were: (i) control animals without any treatment; (ii) animals exposed to the AMF but without the MNP injection (AMF); (iii) animals that received the MNP injection but were not exposed to the AMF (MNPs); and (iv) animals that received the MNP injection and were then exposed to the AMF (AMF+MNPs). In this last group the mice were exposed to the AMF the same day of the MNPs injection and the next two consecutive days. In all cases the evolution of the tumor volume and the animals' weight were followed twice a week during four weeks after treatment, with the exception of the animals in which the CALR expression was studied, which were monitored just for two weeks.

At around 20 days after the MNP administration, we assessed the expression of a marker of immunogenic cell death (ICD) during *in vivo* MH treatment in order to know whether the cells that die during the treatment could trigger an immune response that would help in the tumor treatment.

The generation of some damage-associated molecular patterns (DAMPs) is related to immunogenic cell death activation.[406, 541] The expression of these molecules in cells responding to a death stimulus leads to a robust immunostimulatory effect since they bind to pattern recognition receptors (PRRs) in the immune cells. Chaperone calreticulin (CALR) molecules, normally located in cellular storage compartments, are exposed on the outer side of the plasmatic membrane in the beginning of the ICD, before the translocation of the phosphatidyl serine typical of apoptosis.[542] CALR is exposed as a consequence of the activation of caspase 8 and other molecules involved in apoptosis. When CALR is recognized by a lipoprotein receptor (low density lipoprotein receptor LRP1 or CD91), an important phagocytic signal is triggered, stimulating antigen presenting cells (APCs) like the dendritic cells. CALR exposure can be detected by flow cytometry using the corresponding antibodies.
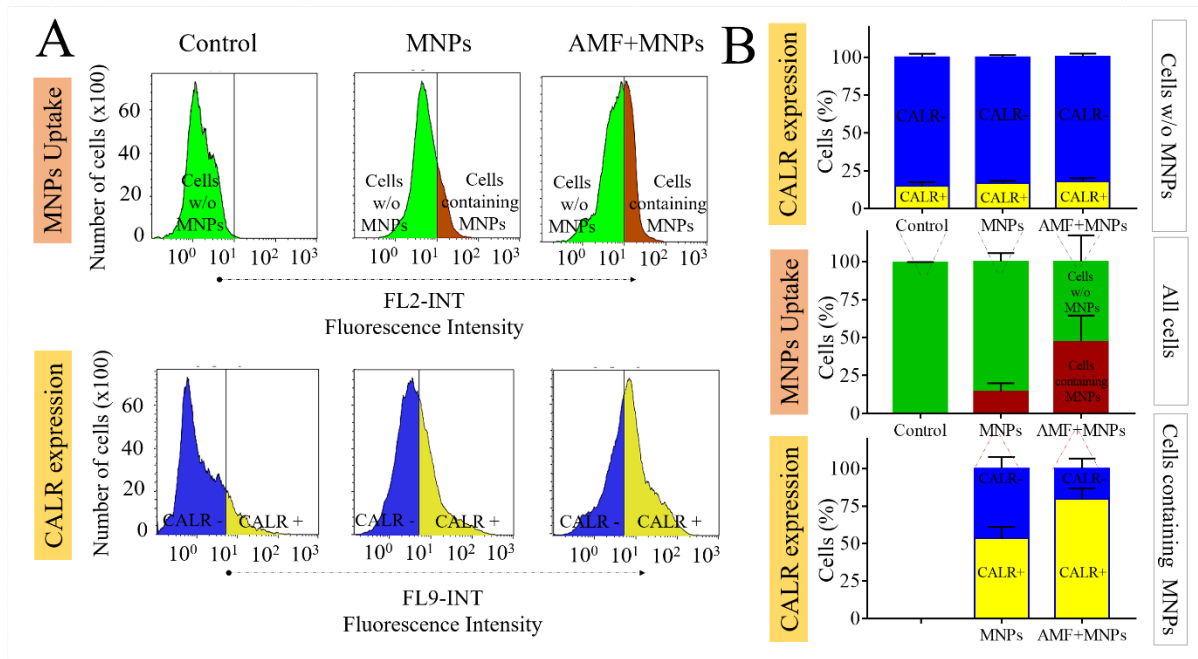
Figure 3. Magnetic nanoparticle uptake and calreticulin expression of different groups analyzed. (A) Flow cytometry histograms showing MNP internalization (up) and CARL expression (down) in cells obtained after digesting the tumor after the MH treatment. (B) Summarized data from flow cytometry experiments showing the percentage of cells that express CARL in the membrane in the cells that do not contain MNPs (up) and in the MNPs-loaded cells (down). n=2.

Figure 3 shows the results of the CALR expression of three groups of mice; Control, MNPs and AMF+MNPs sacrificed at around 2 weeks after the beginning of the study. After euthanizing the animals, tumors were extracted and a cell dissociation protocol was followed to obtain a homogeneous cell suspension formed by tumor cells and extracellular tumor matrix infiltrating cells. The complete suspension was then analyzed by flow cytometry determining two parameters: the MNP internalization and the expression of CALR molecules in the cells obtained after digesting the tumor mass that contain tumor and other infiltrating cells. Results indicate that, in the AMF+MNPs group the percentage of cells that internalized MNPs is higher compared to the animals that only received the MNPs *(Figure 3)*. The increase of the number of cells with internalized MNPs after the AMF exposure was not observed in the *in vitro* experiments with this cell line, probably, this is related to the longer time after the AMF exposure at which the study of the internalization has been carried out in the animal study compared with the *in vitro* one.

Concerning the CALR expression, it was observed that in the MNPs group there was a portion of cells that expressed CALR in their plasmatic membrane, which indicated that the MNPs

were causing some stress to the cells even in the case of not being exposed to the AMF. Interestingly, the expression of this molecule increased considerably for the complete treatment (AMF+MNPs group).

These results were analyzed more in detail by comparing the percentage of cells expressing CALR in cells with and without MNP internalization. MNP-loaded cells are more affected by the heat generated during the MH treatment and therefore are expected to express DAMPs. However, we considered that it was also worth studying the levels of CALR expression in the non-loaded cells, in order detect if there was any bystander effect that could sensitize them.

The percentage of MNP-loaded cells that express CALR on their surface both with and without AMF exposure was evaluated *(Figure 3)*. In the MNPs group the percentage of cells positive for CALR expression was of 54%, indicating some degree of toxicity associated to the presence of the MNPs. Interestingly, this percentage significantly increased up to 80% in the AMF+MNPs group, indicating that the activation of the immune system was triggered after the MH treatment. The basal expression of the CALR levels was evaluated in those cells that did not contain any particle (Figure 3). CALR expression levels were similar in all the samples analyzed, indicating that no bystander effect was occurring, at least in terms of this molecule expression.

Very little work has been performed on the study of the immunomodulatory effect of the MH treatment,[512, 543-544] though none of these studies used iron oxide spherical magnetic nanoparticles as thermal sources as in this work. Some recent work had also evaluated the activation of the immune system in the tumor environment related to the heat produced by photothermal therapy with gold nanoparticles.[545] A more complete analysis of other relevant players in the immune system response to the MH treatment would be required to have a complete knowledge of the pathways that are being activated by this treatment.[359] Nevertheless, our results indicated that tumor cells that die during the magnetic hyperthermia treatment expressed the selected DAMP, indicating an increase of activation of immunogenic cell death routes. Our results agreed with recent publications, that showed that after heating up tumors with MNPs, in this case with light radiation, there was an immune response, observing the activation of dendritic cells and T cells in *in vivo* experiments, resulting in the inhibition of distant tumors.[546] Stimulating the adaptive immune response would have very important advantages, such as generating a systemic antitumor reaction that could act in metastatic tumors and triggering an immune memory effect[547] that could prevent the patients from relapsing.

2.2.2 In vivo antitumor effectiveness of the MH treatment

In order to evaluate the MH treatment effectiveness *in vivo*, the evolution of the tumor volume along time for the different groups was followed during approximately 30 days *(Figure 4)*. In general, this is the main parameter that has been used in previous works assessing the effectiveness of the treatment.[369] In general, in many previous works, the growth inhibition of the tumor was observed and there are only scarce works where a complete regression of the tumor occurred.[94, 274, 280-281]

In our work, as expected, the control and the AMF groups showed the highest tumor growth rates, very similar in both cases. The MNPs group, that received the particle injection, did not reach tumor volumes as high as the other two control groups (Control and AMF groups). These results agreed with the effect observed in the analysis of the CALR expression that showed an activation of the immunogenic cell death associated to the presence of particles, even though they were not exposed to the AMF. Finally, the AMF+MNPs group, animals that received the complete treatment consisting of three cycles of MH, showed a heterogenous antitumor effect that could be divided into two different subgroups *(Figure 4B)*. One of these subgroups showed a lower antitumor effect (Subgroup A), with final volume sizes very similar to those of the MNPs group. The other subgroup of animals (Subgroup B) showed a higher inhibition of the tumor growth. The differences in the tumor growth behavior between these two subgroups were statistically different. In order to evaluate the reasons for these differences, further histopathological analysis and magnetic measurements of the MNP biodistribution were performed.
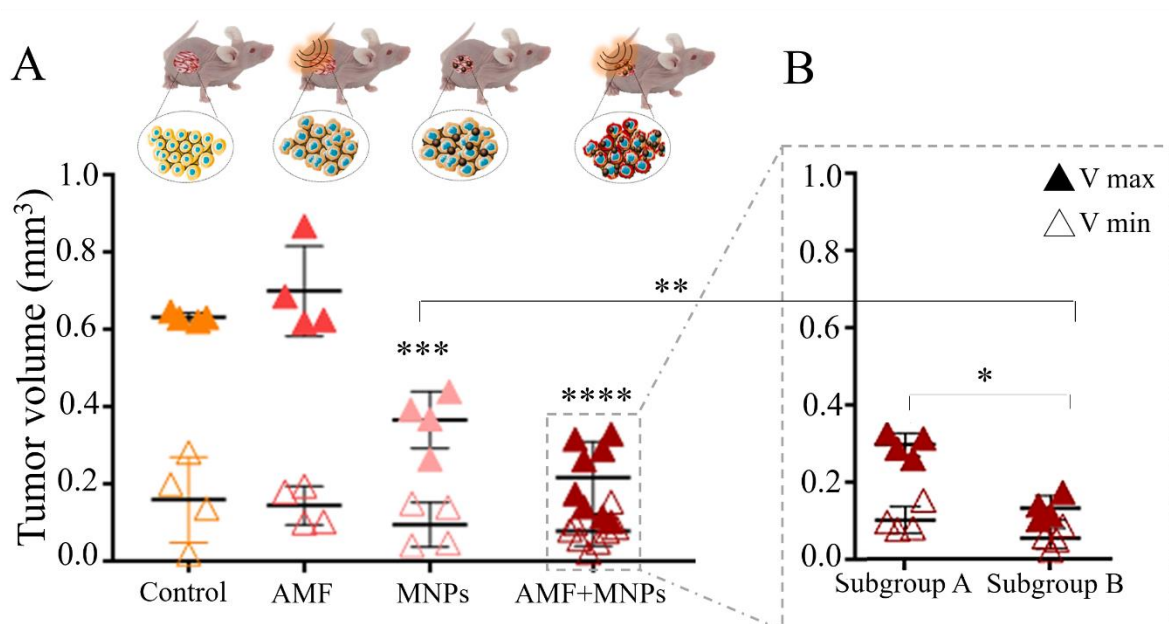
Figure 4. (A) Tumor evolution represented as the starting volume (V min) and maximum volume reached during the experiment (V max) (B) Same data as in panel A for the AMF+MNPs group but divided into two subgroups with different behavior. Significant differences with respect to the control were analyzed using a two-way ANOVA followed by a Sidak's multiple comparisons test (****p < 0.0001; *** p < 0.001;**p < 0.01; *p < 0.05; p > 0.05 no significance). In cases where more than one group generated significant differences with respect to control, the means between those groups were also compared. This figure was produced using images from Servier Medical Art PPT image bank.

2.2.3 Histological analysis: Effect of the MH treatment on the MNP intratumor distribution

Histological assessment of tumor sections from the different groups provided further information regarding the effect of the treatment. The nanoparticle distribution in the tissue was observed trough specific iron staining with Prussian Blue. In both models containing nanoparticles (MNPs and AFM+MNPs), the particles were mainly located in the outer areas of the tumor (Fig. 5A). This non-homogeneous particle distribution within the tumor also had been previously reported in other studies using intratumor administration.[528-529] Some factors had already been proposed as the cause of the variation of spatial distribution of the nanoparticles in the tumor such as the flow rate injection,[530] the time between the injection and the MH treatment or the exposure or not to the AMF.[490] This non-homogeneous distribution of the MNPs could be one of the reasons why the complete inhibition of the tumor growth was not observed in our case, as the heat released by the particles may not be enough to reach the inner areas of the tumor.[489]

In our work, we quantified the necrotic and apoptotic cells in each tumor section *(Figures 5; S3)* to obtain more information about the effects caused by the MH treatment. Ten different zones of the same area per tissue section were selected for the analysis. No significant differences in the number of dead cells per area were observed between the three control groups: mice treated with PBS (Control), mice exposed to the AMF field (AMF) or mice treated with the MNPs but not exposed to the AMF (MNPs) (Fig. 5B). In contrast, significant differences were found for the group that received the complete MH treatment (AMF+MNPs) (Fig. 5B). These differences were higher in the sub-group of mice where a clear tumor growth inhibition was observed (p=0.0014 for Subgroup B). In contrast, a smaller effect was observed in the other subgroup of mice (p=0.0187 for the Subgroup A). These results agreed with the effect observed in the evolution of the tumor volume found for these two sub-groups.

Interestingly, in all the mice exposed to an AMF after the MNP injection, the penetration of the particles towards the inner parts of the tumor was observed *(Figure 5)*. This is the same effect previously reported in our studies with 3D cell cultures models[336] and in previous *in vivo* works.[489-490] The reason for this penetration is probably the temperature increase triggered by the MH treatment, that can have an important effect on the ECM structure, facilitating the penetration of MNPs towards the inner areas of the tumor. As mentioned before, these results were especially relevant in the frame pancreatic ductal adenocarcinoma, given its high content of stroma that acts as a barrier against chemotherapeutic agents[533]. It could be envisaged that the MH treatment could act as a tool able the increase the permeability of the stroma, having potential synergistic effects on the treatments for pancreatic cancer with chemotherapy.

Nevertheless, further experiments were still needed to clarify the cause of the differences between the two sub-groups with significantly different effectiveness of the MH treatment (Subgroup A and Subgroup B).
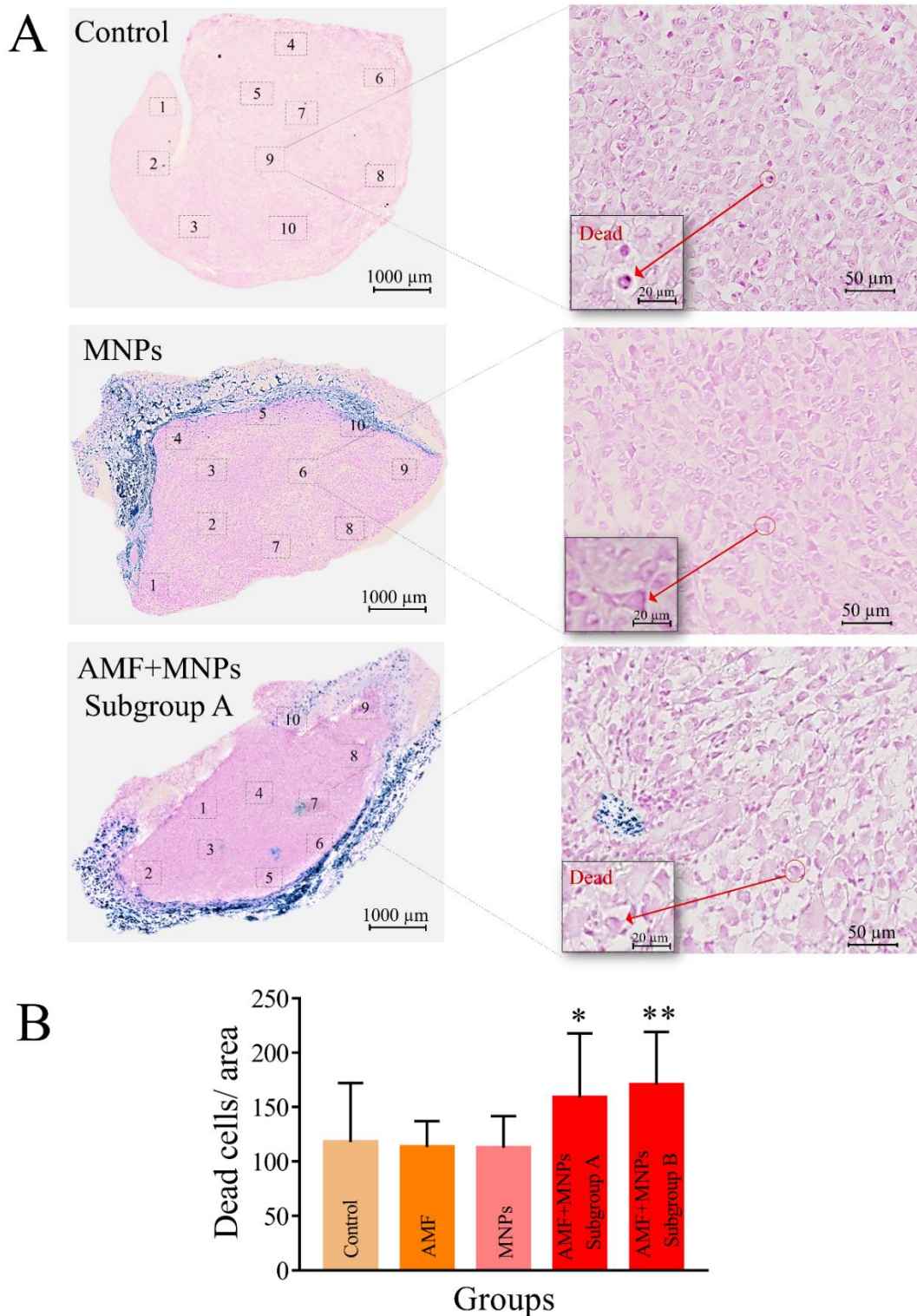
Figure 5. (A) Representative tumor sections after Perls blue staining. The numbers represent the ten random areas used for the dead cell quantification in each section. (B) Summarized analysis of the dead cells per area in the different groups analyzed. The data are represented as the mean ± SD. The statistical differences respect to the control group were determined using a one-way ANOVA (**p < 0.01; *p < 0.05; p > 0.05 no significance).

2.2.4 Effect of the MNP biodistribution on the MH effectiveness

In order to analyze the possible causes of these differences between the groups of animals that received the complete treatment, we performed an analysis of the MNP concentration in the tumor tissue together with the analysis of their biodistribution among other organs.

Few studies had analyzed the biodistribution of nanoparticles towards the internal organs after intratumor injection.[94, 528] One of the main difficulties is that, given the relatively high amount of endogenous iron in the liver and the spleen, conventional elemental analysis techniques are not specific enough to detect variations in small amounts of iron coming from the particles. For this reason, a technique as the AC susceptibility measurements was selected, as this technique is able to distinguish between the endogenous iron and the iron originating from the MNPs, allowing their detection with high sensitivity and specificity.[548]

After sacrificing the mice at the end of the study, some organs were extracted (tumor, skin in contact with the tumor, liver, spleen and blood) and the amount of particles in each of them was analyzed using magnetic measurements. The temperature dependence of the AC magnetic susceptibility for all the organs was measured and compared with that of the injected particles. Previous works had validated this technique as a very sensitive way to detect the MNP biodistribution.[28, 289, 314, 549-550] The susceptibility maxima observed in *Figures 6A* and *6B* was a fingerprint of the presence of particles in a given tissue.[548, 551] The height of the out-of-phase susceptibility maxima *(Figure S4)* was related to the number of particles within a given tissue and was used to quantify the iron concentration in the form of MNPs in each tissue sample.

The quantification process was performed in the tumors. However, as the tumor was split in several parts to be also analyzed by histology, some errors may had been introduced in the calculation related to the heterogeneous MNPs biodistribution. An average concentration of 0.7 ± 0.6 μg of iron/mg of tissue was found for Subgroup A while for Subgroup B this value was 2.5 fold-higher (1.7 ± 0.6 μg of iron/mg of tissue). The total iron content in the tumors analyzed, calculated considering the whole tumor mass was found to be quite heterogeneous ($\approx 5 - 80$ μg of iron, that corresponded to $\approx 2.5 - 40\%$ of mass of iron from the initial injection, resulting in an average value of 31 ± 29 μg of iron). In the skin samples, although still quite heterogeneous, a shorter range of iron amounts was found ($\approx 3.5 - 17\%$ of mass of iron from the initial injection).

It was interesting to compare the different biodistribution patterns observed in animals that had a different response to the MH treatment. Those animals that showed a weaker response (Subgroup A) presented detectable amounts of particles in the liver and the spleen (≈ 3 μg of iron in the form of MNPs in the liver and ≈ 0.1 μg of iron in the spleen). In contrast, in animals belonging to the Subgroup B, with a better response to the MH treatment, no particles in other organs (or at least under the detection limits of the technique) were found *(Figure 6C and Fig. S4)*. These data indicated that, in Subgroup A, part of the injected dose had travelled from the tumor to other organs, reducing the potential effect of the treatment. The amount of particles found in the liver and spleen was significantly lower than in the tumor, as previously described by other authors.[528] However, it should also be noted that it had been previously shown that the degradation of MNPs in these two organs, spleen and liver, can occur within this time frame,[314, 549] so the total amount of nanoparticles that may had travelled to these organs was probably underestimated in our analysis.

One of the causes of the observation of MNPs in the liver and the spleen could be the filtration of the particles through the tumor vasculature. Leakage of the MNPs towards blood vessels would result in their accumulation in the liver and spleen, the main organs for MNP accumulation after intravenous administration.[28, 314, 550] In our case, no signal of the MNPs was found in blood samples collected during the animal sacrifice, but this could be explained by a leakage at short times after the intravenous injection.

Our results point towards the important effect that an inadequate biodistribution of the MNPs in the body could have on the effectiveness of the treatment. Therefore, we would suggest that this kind of studies should be routinely performed after intratumor administration to verify that the intended amount of particles remain in the tumor area.
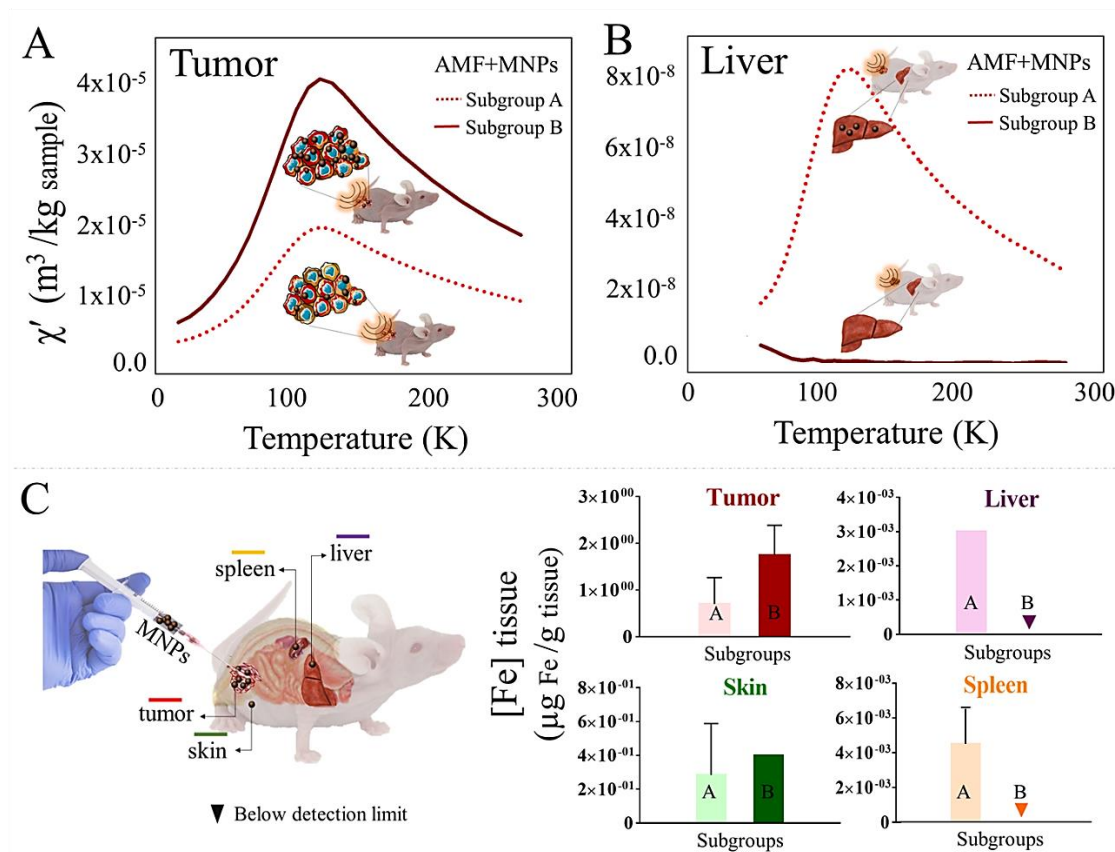
Figure 6. MNP biodistribution assessed by AC magnetic susceptibility 30 days after their intratumor injection. Temperature dependence of the in-phase susceptibility from (A) Tumor and (B) Liver 30 days after of the intratumor injection. (C) Average iron content (associated to MNPs) calculated from the magnetic characterization analysis for each of the analyzed tissues (tumor, liver, spleen and skin next to the tumor) for the two sub-groups of animals that received the complete treatment (AMF+MNPs). This figure was produced using images from Servier Medical Art PPT image bank.

3. Conclusions

Two different 3D cell culture models of MIA PaCa-2 cell line, one with the particles just inside the cells, and other with the particles both inside and outside the cells were prepared and the MNP internalization and viability after the treatment were assessed for three different combinations of magnetic field amplitude and frequency. It was found that a decrease in the cell viability in both models was achieved using the AMF 3 conditions (228 kHz; 23.9 kA/m). Therefore, these conditions were selected to be used in the *in vivo* experiment.

The analysis of the CALR expression suggested that an enhanced immune response was triggered in those cells containing MNPs after the MH treatment, opening the way to further

studies on the immune response after MH using animal models with a complete immune system.

The histological analysis of tumor sections indicated a heterogeneous distribution of the particles within the tumor, being most of them located in the outer areas. Nevertheless, the MH-treated mice showed the presence of significant amounts of particles in inner areas of the tumor. This is probably the result of the increased penetration of the particles towards the inner parts of the tumor after the exposure to several cycles of AMF. This observation points to future studies combining MH and chemotherapy to evaluate possible synergistic effects of both treatments, especially if the heat produced by the particles is also able to improve the permeability of drugs towards the inner parts of the tumor.

Finally, even though a decrease on the tumor growth rate was observed for all animals that received the complete MH treatment in comparison with the controls, it was possible to divide the animals treated in two subgroups depending on the growth rate. A clear relationship was then found between those subgroups and their whole-body particles biodistribution pattern. The sub-group of animals in which the treatment was not so satisfactory presented particles in the liver and the spleen. These results indicate the importance of the correct biodistribution of the nanoparticles in order to achieve the most effective treatment.

In summary, our results have reveled key parameters to be considered for a successful treatment of pancreatic cancer using magnetic hyperthermia and have opened the way to future studies on the enhanced permeability of the tumors after the AMF exposure that could be key factors for the development of new treatments for this disease.

4. Materials and Methods

4.1 Synthesis, functionalization and characterization of magnetic nanoparticles

Iron oxide MNPs ($\approx$ 11 nm) were synthesized by thermal decomposition in organic media based on a previously reported seed-mediated growth method[69] using iron (III) acetylacetonate (Fe(acac)$_3$) as a precursor.[314] This procedure rendered oleic-acid coated hydrophobic MNPs that were then transferred to water using a protocol based on the coating with an amphiphilic polymer (poly(maleic anhydride-alt-1-octadecene, PMAO, MW 30000–50000 Da) modified with TAMRA (tetramethylrhodamine 5(6)-carboxamide cadaverine (Anaspec, Seraing, Belgium), a fluorophore that allows the *in vitro* tracking of the MNPs.[314]

Then, the coated MNPs were functionalized with glucose to provide further stability in biological media. The coated nanoparticles (1 mg of iron) were incubated with 42 µmol of N-(3-dimethylaminopropyl)-N'-ethylcarbodiimide hydrochloride (EDC) and 30 µmol of 4-aminophenyl β-D-glucopyranoside in 250 µL of SSB buffer (50 mM of boric acid and 50 mM of sodium borate) at pH 9. After 3 h at room temperature, the excess of reagents was removed by washing the sample with phosphate-buffered saline buffer (PBS) at pH 7.4 in a centrifugal filter[74]. Finally, nanoparticles were passed through syringe filters with a pore size of 0.22 µm (Merck Millipore, Darmstadt, Germany).

Dynamic light scattering and ζ-potential measurements were performed in water and in complete Dulbecco's Modified Eagle's Medium GlutaMAX™ Supplement (cDMEM; Gibco®, Thermo Fisher Scientific) on a Malvern Zetasizer Nano-ZS, using ten runs per measurement and five replicates at 25 °C and pH 7.

Particle size and morphology were studied by Transmission Electron Microscopy (TEM) using a Tecnai T20 (FEI company, OR, USA) microscope operating at 200 kV. The sample was prepared by placing a drop of a diluted suspension of the MNPs in water onto a carbon-coated grid and allowing it to dry. Particle size was determined by manual measurement of 200 particles using the Digital Micrograph software.

The heating capacity of the MNPs was determined using a commercial Alternating Magnetic Field generator (DM100; Nanoscale Biomagnetics, Spain). A 1 mg Fe/mL MNP suspension was placed in a closed container centered in the inductive coil. The AMF was applied for 5 min using a field amplitude of H = 20 kA/m, and a frequency of 829 kHz while the temperature was recorded using an optic fiber sensor incorporated in the equipment.

For the magnetic characterization, the MNPs liquid sample was allowed to dry at room temperature deposited into a piece of cotton wool that was subsequently placed into a gelatin capsule. An additional sample of the particles dispersed in agar and then freeze-dried was prepared to be used in the quantification protocol. AC magnetic susceptibility measurements were performed in a Quantum Design (USA) MPMS-XL SQUID magnetometer with an AC (alternating current) option. Measurements were acquired using a field amplitude of 0.41 Oe and a frequency of 11 Hz in the temperature range between 5 and 300 K.

4.2 Cell culture

MIA PaCa-2 (ATCC® CRL-1420™) pancreas cancer cell line was cultured and maintained in complete Dulbecco's Modified Eagle's Medium GlutaMAX™ Supplement (cDMEM; Gibco®, Thermo Fisher Scientific) supplemented with 10 % fetal bovine serum (FBS,

Invitrogen), 100 U/mL penicillin G (sodium salt) and 100 μg/mL streptomycin sulfate (Invitrogen) at 37 °C in a humidified atmosphere at 5 % CO_2. Every three or four days in dependence of the confluency, the cell culture was diluted to 1:10. To detach the cells, these were incubated with Trypsin EDTA solution (Sigma Aldrich) for 4 minutes at 37 ºC. Finally, cells were collected in fresh cDMEM.

To prepare the 3D cell culture models, two different strategies of incubation with MNPs were followed based in a previously reported method. [336] The first model where nanoparticles are located only inside the cells - In Model - was prepared by incubation of the cells, cultured in monolayer conditions, with MNPs (0.2 mgFe/mL) during 24 h at 37 ºC. After this time, the medium with MNPs was discarded and the cells were detached and washed by centrifugation (300 x g, 5 min) twice and then, were used to performed the collagen structure. Just after the collagen gelling, 0.5 mL of cDMEM were added to the 3D structure. In the other model where nanoparticles are located both inside and outside the cells In&Out Model-, the 3D cell culture was generated first with the cells in suspension, and then, 0.5 mL of a MNPs suspension (0.2 mg Fe/mL) in cDMEM were added and incubated at 37 °C for 24 h. After the incubation time, the supernatant was removed, the 3D cell culture was washed twice, and 0.5 mL of complete culture medium were added to the 3D model.

4.3 Tumor Xenograft Model

Pathogen- free male athymic nude mice (Crl:NU(NCr-*Foxn1^{nu}*)), 6-week old, received a subcutaneous injection into the right flank with the human pancreatic cancer cell line MIA PaCa-2-2 suspended in 0.2 mL of sterile DMEM culture medium without phenol red using a 25 G needle. During the cells injection, animals were anesthetized by inhalation of isoflurane (4% for the induction step and 2% for maintenance). The mice were commercially obtained from Charles River Laboratory and were maintained in the Animal facilities of the CIBA (IACS-Universidad de Zaragoza). Before any procedure, mice were held one week after arriving from the animal facilities for acclimation. Animals were maintained according to the institutional animal use and care regulation of the Centro de Investigaciones Biomédicas de Aragón (CIBA, Zaragoza, Spain). All animal experiments were conducted according to the law RD53/2013 and approved by the Ethics Committee for animal experiments from the University of Zaragoza that is an accredited animal welfare body.

4.4 Magnetic hyperthermia treatment

A commercial AMF generator (DM3, nB nanoscale Biomagnetics, Zaragoza, Spain) was used in all scenarios. The exposure time to AMF was 30 min in each case.

4.4.1 In vitro

MIA PaCa-2 cells cultured 3D conditions in a 24 wells plates, were thermalized at 37 °C using a water bath pump (Stryker - Medical Devices & Equipment Manufacturing Company) connected to a water tubing jacket. Then, cells were exposed to AMF using different schemes of frequency and field amplitude: AMF1 (377 kHz; 13 kA/m), AMF2 (110 kHz; 31.9 kA/m) and AMF3 (228 kHz; 23.9 kA/m).

4.4.2 In vivo

Immunodeficient mice were inoculated with human pancreatic cancer cells. About 3 weeks later, when the tumor size was about 0.1 mm^3, 3 mg/mL of MNPs in a final volume of 0.05 mL per tumor, were injected intratumorally using a 30 G needle. Mice were divided randomly into four different groups (Control - tumor control; AMF - tumor exposed to AMF; MNP - tumor injected with MNPs; AMF+MNPs - tumor injected with MNPs and exposed to the AMF). The same day of the MNPs injection and the following two days, mice were exposed to the AMF (f = 196 kHz; H = 26 kA/m). Mice were anesthetized with isoflurane and maintained during the AMF exposure onto a hot water bath system that prevents the mice from suffering hypothermia. The rectal temperature was registered during the AMF exposure to control the general state of the animals. After the last AMF exposure, mice were maintained to evaluate the response to the treatment. Tumor dimensions (length, width, and height) were measured twice a week with a digital caliper. The weight was followed during the experiment as indicator of the wellness of mice.

4.5 Confocal microscopy

To study the MNPs cell internalization, the 3D cell cultures were fixed during 20 min with 0.5 mL of paraformaldehyde (4%). Then, the nuclei were stained with DAPI (4′,6-diamidino-2-phenylindole) and the cytoskeleton with Phalloidin 488. A Zeiss LSM 880 Confocal Microscope equipped with a 63x/1.40 Plan Apochromat objective was used to acquire the images of the cells. The laser sources used were 458 nm, 488 nm (Argon Ion) and 561 nm (DPSS- Diode-pumped solid state). ZEN Microscope and Imaging Software were used for the image analysis.

4.6 Flow cytometry studies

All samples were analyzed in a Gallios™ Flow Cytometer (Beckman Coulter) and the data interpreted with Kaluza 2.1 Software (Beckman Coulter).

4.6.1 In vitro assay

Cells were released from the 3D cell cultures using a treatment with collagenase type I (isolated from *Cl. histolyticum* lyophilized, non-sterile, Gibco™ Thermo Fisher Scientific) at 2 mg/mL in HBSS (Hank's Balanced Salt Solution) during 30 min at 37 ºC. Then, in each case, cells were washed by centrifugation (300 x g, 5 min) and re-suspended in PBS (Phosphate Buffer Saline pH=7.4). To determine the MNPs uptake, cells re-suspended in PBS at a concentration of 2.5×10^4 cells/mL were analyzed by flow cytometry in the FL2 channel at 575 nm. To study the cell viability, cells were re-suspended in 1X Annexin V Binding Buffer (10 mM Hepes/NaOH (pH=7.4) 140 mM NaCl, 2,5 mM $CaCl_2$) at a concentration of 10^6 cells/mL. Then, 5×10^{-3} mL of the Annexin V-FITC (Fluorescein Isothiocyanate) and 5×10^{-3} mL of Propidium Iodide (PI) were added to 0.1 mL of cell suspension and incubated at room temperature for 15 minutes in the dark (FITC-Annexin V Apoptosis Detection Kit). After the incubation period, 0.4 mL of 1X Annexin binding buffer was added and the sample was analyzed by flow cytometry.

4.6.2 Ex vivo assays

Subcutaneous tumors from euthanized mice were placed into a corning tube with DMEM medium. Then, on a glass surface, each tumor was disengaged in small pieces with scalpels and transferred into a 15 mL corning tube with 3 mL of Collagenase P (1.5 mg/mL). The mix was placed in continuous rotation for 10-12 min in incubator at 37 ºC. The reaction was stopped by addition of 1 mL of FBS and DMEM medium until 10 mL final volume and then was centrifuged during 5 min at 300 xg. The supernatant was removed and 2 mL of Trypsin/EDTA was added to pellet and mixed gently to incubated in continuous rotation for 3 min at 37 ºC. The trypsin was neutralized by addition of 2 mL of FBS and DMEM until 15 mL final volume. After a strong mixture, the suspension was centrifuged during 5 min at 300xg and the supernatant was discarded. The pellet was resuspended in 5 mL of DMEM and filtered through a 100 µm filter and then in a 40 µm strainer into a 50 mL corning tube. The sample was transferred into a 15 mL tube and centrifuged 5 min at 300xg. The supernatant was discarded and the pellet was resuspended in 0.8 mL of 1X Red Blood Cell (RBC) Lysis Buffer (Invitrogen™ by Thermo Fisher Scientific) continuously agitating with the pipette for 20-30 seconds. The reaction was stopped by addition of DMEM medium (5-10 mL) and then, the mix

was washed by centrifugation (5 min at 300xg). The supernatant was discarded and re-suspended in PBS. To evaluate immunogenic death signals, cells from the tumor samples were re-suspended in 1X Binding Buffer at a concentration of 1×10^4 cells/mL. Then, 2×10^{-3} mL of α-Calreticulin antibody-Alexa Fluor® 405 (Abcam ab210431) were added to 0.05 mL of cell suspension and incubated at room temperature for 30 minutes in the dark. After the incubation period, the cells were washed 3 times by centrifugation (300 x g, 5 min). Finally, 0.4 mL of 1X Binding buffer were added and the sample was analyzed by flow cytometry. To determine the MNP uptake, the cells were analyzed in the FL2 channel at 575 nm.

4.7 Mice Sample Preparation and Analysis

Mice were euthanized by CO_2 inhalation, and blood was directly extracted from the heart. In addition, the tumor, the skin next to it, liver and spleen were removed.

Tumor pieces were fixed in 4% PFA and processed to perform Hematoxylin/Eosin and Blue Perls staining. All the sample preparation including the scanning in light field was made by the "Servicio Científico Técnico-Microscopía y Anatomía Patológica" of the CIBA (IACS-Universidad de Zaragoza).

For the magnetic measurements, tissue samples (liver, spleen, skin and tumor pieces) were freeze-dried in Telstar cryodos-50 during 24 h and placed directly into gelatin capsules for their characterization. Magnetic susceptibility measurements were performed in a Quantum Design (USA) MPMS-XL SQUID magnetometer with an AC (alternating current) amplitude of 0.41 Oe, in the temperature range between 5 and 300 K and at a frequency of 11 Hz.

4.8 Statistical Analysis

All data were expressed as mean ± SD of a minimum three biological replicas. Statistical significance of difference in means was evaluated using GraphPad Prism v7.00. Two-way ANOVA and one-way ANOVA tests were used for the analysis of the data. The confidence interval was 95%. Sidak's and Bonferroni´s multiple comparation post-tests were used to determine which means differed.

5. Associated content
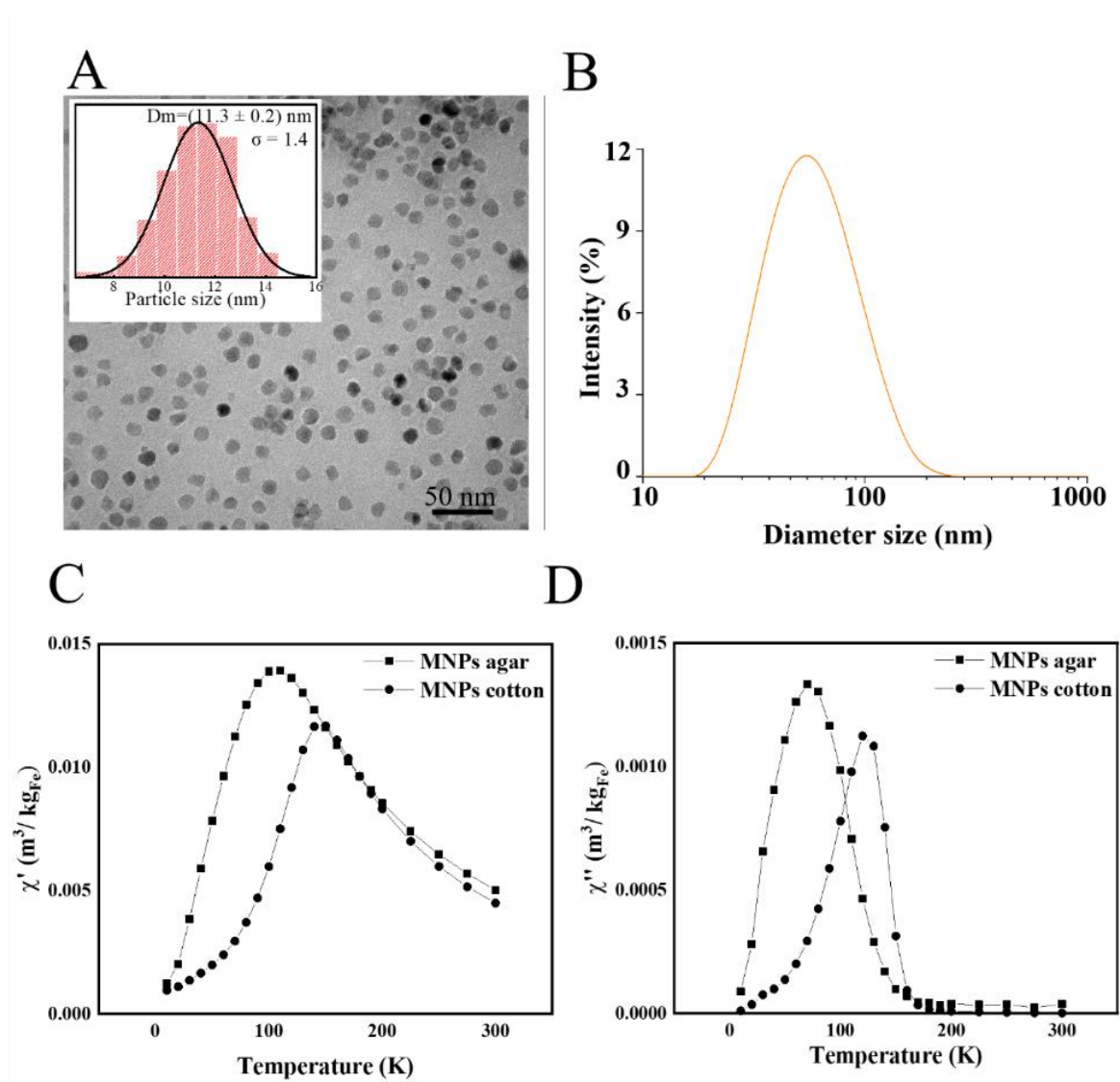
Figure S1. (A) TEM image and nanoparticles size distribution analysis. (B) DLS size distribution histogram of MNPs functionalized with glucose in PBS.
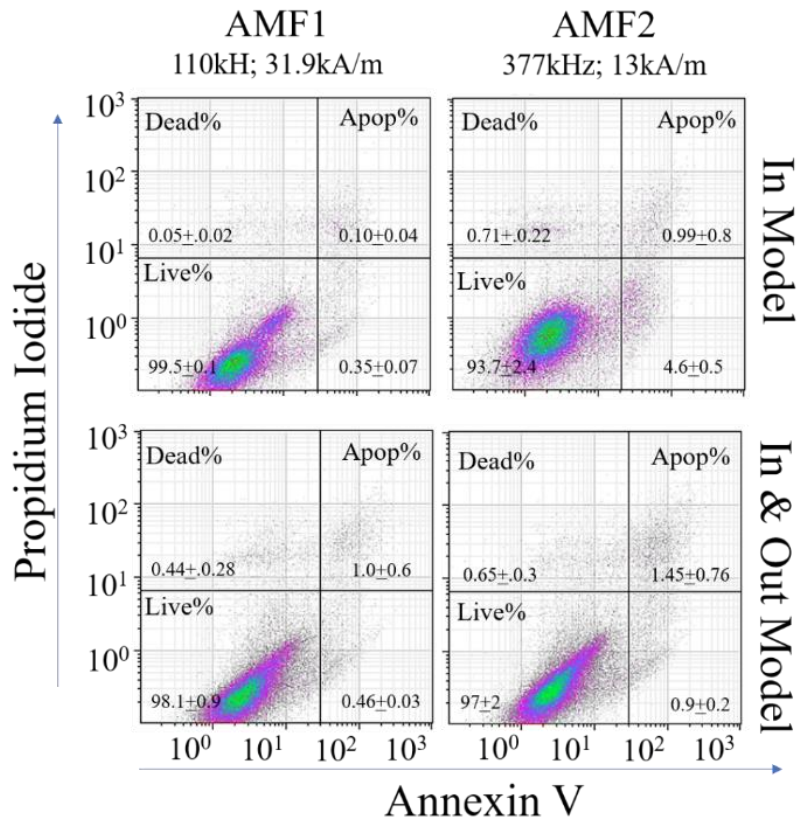
Figure S2: Cell death induction under different hyperthermia controls for In Model (above) and In &Out Model (below). 3D cell culture of empty cells were exposure at different AMF. 24h after one-single dose Annexin V/PI staining was made. The data are represented as density plot representative of three independent experiment (supporting data Figure 2).
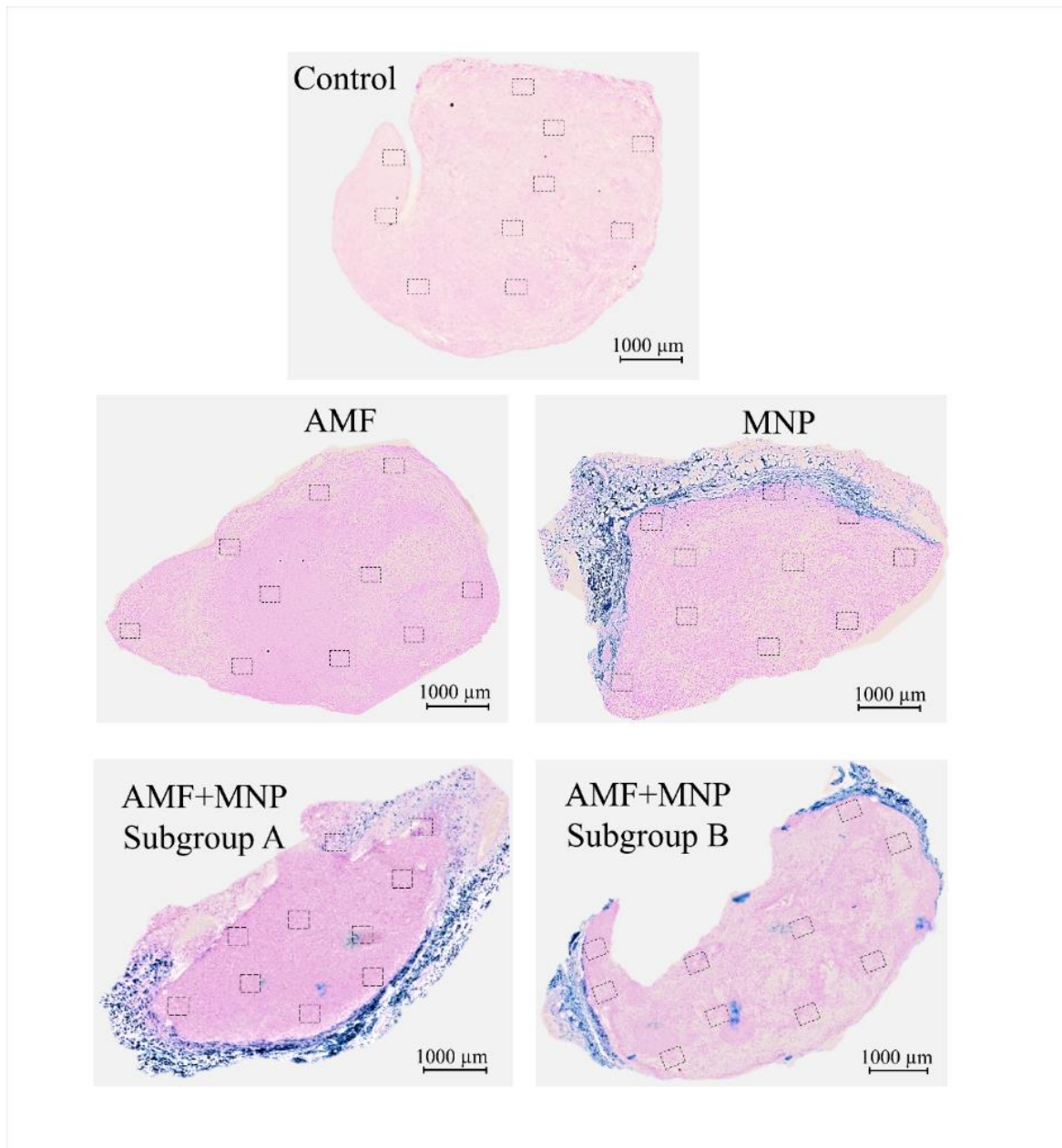
Fig.S3 Histologic assessments from Perls stained images. The numbers represent the ten random areas used for the dead cells quantification in each section.(supporting data Figure 5)
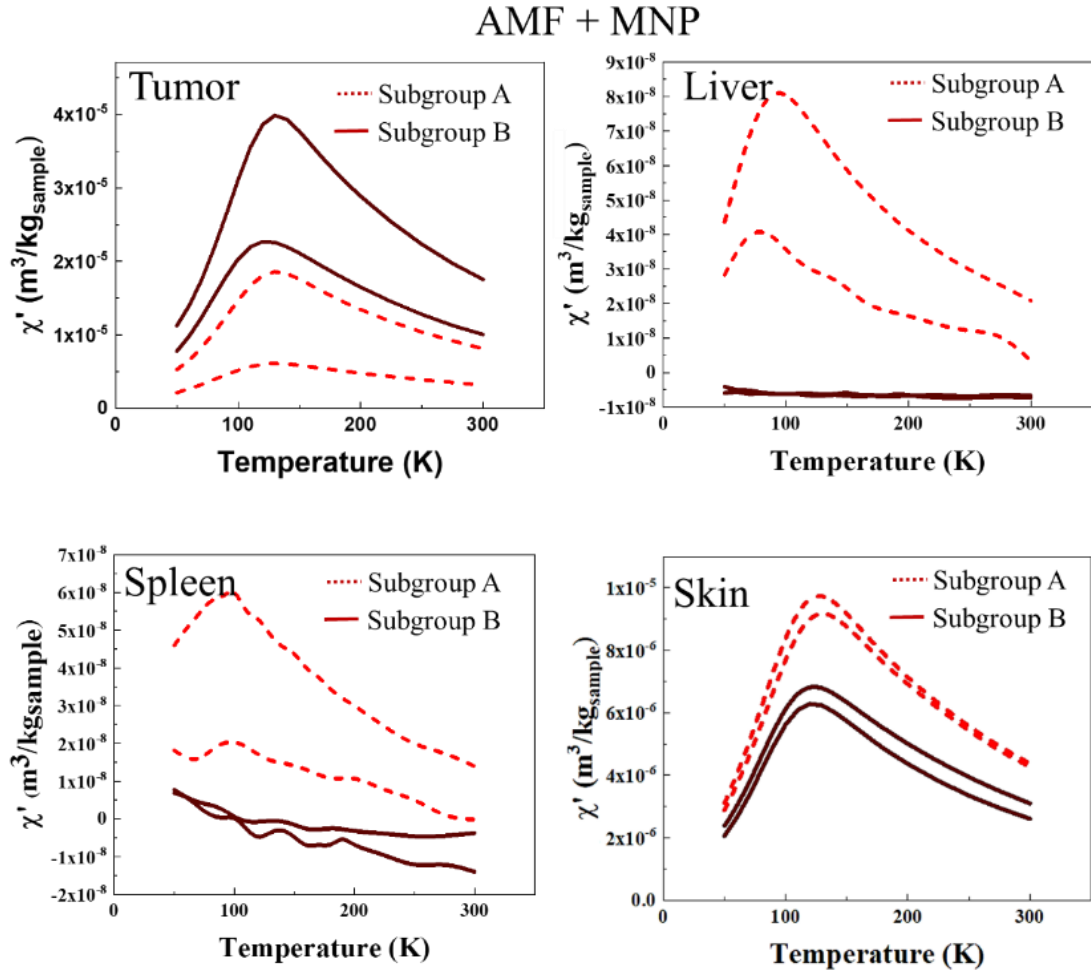
Figure S4: Tissue magnetic characterization. Temperature dependence of the AC magnetic susceptibility in the tumor, liver , skin and spleen four weeks after the intratumoral MNP administration (supporting data of Figure 6) .

6. Acknowledgements

5.3 Aportes al tema, visión crítica y perspectivas de futuro

A pesar de que el pronóstico clínico de pacientes con cáncer de páncreas ha mejorado ligeramente con los años mediante el uso de terapias estándar (ej. cirugía, radio- y quimioterapia), la tasa relativa de supervivencia en cinco años permanece por debajo del 30% para estadios localizados de la enfermedad, y sobre un 8% para todas las etapas combinadas.[160, 552] En este contexto, el tratamiento de tumores pancreáticos con hipertermia es una alternativa prometedora para aumentar la permeabilidad de la gruesa matriz extracelular que los caracteriza y mejorar la sensibilidad de las células tumorales a la terapia.[211, 510]

Estudios anteriores al nuestro (véase sección 5.2) han evaluado, tanto *in vitro* como *in vivo*, el efecto potencialmente beneficioso de la hipertermia magnética en el tratamiento de tumores pancreáticos. [211, 328, 517, 553-556] Sin embargo, pocos abordan el impacto directo de la hipertermia magnética sobre la respuesta de las células y/o la matriz extracelular a la terapia térmica. Al respecto, la mayoría de las investigaciones encontradas en la literatura investigan estrategias duales de tratamiento con quimio-, radio- o inmuno-terapia, o el uso combinado de las nanopartículas magnéticas para hipertermia y técnicas de imagen.[328, 553-555] Además, pocos reportes experimentales estudian el tratamiento de células tumorales pancreáticas desde una perspectiva de cultivo tridimensional, al menos en lo que a la terapia por hipertermia magnética se refiere. [211, 517] Hasta el momento, solo hemos encontrado un estudio publicado este año por Piehler y colaboradores,[211] que enfatice en el efecto multifacético del calentamiento magnéticamente inducido para afectar la estructura fibrilar del colágeno, y a la vez inducir la muerte celular apoptótica o necrótica. En este contexto, una de las novedades de nuestro trabajo, es la evaluación, desde una perspectiva tanto *in vitro* como *in vivo,* de la influencia de parámetros como la biodistribución, disposición y eficiente acumulación intratumoral de las nanopartículas en la efectividad del tratamiento térmico. Aunque las ventajas de la utilización de nanopartículas magnéticas como "hot spot" para inducir la liberación de calor localizado y afectar simultáneamente la matriz extracelular y la viabilidad celular ya habían sido demostradas en trabajos previos desarrollados en la línea celular de macrófagos murinos RAW264.7,[336] el estudio y traslación de estos resultados a un modelo tumoral humano con tan malos pronósticos en la clínica, como el de cáncer de páncreas, es esencial para proporcionar información sobre el papel de las nanopartículas como agentes térmicos en el tratamiento de la enfermedad, y en consecuencia generar nuevas hipótesis para futuras intervenciones terapéuticas.

A pesar de sus múltiples ventajas, los estudios que emplean cultivo 3D para evaluar la efectividad de la hipertermia magnética *in vitro* aún son muy limitados en número. De hecho, la mayoría de las investigaciones suelen pasar directamente del cultivo celular bidimensional a la experimentación animal. Razón por la cual, en muchos casos, la respuesta observada *in vitro* no es reproducible con los resultados posteriores del modelo *in vivo*. En este sentido, el estudio y optimización de las posibles condiciones terapéuticas *in vivo* mediante el uso de un enfoque tridimensional *in vitro* previo, como se ha realizado en este trabajo, es algo que ha sido muy poco abordado en los ensayos de hipertermia magnética para el tratamiento de tumores pancreáticos. Los diferentes modelos de cultivo celular basados en soportes de hidrogel que se han desarrollado en este estudio para intentar reproducir diferentes escenarios de acumulación *in vivo* de nanopartículas en el tejido tumoral, [336] nos permitieron comprender y regular la respuesta de las células tumorales a la terapia térmica en un entorno 3D, contribuyendo a llenar el vacío existente entre los estudios basados en el cultivo 2D de líneas tumorales pancreáticas (adecuadas para el cribado de numerosas condiciones con un alto rendimiento), y los modelos de xenoinjertos *in vivo* (complicados para su establecimiento, pero fisiológicamente relevantes). Por otro lado, cabe resaltar que en este trabajo fue empleado el mismo generador de AMF tanto en los ensayos *in vitro* como en los estudios *in vivo*. Hecho que adquiere relevancia para la modelación *in vitro* de las posibles respuesta de las nanopartículas en escenario pre-clínico; porque aunque el parámetro SAR se usa con bastante frecuencia en la literatura para caracterizar la capacidad de calentamiento de las nanopartículas, tiene la limitación de presentar un potente componente extrínseco (específico del equipo).[105] Por lo cual, para un mismo fluido magnético, este valor puede cambiar dependiendo de las condiciones de frecuencias y campo aplicado, como puede deducirse de la fórmula para la disipación de potencia volumétrica (véase sección 1.3.1).[254] Por lo tanto, contar con un modelo *in vitro* que permitiera evaluar las posibles respuestas *in vivo* del calentamiento intracelular generado por las partículas, además de ser útil para ensayar un mayor número de condiciones terapéuticas previas al estudio *in vivo*, es necesario para minimizar el número de animales de experimentación empleados en pre-clínica.

Por otro lado, aunque numerosos trabajos han abordado la biodistribución de las nanopartículas *in vivo* después de su administración sistémica,[40, 314-315, 525-526, 557] aún se conoce poco acerca del comportamiento de las nanopartículas después de la inyección intratumoral.[153, 245, 267, 490, 529, 531] Estudios previos al nuestro han planteado que la retención intracelular de partículas permanece prácticamente inalterable después del tratamiento térmico.[267] Sin embargo, nuestros

resultados experimentales evidenciaron que hasta 3 semanas después la administración intratumoral podía detectarse acumulación de nanopartículas, en órganos como el hígado y el bazo, tanto en ratones pertenecientes al grupo control de nanopartículas como en los tratados hipertermia magnética. Este hecho a su vez se correlacionó con una menor cantidad de partículas en el tumor y por consiguiente, una menor efectividad terapéutica; en comparación con los animales donde la concentración intratumoral de partículas era cuantitativamente superior, y la detección en hígado y bazo prácticamente imperceptible. Estas diferencias con otros resultados reportados en la literatura resaltan que los efectos de la biodistribución y disposición de las nanopartículas después de la inyección intratumoral en la efectividad del tratamiento térmico aún siguen siendo bastante desconocidos, a pesar de que esta sea una de las metodologías más comunes y ampliamente utilizadas para la administración de material magnético para tratamiento por hipertermia. Lo que resalta la importancia de estudios como los realizados en este trabajo para comprender las posibles respuestas terapéuticas *in vivo*; debido a que la existencia de zonas tumorales con alta, baja o nula concentración de nanopartículas determina la exposición a dosis térmicas diferentes dentro de un mismo tumor, afectando la respuesta global del tejido al choque térmico.[491, 558] Los mecanismos que favorecen la acumulación de nanopartículas en otros órganos luego de su inyección directa en el tumor, requieren de mayor estudio y profundización, tanto para entender las vías fisiológicas implicadas en la circulación de las nanopartículas fuera del microambiente tumoral al que son administradas; como para evaluar si este fenómeno está relacionado con el modelo tumoral utilizado, o con fallos experimentales asociados a un pobre control de la inyección intratumoral. Análisis que podrían ser objeto de investigación de futuros ensayos con diferentes tipos de modelos de xenoinjerto tumoral, que permitan modelar diferentes niveles de estroma celular, ya sea mediante el uso de líneas células tumorales, o a través de la implantación de piezas de tumores resecadas de pacientes en el huésped inmunocomprometido.

En este sentido, aunque el modelo murino de xenoinjerto utilizado (cepa Balb/c *nude*) presenta limitaciones en la respuesta adaptativa de linfocitos T, si que es posible evaluar el efecto de la hipertermia magnética en el posible reclutamiento de componentes moleculares y celulares implicados en la respuesta inmunológica innata.[231, 234] Nuestros resultados sugieren que el tratamiento térmico de tumores pancreáticos puede inducir dos mecanismos potenciales de inmunoestimulación. Por un lado, la sobreexpresión de patrones moleculares asociados a daños (DAMP, por sus siglas en inglés) después del tratamiento con hipertermia magnética, como es el caso de la proteína Calreticulina (que se ha descrito que puede participar en la inducción de

muerte celular inmunogénica),[359] sugiere la movilización de elementos de la respuesta innata en respuesta el estrés térmico, que puede contribuir a la respuesta inmunológica sistémica del organismo frente al cáncer.[418, 559] Mientras que, por otro lado, la permeabilización de la matriz extracelular también podría favorecer la infiltración de células del sistema inmunológico al tumor, contribuyendo a contrarrestar la señal inmunosupresora que caracteriza a los tumores pancreáticos.[507, 510, 534] Sin embargo, estas hipótesis requieren de un mayor número de evidencias experimentales, por lo cual estudios futuros al respecto podrían estar dirigidos a evaluar la infiltración inmunológica al tumor relacionada con el efecto desestabilizante de la hipertermia sobre la matriz extracelular, y al análisis de la secreción y/o expresión de otras moléculas y marcadores asociados a los posibles mecanismos de muerte inmunogénica inducida por la hipertermia magnética.

En resumen, los resultados de esta investigación evidencian las posibilidades multimodales que ofrecen las nanopartículas magnéticas para el tratamiento prospectivo del cáncer, al actuar simultáneamente como disruptores físicos de la matriz extracelular y como sistemas de suministro de calor clínicamente relevantes. En este sentido, el enfoque más prometedor para la mejora de la investigación actual de los procesos carcinogénicos en humanos, es la combinación de los modelos *in vitro* y preclínicos disponibles para garantizar un estudio más integral a diferentes niveles. Investigaciones futuras al respecto pudieran estar encaminadas a la generación de hidrogeles o esferoides más complejos, que nos permitieran incorporar en su interior, tanto células tumorales como del estroma, para delinear el papel de las diferentes tipologías celulares que contribuyen a la respuesta antitumoral a la hipertermia magnética. Además, la utilización de matrices tridimensionales con diversas formas y grados de rigidez también pudiera ser útil para estudiar los efectos térmicos de la hipertermia magnética sobre otros soportes matriciales mecánicamente más fuertes. Al respecto, el empleo y estandarización de técnicas de microscopía electrónica, fuerza atómica y confocal, así como inmunohistoquímicas, sería esencial para analizar las alteraciones de las proteínas de la matriz extracelular, como el colágeno; y estudiar la respuesta mecánica y celular al tratamiento térmico que presentan los tumores pancreáticos tanto *in vitro* como *in vivo*.

CONCLUSIONES GENERALES ·

En esta tesis se optimizaron dos modelos tridimensionales de cultivo celular utilizando la línea de macrófagos murinos RAW264.7. Estos modelos se diferenciaban en la localización de las nanopartículas dentro de los hidrogeles de colágeno I desarrollados: en el Modelo *In*, las nanopartículas se localizaban solamente en el interior de las células que conformaban el hidrogel; y en el Modelo *In&Out*, las nanopartículas se localizaban tanto en el interior celular como en la matriz de colágeno. Los datos experimentales evidenciaron una penetración exitosa de las nanopartículas en los hidrogeles del Modelo *In&Out*, evidenciando que el empleo de geles de colágeno es un modelo factible y sencillo, que permite un acercamiento a la estructura de la matriz extracelular, para estudiar los efectos de la hipertermia magnética. Las imágenes de microscopía confocal obtenidas en este trabajo revelaron una mejora notable en migración de las nanopartículas a través de la matriz de colágeno hacia el interior de la estructura tridimensional, tras su exposición al campo magnético alterno. Fenómeno probablemente asociado a un aumento de la fluidez de dicha matriz debido al aumento de temperatura durante el tratamiento térmico. Los análisis de citometría demostraron, además, que esta mejora en la biodistribución también inducía un incremento en la captura de las nanopartículas por las células, asociado a una distribución más homogénea del material magnético a través del gel de colágeno. La viabilidad celular y el mecanismo de muerte celular fue diferente dependiendo de la cantidad de partículas internalizadas: mientras que la necrosis rápida fue el mecanismo de muerte en células con altas concentraciones de partículas (Modelo *In)*, la apoptosis fue la vía principal de muerte celular cuando la internalización de nanopartículas era 10 veces menor (Modelo *In & Out*). Este efecto evidenció una correlación directa de la concentración intracelular de las partículas con el nivel de estrés térmico generado a las células.

Para estudiar con más detalle el efecto de la concentración intracelular de nanopartículas sobre los diferentes mecanismos de muerte celular regulada inducidos por la hipertermia magnética, se prepararon geles de colágeno del Modelo *In,* pre-incubando las células con diferentes concentraciones de nanopartículas; y se evaluaron las diferencias en la expresión de genes pro-apoptóticos y anti-apoptóticos en los cultivos 3D generados, antes y después de su exposición al campo magnético alterno. Además, se realizaron estudios computacionales para evaluar el

calor inducido por las partículas a nivel intracelular. Las simulaciones teóricas realizadas para este trabajo se centraron en evaluar el calor generado a nivel local, específicamente en los lisosomas, ya que es conocido que son el compartimento principal para el almacenamiento y posterior degradación de las nanopartículas dentro de las células. Nuestros resultados demostraron que las vías de señalización iniciadoras de la apoptosis pueden variar dependiendo de la cantidad de nanopartículas de óxido de hierro internalizadas. Los análisis de citometría de flujo conjuntamente con los estudios de biología molecular, demostraron que, a bajas cantidades intracelulares de nanopartículas, el tratamiento de hipertermia magnética induce la muerte celular apoptótica por vía *intrínseca* o mitocondrial. Mientras que la vía de señalización *extrínseca* es la que ocurre preferencialmente en células donde la cantidad de nanopartículas internalizadas es muy elevada. En ninguno de los modelos estudiados se apreció un incremento perceptible de la temperatura global de la muestra tratada. Por tanto, las diferentes vías apoptóticas desencadenadas por la hipertermia magnética en función de la cantidad intracelular de partículas, podrían estar relacionadas con la permeabilización de la membrana lisosomal y la consecuente liberación de sus enzimas proteolíticas en respuesta al calentamiento local, que pueden activar y/o potenciar los diferentes mecanismos de muerte celular apoptótica. Esta hipótesis requiere de futuros experimentos para su completa elucidación.

Finalmente, la efectividad del tratamiento de hipertermia magnética fue estudiada *in vivo* en un modelo de xenoinjerto de la línea celular MIAPaca-2. Antes de los ensayos *in vivo*, se realizaron estudios *in vitro* donde se utilizaron los dos modelos celulares tridimensionales previamente descritos (Modelo *In* y Modelo *In&Out*). Estas dos aproximaciones de cultivo celular 3D nos permitieron evaluar los efectos citotóxicos de la aplicación de diferentes condiciones de campo y frecuencia del campo magnético alterno. Los ensayos *in vitro* permitieron, además, estudiar y seleccionar las condiciones óptimas de respuesta de la línea tumoral pancreática MIAPaca-2 al tratamiento térmico. Los resultados del estudio *in vivo* demostraron una clara correlación entre la eficiente acumulación y biodistribución de las nanopartículas en el tumor y la efectividad del tratamiento térmico. Nuestras observaciones experimentales evidenciaron dos respuestas distintas al tratamiento dentro del grupo tratado con hipertermia magnética: por un lado, en un subgrupo de animales se observó un aumento del crecimiento tumoral, mientras que en otro subgrupo se apreció una inhibición del crecimiento del tumor asociado a una efectiva respuesta al tratamiento. Los análisis posteriores de la biodistribución de las nanopartículas revelaron importantes diferencias asociadas a la acumulación intratumoral de partículas en cada uno de estos dos subgrupos , demostrando que

a mayor concentración de partículas, el efecto terapéutico observado era mayor. Estos resultados evidenciaron la importancia de un control estricto de la biodistribución de las nanopartículas después de su inyección intratumoral, ya que la obtención de concentraciones efectivas del material magnético, y su distribución en el entorno tumoral constituyen parámetros determinantes para alcanzar dosis térmicas adecuadas que aseguren la eficacia terapéutica. Posibles mecanismos de muerte celular inmunogénica también parecen activarse en respuesta al tratamiento con hipertermia magnética, aspecto de gran relevancia para contribuir a la estimulación del sistema inmunológico frente al cáncer.

GENERAL CONCLUSIONS

In this thesis, two three-dimensional models of cell culture were optimized, using the RAW264.7 murine macrophage cell line, based on differences in the location of the nanoparticles within the collagen I hydrogels developed: in the *In Model*, the nanoparticles were located only in the interior of the cells that made up the hydrogel, and in the *In & Out Model*, the nanoparticles were located both inside the cell and within of the collagen matrix. The experimental data evidenced an effective penetration of the nanoparticles in the *In & Out Model* hydrogels, evidencing that the use of collagen type I gels is a feasible and simple model, which allows an approach to the structure of the extracellular matrix, to study the effects of magnetic hyperthermia. Confocal microscopy images revealed a notable enhancement of the of nanoparticles migration towards the inner part of the 3D structure, after exposure to the alternating magnetic field. Phenomenon probably associated to an increase of the matrix fluidity as a result of the temperature increase during the thermal treatment. Flow cytometry analysis demonstrated that this improvement in biodistribution also induced an increase in the nanoparticles uptake, associated with a more homogeneous distribution of the magnetic material through the collagen gel. Cell viability and the cell death mechanisms were different depending on the amount of internalized particles: while rapid necrosis was the mechanism of death in cells with high intracellular number of particles (*In Model*), apoptosis was the main route of cell death when the nanoparticle internalization was 10 times less (*In & Out Model*). This effect evidenced a direct correlation of the intracellular particle concentration with the level of heat stress generated to the cells.

To study in more detail the effect of the intracellular nanoparticles concentration on the different mechanisms of regulated cell death induced by magnetic hyperthermia, *In Model* hydrogels were prepared pre-incubating the cells with different nanoparticles concentrations. Then, the differences in the expression of pro-apoptotic and anti-apoptotic genes were evaluated, before and after of the gel exposure to an alternating magnetic field. In addition, computational studies were performed to assess the intracellular heating effects induced by magnetic hyperthermia. The theoretical simulations carried out for this work focused on the evaluation of the heat generated locally, specifically in lysosomes, taking in account that it is

the main compartment for the for the storage and subsequent degradation of nanoparticles into the cells. Our results demonstrated that signalling apoptosis pathways can vary depending on the amount of internalized iron oxide nanoparticles, and that this effect appears to be mediated by the localized heating, specifically within lysosomes. Flow cytometry analysis in conjunction with molecular biology studies demonstrated that at low intracellular amounts of nanoparticles, the treatment of magnetic hyperthermia induces apoptotic cell death trough the intrinsic or mitochondrial pathway. While the extrinsic signalling pathway is the one that occurs preferentially, in cells where the amount of internalized nanoparticles is higher. In none of these models was observed a perceptible increase in the global temperature of the treated sample. Therefore, the different apoptotic pathways triggered by magnetic hyperthermia depending on the intracellular amount of particles, could be related to the permeabilization of the lysosomal membrane and the consequent release of its proteolytic enzymes in response to local heating, which can activate and / or enhance the different mechanisms of apoptotic cell death. This hypothesis requires future experiments for its complete elucidation.

Finally, the effectiveness of magnetic hyperthermia treatment was studied in a xenograft *in vivo* model of the MIAPaca-2 cell line. Before the *in vivo* tests, *in vitro* studies were conducted using the two 3D cell culture models previously described (*In Model* and *In&Out Model*). These two 3D cell culture approaches allowed assessing the cytotoxic effects of applying different field conditions and frequency of the alternating magnetic field. The *in vitro* tests also allowed studying and selecting the optimal conditions for the MIAPaca-2 cells treatment. The results of the *in vivo* study demonstrated a clear correlation between the efficient accumulation and biodistribution of nanoparticles in the tumor and the effectiveness of heat treatment. Our experimental observations revealed two different responses to treatment within the group treated with magnetic hyperthermia: in one animals subgroup, an increase in tumor growth was observed; while in another subgroup, an inhibition of tumor growth associated with an effective response to treatment was observed. Subsequent analysis of the nanoparticles biodistribution revealed important differences in the intratumoral nanoparticle accumulation in each of these two subgroups, demonstrating that at a higher concentration of particles, the observed therapeutic effect was better. These results evidenced the importance of strict control of the biodistribution of the nanoparticles after the intratumoral administration, since obtaining effective concentrations of the magnetic material within the tumor constitute fundamental parameters to achieve adequate thermal doses that ensure the possitive therapeutic efficacy. Possible mechanisms of immunogenic cell death also appear to be activated in response to the

magnetic hyperthermia treatment, an aspect of great relevance to contribute to the stimulation of the immune system against cancer.

1.   Rauscher, H.; Roebben, G.; Mech, A.; Gibson, N.; Kestens, V.; Linsinger, T.; Sintes, J. R., An Overview of Concepts and Terms Used in the European Commission's Definition of Nanomaterial. *Chem. Ing. Tech* **2019**, 224-231.

2.   Marchesan, S.; Prato, M., Nanomaterials for (Nano) Medicine. ACS Publications: 2013.

3.   Mozafari, M. R., *Nanomaterials and Nanosystems for Biomedical Applications*. Springer Science & Business Media: 2007.

4.   Zhang, L.; Gu, F.; Chan, J.; Wang, A.; Langer, R.; Farokhzad, O., Nanoparticles in Medicine: Therapeutic Applications and Developments. *Clinical pharmacology & therapeutics* **2008,** *83* (5), 761-769.

5.   Makvandi, P.; Wang, C.-y.; Zare, E. N.; Borzacchiello, A.; Niu, L.-n.; Tay, F. R., Metal-Based Nanomaterials in Biomedical Applications: Antimicrobial Activity and Cytotoxicity Aspects. *Adv. Funct. Mater. n/a* (n/a), 1910021.

6.   Venditti, I., Engineered Gold-Based Nanomaterials: Morphologies and Functionalities in Biomedical Applications. A Mini Review. *Bioengineering* **2019,** *6* (2), 53.

7.   Patra, J. K.; Das, G.; Fraceto, L. F.; Campos, E. V. R.; del Pilar Rodriguez-Torres, M.; Acosta-Torres, L. S.; Diaz-Torres, L. A.; Grillo, R.; Swamy, M. K.; Sharma, S., Nano Based Drug Delivery Systems: Recent Developments and Future Prospects. *Journal of nanobiotechnology* **2018,** *16* (1), 71.

8.   Lee, J. H.; Choi, H. K.; Lee, S. Y.; Lim, M. W.; Chang, J. H., Enhancing Immunoassay Detection of Antigens with Multimeric Protein Gs. *Biosensors and Bioelectronics* **2011,** *28* (1), 146-151.

9.   Soares, P. I. P.; Laia, C. A. T.; Carvalho, A.; Pereira, L. C. J.; Coutinho, J. T.; Ferreira, I. M. M.; Novo, C. M. M.; Borges, J. P., Iron Oxide Nanoparticles Stabilized with a Bilayer of Oleic Acid for Magnetic Hyperthermia and Mri Applications. *Applied Surface Science* **2016,** *383*, 240-247.

10.   Ferreira, C. A.; Ni, D.; Rosenkrans, Z. T.; Cai, W., Radionuclide-Activated Nanomaterials and Their Biomedical Applications. *Angewandte Chemie International Edition* **2019,** *58* (38), 13232-13252.

11.   Bobo, D.; Robinson, K. J.; Islam, J.; Thurecht, K. J.; Corrie, S. R., Nanoparticle-Based Medicines: A Review of Fda-Approved Materials and Clinical Trials to Date. *Pharmaceutical Research* **2016,** *33* (10), 2373-2387.

12.   Alphandéry, E., Biodistribution and Targeting Properties of Iron Oxide Nanoparticles for Treatments of Cancer and Iron Anemia Disease. *Nanotoxicology* **2019,** *13* (5), 573-596.

13.   Anselmo, A. C.; Mitragotri, S., Nanoparticles in the Clinic. *Bioengineering & translational medicine* **2016,** *1* (1), 10-29.

14.   Anselmo, A. C.; Mitragotri, S., Nanoparticles in the Clinic: An Update. *Bioengineering & translational medicine* **2019,** *4* (3), e10143.

15.   Laurent, S.; Bridot, J.-L.; Elst, L. V.; Muller, R. N., Magnetic Iron Oxide Nanoparticles for Biomedical Applications. *Future medicinal chemistry* **2010,** *2* (3), 427-449.

16.   Reddy, L. H.; Arias, J. L.; Nicolas, J.; Couvreur, P., Magnetic Nanoparticles: Design and Characterization, Toxicity and Biocompatibility, Pharmaceutical and Biomedical Applications. *Chem Rev* **2012,** *112* (11), 5818-5878.

17.   Gupta, A. K.; Naregalkar, R. R.; Vaidya, V. D.; Gupta, M., Recent Advances on Surface Engineering of Magnetic Iron Oxide Nanoparticles and Their Biomedical Applications. *Nanomedicine_UK* **2007,** *2* (1), 23–39.

18.   Osuna, J.; de Caro, D.; Amiens, C.; Chaudret, B.; Snoeck, E.; Respaud, M.; Broto, J.-M.; Fert, A., Synthesis, Characterization, and Magnetic Properties of Cobalt Nanoparticles from an Organometallic Precursor. *The Journal of Physical Chemistry* **1996,** *100* (35), 14571-14574.

19.   Ely, T. O.; Amiens, C.; Chaudret, B.; Snoeck, E.; Verelst, M.; Respaud, M.; Broto, J.-M., Synthesis of Nickel Nanoparticles. Influence of Aggregation Induced by Modification of Poly (Vinylpyrrolidone) Chain Length on Their Magnetic Properties. *Chemistry of Materials* **1999,** *11* (3), 526-529.

20.   Akbarzadeh, A.; Samiei, M.; Davaran, S., Magnetic Nanoparticles: Preparation, Physical Properties, and Applications in Biomedicine. *Nanoscale research letters* **2012,** *7* (1), 144.

21.   Figuerola, A.; Di Corato, R.; Manna, L.; Pellegrino, T., From Iron Oxide Nanoparticles Towards Advanced Iron-Based Inorganic Materials Designed for Biomedical Applications. *Pharmacological research* **2010,** *62* (2), 126-143.

22.   Wu, W.; Wu, Z.; Yu, T.; Jiang, C.; Kim, W. S., Recent Progress on Magnetic Iron Oxide Nanoparticles: Synthesis, Surface Functional Strategies and Biomedical Applications. *Sci Technol Adv Mater* **2015,** *16* (2), 023501.

23.   Ho, D.; Sun, X.; Sun, S., Monodisperse Magnetic Nanoparticles for Theranostic Applications. *Accounts of chemical research* **2011,** *44* (10), 875-882.

24.   Wu, W.; Jiang, C. Z.; Roy, V. A., Designed Synthesis and Surface Engineering Strategies of Magnetic Iron Oxide Nanoparticles for Biomedical Applications. *Nanoscale* **2016,** *8* (47), 19421-19474.

25.   Gutiérrez, L.; Morales, M. P.; Lázaro, F. J., Prospects About Magnetic Nanoparticles for Systemic Administration: Synthesis and Quantitative Detection. *Physical Chemistry Chemical Physics* **2014,** *16*, 4456-4464.

26.   Liu, X.; Zhang, Y.; Wang, Y.; Zhu, W.; Li, G.; Ma, X.; Zhang, Y.; Chen, S.; Tiwari, S.; Shi, K., Comprehensive Understanding of Magnetic Hyperthermia for Improving Antitumor Therapeutic Efficacy. *Theranostics* **2020,** *10* (8), 3793.

27.   Arami, H.; Khandhar, A.; Liggitt, D.; Krishnan, K. M., In Vivo Delivery, Pharmacokinetics, Biodistribution and Toxicity of Iron Oxide Nanoparticles. *Chemical Society reviews* **2015,** *44* (23), 8576-8607.

28.   Rojas, J. M.; Gavilan, H.; Del Dedo, V.; Lorente-Sorolla, E.; Sanz-Ortega, L.; da Silva, G. B.; Costo, R.; Perez-Yague, S.; Talelli, M.; Marciello, M.; Morales, M. P.; Barber, D. F.; Gutierrez, L., Time-Course Assessment of the Aggregation and Metabolization of Magnetic Nanoparticles. *Acta Biomater* **2017,** *58*, 181-195.

29.   Levy, M.; Luciani, N.; Alloyeau, D.; Elgrabli, D.; Deveaux, V.; Pechoux, C.; Chat, S.; Wang, G.; Vats, N.; Gendron, F.; Factor, C.; Lotersztajn, S.; Luciani, A.; Wilhelm, C.; Gazeau,

F., Long Term in Vivo Biotransformation of Iron Oxide Nanoparticles. *Biomaterials* **2011,** *32* (16), 3988-3999.

30.   Rojas, J. M.; Sanz-Ortega, L.; Mulens-Arias, V.; Gutierrez, L.; Perez-Yague, S.; Barber, D. F., Superparamagnetic Iron Oxide Nanoparticle Uptake Alters M2 Macrophage Phenotype, Iron Metabolism, Migration and Invasion. *Nanomedicine_UK* **2016,** *12* (4), 1127-1138.

31.   Wang, J.; Pantopoulos, K., Regulation of Cellular Iron Metabolism. *Biochemical Journal* **2011,** *434*, 365-381.

32.   Singh, N.; Jenkins, G. J.; Asadi, R.; Doak, S. H., Potential Toxicity of Superparamagnetic Iron Oxide Nanoparticles (Spion). *Nano reviews* **2010,** *1* (1), 5358.

33.   Askri, D.; Cunin, V.; Béal, D.; Berthier, S.; Chovelon, B.; Arnaud, J.; Rachidi, W.; Sakly, M.; Amara, S.; Sève, M., Investigating the Toxic Effects Induced by Iron Oxide Nanoparticles on Neuroblastoma Cell Line: An Integrative Study Combining Cytotoxic, Genotoxic and Proteomic Tools. *Nanotoxicology* **2019,** *13* (8), 1021-1040.

34.   Singh, S. P.; Rahman, M. F.; Murty, U. S.; Mahboob, M.; Grover, P., Comparative Study of Genotoxicity and Tissue Distribution of Nano and Micron Sized Iron Oxide in Rats after Acute Oral Treatment. *Toxicol Appl Pharmacol* **2013,** *266* (1), 56-66.

35.   Calero, M.; Gutierrrez, L.; Salas, G.; Luengo, Y.; Lazaro, A.; Acedo, P.; Morales, M. P.; Miranda, R.; Villanueva, A., Efficient and Safe Internalization of Magnetic Iron Oxide Nanoparticles: Two Fundamental Requirements for Biomedical Applications. *Nanomedicine_UK* **2013**.

36.   Chamorro, S.; Gutierrez, L.; Vaquero, M. P.; Verdoy, D.; Salas, G.; Luengo, Y.; Brenes, A.; Teran, F. J., Safety Assessment of Chronic Oral Exposure to Iron Oxide Nanoparticles. *Nanotechnology* **2015,** *26* (20), 205101.

37.   Gautier, J.; Allard-Vannier, E.; Burlaud-Gaillard, J.; Domenech, J.; Chourpa, I., Efficacy and Hemotoxicity of Stealth Doxorubicin-Loaded Magnetic Nanovectors on Breast Cancer Xenografts. *J. Biomed. Nanotechnol.* **2014,** *10*, 1-13.

38.   Hong, S. C.; Lee, J. H.; Lee, J.; Kim, H. Y.; Park, J. Y.; Cho, J.; Lee, J.; Han, D.-W., Subtle Cytotoxicity and Genotoxicity Differences in Spion Coated with Varius Funtional Groups. *Int J Nanomedicine* **2011,** *6*, 3219–3231.

39.   Ruiz, A.; Ali, L. M. A.; Cáceres-Vélez, P. R.; Cornudella, R.; Gutiérrez, M.; Moreno, J. A.; Piñol, R.; Palacio, F.; Fascineli, M. L.; Azevedo, R. B.; Morales, M. P.; Millán, A., Hematotoxicity of Magnetite Nanoparticles Coated with Polyethylene Glycol: In Vitro and in Vivo Studies. *Toxicology Research* **2015**.

40.   Ruiz, A.; Mancebo, A.; Beola, L.; Sosa, I.; Gutiérrez, a. L., Dose-Response Bioconversion and Toxicity Analysis of Magnetite Nanoparticles. *IEEE MAGNETICS LETTERS,* **2016,** *7*.

41.   Anzai, Y.; Piccoli, C. W.; Outwater, E. K.; Stanford, W.; Bluemke, D. A.; Nurenberg, P.; Saini, S.; Maravilla, K. R.; Feldman, D. E.; Schmiedl, U. P., Evaluation of Neck and Body Metastases to Nodes with Ferumoxtran 10–Enhanced Mr Imaging: Phase Iii Safety and Efficacy Study. *Radiology* **2003,** *228* (3), 777-788.

42.   Thoeny, H. C.; Triantafyllou, M.; Birkhaeuser, F. D.; Froehlich, J. M.; Tshering, D. W.; Binser, T.; Fleischmann, A.; Vermathen, P.; Studer, U. E., Combined Ultrasmall Superparamagnetic Particles of Iron Oxide–Enhanced and Diffusion-Weighted Magnetic

Resonance Imaging Reliably Detect Pelvic Lymph Node Metastases in Normal-Sized Nodes of Bladder and Prostate Cancer Patients. *European urology* **2009,** *55* (4), 761-769.

43. Auerbach, M.; Ballard, H.; Glaspy, J., Clinical Update: Intravenous Iron for Anaemia. *The Lancet* **2007,** *369* (9572), 1502-1504.

44. Nel, A.; Xia, T.; Mädler, L.; Li, N., Toxic Potential of Materials at the Nanolevel. *Science* **2006,** *311* (5761), 622-627.

45. Shubayev, V. I.; Pisanic, T. R.; Jin, S., Magnetic Nanoparticles for Theragnostics. *Adv Drug Deliv Rev* **2009,** *61* (6), 467-477.

46. Rosensweig, R. E., Magnetic Fluids. *Scientific American* **1982,** *247* (4), 136-145.

47. Hao, R.; Xing, R.; Xu, Z.; Hou, Y.; Gao, S.; Sun, S., Synthesis, Functionalization, and Biomedical Applications of Multifunctional Magnetic Nanoparticles. *Advanced Materials* **2010,** *22*, 2729-2742.

48. Laurent, S.; Forge, D.; Port, M.; Roch, A.; Robic, C.; Elst, L. V.; Muller, R. N., Magnetic Iron Oxide Nanoparticles: Synthesis, Stabilization, Vectorization, Physicochemical Characterizations, and Biological Applications. *Chem Rev* **2008,** *108* (6), 2064-2110.

49. Tartaj, P.; Morales, M. P.; González-Carreño, T.; Veintemillas-Verdaguer, S.; Serna, C. J., The Iron Oxides Strike Back: From Biomedical Applications to Energy Storage Devices and Photoelectrochemical Water Splitting. *Advanced Materials* **2011,** *23* (44), 5243-5249.

50. Veintemillas-Verdaguer, S.; Morales, M.; Serna, C., Continuous Production of Γ-Fe2o3 Ultrafine Powders by Laser Pyrolysis. *Materials Letters* **1998,** *35* (3-4), 227-231.

51. Bautista, M. C.; Bomati-Miguel, O.; del Puerto Morales, M.; Serna, C. J.; Veintemillas-Verdaguer, S., Surface Characterisation of Dextran-Coated Iron Oxide Nanoparticles Prepared by Laser Pyrolysis and Coprecipitation. *J Magn Magn Mater* **2005,** *293* (1), 20-27.

52. Celis, J. A.; Mejía, O. O.; Cabral-Prieto, A.; García-Sosa, I.; Derat-Escudero, R.; Saitovitch, E. B.; Camarena, M. A., Synthesis and Characterization of Nanometric Magnetite Coated by Oleic Acid and the Surfactant Ctab. *Hyperfine Interactions* **2017,** *238* (1), 43.

53. Todaka, Y.; Nakamura, M.; Hattori, S.; Tsuchiya, K.; Umemoto, M., Synthesis of Ferrite Nanoparticles by Mechanochemical Processing Using a Ball Mill. *Materials Transactions* **2003,** *44* (2), 277-284.

54. Baker, C.; Shah, S. I.; Hasanain, S.; Ali, B.; Shah, L.; Li, G.; Ekiert, T.; Unruh, K., Inert Gas Condensation of Iron and Iron-Oxide Nanoparticles. *MRS Online Proceedings Library Archive* **2002,** *746*.

55. Suryanarayana, C.; Prabhu, B., Synthesis of Nanostructured Materials by Inert-Gas Condensation Methods. In *Nanostructured Materials*, Elsevier: 2007; pp 47-90.

56. Tavakoli, A.; Sohrabi, M.; Kargari, A., A Review of Methods for Synthesis of Nanostructured Metals with Emphasis on Iron Compounds. *chemical papers* **2007,** *61* (3), 151-170.

57. Gutiérrez, L.; Costo, R.; Grüttner, C.; Westphal, F.; Gehrke, N.; Heinke, D.; Fornara, A.; Pankhurst, Q. A.; Johansson, C.; Veintemillas-Verdaguer, S., Synthesis Methods to Prepare Single-and Multi-Core Iron Oxide Nanoparticles for Biomedical Applications. *Dalton Transactions* **2015,** *44* (7), 2943-2952.

58. Khomane, R. B.; Kulkarni, B. D., Nanoreactors for Nanostructured Materials. *International Journal of Chemical Reactor Engineering* **2008,** *6* (1).

59.   Lu, Y.; Yin, Y.; Mayers, B. T.; Xia, Y., Modifying the Surface Properties of Superparamagnetic Iron Oxide Nanoparticles through a Sol− Gel Approach. *Nano Lett* **2002,** *2* (3), 183-186.

60.   Liu, H.-L.; Ko, S. P.; Wu, J.-H.; Jung, M.-H.; Min, J. H.; Lee, J. H.; An, B. H.; Kim, Y. K., One-Pot Polyol Synthesis of Monosize Pvp-Coated Sub-5 Nm Fe3o4 Nanoparticles for Biomedical Applications. *J Magn Magn Mater* **2007,** *310* (2), e815-e817.

61.   Caruntu, D.; Caruntu, G.; Chen, Y.; O'Connor, C. J.; Goloverda, G.; Kolesnichenko, V. L., Synthesis of Variable-Sized Nanocrystals of Fe3o4 with High Surface Reactivity. *Chemistry of Materials* **2004,** *16* (25), 5527-5534.

62.   Capek, I., Preparation of Metal Nanoparticles in Water-in-Oil (W/O) Microemulsions. *Adv Colloid Interfac* **2004,** *110* (1-2), 49-74.

63.   Massart, R., Preparation of Aqueous Magnetic Liquids in Alkaline and Acidic Media *Magnetics, IEEE Transactions* **1981,** *17* (2), 1247-1248.

64.   Martínez-Mera, I.; Espinosa-Pesqueira, M.; Pérez-Hernández, R.; Arenas-Alatorre, J., Synthesis of Magnetite (Fe3o4) Nanoparticles without Surfactants at Room Temperature. *Materials Letters* **2007,** *61* (23-24), 4447-4451.

65.   Liang, M.-T.; Wang, S.-H.; Chang, Y.-L.; Hsiang, H.-I.; Huang, H.-J.; Tsai, M.-H.; Juan, W.-C.; Lu, S.-F., Iron Oxide Synthesis Using a Continuous Hydrothermal and Solvothermal System. *Ceramics International* **2010,** *36* (3), 1131-1135.

66.   Mao, B.; Kang, Z.; Wang, E.; Lian, S.; Gao, L.; Tian, C.; Wang, C., Synthesis of Magnetite Octahedrons from Iron Powders through a Mild Hydrothermal Method. *Materials Research Bulletin* **2006,** *41* (12), 2226-2231.

67.   Haw, C. Y.; Mohamed, F.; Chia, C. H.; Radiman, S.; Zakaria, S.; Huang, N.; Lim, H., Hydrothermal Synthesis of Magnetite Nanoparticles as Mri Contrast Agents. *Ceramics International* **2010,** *36* (4), 1417-1422.

68.   Sun, S.; Zeng, H., Size-Controlled Synthesis of Magnetite Nanoparticles. *J. Am. Chem. Soc.* **2002,** *124*, 8204-8205.

69.   Sun, S.; Zeng, H.; Robinson, D. B.; Raoux, S.; Rice, P. M.; Wang, S. X.; Li, G., Monodisperse Mfe$_2$o$_4$ (M = Fe, Co, Mn) Nanoparticles. *J. Am. Chem. Soc.* **2004,** *126*, 273-279.

70.   Salas, G.; Casado, C.; Teran, F.; Miranda, R.; Serna, C. J.; Morales, M. P., Controlled Synthesis of Uniform Magnetite Nanocrystals with High-Quality Properties for Biomedical Applications. *Journal of Materials Chemistry* **2012,** *22* (39), 21065.

71.   Roca, A. G.; Costo, R.; Rebolledo, A. F.; Veintemillas-Verdaguer, S.; Tartaj, P.; González-Carreño, T.; Morales, M. P.; Serna, C. J., Progress in the Preparation of Magnetic Nanoparticles for Applications in Biomedicine. *Journal of Physics D: Applied Physics* **2009,** *42* (22), 224002.

72.   LaMer, V. K.; Dinegar, R. H., Theory, Production and Mechanism of Formation of Monodispersed Hydrosols. *J. Am. Chem. Soc.* **1950,** *72*, 4847-4854.

73.   Zhang, L.; He, R.; Gu, H.-C., Oleic Acid Coating on the Monodisperse Magnetite Nanoparticles. *Applied Surface Science* **2006,** *253*, 2611–2617.

74.   Moros, M.; Pelaz, B.; Lopez-Larrubia, P.; Garcia-Martin, M. L.; Grazu, V.; de la Fuente, J. M., Engineering Biofunctional Magnetic Nanoparticles for Biotechnological Applications. *Nanoscale* **2010,** *2* (9), 1746-55.

75.   Bica, D.; Vékás, L.; Avdeev, M. V.; Marinică, O.; Socoliuc, V.; Bălăsoiu, M.; Garamus, V. M., Sterically Stabilized Water Based Magnetic Fluids: Synthesis, Structure and Properties. *J Magn Magn Mater* **2007,** *311* (1), 17-21.

76.   Gutierrez, L.; Romero, S.; daSilva, G. B.; Costo, R.; Vargas, M. D.; Ronconi, C. M.; Serna, C. J.; Veintemillas-Verdaguer, S.; Morales, M. P., Degradation of Magnetic Nanoparticles Mimicking Lysosomal Conditions Followed by Ac Susceptibility. *Biomedical Engineering / Biomedizinische Technik* **2015**.

77.   Dell´Orco, D.; Lundqvist, M.; Oslakovic, C.; Cedervall, T.; Linse, S., Modeling the Time Evolution of the Nanoparticle-Protein Corona in a Body Fluid. *PLoS One* **2010,** *5* (6), e10949.

78.   Gupta, M. N.; Roy, I., How Corona Formation Impacts Nano-Materials as Drug Carriers? *Molecular Pharmaceutics* **2020**.

79.   Palma, S. I.; Marciello, M.; Carvalho, A.; Veintemillas-Verdaguer, S.; Morales, M. P.; Roque, A. C., Effects of Phase Transfer Ligands on Monodisperse Iron Oxide Magnetic Nanoparticles. *Journal of Colloid Interface Science* **2015,** *437C*, 147-155.

80.   Schweiger, C.; Pietzonka, C.; Heverhagen, J.; Kissel, T., Novel Magnetic Iron Oxide Nanoparticles Coated with Poly(Ethylene Imine)-G-Poly(Ethylene Glycol) for Potential Biomedical Application: Synthesis, Stability, Cytotoxicity and Mr Imaging. *Int J Pharm* **2011,** *408* (1-2), 130-7.

81.   Guardia, P.; Di Corato, R.; Lartigue, L.; Wilhelm, C.; Espinosa, A.; Garcia-Hernandez, M.; Gazeau, F.; Manna, L.; Pellegrino, T., Water-Soluble Iron Oxide Nanocubes with High Values of Specific Absorption Rate for Cancer Cell Hyperthermia Treatment. *ACS nano* **2012,** *6* (4), 3080-3091.

82.   Dias, J. T.; Moros, M.; Del Pino, P.; Rivera, S.; Grazu, V.; de la Fuente, J. M., DNA as a Molecular Local Thermal Probe for the Analysis of Magnetic Hyperthermia. *Angew Chem Int Ed Engl* **2013,** *52* (44), 11526-9.

83.   Li, T.-J.; Huang, C.-C.; Ruan, P.-W.; Chuang, K.-Y.; Huang, K.-J.; Shieh, D.-B.; Yeh, C.-S., In vivo Anti-Cancer Efficacy of Magnetite Nanocrystal - Based System Using Locoregional Hyperthermia Combined with 5-Fluorouracil Chemotherapy. *Biomaterials* **2013,** *34* (32), 7873-7883.

84.   Rodriguez, I.; Perez-Rial, S.; Gonzalez-Jimenez, J.; Perez-Sanchez, J.; Herranz, F.; Beckmann, N.; Ruiz-Cabello, J., Magnetic Resonance Methods and Applications in Pharmaceutical Research. *J Pharm Sci* **2008,** *97* (9), 3637-3665.

85.   Lima-Tenorio, M. K.; Pineda, E. A.; Ahmad, N. M.; Fessi, H.; Elaissari, A., Magnetic Nanoparticles: In Vivo Cancer Diagnosis and Therapy. *Int J Pharm* **2015,** *493* (1-2), 313-27.

86.   Perez-Lopez, B.; Merkoci, A., Nanoparticles for the Development of Improved (Bio)Sensing Systems. *Anal Bioanal Chem* **2011,** *399* (4), 1577-90.

87.   Perez, J. M.; Josephson, L.; O'Loughlin, T.; Högemann, D.; Weissleder, R., Magnetic Relaxation Switches Capable of Sensing Molecular Interactions. *Nature biotechnology* **2002,** *20* (8), 816-820.

88.   Lee, H.; Yoon, T.-J.; Figueiredo, J.-L.; Swirski, F. K.; Weissleder, R., Rapid Detection and Profiling of Cancer Cells in Fine-Needle Aspirates. *Proc. Natl. Acad. Sci. U S A* **2009,** *106* (30), 12459-12464.

89.	Cui, Y. R.; Hong, C.; Zhou, Y. L.; Li, Y.; Gao, X. M.; Zhang, X. X., Synthesis of Orientedly Bioconjugated Core/Shell Fe_3O_4@Au Magnetic Nanoparticles for Cell Separation. *Talanta* **2011,** *85* (3), 1246-1252.

90.	Cavill, I.; Auerbach, M.; Bailie, G. R.; Barrett-Lee, P.; Beguin, Y.; Kaltwasser, P.; Littlewood, T.; Macdougall, I. C.; Wilson, K., Iron and the Anaemia of Chronic Disease: A Review and Strategic Recommendations. *Current medical research and opinion* **2006,** *22* (4), 731-737.

91.	Medarova, Z.; Pham, W.; Farrar, C.; Petkova, V.; Moore, A., In Vivo Imaging of Sirna Delivery and Silencing in Tumors. *Nature medicine* **2007,** *13* (3), 372-377.

92.	Dilnawaz, F.; Sahoo, S. K., Therapeutic Approaches of Magnetic Nanoparticles for the Central Nervous System. *Drug Discov Today* **2015,** *20* (10), 1256-1264.

93.	Lu, Y.-J.; Chuang, E.-Y.; Cheng, Y.-H.; Anilkumar, T.; Chen, H.-A.; Chen, J.-P., Thermosensitive Magnetic Liposomes for Alternating Magnetic Field-Inducible Drug Delivery in Dual Targeted Brain Tumor Chemotherapy. *Chemical Engineering Journal* **2019,** *373*, 720-733.

94.	Kossatz, S.; Grandke, J.; Couleaud, P.; Latorre, A.; Aires, A.; Crosbie-Staunton, K.; Ludwig, R.; Dähring, H.; Ettelt, V.; Lazaro-Carrillo, A.; Calero, M.; Sader, M.; Courty, J.; Volkov, Y.; Prina-Mello, A.; Villanueva, A.; Somoza, Á.; Cortajarena, A. L.; Miranda, R.; Hilger, I., Efficient Treatment of Breast Cancer Xenografts with Multifunctionalized Iron Oxide Nanoparticles Combining Magnetic Hyperthermia and Anti-Cancer Drug Delivery. *Breast Cancer Research* **2015,** *17* (1), 66.

95.	Kossatz, S.; Ludwig, R.; Dähring, H.; Ettelt, V.; Rimkus, G.; Marciello, M.; Salas, G.; Patel, V.; Teran, F. J.; Hilger, I., High Therapeutic Efficiency of Magnetic Hyperthermia in Xenograft Models Achieved with Moderate Temperature Dosages in the Tumor Area. *Pharmaceutical Research* **2014,** *31* (12), 3274-3288.

96.	Guisasola, E.; Asín, L.; Beola, L.; de la Fuente, J. M.; Baeza, A.; Vallet-Regí, M., Beyond Traditional Hyperthermia: In Vivo Cancer Treatment with Magnetic-Responsive Mesoporous Silica Nanocarriers. *ACS Appl Mater Interfaces* **2018,** *10* (15), 12518-12525.

97.	Hilger, I., In Vivo Applications of Magnetic Nanoparticle Hyperthermia. *International Journal of Hyperthermia* **2013,** *29* (8), 828-834.

98.	Attaluri, A.; Kandala, S. K.; Wabler, M.; Zhou, H.; Cornejo, C.; Armour, M.; Hedayati, M.; Zhang, Y.; DeWeese, T. L.; Herman, C.; Ivkov, R., Magnetic Nanoparticle Hyperthermia Enhances Radiation Therapy: A Study in Mouse Models of Human Prostate Cancer. *International Journal of Hyperthermia* **2015,** *31* (4), 359-374.

99.	Asín, L.; Ibarra, M. R.; Tres, A.; Goya, G. F., Controlled Cell Death by Magnetic Hyperthermia: Effects of Exposure Time, Field Amplitude, and Nanoparticle Concentration. *Pharm. Res.* **2012,** *29* (5), 1319-1327.

100.	Laurent, S.; Dutz, S.; Häfeli, U. O.; Mahmoudi, M., Magnetic Fluid Hyperthermia: Focus on Superparamagnetic Iron Oxide Nanoparticles. *Advances in Colloid and Interface Science* **2011,** *166* (1), 8-23.

101.	Abenojar, E. C.; Wickramasinghe, S.; Bas-Concepcion, J.; Samia, A. C. S., Structural Effects on the Magnetic Hyperthermia Properties of Iron Oxide Nanoparticles. *Progress in Natural Science: Materials International* **2016,** *26* (5), 440-448.

102.   Verde, E. L.; Landi, G. T.; Gomes, J. A.; Sousa, M. H.; Bakuzis, A. F., Magnetic Hyperthermia Investigation of Cobalt Ferrite Nanoparticles: Comparison between Experiment, Linear Response Theory, and Dynamic Hysteresis Simulations. *Journal of Applied Physics* **2012,** *111* (12), 123902.

103.   Suto, M.; Hirota, Y.; Mamiya, H.; Fujita, A.; Kasuya, R.; Tohji, K.; Jeyadevan, B., Heat Dissipation Mechanism of Magnetite Nanoparticles in Magnetic Fluid Hyperthermia. *Journal of Magnetism and Magnetic Materials* **2009,** *321* (10), 1493-1496.

104.   Conde-Leboran, I.; Baldomir, D.; Martinez-Boubeta, C.; Chubykalo-Fesenko, O.; del Puerto Morales, M.; Salas, G.; Cabrera, D.; Camarero, J.; Teran, F. J.; Serantes, D., A Single Picture Explains Diversity of Hyperthermia Response of Magnetic Nanoparticles. *The Journal of Physical Chemistry C* **2015,** *119* (27), 15698-15706.

105.   Wildeboer, R.; Southern, P.; Pankhurst, Q., On the Reliable Measurement of Specific Absorption Rates and Intrinsic Loss Parameters in Magnetic Hyperthermia Materials. *Journal of Physics D: Applied Physics* **2014,** *47* (49), 495003.

106.   Soetaert, F.; Kandala, S. K.; Bakuzis, A.; Ivkov, R., Experimental Estimation and Analysis of Variance of the Measured Loss Power of Magnetic Nanoparticles. *Sci Rep* **2017,** *7* (1), 1-15.

107.   Fields, R. E., Evaluating Compliance with Fcc Guidelines for Human Exposure to Radiofrequency Electromagnetic Fields. *OET bulletin* **1997,** *65* (10).

108.   LeBrun, A.; Ma, R.; Zhu, L., Microct Image Based Simulation to Design Heating Protocols in Magnetic Nanoparticle Hyperthermia for Cancer Treatment. *J Therm Biol* **2016,** *62* (Pt B), 129-137.

109.   Andreu, I.; Natividad, E., Accuracy of Available Methods for Quantifying the Heat Power Generation of Nanoparticles for Magnetic Hyperthermia. *International Journal of Hyperthermia* **2013,** *29* (8), 739-751.

110.   Kallumadil, M.; Tada, M.; Nakagawa, T.; Abe, M.; Southern, P.; Pankhurst, Q. A., Suitability of Commercial Colloids for Magnetic Hyperthermia. *J Magn Magn Mater* **2009,** *321* (10), 1509-1513.

111.   Kallumadil, M.; Tada, M.; Nakagawa, T.; Abe, M.; Southern, P.; Pankhurst, Q. A., Corrigendum to "Suitability of Commercial Colloids for Magnetic Hyperthermia"[J. Magn. Magn. Mater. 321 (2009) 1509-1513]. *JMMM* **2009,** *321* (21), 3650-3651.

112.   Ortega, D.; Pankhurst, Q. A., Magnetic Hyperthermia. *Nanoscience* **2013,** *1* (60), e88.

113.   Kumar, C. S.; Mohammad, F., Magnetic Nanomaterials for Hyperthermia-Based Therapy and Controlled Drug Delivery. *Adv Drug Deliv Rev* **2011,** *63* (9), 789-808.

114.   Moros, M.; Idiago-López, J.; Asín, L.; Moreno-Antolín, E.; Beola, L.; Grazú, V.; Fratila, R. M.; Gutiérrez, L.; de la Fuente, J. M., Triggering Antitumoural Drug Release and Gene Expression by Magnetic Hyperthermia. *Adv Drug Deliv Rev* **2018**.

115.   James, G. A.; Swogger, E.; Wolcott, R.; Pulcini, E. d.; Secor, P.; Sestrich, J.; Costerton, J. W.; Stewart, P. S., Biofilms in Chronic Wounds. *Wound Repair and regeneration* **2008,** *16* (1), 37-44.

116.   Hall, C. W.; Mah, T.-F., Molecular Mechanisms of Biofilm-Based Antibiotic Resistance and Tolerance in Pathogenic Bacteria. *FEMS microbiology reviews* **2017,** *41* (3), 276-301.

117.   Ricker, E. B.; Nuxoll, E., Synergistic Effects of Heat and Antibiotics on Pseudomonas Aeruginosa Biofilms. *Biofouling* **2017,** *33* (10), 855-866.

118.   Sturtevant, R. A.; Sharma, P.; Pavlovsky, L.; Stewart, E. J.; Solomon, M. J.; Younger, J. G., Thermal Augmentation of Vancomycin against Staphylococcal Biofilms. *Shock (Augusta, Ga.)* **2015,** *44* (2), 121.

119.   Alumutairi, L.; Yu, B.; Filka, M.; Nayfach, J.; Kim, M. H., Mild Magnetic Nanoparticle Hyperthermia Enhances the Susceptibility of Staphylococcus Aureus Biofilm to Antibiotics. *Int J Hyperthermia* **2020,** *37* (1), 66-75.

120.   Asin, L.; Goya, G.; Tres, A.; Ibarra, M., Induced Cell Toxicity Originates Dendritic Cell Death Following Magnetic Hyperthermia Treatment. *Cell death & disease* **2013,** *4* (4), e596-e596.

121.   Asín, L.; Stepien, G.; Moros, M.; Fratila, R. M.; de la Fuente, J. M., 16 Magnetic Nanoparticles for Cancer Treatment Using Magnetic Hyperthermia. *Clinical Applications of Magnetic Nanoparticles: From Fabrication to Clinical Applications* **2018**, 305.

122.   Badjatia, N., Hyperthermia and Fever Control in Brain Injury. *Critical care medicine* **2009,** *37* (7), S250-S257.

123.   Roussakow, S. In *The History of Hyperthermia Rise and Decline*, Conference Papers in Science, Hindawi: 2013.

124.   Jia, D.; Liu, J., Current Devices for High-Performance Whole-Body Hyperthermia Therapy. *Expert review of medical devices* **2010,** *7* (3), 407-423.

125.   Dähring, H.; Grandke, J.; Teichgräber, U.; Hilger, I., Improved Hyperthermia Treatment of Tumors under Consideration of Magnetic Nanoparticle Distribution Using Micro-Ct Imaging. *Molecular imaging and biology* **2015,** *17* (6), 763-769.

126.   Gilchrist, R. K.; Medal, R.; Shorey, W. D.; Hanselman, R. C.; Parrott, J. C.; Taylor, C. B., Selective Inductive Heating of Lymph Nodes. *Annals of Surgery* **1957,** *146* (4), 596-606.

127.   Muller, S., Magnetic Fluid Hyperthermia Therapy for Malignant Brain Tumors--an Ethical Discussion. *Nanomedicine* **2009,** *5* (4), 387-93.

128.   Beik, J.; Abed, Z.; Ghoreishi, F. S.; Hosseini-Nami, S.; Mehrzadi, S.; Shakeri-Zadeh, A.; Kamrava, S. K., Nanotechnology in Hyperthermia Cancer Therapy: From Fundamental Principles to Advanced Applications. *J Control Release* **2016,** *235*, 205-221.

129.   Banobre-Lopez, M.; Teijeiro, A.; Rivas, J., Magnetic Nanoparticle-Based Hyperthermia for Cancer Treatment. *Rep Pract Oncol Radiother* **2013,** *18* (6), 397-400.

130.   Espinosa, A.; Kolosnjaj-Tabi, J.; Abou-Hassan, A.; Plan Sangnier, A.; Curcio, A.; Silva, A. K.; Di Corato, R.; Neveu, S.; Pellegrino, T.; Liz-Marzán, L. M., Magnetic (Hyper) Thermia or Photothermia? Progressive Comparison of Iron Oxide and Gold Nanoparticles Heating in Water, in Cells, and in Vivo. *Adv. Funct. Mater.* **2018,** *28* (37), 1803660.

131.   Laurent, S.; Dutz, S.; Hafeli, U. O.; Mahmoudi, M., Magnetic Fluid Hyperthermia: Focus on Superparamagnetic Iron Oxide Nanoparticles. *Adv Colloid Interface Sci* **2011,** *166* (1-2), 8-23.

132.   Ohtake, M.; Umemura, M.; Sato, I.; Akimoto, T.; Oda, K.; Nagasako, A.; Kim, J.-H.; Fujita, T.; Yokoyama, U.; Nakayama, T.; Hoshino, Y.; Ishiba, M.; Tokura, S.; Hara, M.; Muramoto, T.; Yamada, S.; Masuda, T.; Aoki, I.; Takemura, Y.; Murata, H.; Eguchi, H.; Kawahara, N.; Ishikawa, Y., Hyperthermia and Chemotherapy Using Fe(Salen) Nanoparticles Might Impact Glioblastoma Treatment. *Scientific Reports* **2017,** *7*, 42783.

133. Liu, D.; Hong, Y.; Li, Y.; Hu, C.; Yip, T.-C.; Yu, W.-K.; Zhu, Y.; Fong, C.-C.; Wang, W.; Au, S.-K., Targeted Destruction of Cancer Stem Cells Using Multifunctional Magnetic Nanoparticles That Enable Combined Hyperthermia and Chemotherapy. *Theranostics* **2020,** *10* (3), 1181.

134. Niiyama, E.; Uto, K.; Lee, C. M.; Sakura, K.; Ebara, M., Hyperthermia Nanofiber Platform Synergized by Sustained Release of Paclitaxel to Improve Antitumor Efficiency. *Advanced healthcare materials* **2019,** *8* (13), 1900102.

135. Issels, R. D., Hyperthermia Adds to Chemotherapy. *Eur J Cancer* **2008,** *44* (17), 2546-54.

136. Huilgol, N. G.; Pemmaraju, G.; Dusane, R., Promising Role of Hyperthermia Concurrent with Radiation in the Treatment of Head-and-Neck Cancers: A Retrospective Comparative Study. *Journal of Radiation and Cancer Research* **2019,** *10* (4), 165.

137. Quinto, C. A.; Mohindra, P.; Tong, S.; Bao, G., Multifunctional Superparamagnetic Iron Oxide Nanoparticles for Combined Chemotherapy and Hyperthermia Cancer Treatment. *Nanoscale* **2015,** *7* (29), 12728-12736.

138. Oei, A.; Kok, H.; Oei, S.; Horsman, M.; Stalpers, L.; Franken, N.; Crezee, J., Molecular and Biological Rationale of Hyperthermia as Radio-and Chemosensitizer. *Adv Drug Deliv Rev* **2020**.

139. Ariyafar, T.; Mahdavi, S. R.; Geraily, G.; Fadavi, P.; Farhood, B.; Najafi, M.; Ashouri, A.; Khalafi, L.; Shirazi, A., Evaluating the Effectiveness of Combined Radiotherapy and Hyperthermia for the Treatment Response of Patients with Painful Bony Metastases: A Phase 2 Clinical Trial. *J Therm Biol* **2019,** *84*, 129-135.

140. Westermann, A. M.; Jones, E. L.; Schem, B. C.; van der Steen-Banasik, E. M.; Koper, P.; Mella, O.; Uitterhoeve, A. L.; de Wit, R.; van der Velden, J.; Burger, C., First Results of Triple-Modality Treatment Combining Radiotherapy, Chemotherapy, and Hyperthermia for the Treatment of Patients with Stage Iib, Iii, and Iva Cervical Carcinoma. *Cancer* **2005,** *104* (4), 763-770.

141. Badgwell, B. D.; Ikoma, N.; Blum Murphy, M. A.; Wang, X.; Estrella, J.; Roy-Chowdhuri, S.; Das, P.; Minsky, B. D.; Mansfield, P. F.; Ajani, J. A., A Phase Ii Trial of Cytoreduction, Gastrectomy, and Hyperthermic Intraperitoneal Perfusion with Chemotherapy for Patients with Gastric Cancer and Stage Iv Peritoneal Disease. American Society of Clinical Oncology: 2020.

142. Lu, Y.-D.; Zheng, S., Hyperthermic Intraperitoneal Chemotherapy for Gastric Cancer with Peritoneal Metastasis: A Meta-Analysis. *TMR Cancer* **2020,** *3* (2), 62-73.

143. Issels, R. D.; Lindner, L. H.; Verweij, J.; Wust, P.; Reichardt, P.; Schem, B.-C.; Abdel-Rahman, S.; Daugaard, S.; Salat, C.; Wendtner, C.-M., Neo-Adjuvant Chemotherapy Alone or with Regional Hyperthermia for Localised High-Risk Soft-Tissue Sarcoma: A Randomised Phase 3 Multicentre Study. *Lancet Oncol* **2010,** *11* (6), 561-570.

144. Moy, A. J.; Tunnell, J. W., Combinatorial Immunotherapy and Nanoparticle Mediated Hyperthermia. *Adv Drug Deliv Rev* **2017,** *114*, 175-183.

145. Hurwitz, M. D., Hyperthermia and Immunotherapy: Clinical Opportunities. *International Journal of Hyperthermia* **2019,** *36* (sup1), 4-9.

146. Clarke, M. F.; Hass, A. T., Cancer Stem Cells. *Reviews in Cell Biology and Molecular Medicine* **2006**.

147.   Alekseenko, L. L.; Zemelko, V. I.; Domnina, A. P.; Lyublinskaya, O. G.; Zenin, V. V.; Pugovkina, N. A.; Kozhukharova, I. V.; Borodkina, A. V.; Grinchuk, T. M.; Fridlyanskaya, I. I., Sublethal Heat Shock Induces Premature Senescence Rather Than Apoptosis in Human Mesenchymal Stem Cells. *Cell Stres Chaperon* **2014,** *19* (3), 355-366

148.   Sadhukha, T.; Niu, L.; Wiedmann, T. S.; Panyam, J., Effective Elimination of Cancer Stem Cells by Magnetic Hyperthermia. *Molecular Pharmaceutics* **2013,** *10* (4), 1432-1441.

149.   Yin, P. T.; Shah, S.; Pasquale, N. J.; Garbuzenko, O. B.; Minko, T.; Lee, K.-B., Stem Cell-Based Gene Therapy Activated Using Magnetic Hyperthermia to Enhance the Treatment of Cancer. *Biomaterials* **2016,** *81* (Supplement C), 46-57.

150.   Arriortua, O. K.; Garaio, E.; Herrero de la Parte, B.; Insausti, M.; Lezama, L.; Plazaola, F.; García, J. A.; Aizpurua, J. M.; Sagartzazu, M.; Irazola, M.; Etxebarria, N.; García-Alonso, I.; Saiz-López, A.; Echevarria-Uraga, J. J., Antitumor Magnetic Hyperthermia Induced by Rgd-Functionalized Fe(3)O(4) Nanoparticles, in an Experimental Model of Colorectal Liver Metastases. *Beilstein Journal of Nanotechnology* **2016,** *7*, 1532-1542.

151.   Wang, P.; Xie, X.; Wang, J.; Shi, Y.; Shen, N.; Huang, X., Ultra-Small Superparamagnetic Iron Oxide Mediated Magnetic Hyperthermia in Treatment of Neck Lymph Node Metastasis in Rabbit Pyriform Sinus Vx2 Carcinoma. *Tumor Biology* **2015,** *36* (10), 8035-8040.

152.   Sadhukha, T.; Wiedmann, T. S.; Panyam, J., Inhalable Magnetic Nanoparticles for Targeted Hyperthermia in Lung Cancer Therapy. *Biomaterials* **2013,** *34* (21), 5163-5171.

153.   Zadnik, P. L.; Molina, C. A.; Sarabia-Estrada, R.; Groves, M. L.; Wabler, M.; Mihalic, J.; McCarthy, E. F.; Gokaslan, Z. L.; Ivkov, R.; Sciubba, D., Characterization of Intratumor Magnetic Nanoparticle Distribution and Heating in a Rat Model of Metastatic Spine Disease. *Journal of Neurosurgery: Spine* **2014,** *20* (6), 740-750.

154.   Maier-Hauff, K.; Ulrich, F.; Nestler, D.; Niehoff, H.; Wust, P.; Thiesen, B.; Orawa, H.; Budach, V.; Jordan, A., Efficacy and Safety of Intratumoral Thermotherapy Using Magnetic Iron-Oxide Nanoparticles Combined with External Beam Radiotherapy on Patients with Recurrent Glioblastoma Multiforme. *Journal of neuro-oncology* **2011,** *103* (2), 317-324.

155.   Bullivant, J. P.; Zhao, S.; Willenberg, B. J.; Kozissnik, B.; Batich, C. D.; Dobson, J., Materials Characterization of Feraheme/Ferumoxytol and Preliminary Evaluation of Its Potential for Magnetic Fluid Hyperthermia. *International journal of molecular sciences* **2013,** *14* (9), 17501-17510.

156.   Hilger, I.; Kaiser, W. A., Iron Oxide-Based Nanostructures for Mri and Magnetic Hyperthermia. *Nanomedicine* **2012,** *7* (9), 1443-1459.

157.   Thiesen, B.; Jordan, A., Clinical Applications of Magnetic Nanoparticles for Hyperthermia. *International Journal of Hyperthermia* **2008,** *24* (6), 467-474.

158.   Silva, A. K.; Nicolas-Boluda, A.; Fouassier, L.; Gazeau, F., Overcoming the Tumor Microenvironment: The Role of Nanohyperthermia. *Nanomedicine* **2017,** *12* (11), 1213-1215.

159.   Lee, S.; Schmitt, C. A., The Dynamic Nature of Senescence in Cancer. *Nature cell biology* **2019,** *21* (1), 94-101.

160.   Ferlay, J.; Colombet, M.; Soerjomataram, I.; Mathers, C.; Parkin, D.; Piñeros, M.; Znaor, A.; Bray, F., Estimating the Global Cancer Incidence and Mortality in 2018: Globocan Sources and Methods. *International journal of cancer* **2019,** *144* (8), 1941-1953.

161.   Hanahan, D.; Weinberg, R. A., The Hallmarks of Cancer. *Cell* **2000,** *100* (1), 57-70.

162.   Hanahan, D.; Weinberg, R. A., Hallmarks of Cancer: The Next Generation. *Cell* **2011,** *144* (5), 646-674.

163.   van Kempen, L. C.; Ruiter, D. J.; van Muijen, G. N.; Coussens, L. M., The Tumor Microenvironment: A Critical Determinant of Neoplastic Evolution. *Eur. J. Cell Biol.* **2003,** *82* (11), 539-548.

164.   Whiteside, T. L., The Tumor Microenvironment and Its Role in Promoting Tumor Growth. *Oncogene* **2008,** *27* (45), 5904-5912.

165.   Larson, B., 3d Cell Culture: A Review of Current Techniques. *BioTek* **2015,** *6*, 1-10.

166.   Deisboeck, T. S.; Wang, Z.; Macklin, P.; Cristini, V., Multiscale Cancer Modeling. *Annual review of biomedical engineering* **2011,** *13*, 127-155.

167.   Sachs, N.; Clevers, H., Organoid Cultures for the Analysis of Cancer Phenotypes. *Current opinion in genetics & development* **2014,** *24*, 68-73.

168.   Favaro, E.; Bottelli, A.; Lozanoska-Ochser, B.; Ferioli, E.; Huang, G.; Klein, N.; Chiaravalli, A.; Perin, P. C.; Camussi, G.; Peakman, M., Primary and Immortalised Human Pancreatic Islet Endothelial Cells: Phenotypic and Immunological Characterisation. *Diabetologia* **2005,** *48* (12), 2552-2562.

169.   Stacey, G.; MacDonald, C., Immortalisation of Primary Cells. In *Cell Culture Methods for in Vitro Toxicology*, Springer: 2001; pp 27-42.

170.   Shepherd, T. G.; Thériault, B. L.; Campbell, E. J.; Nachtigal, M. W., Primary Culture of Ovarian Surface Epithelial Cells and Ascites-Derived Ovarian Cancer Cells from Patients. *Nature protocols* **2006,** *1* (6), 2643.

171.   Saeed, K.; Ojamies, P.; Pellinen, T.; Eldfors, S.; Turkki, R.; Lundin, J.; Järvinen, P.; Nisen, H.; Taari, K.; Af Hällström, T. M., Clonal Heterogeneity Influences Drug Responsiveness in Renal Cancer Assessed by Ex Vivo Drug Testing of Multiple Patient-Derived Cancer Cells. *International journal of cancer* **2019,** *144* (6), 1356-1366.

172.   Van Wezel, A., Growth of Cell-Strains and Primary Cells on Micro-Carriers in Homogeneous Culture. *Nature* **1967,** *216* (5110), 64-65.

173.   Cayrefourcq, L.; Mazard, T.; Joosse, S.; Solassol, J.; Ramos, J.; Assenat, E.; Schumacher, U.; Costes, V.; Maudelonde, T.; Pantel, K., Establishment and Characterization of a Cell Line from Human Circulating Colon Cancer Cells. *Cancer research* **2015,** *75* (5), 892-901.

174.   Masters, J. R., Human Cancer Cell Lines: Fact and Fantasy. *Nat. Rev. Mol. Cell Biol.* **2000,** *1* (3), 233-236.

175.   Palmini, G.; Zonefrati, R.; Mavilia, C.; Aldinucci, A.; Luzi, E.; Marini, F.; Franchi, A.; Capanna, R.; Tanini, A.; Brandi, M. L., Establishment of Cancer Stem Cell Cultures from Human Conventional Osteosarcoma. *JoVE (Journal of Visualized Experiments)* **2016,** (116), e53884.

176.   O'Hare, M. J.; Bond, J.; Clarke, C.; Takeuchi, Y.; Atherton, A. J.; Berry, C.; Moody, J.; Silver, A. R.; Davies, D. C.; Alsop, A. E., Conditional Immortalization of Freshly Isolated Human Mammary Fibroblasts and Endothelial Cells. *Proc. Natl. Acad. Sci. U S A* **2001,** *98* (2), 646-651.

177.   Christophe, J., Pancreatic Tumoral Cell Line Ar42j: An Amphicrine Model. *American Journal of Physiology-Gastrointestinal and Liver Physiology* **1994,** *266* (6), G963-G971.

178.   Kamalidehghan, B.; Houshmand, M.; Kamalidehghan, F.; Jafarzadeh, N.; Azari, S.; Akmal, S. N.; Rosli, R., Establishment and Characterization of Two Human Breast Carcinoma Cell Lines by Spontaneous Immortalization: Discordance between Estrogen, Progesterone and Her2/Neu Receptors of Breast Carcinoma Tissues with Derived Cell Lines. *Cancer cell international* **2012,** *12* (1), 43.

179.   Goodspeed, A.; Heiser, L. M.; Gray, J. W.; Costello, J. C., Tumor-Derived Cell Lines as Molecular Models of Cancer Pharmacogenomics. *Molecular Cancer Research* **2016,** *14* (1), 3-13.

180.   Sharma, S. V.; Haber, D. A.; Settleman, J., Cell Line-Based Platforms to Evaluate the Therapeutic Efficacy of Candidate Anticancer Agents. *Nat. Rev. Cancer* **2010,** *10* (4), 241-253.

181.   Ghandi, M.; Huang, F. W.; Jané-Valbuena, J.; Kryukov, G. V.; Lo, C. C.; McDonald, E. R.; Barretina, J.; Gelfand, E. T.; Bielski, C. M.; Li, H., Next-Generation Characterization of the Cancer Cell Line Encyclopedia. *Nature* **2019,** *569* (7757), 503-508.

182.   Barretina, J.; Caponigro, G.; Stransky, N.; Venkatesan, K.; Margolin, A. A.; Kim, S.; Wilson, C. J.; Lehár, J.; Kryukov, G. V.; Sonkin, D., The Cancer Cell Line Encyclopedia Enables Predictive Modelling of Anticancer Drug Sensitivity. *Nature* **2012,** *483* (7391), 603-607.

183.   Gillet, J.-P.; Varma, S.; Gottesman, M. M., The Clinical Relevance of Cancer Cell Lines. *J. Ntl. Cancer Inst.* **2013,** *105* (7), 452-458.

184.   Masters, J. R.; Thomson, J. A.; Daly-Burns, B.; Reid, Y. A.; Dirks, W. G.; Packer, P.; Toji, L. H.; Ohno, T.; Tanabe, H.; Arlett, C. F., Short Tandem Repeat Profiling Provides an International Reference Standard for Human Cell Lines. *Proc. Natl. Acad. Sci. U S A* **2001,** *98* (14), 8012-8017.

185.   Romano, P.; Manniello, A.; Aresu, O.; Armento, M.; Cesaro, M.; Parodi, B., Cell Line Data Base: Structure and Recent Improvements Towards Molecular Authentication of Human Cell Lines. *Nucleic acids research* **2009,** *37* (suppl_1), D925-D932.

186.   Freshney, R. I., *Culture of Animal Cells: A Manual of Basic Technique and Specialized Applications*. John Wiley & Sons: 2015.

187.   Bissell, M. J., The Differentiated State of Normal and Malignant Cells or How to Define a "Normal" Cell in Culture. In *International Review of Cytology*, Elsevier: 1981; Vol. 70, pp 27-100.

188.   Vinci, V. A.; Parekh, S. R., *Handbook of Industrial Cell Culture: Mammalian, Microbial, and Plant Cells*. Springer Science & Business Media: 2002.

189.   Place, T. L.; Domann, F. E.; Case, A. J., Limitations of Oxygen Delivery to Cells in Culture: An Underappreciated Problem in Basic and Translational Research. *Free Radical Biology and Medicine* **2017,** *113*, 311-322.

190.   Eglen, R. M.; Klein, J.-L., Three-Dimensional Cell Culture: A Rapidly Emerging Approach to Cellular Science and Drug Discovery. *SLAS DISCOVERY: Advancing the Science of Drug Discovery* **2017,** *22* (5), 453-455.

191.   Fang, Y.; Eglen, R. M., Three-Dimensional Cell Cultures in Drug Discovery and Development. *Slas discovery: Advancing Life Sciences R&D* **2017,** *22* (5), 456-472.

192.   Justice, B. A.; Badr, N. A.; Felder, R. A., 3d Cell Culture Opens New Dimensions in Cell-Based Assays. *Drug Discov Today* **2009,** *14* (1-2), 102-7.

193. Roth, A.; Singer, T., The Application of 3d Cell Models to Support Drug Safety Assessment: Opportunities & Challenges. *Adv Drug Deliv Rev* **2014,** *69*, 179-189.

194. Li, Y.; Kumacheva, E., Hydrogel Microenvironments for Cancer Spheroid Growth and Drug Screening. *Science advances* **2018,** *4* (4), eaas8998.

195. Khawar, I. A.; Kim, J. H.; Kuh, H.-J., Improving Drug Delivery to Solid Tumors: Priming the Tumor Microenvironment. *Journal of Controlled Release* **2015,** *201*, 78-89.

196. De Angelis, M. L.; Bruselles, A.; Francescangeli, F.; Pucilli, F.; Vitale, S.; Zeuner, A.; Tartaglia, M.; Baiocchi, M., Colorectal Cancer Spheroid Biobanks: Multi-Level Approaches to Drug Sensitivity Studies. *Cell Biology and Toxicology* **2018,** *34* (6), 459-469.

197. Ioachim, E.; Charchanti, A.; Briasoulis, E.; Karavasilis, V.; Tsanou, H.; Arvanitis, D. L.; Agnantis, N. J.; Pavlidis, N., Immunohistochemical Expression of Extracellular Matrix Components Tenascin, Fibronectin, Collagen Type Iv and Laminin in Breast Cancer: Their Prognostic Value and Role in Tumour Invasion and Progression. *Eur J Cancer* **2002,** *38* (18), 2362-2370

198. Netti, P. A.; Berk, D. A.; Swartz, M. A.; Grodzinsky, A. J.; Jain, R. K., Role of Extracellular Matrix Assembly in Interstitial Transport in Solid Tumors. *Cancer research* **2000,** *60* (9), 2497-2503.

199. Del Bufalo, F.; Manzo, T.; Hoyos, V.; Yagyu, S.; Caruana, I.; Jacot, J.; Benavides, O.; Rosen, D.; Brenner, M. K., 3d Modeling of Human Cancer: A Peg-Fibrin Hydrogel System to Study the Role of Tumor Microenvironment and Recapitulate the in Vivo Effect of Oncolytic Adenovirus. *Biomaterials* **2016,** *84*, 76-85.

200. Hoffmann, O. I.; Ilmberger, C.; Magosch, S.; Joka, M.; Jauch, K.-W.; Mayer, B., Impact of the Spheroid Model Complexity on Drug Response. *Journal of biotechnology* **2015,** *205*, 14-23.

201. Hennink, W. E.; van Nostrum, C. F., Novel Crosslinking Methods to Design Hydrogels. *Adv Drug Deliv Rev* **2012,** *64*, 223-236.

202. Jeong, B.; Kim, S. W.; Bae, Y. H., Thermosensitive Sol–Gel Reversible Hydrogels. *Adv Drug Deliv Rev* **2012,** *64*, 154-162.

203. Nguyen, K. T.; West, J. L., Photopolymerizable Hydrogels for Tissue Engineering Applications. *Biomaterials* **2002,** *23* (22), 4307-4314.

204. DJ, L. K. M., Hydrogels for Tissue Engeneering. *Chem. Rev* **2001,** *101*, 1869-1880.

205. Szot, C. S.; Buchanan, C. F.; Freeman, J. W.; Rylander, M. N., 3d in Vitro Bioengineered Tumors Based on Collagen I Hydrogels. *Biomaterials* **2011,** *32* (31), 7905-7912.

206. Liu, J.; Tan, Y.; Zhang, H.; Zhang, Y.; Xu, P.; Chen, J.; Poh, Y.-C.; Tang, K.; Wang, N.; Huang, B., Soft Fibrin Gels Promote Selection and Growth of Tumorigenic Cells. *Nat Mater* **2012,** *11* (8), 734-741.

207. Cavo, M.; Caria, M.; Pulsoni, I.; Beltrame, F.; Fato, M.; Scaglione, S., A New Cell-Laden 3d Alginate-Matrigel Hydrogel Resembles Human Breast Cancer Cell Malignant Morphology, Spread and Invasion Capability Observed "in Vivo". *Sci Rep* **2018,** *8* (1), 1-12.

208. Stamov, D. R.; Pompe, T., Structure and Function of Ecm-Inspired Composite Collagen Type I Scaffolds. *Soft Matter* **2012,** *8* (40), 10200-10212.

209. Egeblad, M.; Rasch, M. G.; Weaver, V. M., Dynamic Interplay between the Collagen Scaffold and Tumor Evolution. *Current opinion in cell biology* **2010,** *22* (5), 697-706.

210.   Kondo, J.; Endo, H.; Okuyama, H.; Ishikawa, O.; Iishi, H.; Tsujii, M.; Ohue, M.; Inoue, M., Retaining Cell–Cell Contact Enables Preparation and Culture of Spheroids Composed of Pure Primary Cancer Cells from Colorectal Cancer. *Proc. Natl. Acad. Sci. U S A* **2011,** *108* (15), 6235-6240.

211.   Piehler, S.; Wucherpfennig, L.; Tansi, F. L.; Berndt, A.; Quaas, R.; Teichgraeber, U. K.; Hilger, I., Hyperthermia Affects Collagen Fiber Architecture and Induces Apoptosis in Pancreatic and Fibroblast Tumor Hetero-Spheroids in Vitro. *Nanomedicine: Nanotechnology, Biology and Medicine* **2020**, 102183.

212.   Kundu, B.; Bastos, A.; Brancato, V.; Cerqueira, M. T.; Oliveira, J. M.; Correlo, V. M.; Reis, R. L.; Kundu, S. C., Mechanical Property of Hydrogels and the Presence of Adipose Stem Cells in Tumor Stroma Affect Spheroid Formation in the 3d Osteosarcoma Model. *ACS Appl Mater Interfaces* **2019,** *11* (16), 14548-14559.

213.   Sokol, E. S.; Miller, D. H.; Breggia, A.; Spencer, K. C.; Arendt, L. M.; Gupta, P. B., Growth of Human Breast Tissues from Patient Cells in 3d Hydrogel Scaffolds. *Breast Cancer Research* **2016,** *18* (1), 19.

214.   Meinert, C.; Theodoropoulos, C.; Klein, T. J.; Hutmacher, D. W.; Loessner, D., A Method for Prostate and Breast Cancer Cell Spheroid Cultures Using Gelatin Methacryloyl-Based Hydrogels. In *Prostate Cancer*, Springer: 2018; pp 175-194.

215.   Vail, D. M.; Macewen, E. G., Spontaneously Occurring Tumors of Companion Animals as Models for Human Cancer. *Cancer Investigation* **2000,** *18* (8), 781-792.

216.   Day, C.-P.; Merlino, G.; Van Dyke, T., Preclinical Mouse Cancer Models: A Maze of Opportunities and Challenges. *Cell* **2015,** *163* (1), 39-53.

217.   Workman, P.; Aboagye, E. O.; Balkwill, F.; Balmain, A.; Bruder, G.; Chaplin, D. J.; Double, J. A.; Everitt, J.; Farningham, D. A. H.; Glennie, M. J.; Kelland, L. R.; Robinson, V.; Stratford, I. J.; Tozer, G. M.; Watson, S.; Wedge, S. R.; Eccles, S. A.; An ad hoc committee of the National Cancer Research, I., Guidelines for the Welfare and Use of Animals in Cancer Research. *British journal of cancer* **2010,** *102* (11), 1555-1577.

218.   Bibby, M. C., Orthotopic Models of Cancer for Preclinical Drug Evaluation: Advantages and Disadvantages. *Eur J Cancer* **2004,** *40* (6), 852-857.

219.   Becher, O. J.; Holland, E. C., Genetically Engineered Models Have Advantages over Xenografts for Preclinical Studies. *Cancer research* **2006,** *66* (7), 3355.

220.   Mosely, S. I. S.; Prime, J. E.; Sainson, R. C. A.; Koopmann, J.-O.; Wang, D. Y. Q.; Greenawalt, D. M.; Ahdesmaki, M. J.; Leyland, R.; Mullins, S.; Pacelli, L.; Marcus, D.; Anderton, J.; Watkins, A.; Coates Ulrichsen, J.; Brohawn, P.; Higgs, B. W.; McCourt, M.; Jones, H.; Harper, J. A.; Morrow, M.; Valge-Archer, V.; Stewart, R.; Dovedi, S. J.; Wilkinson, R. W., Rational Selection of Syngeneic Preclinical Tumor Models for Immunotherapeutic Drug Discovery. *Cancer Immunology Research* **2017,** *5* (1), 29.

221.   Delfino, T.; Wang, Y.; Schartner, J.; Rutz, S., Targeted Ablation of Foxp3+ T Cells Activates Peripheral and Tumor-Infiltrating Cytotoxic Cd8+ T Cells in Multiple Syngeneic Mouse Tumor Models. *The Journal of Immunology* **2019,** *202* (1 Supplement), 134.18.

222.   Teicher, B. A., Tumor Models for Efficacy Determination. *Molecular Cancer Therapeutics* **2006,** *5* (10), 2435.

223.   Combest, A. J.; Roberts, P. J.; Dillon, P. M.; Sandison, K.; Hanna, S. K.; Ross, C.; Habibi, S.; Zamboni, B.; Müller, M.; Brunner, M.; Sharpless, N. E.; Zamboni, W. C.,

Genetically Engineered Cancer Models, but Not Xenografts, Faithfully Predict Anticancer Drug Exposure in Melanoma Tumors. *The oncologist* **2012,** *17* (10), 1303-1316.

224.   Martin, E. S.; Belmont, P. J.; Sinnamon, M. J.; Richard, L. G.; Yuan, J.; Coffee, E. M.; Roper, J.; Lee, L.; Heidari, P.; Lunt, S. Y.; Goel, G.; Ji, X.; Xie, Z.; Xie, T.; Lamb, J.; Weinrich, S. L.; VanArsdale, T.; Bronson, R. T.; Xavier, R. J.; Vander Heiden, M. G.; Kan, J. L. C.; Mahmood, U.; Hung, K. E., Development of a Colon Cancer Gemm-Derived Orthotopic Transplant Model for Drug Discovery and Validation. *Clinical Cancer Research* **2013,** *19* (11), 2929.

225.   Voskoglou-Nomikos, T.; Pater, J. L.; Seymour, L., Clinical Predictive Value of the in Vitro Cell Line, Human Xenograft, and Mouse Allograft Preclinical Cancer Models. *Clinical Cancer Research* **2003,** *9* (11), 4227.

226.   Kim, M. P.; Evans, D. B.; Wang, H.; Abbruzzese, J. L.; Fleming, J. B.; Gallick, G. E., Generation of Orthotopic and Heterotopic Human Pancreatic Cancer Xenografts in Immunodeficient Mice. *Nature protocols* **2009,** *4* (11), 1670.

227.   Tentler, J. J.; Tan, A. C.; Weekes, C. D.; Jimeno, A.; Leong, S.; Pitts, T. M.; Arcaroli, J. J.; Messersmith, W. A.; Eckhardt, S. G., Patient-Derived Tumour Xenografts as Models for Oncology Drug Development. *Nature Reviews Clinical Oncology* **2012,** *9* (6), 338-350.

228.   Liu, Q.; Huang, J.; Feng, Q.; Zhang, T.; Chen, X.; Li, X.; Liu, X.; Li, H.; Zhong, Z.; Xiao, K., Multi-Modal Visualization of Uptake and Distribution of Iron Oxide Nanoparticles in Macrophages, Cancer Cells, and Xenograft Models. *Journal of Biomedical Nanotechnology* **2019,** *15* (8), 1801-1811.

229.   Walsh, N. C.; Kenney, L. L.; Jangalwe, S.; Aryee, K.-E.; Greiner, D. L.; Brehm, M. A.; Shultz, L. D., Humanized Mouse Models of Clinical Disease. *Annual Review of Pathology: Mechanisms of Disease* **2017,** *12*, 187-215.

230.   Zitvogel, L.; Pitt, J. M.; Daillère, R.; Smyth, M. J.; Kroemer, G., Mouse Models in Oncoimmunology. *Nature Reviews Cancer* **2016,** *16* (12), 759.

231.   Xie, X.; Briinnert, N.; Jensen, G.; Albrectsen, J.; Gotthardsen, B.; Rygaard, J., Comparative Studies between Nude and Scid Mice on the Growth and Metastatic Behavior of Xenografted Human Tumors. *Clinical & Experimental Metastasis* **1992,** *10* (3), 201-210.

232.   Watson, S. A.; Kumari, R., Theoretical Considerations in Using Animal Models of Metastasis and Brief Methodology for in Vivo Colorectal Cancer Models in Scid and Nude Mice. In *Metastasis Research Protocols*, Dwek, M.; Schumacher, U.; Brooks, S. A., Eds. Springer New York: New York, NY, 2014; pp 117-129.

233.   Fogh, J.; Fogh, J. M.; Orfeo, T., One Hundred and Twenty-Seven Cultured Human Tumor Cell Lines Producing Tumors in Nude Mice23. *JNCI: Journal of the National Cancer Institute* **1977,** *59* (1), 221-226.

234.   Oliveira, C. F. A.; Lara, N. L. M.; Lacerda, S. M. S. N.; Resende, R. R.; França, L. R.; Avelar, G. F., Foxn1 and Prkdc Genes Are Important for Testis Function: Evidence from Nude and Scid Adult Mice. *Cell and Tissue Research* **2020**.

235.   Pearson, T.; Greiner, D. L.; Shultz, L. D., Humanized Scid Mouse Models for Biomedical Research. In *Humanized Mice*, Nomura, T.; Watanabe, T.; Habu, S., Eds. Springer Berlin Heidelberg: Berlin, Heidelberg, 2008; pp 25-51.

236.   Schroeder, M. A.; DiPersio, J. F., Mouse Models of Graft-Versus-Host Disease: Advances and Limitations. *Disease Models &amp; Mechanisms* **2011,** *4* (3), 318.

237.   Tanaka, H. Y.; Kano, M. R., Stromal Barriers to Nanomedicine Penetration in the Pancreatic Tumor Microenvironment. *Cancer science* **2018,** *109* (7), 2085-2092.

238.   Shaw, T. J.; Senterman, M. K.; Dawson, K.; Crane, C. A.; Vanderhyden, B. C., Characterization of Intraperitoneal, Orthotopic, and Metastatic Xenograft Models of Human Ovarian Cancer. *Molecular therapy* **2004,** *10* (6), 1032-1042.

239.   Johannsen, M.; Thiesen, B.; Wust, P.; Jordan, A., Magnetic Nanoparticle Hyperthermia for Prostate Cancer. *International Journal of Hyperthermia* **2010,** *26* (8), 790-795.

240.   Stapf, M.; Poempner, N.; Kettering, M.; Hilger, I., Magnetic Thermoablation Stimuli Alter Bcl2 and Fgf-R1 but Not Hsp70 Expression Profiles in Bt474 Breast Tumors. *Int J Nanomedicine* **2015,** *10*, 1931.

241.   Krawczyk, P. M.; Eppink, B.; Essers, J.; Stap, J.; Rodermond, H.; Odijk, H.; Zelensky, A.; van Bree, C.; Stalpers, L. J.; Buist, M. R., Mild Hyperthermia Inhibits Homologous Recombination, Induces Brca2 Degradation, and Sensitizes Cancer Cells to Poly (Adp-Ribose) Polymerase-1 Inhibition. *Proc. Natl. Acad. Sci. U S A* **2011,** *108* (24), 9851-9856.

242.   Moros, M.; Ambrosone, A.; Stepien, G.; Fabozzi, F.; Marchesano, V.; Castaldi, A.; Tino, A.; de la Fuente, J. M.; Tortiglione, C., Deciphering Intracellular Events Triggered by Mild Magnetic Hyperthermia in Vitro and in Vivo. *Nanomedicine* **2015,** *10* (14), 2167-2183.

243.   Khot, V. M.; Salunkhe, A. B.; Ruso, J. M.; Pawar, S. H., Improved Magnetic Induction Heating of Nanoferrites for Hyperthermia Applications: Correlation with Colloidal Stability and Magneto-Structural Properties. *J Magn Magn Mater* **2015,** *384*, 335-343.

244.   Patil, R. M.; Thorat, N. D.; Shete, P. B.; Otari, S. V.; Tiwale, B. M.; Pawar, S. H., In Vitro Hyperthermia with Improved Colloidal Stability and Enhanced Sar of Magnetic Core/Shell Nanostructures. *Mater Sci Eng C Mater Biol Appl* **2016,** *59*, 702-709.

245.   Rodrigues, H. F.; Capistrano, G.; Mello, F. M.; Zufelato, N.; Silveira-Lacerda, E.; Bakuzis, A. F., Precise Determination of the Heat Delivery During in Vivo Magnetic Nanoparticle Hyperthermia with Infrared Thermography. *Phys Med Biol* **2017,** *62* (10), 4062-4082.

246.   Shah, R. R.; Davis, T. P.; Glover, A. L.; Nikles, D. E.; Brazel, C. S., Impact of Magnetic Field Parameters and Iron Oxide Nanoparticle Properties on Heat Generation for Use in Magnetic Hyperthermia. *J Magn Magn Mater* **2015,** *387*, 96-106.

247.   Deatsch, A. E.; Evans, B. A., Heating Efficiency in Magnetic Nanoparticle Hyperthermia. *J Magn Magn Mater* **2014,** *354*, 163-172.

248.   Sodano, H. A.; Bae, J.-S.; Inman, D. J.; Belvin, W. K., Improved Concept and Model of Eddy Current Damper. *Journal of Vibration and Acoustics* **2005,** *128* (3), 294-302.

249.   Atkinson, W. J.; Brezovich, I. A.; Chakraborty, D. P., Usable Frequencies in Hyperthermia with Thermal Seeds. *IEEE Transactions on Biomedical Engineering* **1984,** (1), 70-75.

250.   Brezovich, I. A., Low Frequency Hyperthermia: Capacitive and Ferromagnetic Thermoseed Methods. *Medical physics monograph* **1988,** *16*, 82-111.

251.   Hergt, R.; Dutz, S., Magnetic Particle Hyperthermia—Biophysical Limitations of a Visionary Tumour Therapy. *Journal of Magnetism and Magnetic Materials* **2007,** *311* (1), 187-192.

252.   El-Sherbiny, I. M.; El-Sayed, M.; Reda, A., Superparamagnetic Iron Oxide Nanoparticles (Spions) as Multifunctional Cancer Theranostics. In *Magnetic Nanoheterostructures*, Springer: 2020; pp 223-241.

253.   Seynhaeve, A.; Amin, M.; Haemmerich, D.; van Rhoon, G.; Ten Hagen, T., Hyperthermia and Smart Drug Delivery Systems for Solid Tumor Therapy. *Adv Drug Deliv Rev* **2020**.

254.   Dutz, S.; Hergt, R., Magnetic Nanoparticle Heating and Heat Transfer on a Microscale: Basic Principles, Realities and Physical Limitations of Hyperthermia for Tumour Therapy. *Int J Hyperthermia* **2013,** *29* (8), 790-800.

255.   Cervadoro, A.; Giverso, C.; Pande, R.; Sarangi, S.; Preziosi, L.; Wosik, J.; Brazdeikis, A.; Decuzzi, P., Design Maps for the Hyperthermic Treatment of Tumors with Superparamagnetic Nanoparticles. *Plos One* **2013,** *8* (2).

256.   Datta, N.; Krishnan, S.; Speiser, D.; Neufeld, E.; Kuster, N.; Bodis, S.; Hofmann, H., Magnetic Nanoparticle-Induced Hyperthermia with Appropriate Payloads: Paul Ehrlich's "Magic (Nano) Bullet" for Cancer Theranostics? *Cancer treatment reviews* **2016,** *50*, 217-227.

257.   Jordan, A.; Scholz, R.; Wust, P.; Fähling, H.; Krause, J.; Wlodarczyk, W.; Sander, B.; Vogl, T.; Felix, R., Effects of Magnetic Fluid Hyperthermia (Mfh) on C3h Mammary Carcinoma in Vivo. *International Journal of Hyperthermia* **1997,** *13* (6), 587-605.

258.   Yadollahpour, A.; Hosseini, S. A., Magnetic Nanoparticle Based Hyperthermia: A Review of the Physiochemical Properties and Synthesis Methods. *Int J Pharm Res Allied Sci* **2016,** *5*, 242-246.

259.   Salunkhe, A. B.; Khot, V. M.; Pawar, S., Magnetic Hyperthermia with Magnetic Nanoparticles: A Status Review. *Current topics in medicinal chemistry* **2014,** *14* (5), 572-594.

260.   Kafrouni, L.; Savadogo, O., Recent Progress on Magnetic Nanoparticles for Magnetic Hyperthermia. *Progress in biomaterials* **2016,** *5* (3-4), 147-160.

261.   Périgo, E. A.; Hemery, G.; Sandre, O.; Ortega, D.; Garaio, E.; Plazaola, F.; Teran, F. J., Fundamentals and Advances in Magnetic Hyperthermia. *Applied Physics Reviews* **2015,** *2* (4), 041302.

262.   Balivada, S.; Rachakatla, R. S.; Wang, H.; Samarakoon, T. N.; Dani, R. K.; Pyle, M.; Kroh, F. O.; Walker, B.; Leaym, X.; Koper, O. B.; Tamura, M.; Chikan, V.; Bossmann, S. H.; Troyer, D. L., A/C Magnetic Hyperthermia of Melanoma Mediated by Iron(0)/Iron Oxide Core/Shell Magnetic Nanoparticles: A Mouse Study. *BMC Cancer* **2010,** *10* (1), 119.

263.   Rachakatla, R. S.; Balivada, S.; Seo, G.-M.; Myers, C. B.; Wang, H.; Samarakoon, T. N.; Dani, R.; Pyle, M.; Kroh, F. O.; Walker, B.; Leaym, X.; Koper, O. B.; Chikan, V.; Bossmann, S. H.; Tamura, M.; Troyer, D. L., Attenuation of Mouse Melanoma by a/C Magnetic Field after Delivery of Bi-Magnetic Nanoparticles by Neural Progenitor Cells. *ACS nano* **2010,** *4* (12), 7093-7104.

264.   Ling, Y.; Tang, X.; Wang, F.; Zhou, X.; Wang, R.; Deng, L.; Shang, T.; Liang, B.; Li, P.; Ran, H.; Wang, Z.; Hu, B.; Li, C.; Zuo, G.; Zheng, Y., Highly Efficient Magnetic Hyperthermia Ablation of Tumors Using Injectable Polymethylmethacrylate-Fe3o4. *RSC Advances* **2017,** *7* (5), 2913-2918.

265.   Bae, K. H.; Park, M.; Do, M. J.; Lee, N.; Ryu, J. H.; Kim, G. W.; Kim, C.; Park, T. G.; Hyeon, T., Chitosan Oligosaccharide-Stabilized Ferrimagnetic Iron Oxide Nanocubes for Magnetically Modulated Cancer Hyperthermia. *ACS nano* **2012,** *6* (6), 5266-5273.

266.   Johannsen, M.; Thiesen, B.; Jordan, A.; Taymoorian, K.; Gneveckow, U.; Waldöfner, N.; Scholz, R.; Koch, M.; Lein, M.; Jung, K.; Loening, S. A., Magnetic Fluid Hyperthermia (Mfh)Reduces Prostate Cancer Growth in the Orthotopic Dunning R3327 Rat Model. *The Prostate* **2005,** *64* (3), 283-292.

267.   Melanie, K.; Heike, R.; Frank, W.; Sibylle, B.-S.; Lutz, T.; Werner Alois, K.; Ingrid, H., Minimal-Invasive Magnetic Heating of Tumors Does Not Alter Intra-Tumoral Nanoparticle Accumulation, Allowing for Repeated Therapy Sessions: An in Vivo Study in Mice. *Nanotechnology* **2011,** *22* (50), 505102.

268.   Kolosnjaj-Tabi, J.; Di Corato, R.; Lartigue, L.; Marangon, I.; Guardia, P.; Silva, A. K. A.; Luciani, N.; Clément, O.; Flaud, P.; Singh, J. V.; Decuzzi, P.; Pellegrino, T.; Wilhelm, C.; Gazeau, F., Heat-Generating Iron Oxide Nanocubes: Subtle "Destructurators" of the Tumoral Microenvironment. *ACS nano* **2014,** *8* (5), 4268-4283.

269.   Sandre, O.; Genevois, C.; Garaio, E.; Adumeau, L.; Mornet, S.; Couillaud, F., In Vivo Imaging of Local Gene Expression Induced by Magnetic Hyperthermia. *Genes* **2017,** *8* (2).

270.   Lin, W.; Xie, X.; Yang, Y.; Fu, X.; Liu, H.; Yang, Y.; Deng, J., Thermosensitive Magnetic Liposomes with Doxorubicin Cell-Penetrating Peptides Conjugate for Enhanced and Targeted Cancer Therapy. *Drug Delivery* **2016,** *23* (9), 3436-3443.

271.   Yi, G.-q.; Gu, B.; Chen, L.-k., The Safety and Efficacy of Magnetic Nano-Iron Hyperthermia Therapy on Rat Brain Glioma. *Tumor Biology* **2014,** *35* (3), 2445-2449.

272.   Zhang, Z.-Q.; Song, S.-C., Thermosensitive/Superparamagnetic Iron Oxide Nanoparticle-Loaded Nanocapsule Hydrogels for Multiple Cancer Hyperthermia. *Biomaterials* **2016,** *106* (Supplement C), 13-23.

273.   Zhang, Z.-Q.; Song, S.-C., Multiple Hyperthermia-Mediated Release of Trail/Spion Nanocomplex from Thermosensitive Polymeric Hydrogels for Combination Cancer Therapy. *Biomaterials* **2017,** *132* (Supplement C), 16-27.

274.   Brusentsov, N. A.; Nikitin, L. V.; Brusentsova, T. N.; Kuznetsov, A. A.; Bayburtskiy, F. S.; Shumakov, L. I.; Jurchenko, N. Y., Magnetic Fluid Hyperthermia of the Mouse Experimental Tumor. *Journal of Magnetism and Magnetic Materials* **2002,** *252* (Supplement C), 378-380.

275.   Yang, Y.; Wang, F.; Zheng, K.; Deng, L.; Yang, L.; Zhang, N.; Xu, C.; Ran, H.; Wang, Z.; Wang, Z.; Zheng, Y., Injectable Plga/Fe3o4 Implants Carrying Cisplatin for Synergistic Magnetic Hyperthermal Ablation of Rabbit Vx2 Tumor. *Plos One* **2017,** *12* (5), e0177049.

276.   Liu, X. L.; Yang, Y.; Ng, C. T.; Zhao, L. Y.; Zhang, Y.; Bay, B. H.; Fan, H. M.; Ding, J., Magnetic Vortex Nanorings: A New Class of Hyperthermia Agent for Highly Efficient in Vivo Regression of Tumors. *Advanced Materials* **2015,** *27* (11), 1939-1944.

277.   Cheng, Y.; Muroski, M. E.; Petit, D. C. M. C.; Mansell, R.; Vemulkar, T.; Morshed, R. A.; Han, Y.; Balyasnikova, I. V.; Horbinski, C. M.; Huang, X.; Zhang, L.; Cowburn, R. P.; Lesniak, M. S., Rotating Magnetic Field Induced Oscillation of Magnetic Particles for in Vivo Mechanical Destruction of Malignant Glioma. *Journal of Controlled Release* **2016,** *223* (Supplement C), 75-84.

278.   Hayashi, K.; Nakamura, M.; Miki, H.; Ozaki, S.; Abe, M.; Matsumoto, T.; Sakamoto, W.; Yogo, T.; Ishimura, K., Magnetically Responsive Smart Nanoparticles for Cancer Treatment with a Combination of Magnetic Hyperthermia and Remote-Control Drug Release. *Theranostics* **2014,** *4* (8), 834-844.

279.   Haghniaz, R.; Umrani, R. D.; Paknikar, K. M., Hyperthermia Mediated by Dextran-Coated La(0.7)Sr(0.3)Mno(3) Nanoparticles: In Vivo Studies. *International Journal of Nanomedicine* **2016,** *11*, 1779-1791.

280.   Espinosa, A.; Di Corato, R.; Kolosnjaj-Tabi, J.; Flaud, P.; Pellegrino, T.; Wilhelm, C., Duality of Iron Oxide Nanoparticles in Cancer Therapy: Amplification of Heating Efficiency by Magnetic Hyperthermia and Photothermal Bimodal Treatment. *ACS nano* **2016,** *10* (2), 2436-2446.

281.   Chen, Y.; Jiang, L.; Wang, R.; Lu, M.; Zhang, Q.; Zhou, Y.; Wang, Z.; Lu, G.; Liang, P.; Ran, H.; Chen, H.; Zheng, Y., Injectable Smart Phase-Transformation Implants for Highly Efficient in Vivo Magnetic-Hyperthermia Regression of Tumors. *Advanced Materials* **2014,** *26* (44), 7468-7473.

282.   Baldi, G.; Ravagli, C.; Mazzantini, F.; Loudos, G.; Adan, J.; Masa, M.; Psimadas, D.; Fragogeorgi, E. A.; Locatelli, E.; Innocenti, C.; Sangregorio, C.; Comes Franchini, M., In Vivo Anticancer Evaluation of the Hyperthermic Efficacy of Anti-Human Epidermal Growth Factor Receptor-Targeted Peg-Based Nanocarrier Containing Magnetic Nanoparticles. *International Journal of Nanomedicine* **2014,** *9*, 3037-3056.

283.   Ding, Q.; Liu, D.; Guo, D.; Yang, F.; Pang, X.; Che, R.; Zhou, N.; Xie, J.; Sun, J.; Huang, Z.; Gu, N., Shape-Controlled Fabrication of Magnetite Silver Hybrid Nanoparticles with High Performance Magnetic Hyperthermia. *Biomaterials* **2017,** *124* (Supplement C), 35-46.

284.   Wang, F.; Yang, Y.; Ling, Y.; Liu, J.; Cai, X.; Zhou, X.; Tang, X.; Liang, B.; Chen, Y.; Chen, H.; Chen, D.; Li, C.; Wang, Z.; Hu, B.; Zheng, Y., Injectable and Thermally Contractible Hydroxypropyl Methyl Cellulose/Fe3o4 for Magnetic Hyperthermia Ablation of Tumors. *Biomaterials* **2017,** *128*, 84-93.

285.   Guo, Y.; Zhang, Y.; Ma, J.; Li, Q.; Li, Y.; Zhou, X.; Zhao, D.; Song, H.; Chen, Q.; Zhu, X., Light/Magnetic Hyperthermia Triggered Drug Released from Multi-Functional Thermo-Sensitive Magnetoliposomes for Precise Cancer Synergetic Theranostics. *Journal of Controlled Release* **2017**.

286.   Gao, W.; Zheng, Y.; Wang, R.; Chen, H.; Cai, X.; Lu, G.; Chu, L.; Xu, C.; Zhang, N.; Wang, Z.; Ran, H.; Li, P.; Yang, C.; Mei, Z.; Song, J., A Smart, Phase Transitional and Injectable Dox/Plga-Fe Implant for Magnetic-Hyperthermia-Induced Synergistic Tumor Eradication. *Acta Biomaterialia* **2016,** *29* (Supplement C), 298-306.

287.   Chatterjee, J.; Bettge, M.; Haik, Y.; Jen Chen, C., Synthesis and Characterization of Polymer Encapsulated Cu–Ni Magnetic Nanoparticles for Hyperthermia Applications. *Journal of Magnetism and Magnetic Materials* **2005,** *293* (1), 303-309.

288.   Ban, I.; Stergar, J.; Drofenik, M.; Ferk, G.; Makovec, D., Synthesis of Copper–Nickel Nanoparticles Prepared by Mechanical Milling for Use in Magnetic Hyperthermia. *Journal of Magnetism and Magnetic Materials* **2011,** *323* (17), 2254-2258.

289.   Ruiz, A.; Gutierrez, L.; Caceres-Velez, P. R.; Santos, D.; Chaves, S. B.; Fascineli, M. L.; Garcia, M. P.; Azevedo, R. B.; Morales, M. P., Biotransformation of Magnetic Nanoparticles as a Function of Coating in a Rat Model. *Nanoscale* **2015,** *7* (39), 16321-16329.

290.   Gutiérrez, L.; Lázaro, F. J., Comparative Study of Iron-Containing Haematinics from the Point of View of Their Magnetic Properties. *Journal of Magnetism and Magnetic Materials* **2007,** *316* (2), 136-139.

291.   Martin, M.; Rodriguez-Nogales, A.; Garces, V.; Galvez, N.; Gutierrez, L.; Galvez, J.; Rondon, D.; Olivares, M.; Dominguez-Vera, J. M., Magnetic Study on Biodistribution and Biodegradation of Oral Magnetic Nanostructures in the Rat Gastrointestinal Tract. *Nanoscale* **2016,** *8* (32), 15041-15047.

292.   Lu, Y.; Xu, Y.-J.; Zhang, G.-b.; Ling, D.; Wang, M.-q.; Zhou, Y.; Wu, Y.-D.; Wu, T.; Hackett, M. J.; Kim, B. H., Iron Oxide Nanoclusters for T 1 Magnetic Resonance Imaging of Non-Human Primates. *Nature biomedical engineering* **2017,** *1* (8), 637-643.

293.   Ito, M.; Hiramatsu, H.; Kobayashi, K.; Suzue, K.; Kawahata, M.; Hioki, K.; Ueyama, Y.; Koyanagi, Y.; Sugamura, K.; Tsuji, K., Nod/Scid/Γ C Null Mouse: An Excellent Recipient Mouse Model for Engraftment of Human Cells. *Blood, The Journal of the American Society of Hematology* **2002,** *100* (9), 3175-3182.

294.   Roca, A. G.; Morales, M. P.; O'Grady, K.; Serna, C. J., Structural and Magnetic Properties of Uniform Magnetite Nanoparticles Prepared by High Temperature Decomposition of Organic Precursors. *Nanotechnology* **2006,** *17* (11), 2783.

295.   Hugounenq, P.; Levy, M.; Alloyeau, D.; Lartigue, L.; Dubois, E.; Cabuil, V.; Ricolleau, C.; Roux, S.; Wilhelm, C.; Gazeau, F.; Bazzi, R., Iron Oxide Monocrystalline Nanoflowers for Highly Efficient Magnetic Hyperthermia. *The Journal of Physical Chemistry C* **2012,** *116* (29), 15702-15712.

296.   Massart, R., Preparation of Aqueous Magnetic Liquids in Alkaline and Acidic Media. *IEEE Transactions on Magnetics* **1981,** *17* (2), 1247-1248.

297.   Vergés, M. A.; Costo, R.; Roca, A. G.; Marco, J. F.; Goya, G. F.; Serna, C. J.; Morales, M. P., Uniform and Water Stable Magnetite Nanoparticles with Diameters around the Monodomain–Multidomain Limit. *Journal of Physics D: Applied Physics* **2008,** *41* (13), 134003.

298.   França, A.; Pelaz, B.; Moros, M.; Sánchez-Espinel, C.; Hernández, A.; Fernández-López, C.; Grazu, V.; de la Fuente, J. M.; Pastoriza-Santos, I.; Liz-Marzán, L. M., Sterilization Matters: Consequences of Different Sterilization Techniques on Gold Nanoparticles. *small* **2010,** *6* (1), 89-95.

299.   Talamini, L.; Violatto, M. B.; Cai, Q.; Monopoli, M. P.; Kantner, K.; Krpetić, Z. e.; Perez-Potti, A.; Cookman, J.; Garry, D.; Silveira, C. P., Influence of Size and Shape on the Anatomical Distribution of Endotoxin-Free Gold Nanoparticles. *ACS nano* **2017,** *11* (6), 5519-5529.

300.   Mehdaoui, B.; Tan, R. P.; Meffre, A.; Carrey, J.; Lachaize, S.; Chaudret, B.; Respaud, M., Increase of Magnetic Hyperthermia Efficiency Due to Dipolar Interactions in Low-Anisotropy Magnetic Nanoparticles: Theoretical and Experimental Results. *Physical Review B* **2013,** *87* (17), 174419.

301.   Chu, M.; Shao, Y.; Peng, J.; Dai, X.; Li, H.; Wu, Q.; Shi, D., Near-Infrared Laser Light Mediated Cancer Therapy by Photothermal Effect of Fe3o4 Magnetic Nanoparticles. *Biomaterials* **2013,** *34* (16), 4078-4088.

302.   Javed, Y.; Lartigue, L.; Hugounenq, P.; Vuong, Q. L.; Gossuin, Y.; Bazzi, R.; Wilhelm, C.; Ricolleau, C.; Gazeau, F.; Alloyeau, D., Biodegradation Mechanisms of Iron Oxide Monocrystalline Nanoflowers and Tunable Shield Effect of Gold Coating. *small* **2014,** *10* (16), 3325-3337.

303.   Ito, A.; Tanaka, K.; Kondo, K.; Shinkai, M.; Honda, H.; Matsumoto, K.; Saida, T.; Kobayashi, T., Tumor Regression by Combined Immunotherapy and Hyperthermia Using Magnetic Nanoparticles in an Experimental Subcutaneous Murine Melanoma. *Cancer science* **2003,** *94* (3), 308-313.

304.   Wilhelm, S.; Tavares, A. J.; Dai, Q.; Ohta, S.; Audet, J.; Dvorak, H. F.; Chan, W. C., Analysis of Nanoparticle Delivery to Tumours. *Nature reviews materials* **2016,** *1* (5), 16014.

305.   Jain, R. K.; Stylianopoulos, T., Delivering Nanomedicine to Solid Tumors. *Nature Reviews Clinical Oncology* **2010,** *7* (11), 653-664.

306.   Kherlopian, A. R.; Song, T.; Duan, Q.; Neimark, M. A.; Po, M. J.; Gohagan, J. K.; Laine, A. F., A Review of Imaging Techniques for Systems Biology. *BMC systems biology* **2008,** *2* (1), 74.

307.   Hannecart, A.; Stanicki, D.; Vander Elst, L.; Muller, R. N.; Lecommandoux, S.; Thévenot, J.; Bonduelle, C.; Trotier, A.; Massot, P.; Miraux, S., Nano-Thermometers with Thermo-Sensitive Polymer Grafted Uspios Behaving as Positive Contrast Agents in Low-Field Mri. *Nanoscale* **2015,** *7* (8), 3754-3767.

308.   Yan, H.; Zhao, L.; Shang, W.; Liu, Z.; Xie, W.; Qiang, C.; Xiong, Z.; Zhang, R.; Li, B.; Sun, X.; Kang, F., General Synthesis of High-Performing Magneto-Conjugated Polymer Core–Shell Nanoparticles for Multifunctional Theranostics. *Nano Research* **2016,** *10* (2), 704-717.

309.   Kolosnjaj-Tabi, J.; Di Corato, R.; Lartigue, L.; Marangon, I.; Guardia, P.; Silva, A. K.; Luciani, N.; Clement, O.; Flaud, P.; Singh, J. V., Heat-Generating Iron Oxide Nanocubes: Subtle "Destructurators" of the Tumoral Microenvironment. *ACS nano* **2014,** *8* (5), 4268-4283.

310.   Cabrera, D.; Camarero, J.; Ortega, D.; Teran, F. J., Influence of the Aggregation, Concentration, and Viscosity on the Nanomagnetism of Iron Oxide Nanoparticle Colloids for Magnetic Hyperthermia. *Journal of Nanoparticle Research* **2015,** *17* (3), 121.

311.   Etheridge, M. L.; Hurley, K. R.; Zhang, J.; Jeon, S.; Ring, H. L.; Hogan, C.; Haynes, C. L.; Garwood, M.; Bischof, J. C., Accounting for Biological Aggregation in Heating and Imaging of Magnetic Nanoparticles. *Technology* **2014,** *2* (03), 214-228.

312.   Gutierrez, L.; Moros, M.; Mazario, E.; de Bernardo, S.; de la Fuente, J. M.; del Puerto Morales, M.; Salas, G., Aggregation Effects on the Magnetic Properties of Iron Oxide Colloids. *Nanotechnology* **2019**.

313.   Mejías, R.; Hernández Flores, P.; Talelli, M.; Tajada-Herráiz, J. L.; Brollo, M. E.; Portilla, Y.; Morales, M. a. P.; Barber, D. F., Cell-Promoted Nanoparticle Aggregation Decreases Nanoparticle-Induced Hyperthermia under an Alternating Magnetic Field Independently of Nanoparticle Coating, Core Size, and Subcellular Localization. *ACS Appl Mater Interfaces* **2018,** *11* (1), 340-355.

314.   Stepien, G.; Moros, M.; Perez-Hernandez, M.; Monge, M.; Gutierrez, L.; Fratila, R. M.; Las Heras, M.; Menao Guillen, S.; Puente Lanzarote, J. J.; Solans, C.; Pardo, J.; de la Fuente, J. M., Effect of Surface Chemistry and Associated Protein Corona on the Long-Term Biodegradation of Iron Oxide Nanoparticles in Vivo. *ACS Appl Mater Interfaces* **2018,** *10* (5), 4548-4560.

315.   Ruiz, A.; Alpízar, A.; Beola, L.; Rubio, C.; Gavilán, H.; Marciello, M.; Rodríguez-Ramiro, I.; Ciordia, S.; Morris, C. J.; Morales, M. d. P., Understanding the Influence of a

Bifunctional Polyethylene Glycol Derivative in Protein Corona Formation around Iron Oxide Nanoparticles. *Materials* **2019,** *12* (14), 2218.

316. Silva, A. C.; Oliveira, T. R.; Mamani, J. B.; Malheiros, S. M.; Malavolta, L.; Pavon, L. F.; Sibov, T. T.; Amaro, E., Jr.; Tannus, A.; Vidoto, E. L.; Martins, M. J.; Santos, R. S.; Gamarra, L. F., Application of Hyperthermia Induced by Superparamagnetic Iron Oxide Nanoparticles in Glioma Treatment. *Int J Nanomedicine* **2011,** *6*, 591-603.

317. Stocke, N. A.; Sethi, P.; Jyoti, A.; Chan, R.; Arnold, S. M.; Hilt, J. Z.; Upreti, M., Toxicity Evaluation of Magnetic Hyperthermia Induced by Remote Actuation of Magnetic Nanoparticles in 3d Micrometastasic Tumor Tissue Analogs for Triple Negative Breast Cancer. *Biomaterials* **2017,** *120*, 115-125.

318. Thomas, R. G.; Moon, M. J.; Lee, H.; Sasikala, A. R.; Kim, C. S.; Park, I. K.; Jeong, Y. Y., Hyaluronic Acid Conjugated Superparamagnetic Iron Oxide Nanoparticle for Cancer Diagnosis and Hyperthermia Therapy. *Carbohydr Polym* **2015,** *131*, 439-46.

319. Hildebrandt, B.; Wust, P.; Ahlers, O.; Dieing, A.; Sreenivasa, G.; Kerner, T.; Felix, R.; Riess, H., The Cellular and Molecular Basis of Hyperthermia. *Critical reviews in oncology/hematology* **2002,** *43* (1), 33-56.

320. Kossatz, S.; Ludwig, R.; Dahring, H.; Ettelt, V.; Rimkus, G.; Marciello, M.; Salas, G.; Patel, V.; Teran, F. J.; Hilger, I., High Therapeutic Efficiency of Magnetic Hyperthermia in Xenograft Models Achieved with Moderate Temperature Dosages in the Tumor Area. *Pharmaceutical Research* **2014,** *31* (12), 3274-88.

321. Garanina, A. S.; Naumenko, V. A.; Nikitin, A. A.; Myrovali, E.; Petukhova, A. Y.; Klimyuk, S. V.; Nalench, Y. A.; Ilyasov, A. R.; Vodopyanov, S. S.; Erofeev, A. S., Temperature-Controlled Magnetic Nanoparticles Hyperthermia Inhibits Primary Tumor Growth and Metastases Dissemination. *Nanomedicine: Nanotechnology, Biology and Medicine* **2020,** *25*, 102171.

322. van den Tempel, N.; Laffeber, C.; Odijk, H.; van Cappellen, W. A.; van Rhoon, G. C.; Franckena, M.; Kanaar, R., The Effect of Thermal Dose on Hyperthermia-Mediated Inhibition of DNA Repair through Homologous Recombination. *Oncotarget* **2017,** *8* (27), 44593.

323. Mantso, T.; Goussetis, G.; Franco, R.; Botaitis, S.; Pappa, A.; Panayiotidis, M. In *Effects of Hyperthermia as a Mitigation Strategy in DNA Damage-Based Cancer Therapies*, Seminars in cancer biology, Elsevier: 2016; pp 96-105.

324. Bettaieb, A.; Wrzal, P. K.; Averill-Bates, D. A., Hyperthermia: Cancer Treatment and Beyond. *Cancer treatment-conventional and innovative approaches* **2013**, 257-283.

325. Ikwegbue, P. C.; Masamba, P.; Oyinloye, B. E.; Kappo, A. P., Roles of Heat Shock Proteins in Apoptosis, Oxidative Stress, Human Inflammatory Diseases, and Cancer. *Pharmaceuticals* **2018,** *11* (1), 2.

326. Miyagawa, T.; Saito, H.; Minamiya, Y.; Mitobe, K.; Takashima, S.; Takahashi, N.; Ito, A.; Imai, K.; Motoyama, S.; Ogawa, J., Inhibition of Hsp90 and 70 Sensitizes Melanoma Cells to Hyperthermia Using Ferromagnetic Particles with a Low Curie Temperature. *International journal of clinical oncology* **2014,** *19* (4), 722-730.

327. Shetake, N. G.; Kumar, A.; Gaikwad, S.; Ray, P.; Desai, S.; Ningthoujam, R. S.; Vatsa, R. K.; Pandey, B. N., Magnetic Nanoparticle-Mediated Hyperthermia Therapy Induces Tumour Growth Inhibition by Apoptosis and Hsp90/Akt Modulation. *International Journal of Hyperthermia* **2015,** *31* (8), 909-919.

328.   Rochani, A. K.; Balasubramanian, S.; Girija, A. R.; Raveendran, S.; Borah, A.; Nagaoka, Y.; Nakajima, Y.; Maekawa, T.; Kumar, D. S., Dual Mode of Cancer Cell Destruction for Pancreatic Cancer Therapy Using Hsp90 Inhibitor Loaded Polymeric Nano Magnetic Formulation. *Int J Pharm* **2016,** *511* (1), 648-658.

329.   Kong, G.; Braun, R. D.; Dewhirst, M. W., Characterization of the Effect of Hyperthermia on Nanoparticle Extravasation from Tumor Vasculature. *Cancer research* **2001,** *61* (7), 3027-3032.

330.   Song, C.; Park, H.; Lee, C. K.; Griffin, R., Implications of Increased Tumor Blood Flow and Oxygenation Caused by Mild Temperature Hyperthermia in Tumor Treatment. *International Journal of Hyperthermia* **2005,** *21* (8), 761-767.

331.   Kong, G.; Braun, R. D.; Dewhirst, M. W., Hyperthermia Enables Tumor-Specific Nanoparticle Delivery: Effect of Particle Size. *Cancer research* **2000,** *60* (16), 4440-4445.

332.   Kolosnjaj-Tabi, J.; Marangon, I.; Nicolas-Boluda, A.; Silva, A. K.; Gazeau, F., Nanoparticle-Based Hyperthermia, a Local Treatment Modulating the Tumor Extracellular Matrix. *Pharmacological research* **2017,** *126*, 123-137.

333.   McKee, T. D.; Grandi, P.; Mok, W.; Alexandrakis, G.; Insin, N.; Zimmer, J. P.; Bawendi, M. G.; Boucher, Y.; Breakefield, X. O.; Jain, R. K., Degradation of Fibrillar Collagen in a Human Melanoma Xenograft Improves the Efficacy of an Oncolytic Herpes Simplex Virus Vector. *Cancer research* **2006,** *66* (5), 2509-2513.

334.   Zheng, X.; Goins, B. A.; Cameron, I. L.; Santoyo, C.; Bao, A.; Frohlich, V. C.; Fullerton, G. D., Ultrasound-Guided Intratumoral Administration of Collagenase-2 Improved Liposome Drug Accumulation in Solid Tumor Xenografts. *Cancer Chemotherapy and Pharmacology* **2011,** *67* (1), 173-182.

335.   Jabłońska-Trypuć, A.; Matejczyk, M.; Rosochacki, S., Matrix Metalloproteinases (Mmps), the Main Extracellular Matrix (Ecm) Enzymes in Collagen Degradation, as a Target for Anticancer Drugs. *Journal of Enzyme Inhibition and Medicinal Chemistry* **2016,** *31* (sup1), 177-183.

336.   Beola, L.; Asín, L.; Fratila, R. M.; Herrero, V.; de la Fuente, J. M.; Grazú, V.; Gutiérrez, L., Dual Role of Magnetic Nanoparticles as Intracellular Hotspots and Extracellular Matrix Disruptors Triggered by Magnetic Hyperthermia in 3d Cell Culture Models. *ACS Appl Mater Interfaces* **2018,** *10* (51), 44301-44313.

337.   Frantz, C.; Stewart, K. M.; Weaver, V. M., The Extracellular Matrix at a Glance. *J. Cell Sci.* **2010,** *123* (24), 4195.

338.   Hay, E. D., *Cell Biology of Extracellular Matrix: Second Edition*. Springer US: 2013.

339.   Liu, Y.; Liu, L.; Chen, M.; Zhang, Q., Double Thermal Transitions of Type I Collagen in Acidic Solution. *Journal of Biomolecular Structure and Dynamics* **2013,** *31* (8), 862-873.

340.   Persikov, A. V.; Xu, Y.; Brodsky, B., Equilibrium Thermal Transitions of Collagen Model Peptides. *Protein Science* **2004,** *13* (4), 893-902.

341.   Xu, Y., Thermal Stability of Collagen Triple Helix. In *Methods in Enzymology*, Elsevier: 2009; Vol. 466, pp 211-232.

342.   Chang, L.; Liu, X. L.; Di Fan, D.; Miao, Y. Q.; Zhang, H.; Ma, H. P.; Liu, Q. Y.; Ma, P.; Xue, W. M.; Luo, Y. E.; Fan, H. M., The Efficiency of Magnetic Hyperthermia and in Vivo Histocompatibility for Human-Like Collagen Protein-Coated Magnetic Nanoparticles. *Int J Nanomedicine* **2016,** *11*, 1175-85.

343. Xia, Z.; Calderon-Colon, X.; Trexler, M.; Elisseeff, J.; Guo, Q., Thermal Denaturation of Type I Collagen Vitrified Gels. *Thermochim acta* **2012,** *527*, 172-179.

344. Colombo, M.; Carregal-Romero, S.; Casula, M. F.; Gutierrez, L.; Morales, M. P.; Bohm, I. B.; Heverhagen, J. T.; Prosperi, D.; Parak, W. J., Biological Applications of Magnetic Nanoparticles. *Chemical Society reviews* **2012,** *41* (11), 4306-4334.

345. Eifler, A. C.; Thaxton, C. S., Nanoparticle Therapeutics: Fda Approval, Clinical Trials, Regulatory Pathways, and Case Study. *Methods Mol Biol* **2011,** *726*, 325-38.

346. Jain, K., Advances in the Field of Nanooncology. *BMC medicine* **2010,** *8* (1), 83.

347. Pérez-López, B.; Merkoçi, A., Nanoparticles for the Development of Improved (Bio) Sensing Systems. *Analytical and bioanalytical chemistry* **2011,** *399* (4), 1577-1590.

348. Arruebo, M.; Fernández-Pacheco, R.; Ibarra, R. M.; Santamaría, J., Magnetic Nanoparticles for Drug Delivery. *Nano Today* **2007,** *2* (3), 22-32.

349. Neuberger, T.; Schöpf, B.; Hofmann, H.; Hofmann, M.; von Rechenberg, B., Superparamagnetic Nanoparticles for Biomedical Applications: Possibilities and Limitations of a New Drug Delivery System. *J. Magn. Magn. Matter.* **2005,** *293* (1), 483-496.

350. Rosen, J. E.; Chan, L.; Shieh, D. B.; Gu, F. X., Iron Oxide Nanoparticles for Targeted Cancer Imaging and Diagnostics. *Nanomedicine_UK* **2012,** *8* (3), 275-290.

351. Huh, Y. M.; Jun, Y. W.; Song, H. T.; Kim, S.; Choi, J. S.; Lee, J. H.; Kim, K. S.; Shin, J. S.; Suh, J. S.; Cheon, J., In Vivo Magnetic Resonance Detection of Cancer by Using Multifunctional Magnetic Nanocrystals. *J. Am. Chem. Soc.* **2005,** *127*, 12387-12391.

352. Jordan, A.; Scholz, R.; Wust, P.; Fähling, H.; Roland, F., Magnetic Fluid Hyperthermia (Mfh): Cancer Treatment with Ac Magnetic Field Induced Excitation of Biocompatible Superparamagnetic Nanoparticles. *J. Magn. Magn. Matter.* **1999,** *201* (1–3), 413-419.

353. Wust, P.; Hildebrandt, B.; Sreenivasa, G.; Rau, B.; Gellermann, J.; Riess, H.; Felix, R.; Schlag, P. M., Hyperthermia in Combined Treatment of Cancer. *Lancet Oncol* **2002,** *3* (8), 487-497.

354. Kobayashi, T., Cancer Hyperthermia Using Magnetic Nanoparticles. *Biotechnol J* **2011,** *6* (11), 1342-7.

355. Sato, I., Simultaneous Hyperthermia-Chemotherapy with Controlled Drug Delivery Using Single-Drug Nanoparticles. *Sci Rep* **2016,** *6*, 24629.

356. Thorat, N. D.; Bohara, R.; Yadav, H. M.; Otari, S. V.; Pawar, S. H.; Tofail, S. A. M., Multifunctional Magnetic Nanostructures for Cancer Hyperthermia Therapy. **2016**, 589-612.

357. Grivennikov, S. I.; Greten, F. R.; Karin, M., Immunity, Inflammation, and Cancer. *Cell* **2010,** *140* (6), 883-899.

358. Berghe, T. V.; Linkermann, A.; Jouan-Lanhouet, S.; Walczak, H.; Vandenabeele, P., Regulated Necrosis: The Expanding Network of Non-Apoptotic Cell Death Pathways. *Nat. Rev. Mol. Cell Biol.* **2014,** *15* (2), 135.

359. Krysko, D. V.; Garg, A. D.; Kaczmarek, A.; Krysko, O.; Agostinis, P.; Vandenabeele, P., Immunogenic Cell Death and Damps in Cancer Therapy. *Nat. Rev. Cancer* **2012,** *12* (12), 860.

360. Sanz, B.; Calatayud, M. P.; Torres, T. E.; Fanarraga, M. L.; Ibarra, M. R.; Goya, G. F., Magnetic Hyperthermia Enhances Cell Toxicity with Respect to Exogenous Heating. *Biomaterials* **2017,** *114*, 62-70.

361. Calatayud, M. P.; Soler, E.; Torres, T. E.; Campos-Gonzalez, E.; Junquera, C.; Ibarra, M. R.; Goya, G. F., Cell Damage Produced by Magnetic Fluid Hyperthermia on Microglial Bv2 Cells. *Sci Rep* **2017,** *7* (1), 8627.

362. Lee, J.; Cuddihy, M. J.; Kotov, N. A., Three-Dimensional Cell Culture Matrices: State of the Art. *Tissue Eng Part B Rev* **2008,** *14* (1), 61-86.

363. McHale, G.; Newton, M., Liquid Marbles: Topical Context within Soft Matter and Recent Progress. *Soft Matter* **2015,** *11* (13), 2530-2546.

364. Derda, R.; Laromaine, A.; Mammoto, A.; Tang, S. K.; Mammoto, T.; Ingber, D. E.; Whitesides, G. M., Paper-Supported 3d Cell Culture for

Tissue-Based Bioassays. *Proc. Natl. Acad. Sci. U S A* **2009,** *106* (44), 18457-18462.

365. Cukierman, E.; Pankov, R.; Yamada, K. M., Cell Interactions with Three-Dimensional Matrices. *Current opinion in cell biology* **2002,** *14* (5), 633-640.

366. Tambe, D. T.; Hardin, C. C.; Angelini, T. E.; Rajendran, K.; Park, C. Y.; Serra-Picamal, X.; Zhou, E. H.; Zaman, M. H.; Butler, J. P.; Weitz, D. A.; Fredberg, J. J.; Trepat, X., Collective Cell Guidance by Cooperative Intercellular Forces. *Nat Mater* **2011,** *10* (6), 469-75.

367. Pampaloni, F.; Reynaud, E. G.; Stelzer, E. H., The Third Dimension Bridges the Gap between Cell Culture and Live Tissue. *Nat. Rev. Mol. Cell Biol.* **2007,** *8* (10), 839.

368. Trédan, O.; Galmarini, C. M.; Patel, K.; Tannock, I. F., Drug Resistance and the Solid Tumor Microenvironment. *J. Ntl. Cancer Inst.* **2007,** *99* (19), 1441-1454.

369. Beola, L.; Gutiérrez, L.; Grazú, V.; Asín, L., A Roadmap to the Standardization of in Vivo Magnetic Hyperthermia. In *Nanomaterials for Magnetic and Optical Hyperthermia Applications*, Elsevier: 2019; pp 317-337.

370. Kobayashi, T.; Ito, A.; Honda, H., Magnetic Nanoparticle-Mediated Hyperthermia and Induction of Anti-Tumor Immune Responses. In *Hyperthermic Oncology from Bench to Bedside*, Kokura, S.; Yoshikawa, T.; Ohnishi, T., Eds. Springer Singapore: Singapore, 2016; pp 137-150.

371. Moros, M.; Hernáez, B.; Garet, E.; Dias, J. T.; Sáez, B.; Grazú, V.; González-Fernández, A. f.; Alonso, C.; de la Fuente, J. s. M., Monosaccharides Versus Peg-Functionalized Nps: Influence in the Cellular Uptake. *ACS nano* **2012,** *6* (2), 1565-1577

372. Macheda, M. L.; Rogers, S.; Best, J. D., Molecular and Cellular Regulation of Glucose Transporter (Glut) Proteins in Cancer. *J. Cell. Physiol.* **2005,** *202* (3), 654-662.

373. Fratila, R. M.; Navascuez, M.; Idiago-López, J.; Eceiza, M.; Miranda, J. I.; Aizpurua, J. M.; Jesús, M., Covalent Immobilisation of Magnetic Nanoparticles on Surfaces Via Strain-Promoted Azide–Alkyne Click Chemistry. *New J. Chem.* **2017,** *41* (19), 10835-10840.

374. Privalov, P. L., Stability of Proteins: Proteins Which Do Not Present a Single Cooperative System. In *Advances in Protein Chemistry*, Elsevier: 1982; Vol. 35, pp 1-104 % @ 0065-3233.

375. Stone, L., Prostate Cancer: A Glitch in the Extracellular Matrix. *Nat. Rev. Urol.* **2016,** *14* (1), 1759-4820.

376. Gritsenko, P.; Leenders, W.; Friedl, P., Recapitulating in Vivo-Like Plasticity of Glioma Cell Invasion Along Blood Vessels and in Astrocyte-Rich Stroma. *Histochem. Cell Biol* **2017,** *148* (4), 395-406 % @ 0948-6143.

377.   Miyamoto, H.; Murakami, T.; Tsuchida, K.; Sugino, H.; Miyake, H.; Tashiro, S., Tumor-Stroma Interaction of Human Pancreatic Cancer: Acquired Resistance to Anticancer Drugs and Proliferation Regulation Is Dependent on Extracellular Matrix Proteins. *Pancreas* **2004,** *28* (1), 38-44

378.   Wlodkowic, D.; Skommer, J.; Darzynkiewicz, Z., Flow Cytometry-Based Apoptosis Detection. *Methods Mol Biol* **2009,** *559*, 19-32.

379.   Kühl, N. M.; Rensing, L., Heat Shock Effects on Cell Cycle Progression. *Cell Mol Life Sci* **2000,** *57* (3), 450-463

380.   Szüts, D.; Krude, T., Cell Cycle Arrest at the Initiation Step of Human Chromosomal DNA Replication Causes DNA Damage. *J. Cell Sci.* **2004,** *117* (21), 4897-4908.

381.   Ahmed, M. S. U.; Salam, A. B.; Clayton Yates, K. W.; Jaynes, J.; Turner, T.; Abdalla, M. O., Double-Receptor-Targeting Multifunctional Iron Oxide Nanoparticles Drug Delivery System for the Treatment and Imaging of Prostate Cancer. *Int J Nanomedicine* **2017,** *12*, 6973.

382.   Cabrera, D.; Coene, A.; Leliaert, J.; Artes-Ibanez, E. J.; Dupre, L.; Telling, N. D.; Teran, F. J., Dynamical Magnetic Response of Iron Oxide Nanoparticles inside Live Cells. *ACS nano* **2018,** *12* (3), 2741-2752.

383.   López, A.; Gutiérrez, L.; Lázaro, F. J., The Role of Dipolar Interaction in the Quantitative Determination of Particulate Magnetic Carriers in Biological Tissues. *Physics in Medicine & Biology* **2007,** *52* (16), 5043 %@ 0031-9155.

384.   Gutiérrez, L.; Morales, M.; Lázaro, F. J., Prospects About Magnetic Nanoparticles for Systemic Administration: Synthesis and Quantitative Detection. *Physical Chemistry Chemical Physics* **2014,** *16* (10), 4456-4464.

385.   Cope, D. A.; Dewhirst, M. W.; Friedman, H. S.; Bigner, D. D.; Zalutsky, M. R., Enhanced Delivery of a Monoclonal Antibody F (Ab′) 2 Fragment to Subcutaneous Human Glioma Xenografts Using Local Hyperthermia. *Cancer research* **1990,** *50* (6), 1803-1809.

386.   Hosono, M. N.; Hosono, M.; Endo, K.; Ueda, R.; Onoyama, Y., Effect of Hyperthermia on Tumor Uptake of Radiolabeled Anti-Neural Cell Adhesion Molecule Antibody in Small-Cell Lung Cancer Xenografts. *Journal of nuclear medicine: official publication, Society of Nuclear Medicine* **1994,** *35* (3), 504-509.

387.   Schuster, J.; Zalutsky, M.; Noska, M.; Dodge, R.; Friedman, H.; Bigner, D.; Dewhirst, M., Hyperthermic Modulation of Radiolabelled Antibody Uptake in a Human Glioma Xenograft and Normal Tissues. *International Journal of Hyperthermia* **1995,** *11* (1), 59-72.

388.   Hauck, M.; Coffin, D.; Dodge, R.; Dewhirst, M.; Mitchell, J.; Zalutsky, M., A Local Hyperthermia Treatment Which Enhances Antibody Uptake in a Glioma Xenograft Model Does Not Affect Tumour Interstitial Fluid Pressure. *International Journal of Hyperthermia* **1997,** *13* (3), 307-316.

389.   Serebriiskii, I.; Castello-Cros, R.; Lamb, A.; Golemis, E. A.; Cukierman, E., Fibroblast-Derived 3d Matrix Differentially Regulates the Growth and Drug-Responsiveness of Human Cancer Cells. *Matrix Biol* **2008,** *27* (6), 573-585.

390.   Dangi-Garimella, S.; Krantz, S. B.; Barron, M. R.; Shields, M. A.; Heiferman, M. J.; Grippo, P. J.; Bentrem, D. J.; Munshi, H. G., Three-Dimensional Collagen I Promotes Gemcitabine Resistance in Pancreatic Cancer through Mt1-Mmp–Mediated Expression of Hmga2. *Cancer research* **2011,** *71* (3), 1019-1028.

391.   Navazo, M. D. P.; Valmori, D.; Rüegg, C., The Alternatively Spliced Domain Tnfniii A1a2 of the Extracellular Matrix Protein Tenascin-C Suppresses Activation-Induced T Lymphocyte Proliferation and Cytokine Production. *The Journal of Immunology* **2001,** *167* (11), 6431-6440.

392.   Shultz, L. D.; Ishikawa, F.; Greiner, D. L., Humanized Mice in Translational Biomedical Research. *Nature Reviews Immunology* **2007,** *7* (2), 118-130.

393.   Frey, R. G., Justifying Animal Experimentation. *Society* **2002,** *39* (6), 37-47.

394.   Cole, A. J.; David, A. E.; Wang, J.; Galban, C. J.; Hill, H. L.; Yang, V. C., Polyethylene Glycol Modified, Cross-Linked Starch-Coated Iron Oxide Nanoparticles for Enhanced Magnetic Tumor Targeting. *Biomaterials* **2011,** *32* (8), 2183-93.

395.   Liu, Y.; Chen, Z.; Gu, N.; Wang, J., Effects of Dmsa-Coated Fe3o4 Magnetic Nanoparticles on Global Gene Expression of Mouse Macrophage RAW264.7 Cells. *Toxicology Letters* **2011,** *205* (2), 130-139.

396.   Gu, J.; Xu, H.; Han, Y.; Dai, W.; Hao, W.; Wang, C.; Gu, N.; Xu, H.; Cao, J., The Internalization Pathway, Metabolic Fate and Biological Effect of Superparamagnetic Iron Oxide Nanoparticles in the Macrophage-Like Raw264. 7 Cell. *Science China Life Sciences* **2011,** *54* (9), 793-805.

397.   Park, E.-J.; Choi, D.-H.; Kim, Y.; Lee, E.-W.; Song, J.; Cho, M.-H.; Kim, J.-H.; Kim, S.-W., Magnetic Iron Oxide Nanoparticles Induce Autophagy Preceding Apoptosis through Mitochondrial Damage and Er Stress in Raw264. 7 Cells. *Toxicology in Vitro* **2014,** *28* (8), 1402-1412.

398.   Creixell, M.; Bohorquez, A. C.; Torres-Lugo, M.; Rinaldi, C., Egfr-Targeted Magnetic Nanoparticle Heaters Kill Cancer Cells without a Perceptible Temperature Rise. *ACS nano* **2011,** *5* (9), 7124-7129.

399.   Rodriguez-Luccioni, H. L.; Latorre-Esteves, M.; Méndez-Vega, J.; Soto, O.; Rodríguez, A. R.; Rinaldi, C.; Torres-Lugo, M., Enhanced Reduction in Cell Viability by Hyperthermia Induced by Magnetic Nanoparticles. *Int J Nanomedicine* **2011,** *6*, 373.

400.   Mukherjee, A.; Castanares, M.; Hedayati, M.; Wabler, M.; Trock, B.; Kulkarni, P.; Rodriguez, R.; Getzenberg, R. H.; DeWeese, T. L.; Ivkov, R., Monitoring Nanoparticle-Mediated Cellular Hyperthermia with a High-Sensitivity Biosensor. *Nanomedicine* **2014,** *9* (18), 2729-2743.

401.   Guisasola, E.; Baeza, A.; Talelli, M.; Arcos, D.; Moros, M.; de la Fuente, J. s. M.; Vallet-Regí, M., Magnetic-Responsive Release Controlled by Hot Spot Effect. *Langmuir* **2015,** *31* (46), 12777-12782.

402.   Kettering, M.; Grau, I.; Pömpner, N.; Stapf, M.; Gajda, M.; Teichgräber, U.; Hilger, I., Means to Increase the Therapeutic Efficiency of Magnetic Heating of Tumors. *Biomedical Engineering/Biomedizinische Technik* **2015,** *60* (5), 505-517.

403.   Galluzzi, L.; Maiuri, M.; Vitale, I.; Zischka, H.; Castedo, M.; Zitvogel, L.; Kroemer, G., Cell Death Modalities: Classification and Pathophysiological Implications. Nature Publishing Group: 2007.

404.   Kroemer, G.; Galluzzi, L.; Vandenabeele, P.; Abrams, J.; Alnemri, E. S.; Baehrecke, E.; Blagosklonny, M.; El-Deiry, W.; Golstein, P.; Green, D., Classification of Cell Death: Recommendations of the Nomenclature Committee on Cell Death 2009. *Cell death and differentiation* **2009,** *16* (1), 3.

405.   Galluzzi, L.; Vitale, I.; Abrams, J.; Alnemri, E.; Baehrecke, E.; Blagosklonny, M.; Dawson, T. M.; Dawson, V.; El-Deiry, W.; Fulda, S., Molecular Definitions of Cell Death Subroutines: Recommendations of the Nomenclature Committee on Cell Death 2012. *Cell Death & Differentiation* **2012,** *19* (1), 107-120.

406.   Kroemer, G.; Galluzzi, L.; Kepp, O.; Zitvogel, L., Immunogenic Cell Death in Cancer Therapy. *Annual review of immunology* **2013,** *31*, 51-72.

407.   Galluzzi, L.; Buqué, A.; Kepp, O.; Zitvogel, L.; Kroemer, G., Immunogenic Cell Death in Cancer and Infectious Disease. *Nature Reviews Immunology* **2017,** *17* (2), 97.

408.   Kroemer, G.; El-Deiry, W.; Golstein, P.; Peter, M.; Vaux, D.; Vandenabeele, P.; Zhivotovsky, B.; Blagosklonny, M.; Malorni, W.; Knight, R., Classification of Cell Death: Recommendations of the Nomenclature Committee on Cell Death. *Cell death and differentiation* **2005,** *12* (12), 1463-1467.

409.   Galluzzi, L.; Bravo-San Pedro, J.; Vitale, I.; Aaronson, S.; Abrams, J.; Adam, D.; Alnemri, E.; Altucci, L.; Andrews, D.; Annicchiarico-Petruzzelli, M., Essential Versus Accessory Aspects of Cell Death: Recommendations of the Nccd 2015. *Cell Death & Differentiation* **2015,** *22* (1), 58-73.

410.   Galluzzi, L.; Vitale, I.; Aaronson, S. A.; Abrams, J. M.; Adam, D.; Agostinis, P.; Alnemri, E. S.; Altucci, L.; Amelio, I.; Andrews, D. W., Molecular Mechanisms of Cell Death: Recommendations of the Nomenclature Committee on Cell Death 2018. *Cell Death & Differentiation* **2018,** *25* (3), 486-541.

411.   Galluzzi, L.; Aaronson, S.; Abrams, J.; Alnemri, E.; Andrews, D.; Baehrecke, E.; Bazan, N.; Blagosklonny, M.; Blomgren, K.; Borner, C., Guidelines for the Use and Interpretation of Assays for Monitoring Cell Death in Higher Eukaryotes. *Cell Death & Differentiation* **2009,** *16* (8), 1093-1107.

412.   Blanco-Andujar, C.; Ortega, D.; Southern, P.; Nesbitt, S. A.; Thanh, N. T. K.; Pankhurst, Q. A., Real-Time Tracking of Delayed-Onset Cellular Apoptosis Induced by Intracellular Magnetic Hyperthermia. *Nanomedicine* **2016,** *11* (2), 121-136.

413.   Levine, B.; Yuan, J., Autophagy in Cell Death: An Innocent Convict? *The Journal of clinical investigation* **2005,** *115* (10), 2679-2688.

414.   Kroemer, G.; Jäättelä, M., Lysosomes and Autophagy in Cell Death Control. *Nat. Rev. Cancer* **2005,** *5* (11), 886-897.

415.   Amaravadi, R. K.; Thompson, C. B., The Roles of Therapy-Induced Autophagy and Necrosis in Cancer Treatment. *Clinical Cancer Research* **2007,** *13* (24), 7271-7279.

416.   Zhang, C.; Ren, J.; He, J.; Ding, Y.; Huo, D.; Hu, Y., Long-Term Monitoring of Tumor-Related Autophagy in Vivo by Fe3o4no· Nanoparticles. *Biomaterials* **2018,** *179*, 186-198.

417.   Vakkila, J.; Lotze, M. T., Inflammation and Necrosis Promote Tumour Growth. *Nature Reviews Immunology* **2004,** *4* (8), 641-648.

418.   Martin, S. J., Cell Death and Inflammation: The Case for Il-1 Family Cytokines as the Canonical Damp S of the Immune System. *The FEBS journal* **2016,** *283* (14), 2599-2615.

419.   Leist, M.; Jäättelä, M., Four Deaths and a Funeral: From Caspases to Alternative Mechanisms. *Nat. Rev. Mol. Cell Biol.* **2001,** *2* (8), 589-598.

420.   Kurokawa, M.; Kornbluth, S., Caspases and Kinases in a Death Grip. *Cell* **2009,** *138* (5), 838-854.

421.	Creagh, E. M.; Conroy, H.; Martin, S. J., Caspase-Activation Pathways in Apoptosis and Immunity. *Immunological reviews* **2003,** *193* (1), 10-21.

422.	Riedl, S. J.; Shi, Y., Molecular Mechanisms of Caspase Regulation During Apoptosis. *Nat. Rev. Mol. Cell Biol.* **2004,** *5* (11), 897-907.

423.	McArthur, K.; Kile, B. T., Apoptotic Caspases: Multiple or Mistaken Identities? *Trends in cell biology* **2018,** *28* (6), 475-493.

424.	Chen, M.; Wang, J., Initiator Caspases in Apoptosis Signaling Pathways. *Apoptosis* **2002,** *7* (4), 313-319.

425.	Shi, Y., Apoptosome: The Cellular Engine for the Activation of Caspase-9. *Structure* **2002,** *10* (3), 285-288.

426.	Carrington, P. E.; Sandu, C.; Wei, Y.; Hill, J. M.; Morisawa, G.; Huang, T.; Gavathiotis, E.; Wei, Y.; Werner, M. H., The Structure of Fadd and Its Mode of Interaction with Procaspase-8. *Molecular cell* **2006,** *22* (5), 599-610.

427.	Bressenot, A.; Marchal, S.; Bezdetnaya, L.; Garrier, J.; Guillemin, F.; Plénat, F., Assessment of Apoptosis by Immunohistochemistry to Active Caspase-3, Active Caspase-7, or Cleaved Parp in Monolayer Cells and Spheroid and Subcutaneous Xenografts of Human Carcinoma. *Journal of Histochemistry & Cytochemistry* **2009,** *57* (4), 289-300.

428.	Logue, S. E.; Martin, S. J., Caspase Activation Cascades in Apoptosis. *Biochemical Society Transactions* **2008,** *36* (1), 1-9.

429.	Kalkavan, H.; Green, D. R., Momp, Cell Suicide as a Bcl-2 Family Business. *Cell death and differentiation* **2018,** *25* (1), 46.

430.	Garcia-Saez, A., The Secrets of the Bcl-2 Family. *Cell Death & Differentiation* **2012,** *19* (11), 1733-1740.

431.	McArthur, K.; Whitehead, L. W.; Heddleston, J. M.; Li, L.; Padman, B. S.; Oorschot, V.; Geoghegan, N. D.; Chappaz, S.; Davidson, S.; San Chin, H., Bak/Bax Macropores Facilitate Mitochondrial Herniation and Mtdna Efflux During Apoptosis. *Science* **2018,** *359* (6378), eaao6047.

432.	Hengartner, M. O., The Biochemistry of Apoptosis. *Nature* **2000,** *407* (6805), 770-776.

433.	Suen, D.-F.; Norris, K. L.; Youle, R. J., Mitochondrial Dynamics and Apoptosis. *Genes & development* **2008,** *22* (12), 1577-1590.

434.	Yoo, D.; Jeong, H.; Preihs, C.; Choi, J. s.; Shin, T. H.; Sessler, J. L.; Cheon, J., Double-Effector Nanoparticles: A Synergistic Approach to Apoptotic Hyperthermia. *Angewandte Chemie International Edition* **2012,** *51* (50), 12482-12485.

435.	Tabuchi, Y.; Ahmed, K.; Kondo, T., Induction of Oxidative Stress by Hyperthermia and Enhancement of Hyperthermia-Induced Apoptosis by Oxidative Stress Modification. In *Hyperthermic Oncology from Bench to Bedside*, Springer: 2016; pp 7-18.

436.	Tomitaka, A.; Yamada, T.; Takemura, Y., Magnetic Nanoparticle Hyperthermia Using Pluronic-Coated Fe3o4 Nanoparticles: An in Vitro Study. *Journal of Nanomaterials* **2012,** *2012*.

437.	Demirci, H.; Slimani, N.; Pawar, M.; Kumon, R. E.; Vaishnava, P.; Besirli, C. G., Magnetic Hyperthermia in Y79 Retinoblastoma and Arpe-19 Retinal Epithelial Cells: Tumor Selective Apoptotic Activity of Iron Oxide Nanoparticle. *Translational vision science & technology* **2019,** *8* (5), 18-18.

438. Al-Qubaisi, M. S.; Rasedee, A.; Flaifel, M. H.; Ahmad, S. H.; Hussein-Al-Ali, S.; Hussein, M. Z.; Zainal, Z.; Alhassan, F. H.; Taufiq-Yap, Y. H.; Eid, E. E., Induction of Apoptosis in Cancer Cells by Nizn Ferrite Nanoparticles through Mitochondrial Cytochrome C Release. *Int J Nanomedicine* **2013,** *8*, 4115.

439. Mantso, T.; Vasileiadis, S.; Anestopoulos, I.; Voulgaridou, G. P.; Lampri, E.; Botaitis, S.; Kontomanolis, E. N.; Simopoulos, C.; Goussetis, G.; Franco, R.; Chlichlia, K.; Pappa, A.; Panayiotidis, M. I., Hyperthermia Induces Therapeutic Effectiveness and Potentiates Adjuvant Therapy with Non-Targeted and Targeted Drugs in an in Vitro Model of Human Malignant Melanoma. *Sci Rep* **2018,** *8* (1), 10724.

440. Huang, Y.; Sheikh, M. S., Trail Death Receptors and Cancer Therapeutics. *Toxicology and applied pharmacology* **2007,** *224* (3), 284-289.

441. Rossin, A.; Miloro, G.; Hueber, A.-O., Trail and Fasl Functions in Cancer and Autoimmune Diseases: Towards an Increasing Complexity. *Cancers* **2019,** *11* (5), 639.

442. Sheikh, M. S.; Huang, Y., Death Receptor Activation Complexes: It Takes Two to Activate Tnf Receptor 1. *Cell Cycle* **2003,** *2* (6), 549-551.

443. Rossi, D.; Gaidano, G., Messengers of Cell Death: Apoptotic Signaling in Health and Disease. *Haematologica* **2003,** *88* (2), 212-218.

444. Wang, S.; El-Deiry, W. S., Trail and Apoptosis Induction by Tnf-Family Death Receptors. *Oncogene* **2003,** *22* (53), 8628-8633.

445. Milhas, D.; Cuvillier, O.; Therville, N.; Clavé, P.; Thomsen, M.; Levade, T.; Benoist, H.; Ségui, B., Caspase-10 Triggers Bid Cleavage and Caspase Cascade Activation in Fasl-Induced Apoptosis. *Journal of Biological Chemistry* **2005,** *280* (20), 19836-19842.

446. Albeck, J. G.; Burke, J. M.; Aldridge, B. B.; Zhang, M.; Lauffenburger, D. A.; Sorger, P. K., Quantitative Analysis of Pathways Controlling Extrinsic Apoptosis in Single Cells. *Molecular cell* **2008,** *30* (1), 11-25.

447. Sayers, T. J., Targeting the Extrinsic Apoptosis Signaling Pathway for Cancer Therapy. *Cancer Immunology, Immunotherapy* **2011,** *60* (8), 1173-1180.

448. Li, H.; Zhu, H.; Xu, C.-j.; Yuan, J., Cleavage of Bid by Caspase 8 Mediates the Mitochondrial Damage in the Fas Pathway of Apoptosis. *Cell* **1998,** *94* (4), 491-501.

449. Wei, M. C.; Lindsten, T.; Mootha, V. K.; Weiler, S.; Gross, A.; Ashiya, M.; Thompson, C. B.; Korsmeyer, S. J., Tbid, a Membrane-Targeted Death Ligand, Oligomerizes Bak to Release Cytochrome C. *Genes & development* **2000,** *14* (16), 2060-2071.

450. Ito, A.; Shinkai, M.; Honda, H.; Kobayashi, T., Heat-Inducible Tnf-A Gene Therapy Combined with Hyperthermia Using Magnetic Nanoparticles as a Novel Tumor-Targeted Therapy. *Cancer gene therapy* **2001,** *8* (9), 649-654.

451. El Hajj Diab, D.; Clerc, P.; Serhan, N.; Fourmy, D.; Gigoux, V., Combined Treatments of Magnetic Intra-Lysosomal Hyperthermia with Doxorubicin Promotes Synergistic Anti-Tumoral Activity. *Nanomaterials* **2018,** *8* (7), 468.

452. Clerc, P.; Jeanjean, P.; Hallali, N.; Gougeon, M.; Pipy, B.; Carrey, J.; Fourmy, D.; Gigoux, V., Targeted Magnetic Intra-Lysosomal Hyperthermia Produces Lysosomal Reactive Oxygen Species and Causes Caspase-1 Dependent Cell Death. *Journal of Controlled Release* **2018,** *270*, 120-134.

453.   Domenech, M.; Marrero-Berrios, I.; Torres-Lugo, M.; Rinaldi, C., Lysosomal Membrane Permeabilization by Targeted Magnetic Nanoparticles in Alternating Magnetic Fields. *ACS nano* **2013,** *7* (6), 5091-5101.

454.   Guicciardi, M. E.; Leist, M.; Gores, G. J., Lysosomes in Cell Death. *Oncogene* **2004,** *23* (16), 2881-2890.

455.   Stoka, V.; Turk, B.; Schendel, S. L.; Kim, T.-H.; Cirman, T.; Snipas, S. J.; Ellerby, L. M.; Bredesen, D.; Freeze, H.; Abrahamson, M., Lysosomal Protease Pathways to Apoptosis Cleavage of Bid, Not Pro-Caspases, Is the Most Likely Route. *Journal of Biological Chemistry* **2001,** *276* (5), 3149-3157.

456.   Turk, B.; Stoka, V.; Rozman-Pungercar, J.; Cirman, T.; Droga-Mazovec, G.; Oreic, K.; Turk, V., Apoptotic Pathways: Involvement of Lysosomal Proteases. *Biological chemistry* **2002,** *383* (7-8), 1035-1044.

457.   Stoka, V.; Turk, V.; Turk, B., Lysosomal Cysteine Cathepsins: Signaling Pathways in Apoptosis. *Biological chemistry* **2007,** *388* (6), 555-560.

458.   Repnik, U.; Česen, M. H.; Turk, B., Lysosomal Membrane Permeabilization in Cell Death: Concepts and Challenges. *Mitochondrion* **2014,** *19*, 49-57.

459.   Kirkegaard, T.; Jäättelä, M., Lysosomal Involvement in Cell Death and Cancer. *Biochimica et Biophysica Acta (BBA)-Molecular Cell Research* **2009,** *1793* (4), 746-754.

460.   Eno, C. O.; Zhao, G.; Venkatanarayan, A.; Wang, B.; Flores, E. R.; Li, C., Noxa Couples Lysosomal Membrane Permeabilization and Apoptosis During Oxidative Stress. *Free Radical Biology and Medicine* **2013,** *65*, 26-37.

461.   Heinrich, M.; Neumeyer, J.; Jakob, M.; Hallas, C.; Tchikov, V.; Winoto-Morbach, S.; Wickel, M.; Schneider-Brachert, W.; Trauzold, A.; Hethke, A., Cathepsin D Links Tnf-Induced Acid Sphingomyelinase to Bid-Mediated Caspase-9 and-3 Activation. *Cell Death & Differentiation* **2004,** *11* (5), 550-563.

462.   Nagaraj, N. S.; Vigneswaran, N.; Zacharias, W., Cathepsin B Mediates Trail-Induced Apoptosis in Oral Cancer Cells. *Journal of cancer research and clinical oncology* **2006,** *132* (3), 171-183.

463.   Johansson, A.-C.; Appelqvist, H.; Nilsson, C.; Kågedal, K.; Roberg, K.; Öllinger, K., Regulation of Apoptosis-Associated Lysosomal Membrane Permeabilization. *Apoptosis* **2010,** *15* (5), 527-540.

464.   Pucci, C.; De Pasquale, D.; Marino, A.; Martinelli, C.; Lauciello, S.; Ciofani, G., Hybrid Magnetic Nanovectors Promote Selective Glioblastoma Cell Death through a Combined Effect of Lysosomal Membrane Permeabilization and Chemotherapy. *ACS Appl Mater Interfaces* **2020**.

465.   Marcos-Campos, I.; Asin, L.; Torres, T.; Marquina, C.; Tres, A.; Ibarra, M.; Goya, G., Cell Death Induced by the Application of Alternating Magnetic Fields to Nanoparticle-Loaded Dendritic Cells. *Nanotechnology* **2011,** *22* (20), 205101.

466.   Raj, D. B. T. G.; Khan, N. A., Surface Functionalization Dependent Subcellular Localization of Superparamagnetic Nanoparticle in Plasma Membrane and Endosome. *Nano convergence* **2018,** *5* (1), 4.

467.   Raj, D. B. T. G.; Khan, N. A.; Venkatachalam, S.; Chu, D. T.; Arumugam, S., Step-by-Step Protocol for Superparamagnetic Nanoparticle-Based Endosome and Lysosome Isolation from Eukaryotic Cell. **2019**.

468.   Di Corato, R.; Espinosa, A.; Lartigue, L.; Tharaud, M.; Chat, S.; Pellegrino, T.; Ménager, C.; Gazeau, F.; Wilhelm, C., Magnetic Hyperthermia Efficiency in the Cellular Environment for Different Nanoparticle Designs. *Biomaterials* **2014,** *35* (24), 6400-6411.

469.   P Calatayud, M.; Asin, L.; Tres, A.; F Goya, G.; R Ibarra, M., Cell Bystander Effect Induced by Radiofrequency Electromagnetic Fields and Magnetic Nanoparticles. *Current Nanoscience* **2016,** *12* (3), 372-377.

470.   Lee, Y.; Overholtzer, M., Focus: Death: After-Death Functions of Cell Death. *The Yale Journal of Biology and Medicine* **2019,** *92* (4), 687.

471.   Acebes-Huerta, A.; Lorenzo-Herrero, S.; Folgueras, A. R.; Huergo-Zapico, L.; Lopez-Larrea, C.; López-Soto, A.; Gonzalez, S., Drug-Induced Hyperploidy Stimulates an Antitumor Nk Cell Response Mediated by Nkg2d and Dnam-1 Receptors. *Oncoimmunology* **2016,** *5* (2), e1074378.

472.   Prasad, N.; Rathinasamy, K.; Panda, D.; Bahadur, D., Mechanism of Cell Death Induced by Magnetic Hyperthermia with Nanoparticles of Γ-Mn X Fe 2–X O 3 Synthesized by a Single Step Process. *Journal of Materials Chemistry* **2007,** *17* (48), 5042-5051.

473.   Harunaga, J. S.; Yamada, K. M., Cell-Matrix Adhesions in 3d. *Matrix Biol* **2011,** *30* (7-8), 363-8.

474.   Moore, A.; Weissleder, R.; Bogdanov Jr, A., Uptake of Dextran-Coated Monocrystalline Iron Oxides in Tumor Cells and Macrophages. *Journal of Magnetic Resonance Imaging* **1997,** *7* (6), 1140-1145.

475.   Moros, M.; Ambrosone, A.; Stepien, G.; Fabozzi, F.; Marchesano, V.; Castaldi, A.; Tino, A.; de la Fuente, J. M.; Tortiglione, C., Deciphering Intracellular Events Triggered by Mild Magnetic Hyperthermia in Vitro and in Vivo. *Nanomedicine* **2015,** *10* (14), 2167-2183

476.   Coral, D. F.; Mendoza Zelis, P.; Marciello, M.; Morales, M. a. d. P.; Craievich, A.; Sánchez, F. H.; Fernández van Raap, M. B., Effect of Nanoclustering and Dipolar Interactions in Heat Generation for Magnetic Hyperthermia. *Langmuir* **2016,** *32* (5), 1201-1213.

477.   Serantes, D.; Baldomir, D.; Martinez-Boubeta, C.; Simeonidis, K.; Angelakeris, M.; Natividad, E.; Castro, M.; Mediano, A.; Chen, D.-X.; Sanchez, A., Influence of Dipolar Interactions on Hyperthermia Properties of Ferromagnetic Particles. *Journal of Applied Physics* **2010,** *108* (7), 073918.

478.   Munoz-Menendez, C.; Serantes, D.; Ruso, J. M.; Baldomir, D., Towards Improved Magnetic Fluid Hyperthermia: Major-Loops to Diminish Variations in Local Heating. *Physical Chemistry Chemical Physics* **2017,** *19* (22), 14527-14532.

479.   Martinez-Boubeta, C.; Simeonidis, K.; Serantes, D.; Conde-Leborán, I.; Kazakis, I.; Stefanou, G.; Peña, L.; Galceran, R.; Balcells, L.; Monty, C., Adjustable Hyperthermia Response of Self-Assembled Ferromagnetic Fe-Mgo Core–Shell Nanoparticles by Tuning Dipole–Dipole Interactions. *Adv. Funct. Mater.* **2012,** *22* (17), 3737-3744.

480.   Ruta, S.; Chantrell, R.; Hovorka, O., Unified Model of Hyperthermia Via Hysteresis Heating in Systems of Interacting Magnetic Nanoparticles. *Sci Rep* **2015,** *5*, 9090.

481.   Soukup, D.; Moise, S.; Céspedes, E.; Dobson, J.; Telling, N. D., In Situ Measurement of Magnetization Relaxation of Internalized Nanoparticles in Live Cells. *ACS nano* **2015,** *9* (1), 231-240.

482.   Moise, S.; Céspedes, E.; Soukup, D.; Byrne, J. M.; El Haj, A. J.; Telling, N. D., The Cellular Magnetic Response and Biocompatibility of Biogenic Zinc-and Cobalt-Doped Magnetite Nanoparticles. *Sci Rep* **2017,** *7*, 39922.

483.   Cabrera, D.; Coene, A.; Leliaert, J.; Artés-Ibáñez, E. J.; Dupré, L.; Telling, N. D.; Teran, F. J., Dynamical Magnetic Response of Iron Oxide Nanoparticles inside Live Cells. *ACS nano* **2018,** *12* (3), 2741-2752.

484.   Fox, J. L.; MacFarlane, M., Targeting Cell Death Signalling in Cancer: Minimising 'Collateral Damage'. *British journal of cancer* **2016,** *115* (1), 5.

485.   Goldar, S.; Khaniani, M. S.; Derakhshan, S. M.; Baradaran, B., Molecular Mechanisms of Apoptosis and Roles in Cancer Development and Treatment. *Asian Pac J Cancer Prev* **2015,** *16* (6), 2129-2144.

486.   Martins, M.; Baptista, P. V.; Mendo, A. S.; Correia, C.; Videira, P.; Rodrigues, A. S.; Muthukumaran, J.; Santos-Silva, T.; Silva, A.; da Silva, M. F. C. G., In Vitro and in Vivo Biological Characterization of the Anti-Proliferative Potential of a Cyclic Trinuclear Organotin (Iv) Complex. *Molecular BioSystems* **2016,** *12* (3), 1015-1023.

487.   Svahn, N.; Moro, A. J.; Roma-Rodrigues, C.; Puttreddy, R.; Rissanen, K.; Baptista, P. V.; Fernandes, A. R.; Lima, J. C.; Rodríguez, L., The Important Role of the Nuclearity, Rigidity, and Solubility of Phosphane Ligands in the Biological Activity of Gold (I) Complexes. *Chemistry–A European Journal* **2018,** *24* (55), 14654-14667.

488.   Livak, K. J.; Schmittgen, T. D., Analysis of Relative Gene Expression Data Using Real-Time Quantitative Pcr and the $2-\Delta\delta ct$ Method. *methods* **2001,** *25* (4), 402-408.

489.   Attaluri, A.; Ma, R.; Qiu, Y.; Li, W.; Zhu, L., Nanoparticle Distribution and Temperature Elevations in Prostatic Tumours in Mice During Magnetic Nanoparticle Hyperthermia. *International Journal of Hyperthermia* **2011,** *27* (5), 491-502.

490.   Kuboyabu, T.; Yabata, I.; Aoki, M.; Banura, N.; Nishimoto, K.; Mimura, A.; Murase, K., Magnetic Particle Imaging for Magnetic Hyperthermia Treatment: Visualization and Quantification of the Intratumoral Distribution and Temporal Change of Magnetic Nanoparticles in Vivo. *Open Journal of Medical Imaging* **2016,** *6* (01), 1.

491.   Kandala, S. K.; Liapi, E.; Whitcomb, L. L.; Attaluri, A.; Ivkov, R., Temperature-Controlled Power Modulation Compensates for Heterogeneous Nanoparticle Distributions: A Computational Optimization Analysis for Magnetic Hyperthermia. *International Journal of Hyperthermia* **2019,** *36* (1), 115-129.

492.   Tapeinos, C.; Marino, A.; Battaglini, M.; Migliorin, S.; Brescia, R.; Scarpellini, A.; Fernández, C. D. J.; Prato, M.; Drago, F.; Ciofani, G., Stimuli-Responsive Lipid-Based Magnetic Nanovectors Increase Apoptosis in Glioblastoma Cells through Synergic Intracellular Hyperthermia and Chemotherapy. *Nanoscale* **2019,** *11* (1), 72-88.

493.   Griffin, R. J.; Dings, R. P.; Jamshidi-Parsian, A.; Song, C. W., Mild Temperature Hyperthermia and Radiation Therapy: Role of Tumour Vascular Thermotolerance and Relevant Physiological Factors. *International Journal of Hyperthermia* **2010,** *26* (3), 256-263.

494.   Pallepati, P.; Averill-Bates, D. A., Mild Thermotolerance Induced at 40 C Protects Hela Cells against Activation of Death Receptor-Mediated Apoptosis by Hydrogen Peroxide. *Free Radical Biology and Medicine* **2011,** *50* (6), 667-679.

495.   Stone, R.; Willi, T.; Rosen, Y.; Mefford, O. T.; Alexis, F., Targeted Magnetic Hyperthermia. *Therapeutic delivery* **2011,** *2* (6), 815-838.

496.   Tran, S.; Meinander, A.; Holmström, T.; Rivero-Müller, A.; Heiskanen, K.; Linnau, E.; Courtney, M.; Mosser, D.; Sistonen, L.; Eriksson, J., Heat Stress Downregulates Flip and Sensitizes Cells to Fas Receptor-Mediated Apoptosis. *Cell Death & Differentiation* **2003,** *10* (10), 1137-1147.

497.   Shah, B. P.; Pasquale, N.; De, G.; Tan, T.; Ma, J.; Lee, K.-B., Core–Shell Nanoparticle-Based Peptide Therapeutics and Combined Hyperthermia for Enhanced Cancer Cell Apoptosis. *ACS nano* **2014,** *8* (9), 9379-9387.

498.   Yin, P. T.; Shah, B. P.; Lee, K. B., Combined Magnetic Nanoparticle-Based Microrna and Hyperthermia Therapy to Enhance Apoptosis in Brain Cancer Cells. *Small* **2014,** *10* (20), 4106-4112.

499.   Galluzzi, L.; Bravo-San Pedro, J. M.; Kepp, O.; Kroemer, G., Regulated Cell Death and Adaptive Stress Responses. *Cellular and Molecular Life Sciences* **2016,** *73* (11-12), 2405-2410.

500.   Shellman, Y. G.; Howe, W. R.; Miller, L. A.; Goldstein, N. B.; Pacheco, T. R.; Mahajan, R. L.; LaRue, S. M.; Norris, D. A., Hyperthermia Induces Endoplasmic Reticulum-Mediated Apoptosis in Melanoma and Non-Melanoma Skin Cancer Cells. *Journal of investigative dermatology* **2008,** *128* (4), 949-956.

501.   Curado, M.-P.; Edwards, B.; Shin, H. R.; Storm, H.; Ferlay, J.; Heanue, M.; Boyle, P., *Cancer Incidence in Five Continents, Volume Ix*. IARC Press, International Agency for Research on Cancer: 2007.

502.   Parkin, D. M.; Bray, F.; Ferlay, J.; Pisani, P., Estimating the World Cancer Burden: Globocan 2000. *International journal of cancer* **2001,** *94* (2), 153-156.

503.   Raimondi, S.; Maisonneuve, P.; Lowenfels, A. B., Epidemiology of Pancreatic Cancer: An Overview. *Nature reviews Gastroenterology & hepatology* **2009,** *6* (12), 699.

504.   Rawla, P.; Sunkara, T.; Gaduputi, V., Epidemiology of Pancreatic Cancer: Global Trends, Etiology and Risk Factors. *World journal of oncology* **2019,** *10* (1), 10.

505.   Neesse, A.; Michl, P.; Frese, K. K.; Feig, C.; Cook, N.; Jacobetz, M. A.; Lolkema, M. P.; Buchholz, M.; Olive, K. P.; Gress, T. M., Stromal Biology and Therapy in Pancreatic Cancer. *Gut* **2011,** *60* (6), 861-868.

506.   Demaria, S.; Coleman, C. N.; Formenti, S. C., Radiotherapy: Changing the Game in Immunotherapy. *Trends in cancer* **2016,** *2* (6), 286-294.

507.   Smith, J. P.; Wang, S.; Nadella, S.; Jablonski, S. A.; Weiner, L. M., Cholecystokinin Receptor Antagonist Alters Pancreatic Cancer Microenvironment and Increases Efficacy of Immune Checkpoint Antibody Therapy in Mice. *Cancer Immunology, Immunotherapy* **2018,** *67* (2), 195-207.

508.   Di Michele, F.; Pizzichelli, G.; Mazzolai, B.; Sinibaldi, E., On the Preliminary Design of Hyperthermia Treatments Based on Infusion and Heating of Magnetic Nanofluids. *Math Biosci* **2015,** *262*, 105-16.

509.   Toraya-Brown, S.; Fiering, S., Local Tumour Hyperthermia as Immunotherapy for Metastatic Cancer. *International Journal of Hyperthermia* **2014,** *30* (8), 531-539.

510.   Mahmood, J.; Shukla, H. D.; Soman, S.; Samanta, S.; Singh, P.; Kamlapurkar, S.; Saeed, A.; Amin, N. P.; Vujaskovic, Z., Immunotherapy, Radiotherapy, and Hyperthermia: A Combined Therapeutic Approach in Pancreatic Cancer Treatment. *Cancers* **2018,** *10* (12), 469.

511.   Tanaka, K.; Ito, A.; Kobayashi, T.; Kawamura, T.; Shimada, S.; Matsumoto, K.; Saida, T.; Honda, H., Intratumoral Injection of Immature Dendritic Cells Enhances Antitumor Effect of Hyperthermia Using Magnetic Nanoparticles. *International journal of cancer* **2005,** *116* (4), 624-633.

512.   Chao, Y.; Chen, G.; Liang, C.; Xu, J.; Dong, Z.; Han, X.; Wang, C.; Liu, Z., Iron Nanoparticles for Low-Power Local Magnetic Hyperthermia in Combination with Immune Checkpoint Blockade for Systemic Antitumor Therapy. *Nano Lett* **2019,** *19* (7), 4287-4296.

513.   Erkan, M.; Hausmann, S.; Michalski, C. W.; Fingerle, A. A.; Dobritz, M.; Kleeff, J.; Friess, H., The Role of Stroma in Pancreatic Cancer: Diagnostic and Therapeutic Implications. *Nature reviews Gastroenterology & hepatology* **2012,** *9* (8), 454.

514.   Feigin, M. E.; Tuveson, D. A. In *Challenges and Opportunities in Modeling Pancreatic Cancer*, Cold Spring Harbor symposia on quantitative biology, Cold Spring Harbor Laboratory Press: 2016; pp 231-235.

515.   Brachi, G.; Bussolino, F.; Ciardelli, G.; Mattu, C., Nanomedicine for Imaging and Therapy of Pancreatic Adenocarcinoma. *Frontiers in Bioengineering and Biotechnology* **2019,** *7*.

516.   Gutierrez-Barrera, A. M.; Menter, D. G.; Abbruzzese, J. L.; Reddy, S. A., Establishment of Three-Dimensional Cultures of Human Pancreatic Duct Epithelial Cells. *Biochemical and biophysical research communications* **2007,** *358* (3), 698-703.

517.   Jaidev, L.; Chellappan, D. R.; Bhavsar, D. V.; Ranganathan, R.; Sivanantham, B.; Subramanian, A.; Sharma, U.; Jagannathan, N. R.; Krishnan, U. M.; Sethuraman, S., Multi-Functional Nanoparticles as Theranostic Agents for the Treatment & Imaging of Pancreatic Cancer. *Acta Biomater* **2017,** *49*, 422-433.

518.   Ware, M. J.; Keshishian, V.; Law, J. J.; Ho, J. C.; Favela, C. A.; Rees, P.; Smith, B.; Mohammad, S.; Hwang, R. F.; Rajapakshe, K., Generation of an in Vitro 3d Pdac Stroma Rich Spheroid Model. *Biomaterials* **2016,** *108*, 129-142.

519.   Shields, M. A.; Dangi-Garimella, S.; Redig, A. J.; Munshi, H. G., Biochemical Role of the Collagen-Rich Tumour Microenvironment in Pancreatic Cancer Progression. *Biochemical Journal* **2012,** *441* (2), 541-552.

520.   Hwang, C. I.; Boj, S. F.; Clevers, H.; Tuveson, D. A., Preclinical Models of Pancreatic Ductal Adenocarcinoma. *The Journal of pathology* **2016,** *238* (2), 197-204.

521.   Zhang, Y.; Chen, L.; Yang, J.; Fleming, J. B.; Chiao, P. J.; Logsdon, C. D.; Li, M., Study Human Pancreatic Cancer in Mice: How Close Are They? *Biochimica et Biophysica Acta (BBA)-Reviews on Cancer* **2013,** *1835* (1), 110-118.

522.   Zhao, Y.; Sultan, D.; Liu, Y., Biodistribution, Excretion, and Toxicity of Nanoparticles. In *Theranostic Bionanomaterials*, Elsevier: 2019; pp 27-53.

523.   Maeda, H.; Bharate, G.; Daruwalla, J., Polymeric Drugs for Efficient Tumor-Targeted Drug Delivery Based on Epr-Effect. *European journal of pharmaceutics and biopharmaceutics* **2009,** *71* (3), 409-419.

524.   Bazak, R.; Houri, M.; El Achy, S.; Kamel, S.; Refaat, T., Cancer Active Targeting by Nanoparticles: A Comprehensive Review of Literature. *Journal of cancer research and clinical oncology* **2015,** *141* (5), 769-784.

525.   Huang, H. S.; Hainfeld, J. F., Intravenous Magnetic Nanoparticle Cancer Hyperthermia. *Int J Nanomedicine* **2013,** *8*, 2521.

526.   Huerta-Núñez, L. F. E.; Villanueva-Lopez, G. C.; Morales-Guadarrama, A.; Soto, S.; López, J.; Silva, J. G.; Perez-Vielma, N.; Sacristán, E.; Gudiño-Zayas, M. E.; González, C. A., Assessment of the Systemic Distribution of a Bioconjugated Anti-Her2 Magnetic Nanoparticle in a Breast Cancer Model by Means of Magnetic Resonance Imaging. *Journal of Nanoparticle Research* **2016,** *18* (9), 284.

527.   Buyukhatipoglu, K.; Clyne, A. M., Superparamagnetic Iron Oxide Nanoparticles Change Endothelial Cell Morphology and Mechanics Via Reactive Oxygen Species Formation. *Journal of biomedical materials research Part A* **2011,** *96* (1), 186-195.

528.   Kettering, M.; Richter, H.; Wiekhorst, F.; Bremer-Streck, S.; Trahms, L.; Kaiser, W. A.; Hilger, I., Minimal-Invasive Magnetic Heating of Tumors Does Not Alter Intra-Tumoral Nanoparticle Accumulation, Allowing for Repeated Therapy Sessions: An in Vivo Study in Mice. *Nanotechnology* **2011,** *22* (50), 505102.

529.   Giustini, A.; Ivkov, R.; Hoopes, P., Magnetic Nanoparticle Biodistribution Following Intratumoral Administration. *Nanotechnology* **2011,** *22* (34), 345101.

530.   Javidi, M.; Heydari, M.; Karimi, A.; Haghpanahi, M.; Navidbakhsh, M.; Razmkon, A., Evaluation of the Effects of Injection Velocity and Different Gel Concentrations on Nanoparticles in Hyperthermia Therapy. *Journal of biomedical physics & engineering* **2014,** *4* (4), 151.

531.   Onuki, Y.; Jacobs, I.; Artemov, D.; Kato, Y., Noninvasive Visualization of in Vivo Release and Intratumoral Distribution of Surrogate Mr Contrast Agent Using the Dual Mr Contrast Technique. *Biomaterials* **2010,** *31* (27), 7132-7138.

532.   Kanat, O.; Ertas, H., Shattering the Castle Walls: Anti-Stromal Therapy for Pancreatic Cancer. *World journal of gastrointestinal oncology* **2018,** *10* (8), 202.

533.   Stylianopoulos, T.; Martin, J. D.; Chauhan, V. P.; Jain, S. R.; Diop-Frimpong, B.; Bardeesy, N.; Smith, B. L.; Ferrone, C. R.; Hornicek, F. J.; Boucher, Y., Causes, Consequences, and Remedies for Growth-Induced Solid Stress in Murine and Human Tumors. *Proc. Natl. Acad. Sci. U S A* **2012,** *109* (38), 15101-15108.

534.   Elahi-Gedwillo, K. Y.; Carlson, M.; Zettervall, J.; Provenzano, P. P., Antifibrotic Therapy Disrupts Stromal Barriers and Modulates the Immune Landscape in Pancreatic Ductal Adenocarcinoma. *Cancer research* **2019,** *79* (2), 372-386.

535.   Doane, T. L.; Burda, C., The Unique Role of Nanoparticles in Nanomedicine: Imaging, Drug Delivery and Therapy. *Chemical Society reviews* **2012,** *41* (7), 2885-2911.

536.   Bogart, L. K.; Pourroy, G.; Murphy, C. J.; Puntes, V.; Pellegrino, T.; Rosenblum, D.; Peer, D.; Lévy, R., Nanoparticles for Imaging, Sensing, and Therapeutic Intervention. ACS Publications: 2014.

537.   Hervault, A.; Thanh, N. T. K., Magnetic Nanoparticle-Based Therapeutic Agents for Thermo-Chemotherapy Treatment of Cancer. *Nanoscale* **2014,** *6* (20), 11553-11573.

538.   Rodrigues, M.; Piñol, R.; Antorrena, G.; Brites, C. D.; Silva, N. J.; Murillo, J. L.; Cases, R.; Díez, I.; Palacio, F.; Torras, N., Luminescent Thermometers: Implementing Thermometry on Silicon Surfaces Functionalized by Lanthanide-Doped Self-Assembled Polymer Monolayers (Adv. Funct. Mater. 2/2016). *Adv. Funct. Mater.* **2016,** *26* (2), 312-312.

539.   Incio, J.; Suboj, P.; Chin, S. M.; Vardam-Kaur, T.; Liu, H.; Hato, T.; Babykutty, S.; Chen, I.; Deshpande, V.; Jain, R. K., Metformin Reduces Desmoplasia in Pancreatic Cancer

by Reprogramming Stellate Cells and Tumor-Associated Macrophages. *PLoS One* **2015,** *10* (12).

540.   Gudtskova, T.; Zhukova, G.; Bragina, M.; Garkavi, L.; Mikholap, A.; Barteneva, T., Signs of Cell-Cell Interactions in Sarcoma 45 Tissue under Conditions of Antitumor Effect Caused by Injection of Magnetite Nanoparticles. *Bulletin of Experimental Biology & Medicine* **2013,** *155* (6).

541.   Garg, A. D.; Dudek-Peric, A. M.; Romano, E.; Agostinis, P., Immunogenic Cell Death. *International Journal of Developmental Biology* **2015,** *59* (1-2-3), 131-140.

542.   Obeid, M.; Tesniere, A.; Ghiringhelli, F.; Fimia, G. M.; Apetoh, L.; Perfettini, J.-L.; Castedo, M.; Mignot, G.; Panaretakis, T.; Casares, N., Calreticulin Exposure Dictates the Immunogenicity of Cancer Cell Death. *Nature medicine* **2007,** *13* (1), 54-61.

543.   Liu, X.; Zheng, J.; Sun, W.; Zhao, X.; Li, Y.; Gong, N.; Wang, Y.; Ma, X.; Zhang, T.; Zhao, L.-Y., Ferrimagnetic Vortex Nanoring-Mediated Mild Magnetic Hyperthermia Imparts Potent Immunological Effect for Treating Cancer Metastasis. *ACS nano* **2019,** *13* (8), 8811-8825.

544.   Liu, X.; Yan, B.; Li, Y.; Ma, X.; Jiao, W.; Shi, K.; Zhang, T.; Chen, S.; He, Y.; Liang, X.-J., Graphene Oxide-Grafted Magnetic Nanorings Mediated Magnetothermodynamic Therapy Favoring Reactive Oxygen Species-Related Immune Response for Enhanced Antitumor Efficacy. *ACS nano* **2020**.

545.   Zhang, N.; Song, J.; Liu, Y.; Liu, M.; Zhang, L.; Sheng, D.; Deng, L.; Yi, H.; Wu, M.; Zheng, Y., Photothermal Therapy Mediated by Phase-Transformation Nanoparticles Facilitates Delivery of Anti-Pd1 Antibody and Synergizes with Antitumor Immunotherapy for Melanoma. *Journal of Controlled Release* **2019,** *306*, 15-28.

546.   Guo, Y.; Ran, Y.; Wang, Z.; Cheng, J.; Cao, Y.; Yang, C.; Liu, F.; Ran, H., Magnetic-Responsive and Targeted Cancer Nanotheranostics by Pa/Mr Bimodal Imaging-Guided Photothermally Triggered Immunotherapy. *Biomaterials* **2019,** *219*, 119370.

547.   Netea, M. G.; Joosten, L. A.; Latz, E.; Mills, K. H.; Natoli, G.; Stunnenberg, H. G.; O'Neill, L. A.; Xavier, R. J., Trained Immunity: A Program of Innate Immune Memory in Health and Disease. *Science* **2016,** *352* (6284), aaf1098.

548.   Lopez, A.; Gutierrez, L.; Lazaro, F. J., The Role of Dipolar Interaction in the Quantitative Determination of Particulate Magnetic Carriers in Biological Tissues. *Phys Med Biol* **2007,** *52* (16), 5043-56.

549.   Mejías, R.; Gutiérrez, L.; Salas, G.; Pérez-Yagüe, S.; Zotes, T. M.; Lázaro, F. J.; Morales, M. P.; Barber, D. F., Long Term Biotransformation and Toxicity of Dimercaptosuccinic Acid-Coated Magnetic Nanoparticles Support Their Use in Biomedical Applications. *Journal of Controlled Release* **2013,** *171*, 225-233.

550.   Gutiérrez, L.; Mejías, R.; Barber, D. F.; Veintemillas-Verdaguer, S.; Serna, C. J.; Lázaro, F. J.; Morales, M. P., Ac Magnetic Susceptibility Study of in Vivo Nanoparticle Biodistribution. *Journal of Physics D: Applied Physics* **2011,** *44* (25), 255002.

551.   Gutiérrez, L.; Morales, M. P.; Lázaro, F. J., Prospects for Magnetic Nanoparticles in Systemic Administration: Synthesis and Quantitative Detection. *Physical Chemistry Chemical Physics* **2014,** *16* (10), 4456-4464.

552.   Siegel, R. L.; Miller, K. D.; Jemal, A., Cancer Statistics, 2020. *CA: A Cancer Journal for Clinicians* **2020,** *70* (1), 7-30.

553. Wang, L.; An, Y.; Yuan, C.; Zhang, H.; Liang, C.; Ding, F.; Gao, Q.; Zhang, D., Gem-Loaded Magnetic Albumin Nanospheres Modified with Cetuximab for Simultaneous Targeting, Magnetic Resonance Imaging, and Double-Targeted Thermochemotherapy of Pancreatic Cancer Cells. *Int J Nanomedicine* **2015,** *10*, 2507.

554. Ludwig, R.; Teran, F. J.; Teichgraeber, U.; Hilger, I., Nanoparticle-Based Hyperthermia Distinctly Impacts Production of Ros, Expression of Ki-67, Top2a, and Tpx2, and Induction of Apoptosis in Pancreatic Cancer. *Int J Nanomedicine* **2017,** *12*, 1009.

555. Wang, L.; Dong, J.; Ouyang, W.; Wang, X.; Tang, J., Anticancer Effect and Feasibility Study of Hyperthermia Treatment of Pancreatic Cancer Using Magnetic Nanoparticles. *Oncol Rep* **2012,** *27* (3), 719-726.

556. Basel, M. T.; Balivada, S.; Wang, H.; Shrestha, T. B.; Seo, G. M.; Pyle, M.; Abayaweera, G.; Dani, R.; Koper, O. B.; Tamura, M., Cell-Delivered Magnetic Nanoparticles Caused Hyperthermia-Mediated Increased Survival in a Murine Pancreatic Cancer Model. *Int J Nanomedicine* **2012,** *7*, 297.

557. Yu, E. Y.; Bishop, M.; Zheng, B.; Ferguson, R. M.; Khandhar, A. P.; Kemp, S. J.; Krishnan, K. M.; Goodwill, P. W.; Conolly, S. M., Magnetic Particle Imaging: A Novel in Vivo Imaging Platform for Cancer Detection. *Nano Lett* **2017,** *17* (3), 1648-1654.

558. Wang, J. Simulation of Magnetic Nanoparticle Hyperthermia in Prostate Tumors. Johns Hopkins University, 2014.

559. Zhang, Q.; Raoof, M.; Chen, Y.; Sumi, Y.; Sursal, T.; Junger, W.; Brohi, K.; Itagaki, K.; Hauser, C. J., Circulating Mitochondrial Damps Cause Inflammatory Responses to Injury. *Nature* **2010,** *464* (7285), 104.

(8) Beola L., Grazú V., Fernández-Afonso Y., Fratila R.M., de las Heras M., de la Fuente J.M., Gutiérrez L., Asín L., Effect of the field conditions, MNP biodistribution and immune response in the treatment of a xenograft pancreatic cancer model with magnetic hyperthermia. *Submitted*

(7) Beola L., Asín L., Roma-Rodrigues C., Fernández-Afonso Y., Fratila R.M., Serantes D., Ruta S., Chantrell R.W., Fernandes A.R., Baptista P.V., de la Fuente J.M., Grazú V., Gutiérrez L., Intracellular number of magnetic nanoparticles modulates the apoptotic death pathway after magnetic hyperthermia treatment. *Submitted*

(6) Alfranca, G.; **Beola, L**.; Liu, Y.; Gutiérrez, L.; Zhang, A.; Artiga, A.; Cui, D.; de la Fuente, J. M., *In Vivo* Comparison of the Biodistribution and Long-Term Fate of Colloids–Gold Nanoprisms and Nanorods–with Minimum Surface Modification. **Nanomedicine 2019**, 14 (23), 3035-3055.

(5) Ruiz, A.; Alpízar, A.; **Beola, L.**; Rubio, C.; Gavilán, H.; Marciello, M.; Rodríguez-Ramiro, I.; Ciordia, S.; Morris, C. J.; Morales, M. d. P., Understanding the Influence of a Bifunctional Polyethylene Glycol Derivative in Protein Corona Formation around Iron Oxide Nanoparticles. **Materials 2019, 12 (14), 2218**.

(4) Beola, L.; Gutiérrez, L.; Grazú, V.; Asín, L., A Roadmap to the Standardization of in Vivo Magnetic Hyperthermia. In Nanomaterials for Magnetic and Optical Hyperthermia Applications**, Elsevier: 2019**; pp 317-337.

(3) Moros, M.; Idiago-López, J.; Asín, L.; Moreno-Antolín, E.; **Beola, L**.; Grazú, V.; Fratila, R. M.; Gutiérrez, L.; de la Fuente, J. M., Triggering Antitumoural Drug Release and Gene Expression by Magnetic Hyperthermia. **Adv Drug Deliv Rev 2018**.

(2) Beola, L.; Asín, L.; Fratila, R. M.; Herrero, V.; de la Fuente, J. M.; Grazú, V.; Gutiérrez, L., Dual Role of Magnetic Nanoparticles as Intracellular Hotspots and Extracellular Matrix Disruptors Triggered by Magnetic Hyperthermia in 3D Cell Culture Models. **ACS Appl Mater Interfaces 2018,** 10 (51), 44301-44313.

(1) Guisasola, E.; Asín, L.; **Beola, L.**; de la Fuente, J. M.; Baeza, A.; Vallet-Regí, M., Beyond Traditional Hyperthermia: *In Vivo* Cancer Treatment with Magnetic-Responsive Mesoporous Silica Nanocarriers. **ACS Appl Mater Interfaces 2018**, 10 (15), 12518-12525